Title

MASS TRANSFER COEFFICIENTS AND INTERFACIAL AREA FOR GAS ABSORPTION BY AGITATED AQUEOUS ELECTROLYTE SOLUTIONS

Authors

Robinson, Campbell W.
Wilke, Charles R.

Publication Date

1971-04-01

UCRL-20472

MASS TRANSFER COEFFICIENTS AND INTERFACIAL AREA FOR GAS ABSORPTION BY AGITATED AQUEOUS ELECTROLYTE SOLUTIONS

Campbell W. Robinson* and Charles R. Wilke

April 1971

AEC Contract No. W-7405-eng-48

*Filed as a Ph. D. Thesis

LAWRENCE RADIATION LABORATORY
UNIVERSITY of CALIFORNIA BERKELEY

UCRL-20472

DISCLAIMER

To My Wife, Helen

for her patience, understanding, and encouragement

MASS TRANSFER COEFFICIENTS AND INTERFACIAL AREA FOR GAS ABSORPTION BY AGITATED AQUEOUS ELECTROLYTE SOLUTIONS

Contents

MASS TRANSFER COEFFICIENTS AND INTERFACIAL AREA FOR GAS ABSORPTION BY AGITATED AQUEOUS ELECTROLYTE SOLUTIONS

Campbell W. Robinson and Charles R. Wilke

Lawrence Radiation Laboratory
University of California
Berkeley, California 94720

ABSTRACT

In order to design or optimize the operation of stirred-tank gas absorbers, such as are used for the submerged cultivation of aerobic microorganisms wherein oxygen is supplied by mass transfer from dispersed air bubbles, it is necessary to be able to characterize the oxygen mass transfer capabilities in terms of the physicochemical properties of the aqueous phase, the agitation power input, and the aeration rate. The oxygen mass transfer capability of a particular tank can be described in terms of the overall volumetric mass transfer coefficient, $K_{L4}a$.

$K_{L4}a$ measurements were made in several aqueous electrolyte solutions of varying ionic strength over a wide range of agitation-aeration intensity in a 2.5 litre fully-baffled stirred tank having standard geometric ratios and equipped with a turbine-type impeller. Both steady-state and unsteady-state experimental methods were applied, utilizing a dissolved oxygen probe to measure the aqueous-phase oxygen tension or its rate of change. Unsteady-state oxygen probe response methods are described which permit measurement of $K_{L4}a$ with a

minimum of experimental complexity. Mathematical analysis of and computer solutions for probe response are given.

$K_{L4}a$ values are reported as a function of the agitation power input per unit volume (P_G/V_L), superficial gas velocity (v_S), and solution ionic strength. The results indicate that the ionic strength has a pronounced effect on the value of $K_{L4}a$ at constant P_G/V_L and v_S; the effect of ionic strength heretofore has not been explicitly described in the literature. A generalized correlation for the prediction of $K_{L4}a$ for electrolyte solutions or for water is given for the particular type of stirred tank used. Physical absorption results are compared to oxygen absorption-with-reaction results obtained from the copper-catalysed sulphite oxidation method.

A new simultaneous measuring technique involving concurrent chemical absorption of carbon dioxide and desorption of oxygen is developed for separately evaluating the liquid-phase oxygen mass transfer coefficient, k_{L4}, and the specific interfacial area, a. Results from three different non-viscous aqueous electrolyte solutions show that at high agitation power input levels, such that the average gas bubble diameter is between 0.02 and 0.25 cm, k_{L4} decreases with increasing P_G/V_L. This behavior is in contrast with the results of others at lower agitation levels or in non-electrolytic liquids, but is in general agreement with previous results for the behavior of single bubbles or bubble swarms having the same range of average bubble diameter produced in viscous, non-electrolytic aqueous solutions.

ACKNOWLEDGEMENTS

The authors are grateful to Dr. Dale L. Sortland, Dr. Joseph Dabes and Mr. Argyrios Margaritis for valuable advice and many stimulating discussions. We also want to thank Miss Chiu-chuan Shirley Hsu and Mrs. Moira Ralls for their assistance with the chemical and chromatographic analyses.

This work was performed under the auspices of the United States Atomic Energy Commission.

I. INTRODUCTION

1. Gas-Liquid Mass Transfer in Stirred-Tank Microbial Cultivation Vessels

Stirred-tank gas absorbers or absorber-reactors containing an aqueous electrolyte solution as the liquid phase are frequently used in the chemical processing industries for conducting a diversity of operations and are almost invariably used in the microbial processing industries for the submerged cultivation of aerobic microorganisms. In the latter case, air is the commonly-used sparge gas, and the overall transfer process for the microbially-required oxygen consists of a number of steps in series, each of which has a particular resistance to oxygen mass transfer. First, transfer of oxygen from the bulk dispersed gas phase to the gas-liquid interface; second, establishment of physical gas-liquid equilibrium at the interface and transfer across any interfacial resistance; third, transfer from the liquid interface to the bulk of the liquid phase; fourth, transfer of oxygen from the bulk of the liquid phase to the liquid-organism interface; fifth, transport through the organism's cell wall and cell membrane into the internal cytoplasmic region where, finally, the oxygen is consummed by an enzymatically-catalyzed oxidation-reduction reaction. Theory and experiment have lead to the conclusion that the mass transfer resistance of the third step - transfer of oxygen from the liquid interface to the bulk liquid - is the overall rate-controlling one in many cases. The overall volumetric mass transfer coefficient for this step is $K_{L4}a$, and much attention has been given to its evaluation in fermentation media or in what have been considered to be analog solutions.

Until recent years, organisms were grown in submerged processes in aqueous media containing inorganic salts (sources of nitrogen, phosphorous, sulphur, and trace elements required by all forms of life) and a soluble carbon and/or energy source, e.g., glucose. In such soluble-substrate processes utilizing microbes having a high oxygen demand (high respiration rate) it has been frequently found that if sufficient glucose and inorganic nutrients were supplied then the cell yield was limited by the rate of supply of oxygen (1). In addition to the requirement of oxygen for microbial growth per se, in many processes the yield of a valuable extracellular product, e.g., penicillin, is affected by the oxygen supply capability of the stirred-tank cultivation vessel, the yield increasing with increasing oxygen mass transfer rate, for example (2). Soluble-substrate processes are generally conducted with agitation power inputs per unit volume in the range $200 \leq P_G/V_L \leq 1000$ ft-lb_f/min-ft^3.

Recently, much interest has been expressed in producing protein from microbial cells grown in aqueous electrolyte media containing dispersed n-alkane droplets as the source of cellular carbon and energy, e.g. (3). Unlike glucose, n-alkanes of course contain no oxygen, and hence the microbial oxygen demand from sparged air is greater than in the case of the more-conventional soluble substrate processes. Darlington has shown that hydrocarbon substrate growth requires up to 2.7 times the rate of oxygen transfer from air as microbial growth on glucose (4). In order to disperse the hydrocarbon droplets to a high degree, thereby increasing the rate of supply of organic substrate, agitation power inputs in these systems are relatively high, P_G/V_L

being on the order of 10,000 ft-lb_f/min-ft^3 or greater, as estimated from the impeller rotational speeds used in the works of Webb, Lilly, and Ertola (5), Johnson and Miller (6, 7), and Johnson, Lie, and Miller (8).

The oxygen transfer capability of a particular stirred-tank gas absorber design has generally been characterized by $K_{L4}a$ for a given air-liquid system. Scale-up is usually based on correlations of various kinds to predict $K_{L4}a$ for a specified absorber. Commonly, $K_{L4}a$ has been assumed to be a function of either the agitation power per unit volume, P_G/V_L, or the impeller rotational speed, N, in addition to the superficial gas velocity v_S; some workers have also included the effects of liquid-phase viscosity, density, interfacial tension and diffusion coefficient (9, 10). However, no completely general correlation has been developed, particularly for those cases in which $K_{L4}a$ is strongly influenced by physicochemical factors which are functions of ionic composition and concentration.

2. Previous Results

Many investigators have studied oxygen or other sparingly-soluble gas absorption behavior in stirred tanks. The results have generally been expressed as

$$K_L a \propto (P_G/V_L)^n (v_S)^m \qquad (1.1)$$

or as

$$K_L a \propto (N)^b (v_S)^c \quad . \qquad (1.2)$$

With respect to specifically characterizing the behavior of aqueous fermentation media, two means of evaluating the overall volumetric mass transfer coefficient have generally been used. First, the cupric ion catalysed sulphite oxidation system, where dissolved oxygen is reacted with sulphite ion (usually at concentrations initially greater than 0.5M). The rate of oxidation of sulphite to sulphate is used to evaluate $K^r_{L4}a$, the overall volumetric coefficient for oxygen absorption with reaction (11, 12, 13, 14). Second, the absorption of oxygen in a non-reactive aqueous phase, usually pure water, whereby $K_{L4}a$ is evaluated (10, 14). The properties of neither the sulphite solution nor pure water are synonymous with the physicochemical properties of actual fermentation media, but nonetheless $K^r_{L4}a$ or $K_{L4}a$ results in these systems have commonly been used to design and scale-up aerobic microbial processes.

Further uncertainty in the interpretation or comparison of the various correlations results from the fact that there has been no standardization of the geometry in the stirred tanks used by various workers. Many different combinations of impeller type, D_I/D_T ratio, baffle width and air sparger type have been used; the effect of variations in these geometric factors is uncertain at best.

The results of some examples of previous work are shown on Table 1.1, which clearly illustrates the discrepancies that exist between various empirical correlations for $K_{L4}a$ or $K^r_{L4}a$ in terms of P_G/V_L (or N) and v_S.

Table 1.1. $K_{L4}a$ or $K^r_{L4}a$ Correlating Parameters in Fully-Baffled Stirred Tanks.

System and investigator(s)	Ref.	Impeller type	D_I/D_T	Agitation Range P_G/V_L	Agitation Range N	Exponent of P_G/V_L	Exponent of N	Exponent of v_S
SULPHITE OXIDATION								
Cooper et al.	11	16-blade vaned disc	0.40	0 - 2870		0.95		0.67
Yoshida et al.	14	12-blade turbine	0.40		100 - 550		2.34	
Phillips and Johnson	13	8-blade turbine	0.625		600 - 4500		1.21	
Westerterp et al.	12	6-blade turbine	0.3 - 0.7		600 - 3600		1.00	0.0 ($N>N_0$)
Augenstein and Wang	15	turbine	0.51	500 - 37000		0.57 - 0.85		0.0 - 0.20
WATER								
Calderbank	9,10	6-blade turbine	0.333	330 - 3300		0.40		0.50
Yoshida et al.	14	12-blade turbine	0.40		100 - 550		2.01	0.67

Assuming a Power number of 6.0, and using the Aeration number correlation of Ohyama and Endoh (15), values of P_G/V_L were calculated from known values of N given in the works of Yoshida et al. (14), Phillips and Johnson (13), and Westerterp et al. (12). Comparing the results of various workers on the basis that $K_{L4}a$ or $K^r_{L4}a$ varies as $(v_S)^{0.67}$, Fig. (1.1) shows values of $K_{L4}a/(v_S)^{0.67}$ or $K^r_{L4}a/(v_S)^{0.67}$ correlated with measured or calculated values of P_G/V_L. Where the experimental dependency on the superficial gas velocity was not as $(v_S)^{0.67}$, e.g., as in the works of (9), (10), and (12), then the value of $K_{L4}a/(v_S)^{0.67}$ or $K^r_{L4}a/(v_S)^{0.67}$ at constant P_G/V_L will, course, vary with v_S; the behavior at only one value of v_S is shown for illustrative purposes.

Figure (1.1) shows the wide variation that can result when $K_{L4}a$ or $K^r_{L4}a$ is predicted from the various correlations, which for the most part were obtained at values of P_G/V_L less than 4000. Further, if one assumed that the dependency of $K_{L4}a$ or $K^r_{L4}a$ upon P_G/V_L were constant regardless of the value of P_G/V_L, extrapolation of the low-power data to a power input level characteristic of processes for microbial growth on n-alkane substrates would result in even greater differences between the values of $K_{L4}a$ or $K^r_{L4}a$ given by the various correlations. For example, at an agitation power input of 10,000 ft-lb_f/min-ft^3, $K^r_{L4}a(\text{Cooper})/K_{L4}a(\text{Calderbank}) \approx 38.7$, $K^r_{L4}a(\text{Cooper})/K^r_{L4}a(\text{Westerterp}) \approx 2.7$, $K^r_{L4}a(\text{Cooper})/K^r_{L4}a(\text{Yoshida}) \approx 2.7$, and $K^r_{L4}a(\text{Cooper})/K_{L4}a(\text{Yoshida}) \approx 4.0$.

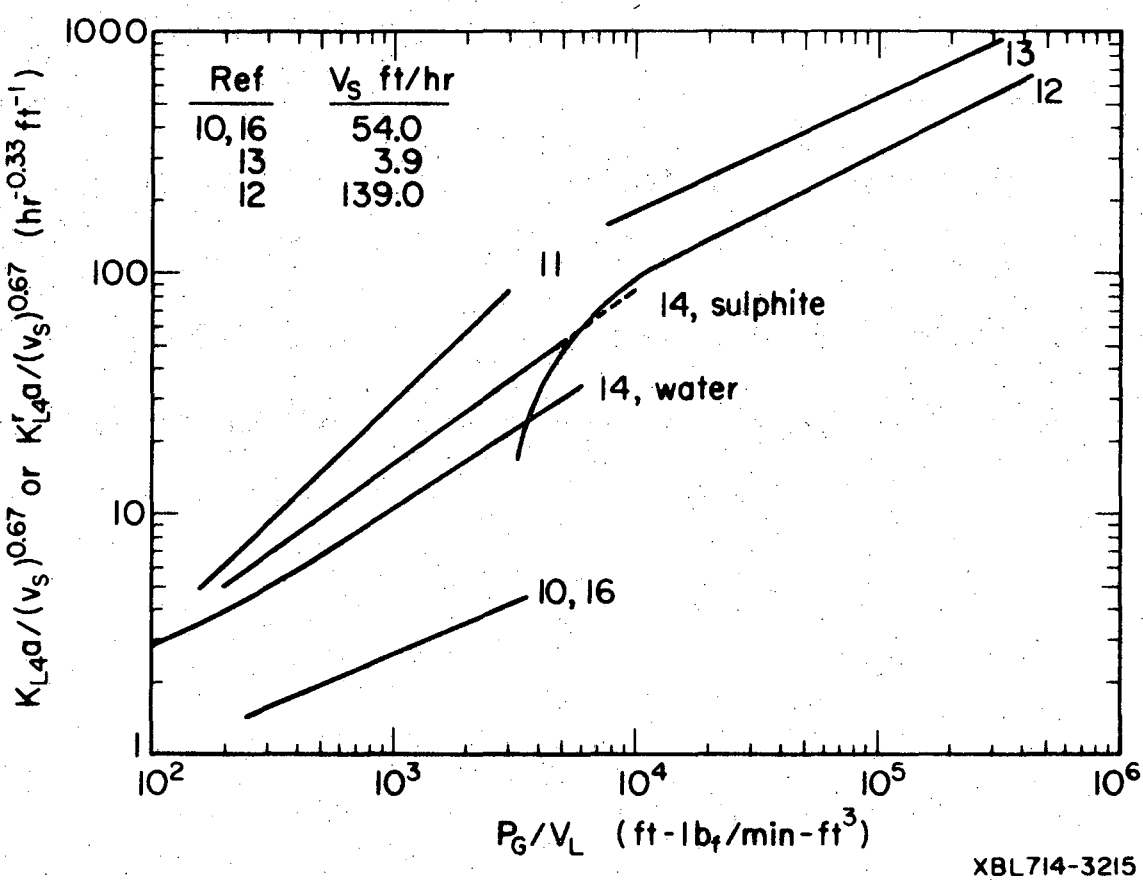

Fig. 1.1. Comparison of Oxygen Mass Transfer Coefficients Estimated from Previous Correlations.

3. Research Goals and Methods

In view of the foregoing, one goal of this present study was to attempt to define a factor or factors, other than geometry, which might explain some of the previous discrepancies in the dependency of $K_{L4}a$ or $K^r_{L4}a$ upon the agitation and aeration parameters at relatively low power inputs, and further to extend the power input range to include the higher power levels associated with the production of biomass from liquid hydrocarbon substrates.

Experimentally, the oxygen mass transfer characteristics of the sulphite oxidation system ($K^r_{L4}a$) and of non-reactive aqueous electrolyte solutions of varying composition and concentration ($K_{L4}a$) were studied in a single, fully-baffled stirred tank of 2.5 litres working liquid volume equipped with a 6-blade turbine impeller having a D_I/D_T ratio of one-third. Both continuous flow, steady-state and semi-batch unsteady-state experiments were conducted. The steady-state dissolved oxygen concentration or its unsteady-state rate of change are related to the value of $K_{L4}a$ as discussed in Section II.2.

The dissolved oxygen tension in the aqueous phase or its rate of change with time was measured in situ using a dissolved oxygen probe of the galvanometric type. A mathematical model of the transient response of the probe was developed to account for the diffusional response lag in the polymeric membrane separating the probe's electrodes from the external solution. The theory of the oxygen probe's behavior in both steady and unsteady-state is developed in Section II.4. When the probe is used in unsteady-state oxygen transfer experiments, the

corresponding value of $K_{L4}a$ is obtained indirectly from a computer non-linear least squares fitting programme which computes the value of a parameter β (which includes $K_{L4}a$) which best fits the transient experimental data to the theoretical response model. The nature of this computer programme is discussed in Section II. 4(e)(iii).

For sparingly-soluble gases such as oxygen, the overall volumetric mass transfer coefficient $K_{L4}a$ is the product of two individual parameters: first, the liquid-phase mass transfer coefficient, k_{L4}, and second, the interfacial area per unit liquid volume, a. Theory and experiment show that in general k_L and a have fundamentally different dependencies upon the physicochemical parameters of the system. For example, at a given hydrodynamic condition (relative motion between the gas bubble and the liquid phase), k_L is primarily dependent upon the liquid-phase viscosity and component diffusivity (9, 17, 18, 19) (in reacting systems, k_L^r may also depend on the kinetics of the reaction), whereas a is primarily dependent upon the interfacial surface tension (10) and the ionic strength, being less dependent on the liquid-phase density and viscosity (10). Therefore, the second goal of this research was to develope and apply a new technique whereby the individual behavior of k_{L4} and a in aqueous solutions of electrolytes could be evaluated under consistent hydrodynamic and physicochemical property conditions. Such consistency has not been a feature of some of the previous methods used to separate the behavior of k_L and a.

In the new technique, the aqueous electrolyte solution contains a small concentration of hydroxide ion (less than 0.1M). The technique

consists of concurrent unsteady-state desorption of oxygen with pseudo-steady state absorption-with-reaction of carbon dioxide from a sparged nitrogen-carbon dioxide gas which is dilute with respect to carbon dioxide (0.10 mole fraction). The oxygen desorption rate is measured by a dissolved oxygen probe, the response of which is used to evaluate $K_{L4}a$; the rate of absorption with reaction of carbon dioxide is used to evaluate a , the corresponding value of k_{L4} being calculated by combining the two results. The general theory of absorption with chemical reaction, and the conditions under which a can be evaluated directly are discussed in Section II. 5. The development of the new technique for the concurrent measurement of $K_{L4}a$ and a and the subsequent evaluation of k_{L4} is presented in Section II. 6.

4. Experimental Results

Following a discussion of the experimental apparatus, its operating characteristics and the analytical methods in Section III, the results of this investigation are given in Section IV. A heretofore unevaluated effect of solution ionic strength upon the relationship between $K_{L4}a$ and P_G/V_L is given in Section IV. 3, wherein a generalized correlation for the prediction of $K_{L4}a$ in agitated and aerated aqueous electrolyte solutions is presented.

The k_{L4} and a results of the new concurrent measurement technique are given in Section IV. 4. It is clearly shown that in aqueous electrolyte solutions subjected to agitation power in the range $1000 \leq P_G/V_L \leq 15{,}000$, k_{L4} and a have distinctly different dependencies upon P_G/V_L . As the agitation power input is increased, k_{L4}

decreases while a increases, the former result being in contrast to previous results of others at lower agitation levels, in non-electrolytic liquids, or with bubbles of a different size range.

The implications of the experimental results and their comparison with those of previous workers are discussed in Section V.

II. THEORY AND PREVIOUS WORK

1. Mass Transfer Driving Forces and Coefficients

a) General Relationships

The transfer of a component from a gaseous phase in direct contact with a liquid phase to that liquid phase will occur at a finite rate whenever the two phases are not at mutual chemical equilibrium with respect to that component; that is, whenever the fugacity of the component is not identical in both phases. The direction of mass transfer will be from that phase having the component at the higher fugacity level to the phase in which the fugacity of the component is the lesser.

The overall process of interphase mass transfer can be considered to consist of a number of sequential steps. For the situation of transfer from the gaseous phase to the liquid phase these steps can be postulated to be:

Step 1: movement of the component from the bulk of the gaseous phase to the interface between the phases. The instantaneous volumetric rate of mass transfer of a component k is proportional to the gas-phase transfer coefficient k_G, defined as

$$k_G \equiv (R_{Vk}/a)(p_{kB} - p_{ki}) , \qquad (2.1)$$

where subscript B denotes a property of the bulk (cup-mixed) phase, and subscript i denotes the parameter value at the interface.

Equation (2.1) is in the form of the classical definition, wherein the more-readily-measurable partial pressure is used in place of the rigorously-exact fugacity. The fugacity is related to the partial pressure by

$$f_k = \phi'_k y_k P_T = \phi'_k p_k \qquad (2.2)$$

where ϕ'_k is defined as the gas phase fugacity coefficient. For ideal gases, or non-associating gases at low (i.e., less than 10 atmospheres) pressure, $\phi'_k = 1.0$.

Step 2: diffusion of the component across any interfacial resistance. Usually, in systems devoid of such obvious resistances as interfacial surfactant films, it is assumed that there is no interfacial resistance to the mass transfer and that instantaneous establishment of gas-liquid physical equilibrium occurs at the interface. Thus, for a component which follows Henry's law,

$$C_{ki} = p_{ki}/H_{kj} . \qquad (2.3)$$

Step 3: movement of the component in the liquid from the interface to the bulk of the liquid phase. Here, the instantaneous volumetric absorption rate is proportional to the liquid phase mass transfer coefficient, k_L, defined classically as

$$k_L \equiv (R_{Vk}/a)\,(C_{ki} - C_{kB}). \qquad (2.4)$$

Steps (1) to (3), inclusive characterize fully the process of physical absorption of a gaseous component into a liquid. However, if the liquid phase contains a non-volatile component which reacts homogeneously with the dissolved gas component, then an additional step is introduced, namely

Step 4: chemical reaction within the liquid phase. Depending upon the relative magnitudes of the reaction rate and the physical absorption rate capabilities of the system, the presence of the reaction can affect the overall absorption rate in either one of two ways, or both. Either the reaction can merely maintain the bulk liquid concentration C_{kB} at its equilibrium value (in the case of an irreversible reaction this means that C_{kB} approaches zero), thereby increasing the concentration-difference driving force, or the reaction rate itself can be rate-controlling or rate-limiting resulting in the overall absorption-with-reaction rate being independent of or not solely dependent on the values of the physical mass transfer coefficients k_G and k_L. The effect of chemical reaction will be further discussed in Section II. 5(b).

At steady-state, equating Eq. (2.1) and Eq. (2.4) in terms of the mass transfer flux, there results

$$k_G(p_{kB} - p_{ki}) = k_L(C_{ki} - C_{kB}) = R_{Vk}/a. \qquad (2.5)$$

Equation (2.5) does not permit the experimental evaluation of either k_G or k_L at measured R_{Vk}/a as it is impossible to measure the interfacial values p_{ki} or C_{ki}. However, for systems where the equilibrium relationship, e.g., Eq. (2.3) gives a straight line distribution over the range of concentrations of interest, and where the ratio k_L/k_G remains constant within the linear portion of the distribution curve, it can be shown that (20)

$$R_{Vk}/a = K_G(p_{kB} - p_k^*) = K_L(C_k^* - C_{kB}), \qquad (2.6)$$

where K_G and K_L are defined as overall mass transfer coefficients based on the overall gas and overall liquid phase driving forces, respectively, p_k^* is the (hypothetical) partial pressure of the component in equilibrium with C_{kB}, and C_k^* is the (hypothetical) liquid concentration in equilibrium with p_{kB}. K_G and K_L incorporate the transfer resistances of both phases expressed in terms of the driving force appropriate to their particular phase.

As is commonly done for stepwise transfer processes that occur in series, the overall coefficients can be written as a function of the individual phase coefficients (21) such that

$$1/K_G = 1/k_G + H/k_L \qquad (2.7)$$

and that

$$1/K_L = 1/Hk_G + 1/k_L \, . \qquad (2.8)$$

b) Sparingly-Soluble Gases in Absorption Without Reaction

Gases which are sparingly-soluble in aqueous media, such as oxygen and carbon dioxide, have Henry's law coefficients of relatively large magnitude. Therefore, when k_L and k_G are of the same order of magnitude, then $Hk_G >> k_L$, and Eq. (2.8) reduces to

$$1/K_L \approx 1/k_L$$

or,

$$k_L \approx K_L \, , \qquad (2.9)$$

in which case the major resistance to interphase mass transfer lies within the liquid phase, and it is then commonly said that the liquid phase controls.

Combining Eqs. (2.5), (2.6), and (2.9) it is readily seen that for sparingly-soluble gases $C_{ki} \approx C_k^*$ and $p_{ki} \approx p_{kB}$. As there is a negligible partial pressure gradient in the gaseous phase, for all practical purposes the interfacial liquid concentration is set by the component's bulk gas-phase partial pressure. Therefore, we can write

$$R_{Vk} = K_L a(C_k^* - C_{kB}) \approx k_L a(C_k^* - C_{kB}). \qquad (2.10)$$

$K_L a$, the overall volumetric mass transfer coefficient, can be evaluated from Eq. (2.10), given values of R_{Vk}, C_k^*, and C_{kB}. Historically, most absorption results have been expressed as the product of K_L and a as the evaluation of the individual parameters requires a second type of experiment to separately evaluate the specific interfacial area a.

c) Some Theoretical Models for Mass Transfer in Gas-Liquid Dispersions

For interphase mass transfer, when the shape of the interface across which the transfer occurs can be mathematically described as a function of both spatial position and time, and in addition when the relative motion between the two phases at the interface (the so-called slip velocity) can be described by a velocity vector, then it is possible in some simple cases to achieve a solution of the general three-dimensional material balance relationship describing the transfer with respect to one of the phases, e.g., Eq. (2.84). To date no such

mathematically-precise description of the behaviour of bubble swarms in randomly-turbulent liquid flow fields, such as those which exist in stirred-tank gas absorbers, has been developed. However, many simplified, and hence approximate models of dispersed gas-liquid phase interactions have been proposed. A number of these models have been reviewed recently by Resnick and Gal-Or (22) and Schaftlein and Russell (23).

Turbulence at a gas bubble - liquid interface promotes heat and mass transfer rates, and, in addition, can result in the break-up of the bubble itself into smaller bubbles (conversely, bubble size growth due to coalescence can occur in those regions of the stirred tank wherein the scale of turbulence is less). Kolmogoroff (24) developed a theory of isotropic turbulence, in which the turbulent fluid is considered to consist of eddies in two distinct size ranges: first, large, unstable primary eddies (being of size magnitude similar to the dimensions of the main flow stream, and which dissipate their energy by viscous flow in breaking up into smaller eddies), and second, small eddies which dissipate most of the energy. The behaviour of the small eddies is considered to be statistically independent of that of the large eddies, such that small-eddy properties are determined solely by the local rate of energy dissipation per unit mass of fluid; that is, local isotropic turbulence exists. Kolmogoroff showed that the size of the small eddies is inversely proportional to the one-quarter power of the agitation power input per unit mass.

Using Kolmogoroff's expression for the small eddy size, and assuming that the Sherwood number could be correlated with the turbulence Reynolds number and the Schmidt number for the case of turbulent gas - liquid dispersions, Calderbank and Moo-Young (16) derived a semiempirical expression in which the liquid phase mass transfer coefficient, k_L, is directly proportional to the one-quarter power of the agitation power per unit volume. Their model is valid only for those dispersions having an average bubble size range for which the value of k_L is independent of the magnitude of the average bubble size.

Gal-Or and co-workers (22, 25, 26, 27) recently have proposed several models to describe the mass and/or heat transfer behaviour of bubble swarms with and without liquid-phase chemical reaction. In the first of these, Gal-Or and Resnick (25) presented a model based on gas residence time in the dispersion. They assumed a time-independent number of bubbles, each of which is surrounded by an identical spherical volume of liquid with which it is in contact for a time period equal to the overall average gas residence time, defined as the volume of the gas holdup divided by the volumetric gas input rate. The model further assumes even distribution of gas bubbles throughout the liquid phase (whereas, in practice, the distribution varies spatially) and uniform bubble diameter (whereas, in practice, there is a distribution of bubble sizes). The model relates, by a complicated expression, the total average mass transfer rate to six parameters: sparge gas volumetric flow rate, bubble mean residence time, first-order reaction velocity constant, liquid phase diffusivity, liquid volume, and the bubble radius.

However, for predictive purposes with respect to the performance of a given stirred-tank, the average bubble diameter and the mean residence time are not known a priori as functions of the agitation rate or the vessel geometry.

In the second model, Gal-Or and Hoelscher (26) considered the case of unsteady-state mass transfer from a swarm of interacting bubbles with bubble size distribution. The theoretical analysis was made by dividing the total volume into "subreactors"; eventually, the total mass transfer rate was obtained by integrating over all the "subreactors". The final result was again expressed in terms of several parameters similar to those in the preceding case, among which is the unknown (a priori) average bubble diameter.

Gal-Or, Hauck, and Hoelscher (28) developed a model for estimating $K_L a$ values for an ensemble of bubbles in terms of eight parameters of which three, namely the average bubble residence time, dispersed gas fractional holdup, and the average bubble size were considered to be the main factors affecting interactions between adjacent bubbles. An experimental test of the model failed to verify its validity in the particular absorption apparatus used as further discussed in Section II. 4(e)(ii).

2. Measurement of Oxygen Supply Rate Capability

a) Operating Methods

Various modes of operation may be used to experimentally measure the value of the overall volumetric mass transfer coefficient for oxygen, $K_{L4}a$, in a stirred-tank absorber, a generalized

representation of which is shown on Fig. (2.1). Two such modes are (i) continuous-flow stirred tank (CFST) wherein both the gas and liquid phases are fed to and removed from the absorber continuously at controlled, invariable rates, and, (ii) semi-batch stirred tank (SBST), wherein one phase-- the aqueous-- is stationary and the other-- the gaseous-- flows continuously into and out of the system. In some experimental systems, the oxygen absorption occurs in the presence of a homogeneous liquid-phase reaction which consummes oxygen, e.g., the sulphite oxidation method; in such systems, the vessel may be described as a stirred-tank reactor, and the operations denoted as CFSTR and SBSTR. The value of the overall volumetric mass transfer coefficient may be affected by the reaction, and is therefore denoted $K^r_{L4}a$.

In order to determine the numerical value of either $K_{L4}a$ or $K^r_{L4}a$, obviously a driving force for mass transfer must be inherent in the system or be induced therein. Three means of providing the necessary driving force or displacement from physical equilibrium which are distinguished by the time dependence of the behaviour of the gas and liquid phases are (i) unsteady-state or transient response method, (ii) steady-state method, and (iii) the pseudo-steady state method.

In the unsteady-state method, the mass transfer driving force is induced in the system, for example by making a step change in the inlet gas composition. One of the time-dependent phase concentration changes is then followed, the rate of approach to the new equilibrium position being dependent upon the value of the overall coefficient. This

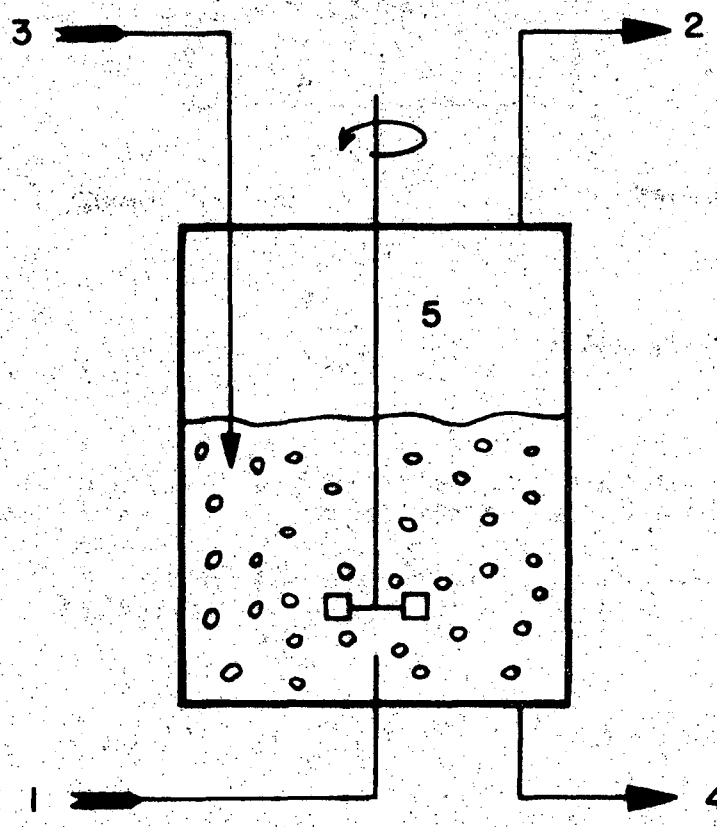

XBL 714-3230

Fig. 2.1. Stirred-Tank Gas Abosrber Schematic Flow Diagram. 1 = Inlet Gas (G_1, y_1), 2 = Outlet Gas (G_2, y_2), 3 = Liquid Feed (F_{L1}, C_{L1}), 4 = Liquid Effluent (F_{L2}, C_{L2}), 5 = Gas-Liquid Dispersion (V_L, C_B, h, y_D).

measurement method can be used in conjunction with any one of the CFST, CFSTR, or SBST operating modes. Here, during the course of measurement, neither phase is in a component concentration steady-state.

In the steady-state method, the mass transfer driving force is inherent in the system, and exists, for example, by virtue of the fact that the inlet aqueous phase oxygen concentration is less than the equilibrium concentration possible at the temperature and pressure conditions of the vessel, and the fact that the gas-liquid contact time is well below the time required to reach equilibrium. The time-independent phase concentration differences between inlet and outlet streams then give a measure of the value of the overall volumetric coefficient. This method can, by definition, be used only with the CFST or CFSTR operating modes; during the course of measurement, both phases are invarient with respect to flow rate and component concentration.

In the pseudo-steady state method, the driving force is inherent in the system due to the fact that the dissolved gaseous component enters into a liquid phase reaction which holds its bulk fluid concentration at its low or zero chemical equilibrium value. Provided that the rate of absorption with chemical reaction is pseudo-first order with respect to the dissolving gaseous component, then the time-independent gas phase concentration difference between inlet and outlet streams or in conjunction with the SBSTR mode of operation the time-dependent liquid-phase reactant concentration and its rate of change can be used to measure $K_{L4}a$. In this case, one phase--the gaseous--is in a steady-state condition, while the aqueous phase is in an unsteady-

state condition with respect to reactant concentration.

To experimentally determine the mass transfer rate capability under defined conditions of aeration and agitation, it is necessary to relate the measured values of component concentration (gas and/or liquid phases) and the system parameters (time, flow rates) to arrive at a value for the overall volumetric coefficient at the particular temperature of operation. The exact nature of the relationship depends, of course, on the mode of operation used in conjunction with a particular method of providing the necessary mass transfer driving force. For the case of mass transfer in the absence of chemical reaction, i.e., purely physical absorption, we will examine two of the possible combinations, namely: SBST/unsteady-state and CFST/steady-state systems.

b) General Material Balances

For the process of absorption of a gaseous component by a liquid the material balances for the gas and liquid phases can be written as (23)

Liquid phase: input - output + transfer from gas

- depletion due to reaction = accumulation,

$$F_1 C_{L1} - F_2 C_{L2} + K_G a P_T (y_2 - C_B \frac{H}{P_T}) V_L - \bar{R}_V V_L = \frac{dC_B}{dt} V_L, \quad (2.11)$$

where $\bar{R}_V$ = rate of chemical reaction, gmole/(unit vol.)(unit time).

Using the relationship

$$K_G a = K_L a / H , \quad (2.12)$$

Eq. (2.11) can be written, for the case of no chemical reaction, as

$$F_1 C_{L1} - F_2 C_{L2} + K_L a \frac{P_T}{H} (y_2 - C_B \frac{H}{P_T}) V_L = \frac{dC_B}{dt} V_L . \qquad (2.13)$$

In the derivation of Eq. (2.11), the assumption has been made that the dispersed gas phase is well mixed, that is, the mole fraction of oxygen in the gas phase throughout the dispersion is time dependent, but is independent of position within the dispersion volume. Hanhart et al. (29) studied the residence time distribution of an air - hydrogen gas mixture dispersed in a well-agitated aqueous phase contained in a fully-baffled vessel equipped with a single six-bladed turbine impeller. They showed that where the liquid height:vessel diameter ratio was not far from unity, in a gas absorption process where the rate of absorption of a gaseous component is proportional to its mole fraction in the gas, the correct driving force for absorption is based on the composition of the gas leaving the dispersion. Thus, we can write

$$C^* = C^*(y_2, H, P_T, t) = P_T y_2(t)/H ; \qquad (2.14)$$

that is, the interfacial concentration in the aqueous phase is in equilibrium with the partial pressure of oxygen in the outlet gas stream, and in the general case represented by Eq. (2.14) is time dependent due to the function of $y_2(t)$.

Gase phase: Input - output - transfer to liquid phase

= accumulation,

$$\frac{G_1 y_1}{V_L} - \frac{G_2 y_2}{V_L} - K_G a P_T (y_2 - C_B \frac{H}{P_T}) = \frac{d(hy_2)}{dt} \qquad (2.15)$$

$$= h \frac{dy_2}{dt} + y_2 \frac{dh}{dt} .$$

The general material balances, Eqs. (2.13) and (2.15) for the liquid and gas phases respectively are coupled, since $C^* = P_T y_2/H$ in the former depends on the value of y_2 in the latter as discussed above. The particular procedure used for solving these coupled equations depends upon the method used to experimentally determine $K_L a$, i.e., whether the mass transfer process is conducted under unsteady-state conditions or steady-state conditions.

c) Semi-batch Stirred-Tank Unsteady-State Mass Transfer

Recall that this approach to determining $K_L a$ utilizes a steady flow rate of gas sparged into a batch liquid volume. Mass transfer driving forces are induced by a step change in inlet gas composition.

In this situation, the liquid phase mass balance Eq. (2.13) simplifies to

$$K_L a \frac{P_T}{H} (y_2 - C_B \frac{H}{P_T}) = \frac{dC_B}{dt} . \qquad (2.16)$$

To achieve an analytical solution of coupled Eqs. (2.15) and (2.16) it is necessary to introduce some simplifying assumptions. First, we assume that the change in inlet gas composition in going from, say, pure nitrogen to air has no effect on the total dispersed gas holdup in the "aerated" liquid; this means that we take the gas holdup to depend solely upon the agitation and gas flow rates and to be independent of

gas phase composition over the range of composition change. This is a very close approximation under experimental conditions where initially the liquid phase is in equilibrium with pure nitrogen at a given pressure, and then it is contacted with air at the same head space pressure and inlet flow rate. The liquid and gas compositions will change toward the final vapor-liquid equilibrium state of equi-fugacity with respect to both components, nitrogen and oxygen; hence, oxygen will leave the gas bubbles, which therefore tend to diminish in volume, but nitrogen is transferred to the air bubbles, partially offsetting the volume change.

$$P_T v_b = n\bar{R}T , \tag{2.17}$$

where v_b = volume of an average gas bubble, cm^3,

n = gmole gas/bubble,

Letting N_b = average number of gas bubbles/cm^3 of gas-free liquid, then

$$h = \frac{\text{gmole total free gas}}{cm^3 \text{ gas-free liquid}} = P_T N_b v_b/\bar{R}T = P_T H'/\bar{R}T , \tag{2.18}$$

where H' = total gas holdup (cm^3)/cm^3 gas-free liquid

$= N_b v_b$.

Applying the assumption of time-invariant total dispersed gas holdup, the time derivative of Eq. (2.18) becomes

$$dh/dt = (P_T/\bar{R}T)(dH'/dt) = 0. \tag{2.19}$$

We know that at 60°F and 1.0 atmosphere (the conditions at which the gas rotometer was calibrated) the volumetric flow rate is

$$Q = 23.7(10^3)G. \tag{2.20}$$

The second simplifying approximation, which is consistent with the first and which also follows from the fact that oxygen transfer efficiencies are low (i.e., only a relatively small fraction of the contained oxygen is transferred from an air bubble during its residence time in the liquid phase) is that the total exit gas flow rate is approximately the same as the inlet gas rate:

$$G_2 \approx G_1 . \tag{2.21}$$

Combining Eqs. (2.15), (2.19), (2.20), and (2.21), the gas phase material balance becomes

$$\frac{Q_1}{(23.7)(10^3)V_L}(y_1 - y_2) - K_L a \frac{P_T}{H}(y_2 - C_B \frac{H}{P_T}) = h \frac{dy_2}{dt}. \tag{2.22}$$

An analytical solution of the coupled material balance Eqs. (2.16) and (2.22) is still not possible as the term C_B, which has an unknown (a priori) time dependency appears in both equations. To achieve an analytical solution, we introduce the third, and final, approximation, namely that the product of the dispersed gas molar holdup (h) and the time variation of the gas phase oxygen mole fraction (dy_2/dt) is negligibly small compared to the other two terms of Eq. (2.22). This criterion may be approached experimentally by using sparingly-solube

gasses such as oxygen, and high gas flow rate:liquid volume ratios. The approximate gas phase material balance equation becomes

$$\frac{Q_1}{(23.7)(10^3)V_L}(y_1 - y_2) - K_L a \frac{P_T}{H}\left(y_2 - C_B \frac{H}{P_T}\right) = 0 . \qquad (2.23)$$

i) Absorption

Equation (2.23) is solved for y_2, and this is substituted in the liquid phase balance, Eq. (2.16), giving a linear, first-order ordinary differential equation describing the time variation of C_B as a function of the system parameters $K_L a$, P_T, H, Q_1, and V_L, namely

$$\frac{dC_B}{dt} + \beta C_B = \alpha , \qquad (2.24)$$

where

$$\beta \equiv \frac{Q_1 H K_L a}{Q_1 H + 23.7(10^3)V_L P_T K_L a} , \ sec^{-1} \qquad (2.25)$$

and

$$\alpha \equiv \frac{Q_1 y_1 P_T K_L a}{Q_1 H + (23.7(10^3)V_L P_T K_L a} , \ \frac{gm\ mole\ O_2}{(cm^3)(sec)} . \qquad (2.26)$$

In a given experimental run where Q_1, P_T, V_L and $K_L a = f(Q_1, N)$ are all constant, then β and α are both constants.

Equation (2.24) is solved by multiplying both sides by an integrating factor

$$\exp \int \beta \, dt = \exp (\beta t)$$

such that the left-hand side of Eq. (2.24) becomes a complete differential, which upon integration results in

$$C_B \exp(\beta t) = \frac{\alpha}{\beta} \exp(\beta t) + A' . \qquad (2.27)$$

The integration constant is evaluated by applying the initial condition

$$t = t_0 = 0 , \quad C_B = C_{B0} .$$

The initial time $t = 0$ is not necessarily synonymous with the point in real time at which the step change in inlet gas concentration was made. At some point along the concentration vs. real time curve we set $C_B = C_{B0}$ and arbitrarily set $t = 0$ there. All other times, t_B, are then expressed relative to the arbitrary initial time and are thus not measured from the actual time of the step change.

Using the initial condition to evaluate the integration constant A' in Eq. (2.27), noting that

$$P_T y_1 / H = C_\infty ,$$

the solution of Eq. (2.27), written in terms of the original variables, becomes

$$\frac{C_\infty - C_{B0}}{C_\infty - C_B} = \exp\left[\frac{Q_1 H K_L a \, t_B}{Q_1 H + 23.7(10^3) V_L P_T K_L a}\right] . \qquad (2.28)$$

Taking the logarithm of Eq. (2.28) and collecting coefficients of $K_L a$, the solution may be expressed in a form more useful for computation purposes:

$$K_L a = \frac{\dfrac{\ln\left(\dfrac{C_\infty - C_{B0}}{C_\infty - C_B}\right)}{t_B}}{1 - (23.7)(10^3)\left[\dfrac{\ln\dfrac{C_\infty - C_{B0}}{C_\infty - C_B}}{t_B}\right]\dfrac{V_L P_T}{Q_1 H}} \quad . \qquad (2.29)$$

In using Eq. (2.29) for computation, all times are expressed relative to the real time at which $C_B = C_{B0}$ where t was arbitrarily taken to be zero. On the other hand, if the time values are measured from the moment of the step change in inlet gas composition (real time zero), then Eq. (2.29) may be generalized to

$$K_L a = \frac{\dfrac{\ln\left(\dfrac{C_\infty - C_{B1}}{C_\infty - C_{B2}}\right)}{t_{B2} - t_{B1}}}{1 - (23.7((10^3)\left[\dfrac{\ln\dfrac{C_\infty - C_{B1}}{C_\infty - C_{B2}}}{t_{B2} - t_{B1}}\right]\dfrac{V_L P_T}{Q_1 H}} \quad . \qquad (2.30)$$

Calderbank used an expression analogous to Eq. (2.24) to describe the variation of $K_L a$ in a series of gas - liquid mass transfer experiments in stirred tanks (9).

It is interesting to note in passing that many of the "standard" references and other works on aeration in fermentation processes (for example: 14, 28, 30, 31, 32) determine $K_L a$ by the "gassing-in" technique considering only the transient behaviour of the liquid phase composition, i.e., they consider only Eq. (2.16). In taking this approach, the exit gas mole fraction y_2 (and hence the interfacial liquid concentration C^*) is considered to be a constant, whereas it in fact varies

not only with time, but with the aeration-agitation parameters Q_1, V_L, and K_La. Therefore, the solution of Eq. (2.16) by itself may be considered to be only the first approximation of K_La. Although it was necessary to neglect the time variation of y_2 in deriving Eq. (2.23), the effect of the above mentioned aeration-agitation parameters is included. In this sense, Eq. (2.24) may be considered a second approximation of K_La, which is particularly better under conditions of low $Q_1:K_LaV_L$ ratios.

ii) Desorption

For the case of transient desorption or stripping of oxygen from liquid solution caused by a step-change (decrease) in inlet gas oxygen mole fraction, the liquid phase material balance is still described by Eq. (2.16), but the approximate gas phase material balance becomes

$$Q_1y_2/23.7(10^3)V_L = (K_LaP_T/H)\,[(C_BH/P_T) - y_2]\,. \qquad (2.31)$$

Equation (2.31) is written for the case where the oxygen mole fraction in the inlet stripping gas, y_1, is zero, and incroporates, as discussed before, the simplifying approximations that $G_2 \approx G_1$ and $h(dy_2/dt)$ is negligibly small. In addition, we have again applied the well-mixed gas phase assumption.

Solving Eq. (2.31) for y_2 and substituting the the result in Eq. (2.16), the differential equation describing the system is found to be

$$dC_B/dt + \beta C_B = 0\,, \qquad (2.32)$$

where β is defined by Eq. (2.25).

The boundary conditions applicable to the desorption model Eq. (2.32) are

$$t = 0, \quad C_B = C_0 ,$$

$$t = t, \quad C_B = C_B .$$

The final solution for the transient behaviour of the liquid-phase oxygen concentration for desorption by a deoxygenated gas is

$$C_B = C_0 \exp(-\beta t) , \tag{2.33}$$

where $C_0 = (P_T/H)(y_1)_{t<0}$, i.e., C_0 is the saturation concentration in equilibrium with the oxygen-containing gas initially in contact with the batch liquid before the step change to deoxygenated inlet gas was made.

As in the absorption case, the solution given by Eq. (2.33) for desorption can be solved explicitly for $K_L a$ which is incorporated in the parameter β . However, for the particular experimental methods used in this work, an explicit solution for $K_L a$ from either of Eqs. (2.24) or (2.33) is not required. The method whereby $K_L a$ was determined is discussed in Section II. 4.

d) CFST Steady-State Absorption

In this experimental situation both the liquid and gas phases flow into and out of the stirred tank absorber at invariant rates. All system parameters are time independent and in the general material balance equations all time derivatives are, therefore, identically zero.

For the liquid phase, $F_1 = F_2$ and Eq. (2.13) becomes

$$K_L a \frac{P_T}{H} \left(y_2 - C_B \frac{H}{P_T}\right) V_L = F_1 (C_B - C_{L1}) . \qquad (2.34)$$

In Eq. (2.34) we have used the well-mixed liquid assumption, $C_{L2} = C_B$, i.e., the exit liquid has the same composition as the bulk liquid in the vessel (the bulk liquid concentration is spatially invariant).

The gas phase material balance Eq. (2.15) becomes

$$\frac{Q_1}{(23.7)(10^3)V_L} (y_1 - y_2) = K_L a \frac{P_T}{H} \left(y_2 - C_B \frac{H}{P_T}\right) \qquad (2.23)$$

where the well-mixed gas phase assumption, $y_D = y_2$, and the approximation that the amount of gas absorbed is small relative to the total gas flow rate, $G_1 \approx G_2$, are incorporated. This is the same functionality as used for the gas phase representation in the unsteady-state procedure discussed previously, but in the steady-state case Eq. (2.23) is exact since dy_2/dt is identically zero here, whereas in the previous case it was not zero but only taken to be negligibly small.

As before, Eq. (2.23) is solved for y_2 which is substituted in Eq. (2.34). After some algebraic manipulation, the solution to the steady-state case becomes

$$K_L a = \frac{\bar{D}}{\left(\frac{C_\infty - C_B}{C_B - C_{L1}}\right) - \frac{23.7(10^3)V_L P_T \bar{D}}{Q_1 H}} \qquad (2.35)$$

where $\bar{D} \equiv$ dilution rate $= F_1/V_L$, and, as before $C_\infty = P_T y_1/H$.

Calderbank (9) gives an expression analogous to Eq. (2.35) for the case of a steady-state CFST absorption process.

For the special case where the inlet feed is completely deoxygenated, i.e., $C_{L1} = 0$, then the relationship between $K_L a$ and the system parameters becomes

$$K_L a = \frac{\bar{D}}{\frac{C_\infty}{C_B} - \left[1 + \frac{23.7(10^3)V_L P_T \bar{D}}{Q_1 H}\right]} . \qquad (2.36)$$

In conclusion, it has been shown how either the SBST unsteady-state procedure or the CFST steady-state procedure may be used to experimentally evaluate the overall volumetric coefficient of mass transfer, $K_L a$, for mass transfer in an agitated liquid. Over a wide range of aeration and agitation conditions either approach will give results having a sufficient degree of accuracy, and the choice of methods is merely a matter of convenience. The transient method has the virtue of relative simplicity as no liquid feed and collection systems are required, and the experimental run times are shorter as only the liquid volume in the absorption vessel need be degassed before re-use, there being no (large) volume of feed liquid. However, the use of the transient method imposes the requirements of being able to accurately detect small differences in dissolved gas concentrations at a low absolute concentration level which is changing rapidly with time. It is preferable to measure the instantaneous concentrations in situ, particularly at high $K_L a$ conditions where dC_B/dt is also large since the finite amount of time required to take a sample for external analysis becomes significant with respect to the time increment over which the dissolved gas concentration changes by a detectable amount.

Where the analytical technique cannot meet the above requirement, it becomes preferable, if not necessary, to use the CSTR steady-state method since all concentrations are time invariant and sampling time is of no significance. In any case, the steady-state method is to be preferred at those experimental conditions characterized by very high $K_L a V_L : Q_1$ ratio, as the assumptions of $G_1 \approx G_2$ and negligible dy_2/dt are then no longer "close" approximations and Eq. (2.23) becomes inadequate.

3. Some Previous Methods of Overall Volumetric Mass Transfer Coefficient Measurement

a) Mass Transfer Without Homogeneous Liquid-Phase Reaction ($K_{L4}a$)

Using an oxygen-free gas to transiently desorb dissolved oxygen from solution (the so-called gassing out technique), the rate of change of dissolved oxygen concentration can be related to the value of $K_{L4}a$, as in, for example, Eq. (2.30). Alternately, using a CFST method, the steady-state oxygen concentration achieved can be used to calculate $K_{L4}a$, for example using Eq. (2.36). Both methods, of course, depend upon the use of suitable analytical methods for determining the dissolved oxygen concentration. Traditional methods have bee been reviewed by Richards (30) and Finn (34), and will be discussed only briefly here.

i) Polarographic Method

Under the influence of an applied potential, the flow of electric current to a fresh mercury surface is dependent upon the liquid-phase oxygen concentration. To avoid polarization at the mercury surface,

the dropping mercury electrode mase be used (35). As such drops are subject to deformation in the turbulent flow field when the electrode is placed inside the stirred tank, and since the flux rate of oxygen to the drop surface is dependent upon the mass transfer coefficient in the hydrodynamic boundary layer around the falling drop, the polarographic method of measurement is not independent of the liquid-phase agitation rate.

ii) Chemical Analysis

Liquid samples can be taken from the absorption vessel and analysed for oxygen concentration by the Winkler method, as was done by Calderbank (10), in which manganous ions are oxidized, the excess manganous ion concentration being determined iodometrically. This method is subject to possible oxygen loss or gain due to the handling of the liquid sample which is not in physical equilibrium with the oxygen content of the environment external to the absorber.

iii) Biological Method

Some species of the microbial genera Pseudomonas, Aspergillus, or Penicillium produce gluconic acid from glucose via the enzymatic reaction-rate controlled metabolism of the growing cells. Tsao and Kempe (36) considered that under oxygen-limited conditions (excess glucose and other essential nutrients) the rate of production of the gluconic acid, which is excreted from the cells into the growth medium, was directly proportional to the rate of oxygen mass transfer into the liquid medium from the dispersed air bubbles, and hence proportional to $K_{L4}a$.

However, as shown by both Humphrey and Reilly (37) and Hsieh, Silver, and Mateles (38), the reaction mechanism does not involve the production of gluconic acid by the direct reaction of oxygen with glucose. Instead, glucose is first oxidized enzymatically (glucose oxidase) to an intermediate, D-glucono-δ-lactone, with concurrent reduction of flavoprotein (FAD); in turn, the $FADH_2$ reduces molecular oxygen. Depending upon the type of organism or cell-free enzyme system used, the gluconolactone intermediate is hydrolysed either non-enzymatically (37) or enzymatically (38) to the gluconic acid end-product. In Humphrey and Reilly's investigation (37), they found that the production rate of gluconic acid from P. ovalis was proportional to the rate of hydrolysis of the gluconolactone, and not to the rate of oxidation of the glucose by the glucose oxidase - FAD coupled reaction, such that the rate of oxygen uptake was not directly proportional to the rate of gluconic acid production.

It appears then that gluconic acid production rates in systems containing either viable cells or cell-free enzyme extracts can be rate-controlled by the reactive activities of two or three enzyme systems rather than being mass-transfer-rate controlled by the availability of oxygen, making this an uncertain method for the direction evaluation of $K_{L4}a$.

b) Sulphite Oxidation Method ($K^r_{L4}a$)

This method utilizes the fact that dissolved oxygen will react in the aqueous phase with sulphite ion (usually supplied by sodium sulphite) in the presence of cupric or cobaltous ion catalyst. The overall reaction may be written as

$$\frac{1}{2}O_2 + SO_3^{=} \xrightarrow{Cu^{++} \text{ or } Co^{++}} SO_4^{=} \qquad (2.37)$$

The absorption-with-reaction has generally been conducted by a semi-batch procedure (continuous air supply with batch liquid). The rate of oxidation of the sulphite ion can be followed very simply by standard iodometric titration. This simplicity of analysis has lead to this method becoming one of the, if not the one most commonly used in fermentation oxygen supply capability studies (2, 11, 13, 14, 33, 39, 40, 110) since its use in 1944 by Cooper, Fernstrom, and Miller (11).

Although this method has been used frequently, it is subject to some uncertainty as far as the reproducibility or the significance of the results are concerned. First, the exact mechanism of the sulphite ion - oxygen reaction is still not clear. Barron and O'Hern (41) found the reaction to be zero order in oxygen and three-halves order in sulphite over a sulphite concentration range of 0.04 to 0.5 molar; in addition, increasing concentrations of cupric ion at the micromolar level increased the rate of reaction, while cuprous ion decreased it. They suggested that a significant amount of cupric ion normally added to the solution is reduced to the cuprous form under the usual conditions of the absorption experiment. Srivastava, McMillan, and Harris (42) found the reaction to be first order with respect to oxygen, but zero order with respect to sulphite concentration in the range 0.08 to 0.16M. In addition, at the typical test pH range of 8 to 9, they found precipitation of the cobaltous hydroxide (cupric ion is also subject to similar precipitation at sufficiently alkaline pH).

In absorption-with-reaction studies, the overall rate of oxygen mass transfer generally has been found to be independent of the concentration of sulphite ion above a minimum value of 0.08 to 0.17M as in, for example, the works of Fuller and Crist (39) and Cooper et al. (11). The absorption-with-reaction rate in sparged, agitated vessels has been found to be directly proportional to the gas-phase oxygen partial pressure (e.g., 11, 13). However, in an unsparged, surface-aerated vessel with both liquid and gas phase stirring, Phillips and Johnson (13) reported that the absorption rate was dependent on the square of the oxygen partial pressure.

The rate of sulphite oxidation reaction is also dependent upon the solution pH (43), and is sensitive to trace contaminants, both organic (44) and inorganic (43).

The behaviour of copper as a reaction catalyst is irregular; the reaction rate may be increased (41) or decreased (41, 43) depending upon the oxidation state of the copper ions. Hence, the absorption-with-reaction may take place in several reaction regimes, ranging from the kinetic regime (wherein the effective absorption rate is unaffected by the agitation rate and the degree of bubble dispersion, being rate-limited by the kinetics) through the diffusional and fast-reaction regimes discussed later in Section II. 5(c). Fortuitously, in many investigations the rate of absorption-with-reaction has been sufficiently enhanced by the reaction kinetic rate to occur in the near-fast reaction regime, such that the measured $K_{L4}^{r}a$ has been greater than values of $K_{L4}a$ for physical absorption in non-reacting solutions of similar solute concentration (2, 11, 13, 110). However, Yoshida et al. (14) found the oxygen

absorption rate to be the same in both sodium sulphite and sulphate solutions of the same concentration, a result which is in disagreement with the theories of mass transfer with chemical reaction. In spite of the foregoing limitations, cupric ion has continued to be the usual choice of catalyst.

Westerterp et al. (12) studied the absorption-with-reaction of oxygen from air dispersed in cupric-catalysed 0.793M sodium sulphite solution at 30°C in a series of geometrically-similar tanks using turbine impellers of varying impeller to tank diameter ratios. Air was admitted through a ring-type sparger, and the gas superficial velocities were about double the maximum used in this work. They reported their results in the form of $K_{L4}^{r}a$, which was found to vary linearly with impeller rotational speed above a minimum rpm (N_0). Their results for $K_{L4}^{r}a$ were independent of superficial gas velocity whenever $N > N_0$.

The use of cobaltous ion catalyst in place of cupric ion can increase the value of the first-order reaction velocity constant by three or four orders of magnitude (12, 43), placing the absorption-with reaction process squarely in the fast-reaction regime. In this particular regime, the overall rate of absorption is independent of the liquid phase coefficient, k_{L4}, but remains dependent upon the specific interfacial area a. Cobaltous-catalysed oxygen absorption-with-reaction has been used by several investigators to measure values of a in stirred tanks (43, 45).

Although the sulphite oxidation absorption-with-reaction has been, and apparently continues to be, a popular method for characterizing the oxygen transfer capabilities of fermentation vessels, its direct applicability remains in doubt. First, the overall absorption rate in the

presence of the homogeneous liquid-phase reaction (which can affect the value of $K_{L4}a$ at the interface) is generally greater than the physical absorption rate of oxygen into a medium containing growing microbial cells. In the latter case, the oxygen is not reacted until it has diffused to an enzymatic reaction site within the cell (heterogeneous case), the rate of oxygen reaction thereby not affecting the value of $K_{L4}a$ at the gas-liquid interface which limits the cell population density. Second, sulphite oxidations are generally conducted at solution ionic strengths which can be much greater than the ionic strengths of some fermentation media. Ionic strength can greatly influence the values of $K_{L4}a$ in stirred tanks, as the results of this investigation will show.

4. Measurement of $K_{L4}a$ Using Dissolved Oxygen Probes

a) Advantages of Use

As discussed in the preceding sections, the measurement of the oxygen supply rate capability of a given system by utilizing such methods as (i) absorption accompanied by chemical reaction, (ii) polarographic measurements using bare electrodes exposed directly to the aqueous solution and its solute components, or (iii) liquid-phase sample withdrawal for external analysis is subject to inherent difficulties. In chemically-reactive systems, the interpretation of the results with respect to physical absorption is open to question, for example, unless caution is exercised to ensure that the kinetic rate constant(s) is not affected by such usually unmeasurable influences as trace contamination of the aqueous solution. In the polarographic methods which employ bare metal surfaces, difficulties in measurement

may arise from instability of the electrochemical cell current-dissolved oxygen concentration calibration curve caused by poisoning or polarization of the metal surface.

One way of retaining the use of electrode systems with their relative convenience (e.g., in situ measurement, fast response) for the measurement of dissolved oxygen concentration without encountering fouling of the electrode surface or interference with the electrochemical reaction at the electrode surface by other soluble species is to encase the electrode system in a protective coating. Such a coating should, of course, be semi-permeable, allowing the transport of oxygen from the aqueous solution to the electrode surface, but being impermeable to water and its contained non-gaseous solutes such as inorganic ions, charged macromolecules (e.g., proteins, amino acids) or neutral species (e.g., glucose). Clark et al. (46) in 1953 were the first to successfully apply this technique; they used a micro-platinum electrode covered with a polyethylene membrane to measure dissolved oxygen in blood.

b) Types of Dissolved Oxygen Probes

Since Clark et al.'s development, many different types of membrane-covered probes have been described in the literature. At present both the anode and the cathode are usually placed, together with the supporting electrolyte, inside an impermeable protective housing - for example, a hollow glass tube - one end of which is covered by the semi-permeable membrane. When the assembly is placed in a turbulent fluid containing dissolved oxygen, molecular oxygen is carried from the bulk of the fluid to the fluid-membrane interface by forced convection,

passes through the membrane by the process of molecular diffusion rate-governed by a gradient in oxygen fugacity across the membrane, and is, finally, reduced electrochemically at the membrane - internal electrolyte - cathode interface. A probe electric current is thereby generated, at a rate which is proportional to the rate of oxygen diffusion.

The types of probes fall into two general categories, polarographic or amperometric (46, 47, 48) in which an external potential of 0.6 - 0.8 volt is applied to the electrodes, both of which are generally noble metals (e.g., platinum-silver), and galvanic (49, 50) in which the cell potential is self-generated, one electrode being sufficiently electronegative to cause spontaneous reduction of molecular oxygen (e.g., lead in a silver/lead cell). In an acetate electrolyte, at the silver cathode

$$O_2 + 2H_2O + 4e^- \longrightarrow 4\,OH^- \xrightarrow{4H^+} 4H_2O\,, \qquad (2.38)$$

while at the lead anode

$$4Pb + 4Ac^- \longrightarrow 4PbAc + 4e^-\,, \qquad (2.39)$$

the overall reaction being

$$O_2 + 2H_2O + 4Ac^- + 4Pb \longrightarrow 4OH^- + 4PbAc\,. \qquad (2.40)$$

Polymeric materials, both naturally-occurring and synthetic, have been used as membrane materials, among which have been Teflon, polyethylene, polypropylene, polystyrene, silicone rubber and gum

rubber. Such materials are non-porous, but instead behave as solid solvents in which dissolved gas molecules migrate by diffusion.

c) General Principles of Probe Operation

The operating principles of membrane-covered probes have been well discussed by Mancy, Okun, and Reilly (49) and further commented on by Johnson et al. (47, 50) and Ricica (51), and will be only summarized here. The mechanism of the transport of gases through polymeric films and the effect thereon of the structural properties of the polymer have been reviewed and studied by Paul and Di Benedetto (52).

The general overall mechanism of oxygen transport across a polymeric membrane has been described consisting of three steps (52). First, "dissolution" of the gas from the bulk fluid in contact with the polymer surface, followed by molecular diffusion through the polymeric matrix, and then finally, the transfer of the gas to another fluid at the second polymer-fluid interface. The ease of "dissolution" of oxygen dissolved in a fluid (vapor or liquid) is a measure of the oxygen's fugacity; therefore, it follows that membrane-covered oxygen probes measure the fugacity ("escaping" tendency) of the oxygen in the fluid. In general, for a component k distributed throughout three phases (gas, liquid, and solid membrane), the component's fugacity is identical in each phase, so that we may write

$$f_{kG} \equiv \phi'_k y_k P_T = \gamma_k x'_k f^\circ_k = f_{kL} = (f_{kM})_i \qquad (2.41)$$

Gas Phase Liquid Phase Membrane

where ϕ'_k and γ_k are the gas-phase fugacity coefficient and the liquid-phase activity coefficient, respectively.

Equation (2.41) follows from the classical description of static equilibrium between phases, i.e., the component's fugacity is uniform throughout all phase spatial volume elements. With respect to the probe's operation, the fugacity of oxygen is not uniform across the membrane thickness as there is a fugacity gradient causing a flux of oxygen through the membrane from the external fluid side to the internal electrolyte side (see Fig. 2.2, reading fugacity for pressure). However, as is commonly done in cases of mass transfer across interfaces, we postulate that a state of dynamic equilibrium exists at each of the membrane-liquid interfaces. Considering the external membrane interface, the fugacity of oxygen in the membrane material at the interface is maintained at all times equal to the fugacity of oxygen in the external fluid phase material immediately adjacent to the interface. For a probe immersed in an aerated liquid under the conditions of bulk gas-bulk liquid equilibrium, and assuming that the liquid phase is well mixed (negligible oxygen fugacity gradient in the liquid film at the membrane interfacial region), since

$$y_k P_T = p_k$$

and

$$\bar{a}_k = \gamma_k x'_k \ ,$$

then Eq. (2.41) can be written as

$$\underset{\text{Liquid}}{\bar{a}_k f_k^\circ} = \underset{\text{Gas}}{\phi_k' p_k} = \underset{\text{Membrane}}{(f_{kM})_i} \qquad (2.42)$$

where $\bar{a}_k$ is the liquid-phase activity of the component, and $(f_{kM})_i$ is the oxygen fugacity in the membrane at the external surface.

When the probe is operative, at the cathode, which is separated from the internal membrane surface by only a thin film of electrolyte, the oxygen is instantaneously reacted; therefore, the oxygen fugacity at the inner membrane surface is negligible, and the fugacity difference across the membrane is numerically the same as $(f_{kM})_i = \phi_k' p_k$. The probe, then, responds to changes in p_k as this establishes the driving force for diffusion across the membrane; that is, the amount of gaseous component transported across the membrane is directly proportional to the "corrected" partial pressure $\phi_k' p_k$ of component k. However, for air as the gas phase at moderately low pressures (e.g., less than 10 atm), $\phi_k' = 1.0$ for oxygen, and the probe measures the partial pressure p_k of oxygen.

For a probe immersed in a liquid phase containing dissolved oxygen, the fugacity relationship at interfacial equilibrium are

$$(f_{kM})_i = f_{kL} = \bar{a}_k f_k^\circ = f_{kG}^* = \phi_k' p_k^* , \qquad (2.44)$$

where p_k^* denotes the partial paressure of component k in the (hypothetical) gas phase which would exist in equilibrium with the liquid phase were there a gas phase present. The probe responds to changes in the applicable fugacity, f_{kL}, which is rigorously identical to $\phi_k' p_k^*$ or for oxygen at near-atmospheric pressure, p_k^* since, as before, $\phi_k' = 1.0$.

p_k^* , for the case of oxygen, is synonymous with the so-called "oxygen tension," a term frequently used in the fermentation literature. Therefore, in a liquid phase containing dissolved oxygen, the probe, in effect, measures an oxygen partial pressure even though no gaseous phase is physically present and does not directly measure the concentration of oxygen dissolved in the liquid phase.

For a gaseous component, such as oxygen, which follows Henry's law,

$$f_{kL} \approx p_k = HC_k \quad , \tag{2.45}$$

where ϕ_k' is taken as ≈ 1.0.

Comparing Eqs. (2.44) and (2.45), it is seen that in liquid solution the dissolved oxygen probe measures the value of HC_k (a quantity independent of the nature of the liquid when the liquid is or has been exposed to a gas phase of fixed oxygen partial pressure) a property which is quite different from C_k (which depends strongly on the nature of the liquid at any fixed oxygen partial pressure in the gas phase). In the literature, statements such as "oxygen concentration was measured by a membrane-covered probe" are still encountered; such statements, therefore, can be misleading.

The vast majority of workers have recognized the foregoing but have generally discussed the operation of dissolved oxygen probes in terms of the "activity" of the oxygen in aqueous solution. Although activity is related to fugacity, it is a less fundamental concept, its numerical value depends upon the arbitrary definition of the standard

state, and its use is generally restricted to describing the behaviour in liquid phases. Since the oxygen probe measures oxygen fugacity, in either the gas or the liquid phase, and at liquid-gas equilibrium will give the same reading regardless of the turbulent phase in which it is placed, we prefer to describe the response of the probe in terms of solution fugacity.

As will be shown later in this section, the current generated by the probe as a result of the electrochemical reduction of molecular oxygen is directly proportional to the flux of oxygen through the membrane, which in turn is related to the partial pressure of oxygen in the bulk solution. Therefore, any circumstance which will alter the flux through the membrane while leaving the solution partial pressure unchanged will change the numerical value of the proportionality constant between the probe current and the bulk solution partial pressure. Such effects occur if the aqueous solution temperature is changed while holding the oxygen partial pressure in the gas phase constant. For example water in equilibrium with air at 1 atm pressure has the same oxygen fugacity at 20°C and 40°C; however, the current from the same probe placed alternately in the two solutions and allowed to come to thermal equilibrium will be greatly different, being higher at the higher temperature. This results from the direct proportionality between the flux of oxygen through the membrane and the molecular diffusivity of oxygen in the polymeric material, i.e., $N = -D_M (dC_M/dx)$. The diffusivity, D_M, has been found to have an Arrhenius type dependency (49, 52):

$$D_M = (D_M)_0 \exp\left(-\frac{E_D}{RT}\right), \qquad (2.46)$$

where E_D is the activation energy for diffusion. The diffusivity increases exponentially with temperature and consequently so does the flux although the partial-pressure-difference driving force remains constant. Therefore, a probe calibrated at one temperature does not give meaningful readings at a significantly different temperature; for example, Teflon membrane probes have a temperature coefficient of about 2% per degree Centigrade (50). Close temperature control of the solutions being analyzed is essential, or alternately, the probe circuitry should include a temperature compensation element (48).

d) Steady-State Characteristics of Dissolved Oxygen Probe

A schematic representation of the oxygen partial pressure profiles and the concentration profiles derived thereform for an oxygen in liquid solution is given in Fig. (2.2) for the steady-state condition, i.e., the partial pressure of dissolved oxygen (or its concentration, in a particular bulk liquid phase) is time invariant. The oxygen diffuses from the bulk liquid phase to the cathode through three distinct mass transfer zones in series, namely the external hydrodynamic boundary layer at the external liquid phase - membrane interface, the membrane itself, and the internal liquid film of probe electrolyte between the inner surface of the membrane and the cathode. The pressure profile (strictly speaking this should be the fugacity profile) is continuous, whereas the concentration profile has, of course, discontinuities at phase interfaces; the magnitude of each discontinuity is a measure of the partition or

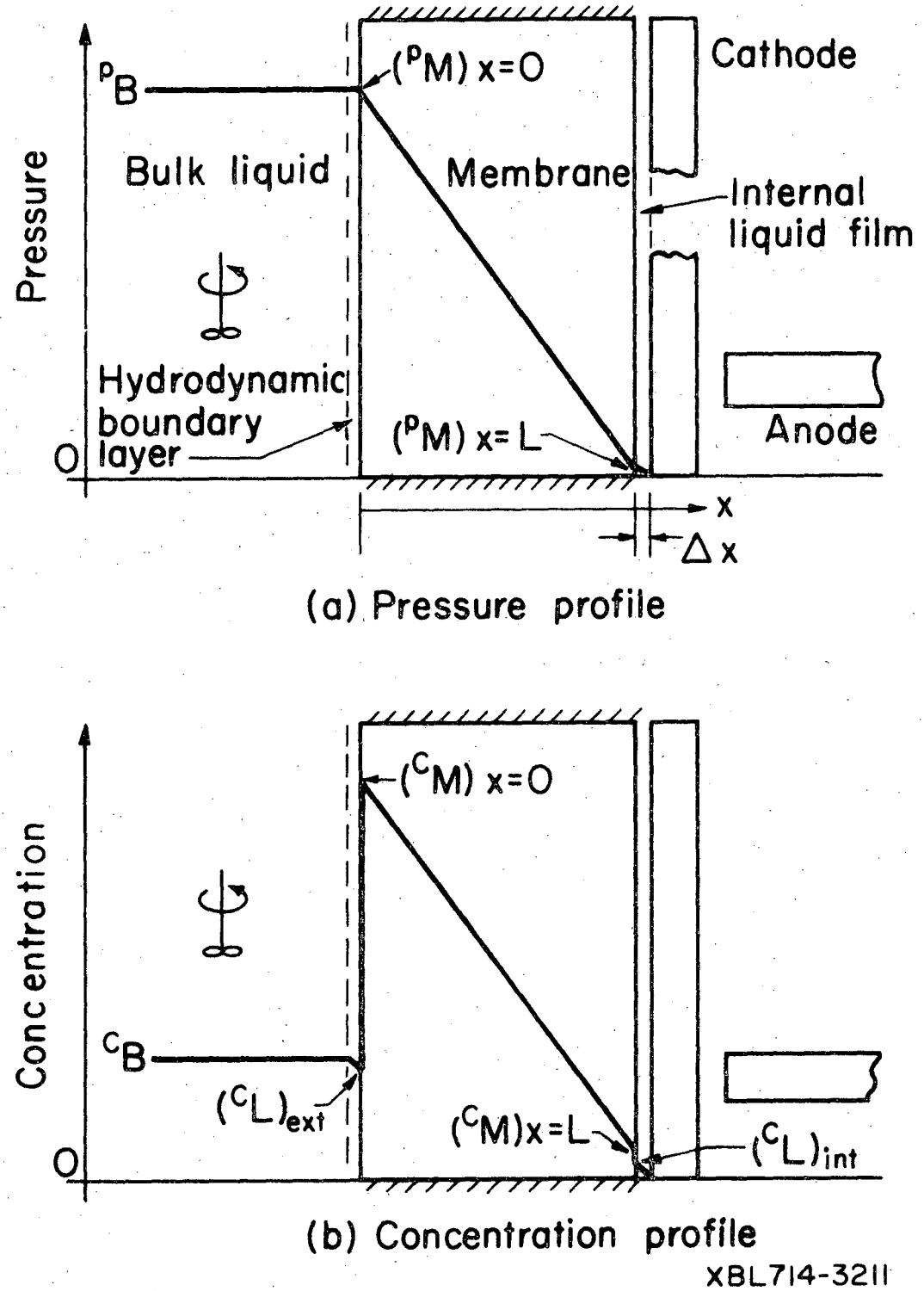

Fig. 2.2. Steady-State Oxygen Pressure and Concentration Profiles for a Membrane-Covered Oxygen Probe.

distribution coefficient of the oxygen concentration between different phases.

In any such series process, the total resistance to oxygen transport is the sum of the individual resistances of each of the transport zones. The individual resistances can be expressed as the ratio of the thickness of the region and the oxygen diffusion coefficient therein if the process is described in terms of the Whitman film theory of mass transfer (53).

$$R_{overall} = (\delta/D_L)_{\substack{hydro.\\bound.\\layer}} + (L/D_M)_{membrane} + (\delta/D_L)_{\substack{internal\\film}} . \quad (2.47)$$

Where one resistance in the series is of much greater magnitude than the sum of the others, it may be considered as the controlling resistance and for all practical purposes the rate of mass transfer can be expressed solely in terms of this resistance and the overall driving force. The representation of Fig. (2.2) is based on the following relationship:

$$(L/D_M)_{membrane} >> (\delta/D_L)_{\substack{hydro.\\bound.\\layer}} > (\delta/D_L)_{\substack{internal,\\film}} \quad (2.48)$$

which expresses the assumption that diffusion in the membrane is the rate-determining step. Equation (2.48) follows from

i) the thickness of the hydrodynamic boundary layer decreases with increasing agitation rate in the bulk solution. As the diffusivity in the aqueous is some two orders of magnitude greater than that in the

polymeric membrane, when the agitation rate exceeds some minimum or threshold value then

$$(\delta/D_L)_{\substack{\text{hydro.}\\ \text{bound.}\\ \text{layer}}} \ll (L/D_M)_{\text{membrane}}.$$

The consequence of this assumption is that the surface of the membrane exposed to the external fluid is in dynamic equilibrium with the bulk of that fluid:

$$(p_M)_{x=0} \approx p_B .$$

Unlike the case of a bare electrode exposed directly to the liquid solution, the probe current - oxygen pressure relationship becomes independent of the solution agitation rate, and does so at a relatively low level of agitation.

ii) the thickness of the internal stagnant liquid film of probe electrolyte between the membrane and the cathode is considered to be negligibly small with respect to the membrane thickness, that is we assume a "tight" fit between the membrane and the cathode such that $\Delta x \rightarrow 0$. Since it is also assumed that the oxygen reacts instantaneously at the cathode, that is, its concentration at the cathode surface is negligibly small, a second consequence is

$$(p_M)_{x=L} \approx 0 .$$

Other assumptions which are implicit in the mathematical derivations which follow are

iii) the oxygen diffusion coefficient in the membrane, D_M, is a constant independent of concentration and position, the latter implying that the polymeric material is isotropic. Polymer films in which the molecules have a preferential direction of orientation in fact are anisotropic media in which the flux of oxygen in the x-direction depends not only on the driving force gradient in the x-direction (isotropic condition) but also on the gradients in the y- and z-directions. For certain geometric conditions, Crank (54) discusses a rigorous treatment of diffusion coefficients in anisotropic materials; in this work, no correction for anisotropy is made, and the diffusion coefficient D_M is therefore an "effective" diffusivity for an overall unidirectional flux.

iv) the membrane edges are sealed and are, therefore, impermeable to oxygen diffusion. All oxygen reacted at the cathode entered the probe through the external membrane face which is parallel to the cathode surface, and the transport of oxygen is solely in the direction normal to the cathode surface.

The electric current (in amperes) produced by the probe as a consequence of the electrochemical cell reactions is directly proportional to the amount of oxygen reduced at the cathode, which in turn is directly related to the molar flux of oxygen through the membrane surface at the cathode by means of Fick's First Law of Diffusion. The relationships are

$$I = n_I \bar{F} A(\underline{N})_{x=L} = - n_I \bar{F} A D_M (dC_M/dx)_{x=L}$$

$$= E/R \, , \qquad (2.49)$$

where $\overline{F}$ = Faraday constant, 96,494 $\frac{\text{coulomb}}{\text{equiv.}}$

n_I = the number of equivalents of electricity (electrons) flowing per mole of reaction as written,

A = area of membrane normal to the direction of oxygen diffusion, cm^2.

The reaction stoichiometry at the anode depends upon the particular type of probe, i.e., upon the nature of the anode material and the supporting electrolyte. For the cathodic reaction of Eq. (2.38), $n_I = 4$.

If we assume a linear absorption isotherm for the membrane polymer, then

$$C_M = Sp , \tag{2.50}$$

where S is defined as the solubility of oxygen in the membrane, g-mole $O_2/(cm^3)(\text{atm } O_2)$.

Substituting Eq. (2.50) in Eq. (2.49), and defining the membrane permeability as

$$K_M = SD_M, \quad \frac{\text{g-mole } O_2}{(\text{cm})(\text{sec})(\text{atm } O_2)} \tag{2.51}$$

the current-flux relationship can be written as

$$I = - n_I \overline{F} A K_M (dp/dx)_{x=L} . \tag{2.52}$$

The numerical value of the membrane permeability, K_M, is ascertained by means of a steady-state current measurement. To determine the value of the effective diffusivity, D_M, the transient behavior of the current in response to a step change in solution oxygen partial pressure is studied.

i) Determination of K_M

The time invariance of oxygen pressure gives rise to a constant gradient through the membrane, and hence a constant flux of oxygen and constant resultant current. At steady state

$$p_M = p_\infty (1 - x/L) , \tag{2.53}$$

$$(dp_M/dx)_{x=L} = (dp_M/dx)_{x=0} = - p_\infty/L = - HC_\infty/L . \tag{2.54}$$

Combining Eqs. (2.52) and (2.54) ,

$$I_\infty = (n_I \bar{F} A K_M/L) (HC_\infty) \tag{2.55}$$

Rather than measuring the current flow in the external wire connecting the cathode to the anode, a precision resistor can be placed in the external circuit and the potential drop across this resistor measured. Utilizing Ohm's law, $E_\infty = I_\infty R$, Eq. (2.55) becomes

$$E_\infty = (n_I \bar{F} A R K_M/L) (HC_\infty) . \tag{2.56}$$

The value of K_M for a particular probe is obtained by applying Eq. (2.56) to measured E_∞ - known C_∞ data taken in a solution of known H.

ii) Measurement of $K_{L4}a$ in CFST Steady-State Oxygen Absorption

Equation (2.56) shows that whenever the oxygen tension in the external solution is time invariant such that a steady-state profile is obtained in the oxygen probe membrane, then at any value of the oxygen tension the corresponding probe external voltage, E, is directly proportional to the oxygen concentration, C. Hence, for measurement of $K_{L4}a$ under steady-state condtions, voltage values E_∞, E_B, and E_{L1} can be substituted directly for their corresponding concentrations C_∞, C_B, and C_{L1} in Eq. (2.35) or Eq. (2.36), from which $K_{L4}a$ may be computed directly for known values of the system parameters Q_1, H, V_L, P_T, and $\bar{D}$.

e) Unsteady-State Characteristics of Oxygen Probes

i) Oxygen Absorption

As previously shown by Eq. (2.30), $K_{L4}a$ may be obtained from a transient "gassing-in" experiment if a means of determining the time-dependent bulk solution oxygen concentration is known. Under steady-state or pseudo-steady-state conditions in the membrane, i.e., whenever there exists a linear or near-linear oxygen concentration profile across the membrane, the external probe voltage is linearly related to bulk solution oxygen concentration. A linear profile will be approximated in the membrane whenever conditions are such that the time interval over which the bulk solution oxygen concentration significantly changes value is relatively much greater than the transient response time lag in the membrane. The rate of change of the bulk solution oxygen concentration is proportional to the volumetric mass

transfer coefficient $K_{L4}a$; the time period over which the membrane transient concentration profile adjusts to an instantaneous, pseudo-steady-state value is directly related to the ratio L^2/D_M.

During a "gassing-in" experiment, the bulk solution oxygen concentration changes continuously with time from an initial value $C_{B0} = 0$ to a final value $C_B = C_\infty = p_\infty/H$. Using these conditions to solve Eq. (2.28) for $C_B(t)$ it follows that

$$C_B = C_\infty \left[1 - \exp(-\beta t)\right] , \tag{2.57}$$

where β is a function of $K_L a$ given by Eq. (2.25).

Using the Henry's law relationship, Eq. (2.45), and the membrane solubility relationship, Eq. (2.50), in conjunction with Eq. (2.57), the time variation of the oxygen concentration in the membrane material at the external solution interface is

$$(C_M)_{x=0} = SHC_\infty \left[1 - \exp(-\beta t)\right] . \tag{2.58}$$

At any given time t, the concentration in the membrane at $x = 0$ takes on an instantaneous value given by Eq. (2.58). Assuming that the probe transient concentration adjusts rapidly enough an instantaneous or pseudo steady-state membrane concentration profile is achieved, and is given by

$$(C_M)_{inst.} = SHC_\infty \left[1 - \exp(-\beta t)\right] (1 - x/L) . \tag{2.59}$$

The pseudo-steady-state condition described by Eq. (2.59) will be approached whenever

$$K_L a \approx \beta \ll 6D_M/L^2 . \qquad (2.60)$$

The right-hand term in Eq. (2.60) is the diffusional time lag in the membrane as defined by Daynes (55) and Barrer (56).

Whenever the criterion of Eq. (2.60) is satisfied, the instantaneous probe voltage, E_t, by analogy with Eq. (2.56), can be written

$$(E_t)_{inst.} = (n_I \bar{F} A H R K_M/L) (C_{Bt})_{inst.} . \qquad (2.70)$$

Therefore, at sufficiently low values of $K_{L4}a$, we anticipate that the substitution of the probe external voltage values for the corresponding concentrations in Eq. (2.30) would lead to calculation of $K_{L4}a$ with reasonable accuracy.

However, at high values of $K_{L4}a$ such that the condition of Eq. (2.60) does not hold, the rate of approach of the transient concentration profile in the membrane to its instantaneous steady-state form lags well behind the rate of change of the solution oxygen concentration (membrane interface concentration at $x = 0$). Under these conditions, the instantaneous concentration profile in the membrane never becomes linear, or even approximately linear, and therefore the probe voltage, E_t, is no longer proportional to the bulk solution concentration, $C_B(t)$, by a simple, linear relationship such as Eq. (2.70). As shown in Fig. (2.3), E_T is directly related only to an apparent bulk solution oxygen concentration, defined as that concentration which would give the same value of E_t determined under steady state conditions, i.e.,

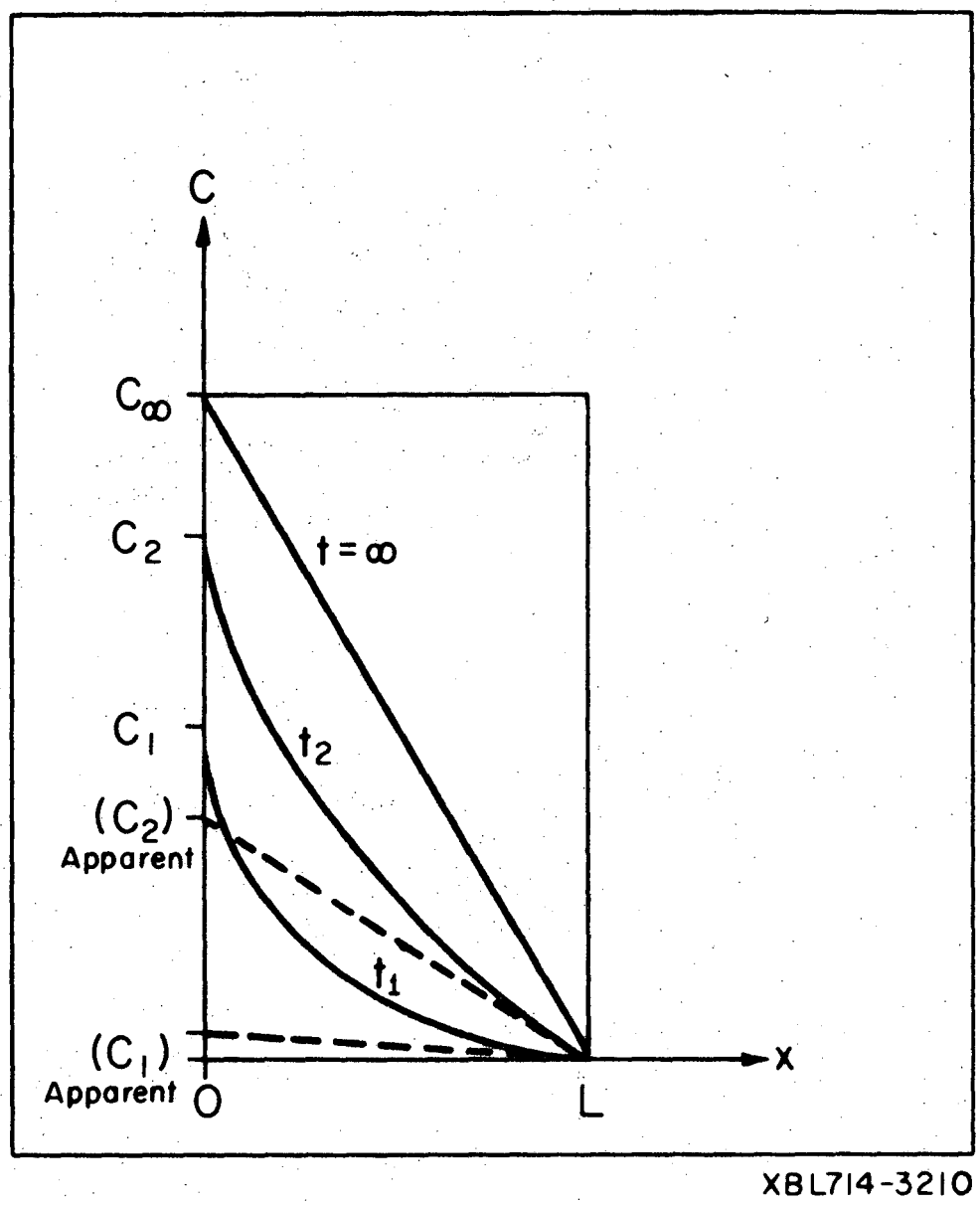

Fig. 2.3. Generalized Transient Oxygen Concentration Profiles in Probe Membrane for Continuous Change in Oxygen Centration in External Liquid; Boundary Conditions Eq. (2.72), (2.73), and (2.74).

if the gradient throughout the membrane were constant and were equal to its instantaneous value at $x = L$. The apparent concentration given by the probe lags behind the true bulk solution concentration; the magnitude of the lag is a variable, depending not only upon the value of $K_{L4}a$, but also upon the elapsed time from the start of the "gassing-in" experiment.

The need to correct for the membrane diffusional lag is illustrated quantitatively on Fig. (2.4) for the case of transient desorption. The hypothetical no-lag probe response [instantaneous establishment of the steady-state gradient in the membrane with the corresponding $C_B(t)$ in the aqueous] is compared to the theoretical real response with diffusional lag in the membrane calculated from Eq. (2.83). It is clear that the evaluation of β from the slope of the real response curve's near-linear section would result in an appreciable error, particularly at high values of β.

In an unsteady-state absorption of oxygen utilizing an oxygen probe to follow the transient composition change, in order to relate E_t to the actual $C_B(t)$ and to relate their rates of change to $K_{L4}a$ it is necessary to characterize the transient behavior of the concentration of oxygen in the membrane under the condition that the concentration in the membrane at $x = 0$ is continuously changing according to Eq. (2.57).

We wish to solve the diffusion relationship commonly known as Fick's Second Law for unsteady-state diffusion in the probe membrane, namely

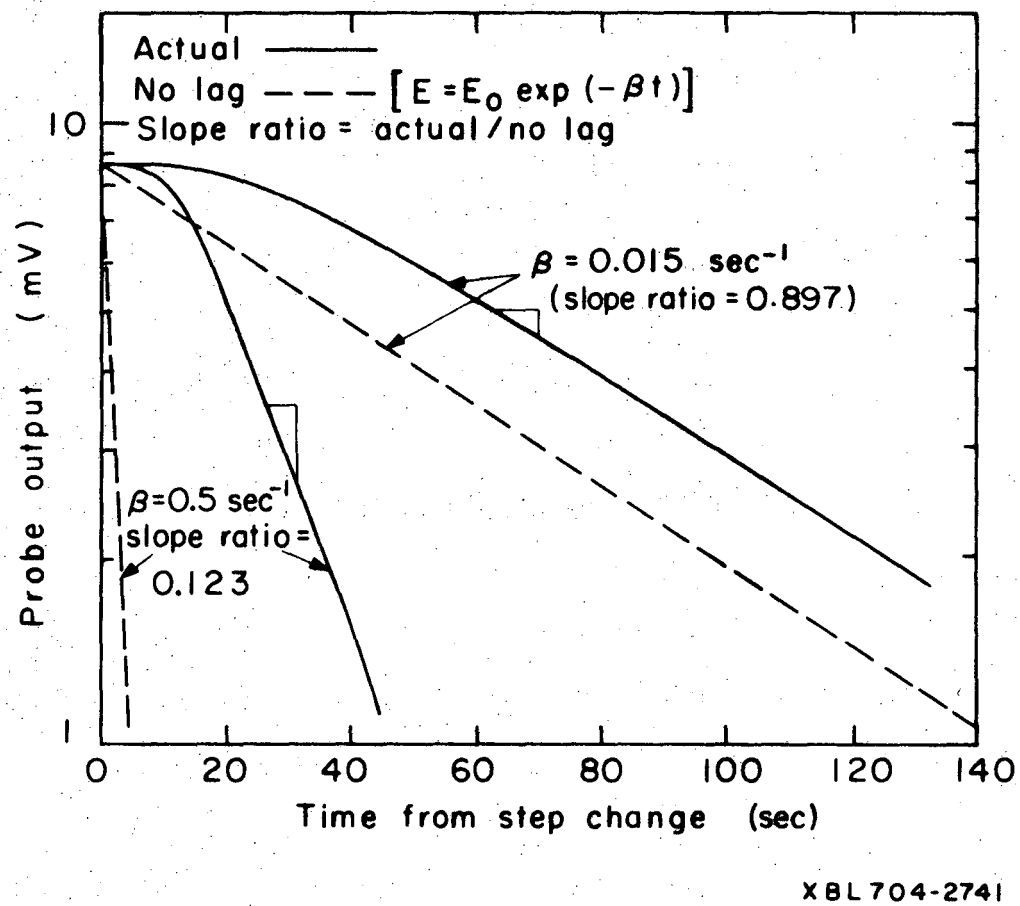

Fig. 2.4. Comparison of Actual and Theoretical No-Lag Responses of Oxygen Probe for Desorption in Unsteady-State.

$$\partial C_M/\partial t = D_M(\partial^2 C_M/\partial x^2) , \tag{2.71}$$

subject to the following conditions:

$$\text{I.C.} \qquad t = 0, \quad C_M = 0, \quad \text{all } x , \tag{2.72}$$

$$\text{B.C.} \qquad x = 0, \quad C_M = SHC_\infty[1 - \exp(-\beta t)] , \tag{2.73}$$

$$\text{B.C.} \qquad x = L, \quad C_M = 0, \quad \text{all } t . \tag{2.74}$$

The solution may be found by the method of Laplace transformation (108), inverting the transform by contour integration (58, 108). The solution is

$$E_t = E_\infty\left[1 + 2\sum_{n=0}^{\infty} \frac{(-1)^n}{1 - \frac{n^2\pi^2}{\tau}} \exp\left(-\frac{n^2\pi^2 D_M t}{L^2}\right) - \frac{\tau^{0.5}}{\sin \tau^{0.5}} \exp(-\beta t)\right] , \tag{2.75}$$

where $\tau = \beta L^2/D_M$, dimensionless (2.76)

τ may be considered as the ratio of the rate at which the bulk solution (membrane interface at $x = 0$), concentration is changing, i.e., the rate of propagation of the instantaneous steady-states ($\beta \approx K_L a$) to the rate at which the transient concentration profile in the membrane can adjust itself from one instantaneous steady state condition to the next (D_M/L^2).

The derivation of Eq. (2.75) is outlined in Appendix II.1. The final form of the solution has been derived independently by Heineken (39).

To use Eq. (2.75) to compute $K_{L4}a$ from transient response data, it is necessary to calculate the best value of β which fits several pairs of data points (E_t, t) to the experimentally-obtained E_t vs. t curve. $K_{L4}a$ is obtained from the best-fit value of β by means of Eq. (2.25) which can be rearranged to give

$$K_{L4}a = Q_1 H\beta/[Q_1 H - 23.7(10^3)V_L P_T \beta] . \qquad (2.77)$$

Gal-Or, Hauck, and Hoelscher (28) made an experimental test of the mass transfer model of Gal-Or and Resnick (25) discussed in Section II. 1(b). They transiently absorbed oxygen by using an oxygen probe of the polarographic type (46) to follow the rate of change of oxygen concentration (sic). Although their probe had a faster response time (90 percent response to step change in about 10 to 20 seconds) than the galvanic-type ones used in this study (90 percent response in about 40 seconds), its rate of response was not independent of the external solution agitation rate, suggesting that oxygen diffusion through the membrane was not the sole rate-controlling resistance. They did not correct for any diffusional response lag in the membrane. Also, their model for the transient concentration behaviour of the liquid phase incorporated only the liquid-phase material balance, Eq. (2.16), neglecting the gas-phase material balance, Eq. (2.22). In effect they assumed that the interfacial concentration over the entire transient absorption time span is the same as the final saturation concentration after infinite time.

Values of $K_{L4}a$ determined experimentally were compared to the predictions of the theoretical model. The experimental $K_{L4}a$'s were found to be three to four times greater than the predicted values.

ii) Oxygen Desorption

During a desorption or "gassing-out" experiment, the oxygen concentration in the aqueous phase varies continuously with time at a rate proportional to $K_{L4}a$ from an initial value of $C_B = C_0 = (P_T/H)(y_1)_{t<0}$ to a final value of $C_B = (P_T/H)(y_1)_{t>0} = 0$ for the case of a step change in inlet gas composition from oxygen-containing gas (e.g., air) to de-oxygenated gas (e.g., nitrogen). Previously, it was shown that the liquid phase behaviour in this case could be approximated by Eq. (2.33).

As in the case of oxygen absorption, the transient behaviour of the oxygen tension in the aqueous phase may be detected by the use of an oxygen probe, but when the oxygen tension is changing rapidly with time, the diffusional lag in the probe membrane results in appreciable deviation from the steady-state linear relationship between oxygen tension and oxygen probe reading. Direct determination of the true bulk aqueous solution oxygen tension and its rate of variation with time is not then possible, and recourse must be made to indirect evaluation of $K_{L4}a$ through a model of the transient behaviour of the probe.

The general membrane diffusional relationships Eq. (2.71) is to be solved subject to the following boundary conditions:

$$\text{I.C.} \qquad t = 0, \quad C_M = SHC_o\,(1 - x/L), \text{ all } x, \tag{2.78}$$

$$\text{B.C.} \qquad x = 0, \quad C_M = SHC_o \exp(-\beta t) \tag{2.79}$$

$$\text{B.C.} \qquad x = L, \quad C_M = 0, \text{ all } t. \tag{2.74}$$

Following the same mathematical procedures used to solve the case of oxygen absorption, that is, solving Eq. (2.71) with its associated initial and boundary conditions by Laplace transformation, and inverting the transform by contour integration, the transient concentration in the probe membrane is described by

$$C_M = SHC_0 \Bigg\{ (2/\pi) \sum_{n=1}^{\infty} (1/n) \sin(n\pi x/L) \times \exp(-n^2\pi^2 D_M t/L^2)/(1 - n^2\pi^2/\tau) + \sin[(\beta/D_M)^{\frac{1}{2}}(L-x)]\exp(-\beta t)/\sin\tau^{\frac{1}{2}} \Bigg\}, \tag{2.80}$$

where, as before, $\tau \equiv \beta L^2/D_M$.

Using the probe external voltage - membrane oxygen flux relationships

$$E_t = -n_I \bar{F} A R D_M (\partial C_M/\partial x)_{x=L} \tag{2.81}$$

and

$$E_0 = n_I \bar{F} A R H S D_M C_0/L \tag{2.82}$$

in conjunction with Eq. (2.80), the probe voltage transient response is given by

$$E_t = E_0\left[\tau^{\frac{1}{2}}\exp(-\beta t)/\sin\tau^{\frac{1}{2}} - 2\sum_{n=1}^{\infty}(-1)^n\exp(-n^2\pi^2 D_M t/L^2)/(1-n^2\pi^2/\tau)\right] \quad (2.83)$$

The theoretical transient response of a probe having a membrane thickness of 0.00509 cm and an effective diffusivity for oxygen of $1.68(10^{-7})$ cm^2/sec is shown for various values of β on Fig. (2.5).

In application of the theory to experimental data, a nonlinear least-squares fitting computer programme was used to determine the best value of β for each run from the experimental (E_t, t) data. $K_{L4}a$ was then computed from the best-fit value of β by using Eq. (2.77).

iii) Computer Evaluation of β

β was evaluated for each experimental run by the nonlinear least-squares procedure of Beals (59) designated LSQVMT. The chi-squared function

$$\text{CHISQ(X)} = \sum_{i=1}^{n}\left[\text{YDATA(i)} - F(\beta, D_M/L^2, t)\right]^2\left[\text{WEIGHT(i)}\right]$$

is minimized with respect to one or both of the parameters β and D_M/L^2 by programme VARMIT (60). VARMIT is an iterative gradient method which uses a variable metric and is a modified version of the method of Davidson (61); VARMIT computes local minima of differentiable functions containing up to 40 variable parameters. In this work all data were given equal weight; WEIGHT(i) = 1 throughout.

Although we had originally assumed D_M to be a constant, in polymeric materials its value in fact depends upon the concentration

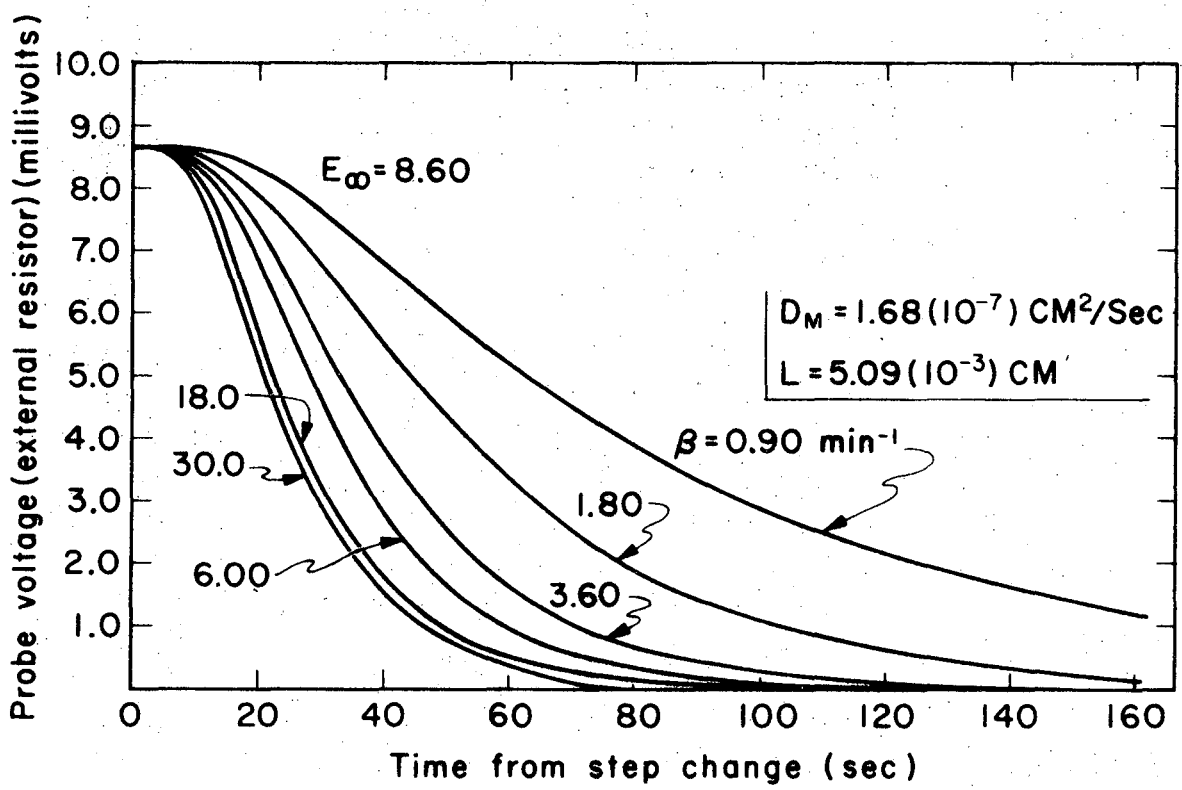

XBL6912-6367

Fig. 2.5. Oxygen Probe Theoretical Transient Response to Step Change in Inlet Gas Composition: Desorption in Stirred Tank.

gradients in all three coordinate directions; in transient response runs, the instantaneous values of the concentration gradients depend upon the value of β. Therefore, one expects the effective value of D_M to vary somewhat from run to run, and as the E_t versus t response is somewhat sensitive to the value of D_M/L^2 chosen, a better value of β [smaller CHISQ(X) value] was obtained by allowing the fitting programme to vary both parameters. The data of a given run were discarded if the computed D_M differed from the experimentally-determined D_M by more than 20 percent. The experimentally-determined value of D_M was $1.68(10^{-7})$ cm^2/sec as obtained from the step change in oxygen tension procedure discussed in Section III. 4(a)(ii).

LSQVMT is a library programme at the Lawrence Radiation Laboratory computer centre. The programme user is, in addition to the data being fitted and initial-guess values for the fitted parameters, merely required to supply a subroutine denoted TABLE. TABLE defines the number of independent variables (t); the number of parameters to be fitted (β, D_M/L^2); the form of the fitting function, e.g., Eq. (2.75) or Eq. (2.83); and the gradient of the fitting function with respect to each of the parameters being fitted. The subroutines for transient oxygen absorption and desorption are given in Appendices II. 2 and II. 3, respectively.

As discussed in Section III, the probe transient voltage was recorded on a high-speed chart. As the recorder was located some distance from the gas-inlet manifold at which the step change in gas composition was made manually, it was not possible to mark accurately

the time axis of the moving chart at the exact instant that the step change was made. From the calculated probe response as shown on Fig. (2.5), there was a theoretical response lag in the membrane of from 5 to 6 seconds from the time the liquid-phase oxygen tension first began to change. There was a further lag of about 5 seconds before the new inlet gas would first come in contact with the stirred liquid phase due to the residence time in the inlet gas piping manifold. Therefore, for computer computation purposes, the time data input was measured relative to zero time being taken as the point of the first deflection of the recorder pen from its pre-step change position; hence, the time parameter t in Eqs. (2.75) and (2.83) was changed to theta, such that in the subroutines TABLE

$$THETA(1) = T(1) + 10. ,$$

the overall time lag of 10 seconds being the value applicable at an inlet gas flow rate corresponding to a superficial gas velocity of 0.01125 ft/sec, the third highest of the four gas sparging rates used in this study. Although the overall time lag depends upon the gas flow rate, this single value was used in the computations of all the four sparging rates; the results from using this one representative value of the time lag did not vary appreciably from those obtained by using the actual time lags which differed by one to three seconds at the other three aeration rates.

5. Measurement of Specific Interfacial Area (a) and Liquid-Phase Mass Transfer Coefficient (k_L)

a) Models of Interphase Mass Transfer

The value of the liquid-phase transfer coefficient, k_L, in a given system is dependent upon the hydrodynamic conditions at the gas - liquid interface. Several different models of interfacial mass transfer are to be found in the literature. We shall consider only two such models, namely the penetration and the random surface renewal theories, both of which are in agreement with the experimentally-observed dependency of the mass transfer rate upon the component's liquid-phase molecular diffusivity over a wide range of dispersed bubble size.

For a component k undergoing simultaneous molecular diffusion and homogeneous reaction in a liquid phase interfacial surface element, a material balance for an incompressible fluid and constant diffusivity leads to (109)

$$\partial C_k/\partial t + \underline{u} \cdot \nabla C_k = D_{Lk} \nabla^2 C_k - \bar{R}_{Vk} . \qquad (2.84)$$

In both aforementioned models, it is assumed that the velocity gradient in the liquid adjacent to the interface is zero ($\underline{u} = 0$). This is a satisfactory assumption for dilute concentrations of the diffusing species. During its lifetime, the surface element behaves as a rigid body even though its spatial position changes. When there is no chemical reaction, $\bar{R}_{VK} = 0$ in both models. Therefore, for both the penetration and the random surface renewal models, Eq. (2.84) simplifies to

$$\partial C_k/\partial t = D_{Lk} (\partial^2 C_k/\partial x^2) - \bar{R}_{Vk} \qquad (2.85)$$

for the case of unidirectional mass transfer.

b) Mass Transfer Without Chemical Reaction

We shall first consider the case of purely physical absorption, $\bar{R}_{Vk} = 0$, and the physical significance given to k_L in each of the models.

i) Penetration Theory

In 1935, Higbie (17) proposed an interfacial hydrodynamic model in which the gas - liquid interface is postulated to consist of numerous small liquid elements which are continuously brought to the interfacial surface from the bulk of the liquid, remain at the interface for a finite average time, and then are subsequently returned to the bulk liquid region by the motion of the liquid phase. During the time each element is at the surface, it absorbs the gaseous component at a transient rate by the process of unsteady-state molecular diffusion into a layer of infinite depth (physically interpreted to mean that the depth of penetration of the gaseous solute is very much less than the depth of the absorbing surface element itself).

Equation (2.85) was solved using appropriate boundary conditions (17), the result being

$$R_{Vk}/a = 2(D_{Lk}/\pi\theta^*)^{1/2} (C_{ki} - C_{kB}) , \qquad (2.86)$$

where θ^* is the average lifetime of the surface elements, that is, the average length of time spent at the interface. For cylindrical gas

bubbles rising through a stagnant liquid, Higbie characterizied θ^* as the bubble length divided by its constant velocity of rise.

Comparing Eqs. (2.4) and (2.86), it is seen that

$$k_L = 2(D_{Lk}/\pi\theta^*)^{1/2} . \qquad (2.87)$$

Equation (2.87) is in agreement with much experimental single-bubble or bubble-swarm evidence that k_L is proportional to $(D_{Lk})^{1/2}$ for relatively large, deformable bubbles (9, 62). On the other hand, small bubbles (less than 0.1 cm diameter) behave as rigid spheres and thus appear to follow Frössling's equation for mass transfer from solid spheres (19) in that small-bubble k_L is proportional to $(D_{Lk})^{2/3}$ (9, 62).

ii) Random Surface Renewal Model

In 1951, Danckwerts (18) extended the conceptual usefulness of the penetration theory by removing the restriction of equal lifetime for all liquid surface elements. He showed that the average absorption rate per unit surface area could be described by

$$R_{Vk}/a = D_{Lk}^{1/2}(C_{ki} - C_{kB}) \int_0^\infty (1/\pi\theta)^{1/2} \psi(\theta) d\theta , \qquad (2.88)$$

where $\psi(\theta)$ is defined as the age distribution function.

Danckwerts postulated that the mean rate of production of fresh interfacial surface was a constant, which he denoted as $\bar{s}$, and, further, that the chance of a surface element being replaced within a given time is independent of the age of the element (e.g., random surface renewal by turbulent eddies). Consequently, he showed that (18)

$$\psi(\theta) = \bar{s} \exp(-\bar{s}\theta) , \qquad (2.89)$$

where $\bar{s}$ is the fractional rate of renewal of surface liquid elements.

Substituting Eq. (2.89) in Eq. (2.88) and performing the integration, the mean rate of absorption-without-reaction per unit area of turbulent surface is given by (18)

$$R_{Vk}/a = (D_{Lk} \bar{s})^{1/2} (C_{ki} - C_{kB}) . \qquad (2.90)$$

Comparing Eq. (2.90) with Eq. (2.4), we see that

$$k_L = (D_{Lk} \bar{s})^{1/2} , \qquad (2.91)$$

in agreement with experimental results for large bubbles (greater than 0.25 cm diameter).

Equations (2.87) and (2.91) cannot be used directly to evaluate k_L from experimentally-determined absorption rates as the parameters θ^* and $\bar{s}$ are usually not independently known.

The basic relationship of the penetration or random surface renewal theories, namely that

$$k_L \propto (D_{Lk})^{1/2}$$

will be used later in the development of a new technique for separately evaluating k_L and a under consistent hydrodynamic conditions [Section II. 5(e)].

c) Reaction Regimes for Mass Transfer with Chemical Reaction

Whenever the absorbing gaseous component k undergoes a homogeneous reaction with a non-volatile component of concentration

B in the liquid phase, the solution of the absorption models requires the inclusion of a separate material balance differential equation for the non-volatile component of the same form as Eq. (2.85). Further boundary conditions are then necessary (18) and the reaction rate relationship $\bar{R}_{Vk} = \bar{R}_{Vk}(C_k, B)$ must also be known. Here, we shall specifically consider only those reactions which exhibit pseudo-first order characteristics.

Depending upon the relative magnitudes of the reaction rate capability and the physical mass transfer rate capability of a given system wherein the absorption is accompanied by chemical reaction, the presence of the chemical reaction may affect the overall absorption rate capability of the system in several ways. Such systems may be classified according to a scheme of more-or-less distinct reaction regimes, as has been done, for example, by Astarita (63) and Danckwerts and Sharma (64). Astarita describes four such regimes which, in order of increasing liquid-phase reaction rate, are the knetic, diffusional, fast-reaction, and instantaneous-reaction regimes. Absorptions with reaction in the diffusional and fast-reaction regimes have particular utility for the experimental evaluation of $K_L a$ and a.

i) Diffusional Regime

In this case, the reaction rate is relatively slow but is still sufficiently fast to keep the dissolved gas concentration in the bulk liquid at or near its chemical equilibrium value, C_{kE}. Reaction occurs only in the bulk of the liquid, and does not directly affect the concentration gradients in the interfacial surface elements. The criterion to be met is (63, 64)

$$(H_L/a)\bar{R}_{Vk} >> k_L(C_{ki} - C_{kE}) \approx K_L(C_k^* - C_{kE}) , \qquad (2.92)$$

which implies that the rate-controlling step is the diffusion of the absorbing species into the liquid surface elements, and is written for the case of a sparingly-soluble gas.

The volumetric absorption rate can then be described by

$$R_{Vk}^r = k_L a(C_{ki} - C_{kE}) \sim K_L a(C_k^* - C_{kE}) . \qquad (2.93)$$

In the diffusional regime, the absorption rate is directly affected by the hydrodynamics as characterized by $k_L a$ (or $K_L a$). The reaction does not influence the value of k_L (or K_L), but merely serves to increase the overall rate of mass transfer by increasing the liquid-phase concentration-difference driving force since

$$\underset{\text{Slow Reaction}}{C_k^* - C_{kE}} > \underset{\text{Physical Absorption}}{C_k^* - C_{kB}} .$$

The true overall volumetric mass transfer coefficient for physical absorption without reaction can be obtained directly from Eq. (2.93), given experimental R_{Vk} data and having knowledge of C_k^* and C_{kE}. However, the separate behaviour of K_L and a cannot be determined in this regime.

ii) Fast-Reaction Regime with Pseudo-first Order Reaction

In the fast-reaction regime, the reaction rate is sufficiently fast such that an appreciable amount of the absorbing gas component is reacted during the lifetime of the liquid surface elements. The

reaction, therefore, has a considerable, direct effect on the absorbing component's concentration profile within the surface elements, thereby altering the apparent mass transfer coefficient which is related to the concentration gradient according to

$$\underline{N}_k^r = - D_{Lk} (\partial C_k / \partial x)_{x=0} \equiv k_L^r \Delta C_k \, . \qquad (2.94)$$

The criterion to be met for the absorption-reaction process to occur in the fast-reaction regime is (64)

$$(D_{Lk} k_2 B_B)^{1/2} \geq 5 k_L \, . \qquad (2.95)$$

For the case of a sparingly-soluble gas, k, reacting in the liquid phase with a large excess of non-volatile reactant, B, the concentration of B at the interfacial surface is nearly identical to its concentration in the bulk liquid, which, in turn, can be nearly constant over the gas-liquid contact time period. In these circumstances, the generalized bimolecular reaction

$$k + ZB \longrightarrow \text{product(s)} \qquad (2.96)$$

becomes, in effect, a pseudo-first order reaction. The criterion for such pseudo-first order behaviour is (64)

$$(D_{Lk} k_2 B_B)^{1/2} \leq \tfrac{1}{2} k_L (1 + B_B / Z C_k^*) \, , \qquad (2.97)$$

where k_2 is the second-order reaction velocity constant for the reaction of Eq. (2.96).

Danckwerts solved the transient diffusion equation with boundary conditions applicable to the random surface renewal model, and for the

case of a first-order, irreversible reaction in the liquid phase obtained (18)

$$R^{r}_{Vk}/a = \left\{C^{*}_{k} - B_{B}\left[\bar{s}/(k_1 + \bar{s})\right]\right\}\left[D_{Lk}(k_1 + \bar{s})\right]^{1/2} \qquad (2.98)$$

where k_1 is the first-order reaction velocity constant. For the case of the pseudo-first order reaction between the absorbing gas and the excess liquid-phase reactant

$$k_1 = k_2 B_B \, . \qquad (2.99)$$

Combining Eqs. (2.91), (2.98), and (2.99), the absorption rate in the presence of a pseudo-first order reaction becomes (64)

$$R^{r}_{Vk} = a\, C^{*}_{k}\,(k^{2}_{L} + D_{Lk} k_2 B_B)^{1/2} \, . \qquad (2.100)$$

Eq. (2.100) forms the basis for the new technique for the simultaneous evaluation of k_{L4} and a, which is discussed in Section II. 5(e).

If the pseudo-first order reaction velocity constant $k_2 B_B$ in Eq. (2.100) is large enough such that the fast-reaction criterion of Eq. (2.95) is concurrently met, then the absorption proceeds in the fast-reaction regime according to

$$R^{r}_{Vk} = a\, C^{*}_{k}\,(D_{Lk} k_2 B_B)^{1/2} \, . \qquad (2.101)$$

The important consequence of Eq. (2.101) is that, by selecting the appropriate experimental conditions (e.g., fast, pseudo-first order reaction) the volumetric absorption rate is independent of the

liquid-phase coefficient, k_L, and hydrodynamically depends solely upon the specific interfacial area. This provides a useful tool for separately evaluating the interfacial area for mass transfer, but gives no information about k_L under the same hydrodynmaic condition and absorbing solution physicochemical properties.

Comparing Eqs. (2.6) and (2.101), we can define an effective overall coefficient of mass transfer in the presence of a homogeneous, liquid-phase reaction, K_L^r, when C_{kB} is zero as

$$K_L^r \approx k_L^r \equiv (D_{Lk} k_2 B_B)^{1/2} \tag{2.102}$$

Combining Eqs. (2.101) and (2.102),

$$R_{Vk}^r = (K_L^r a)\, C_k^* . \tag{2.103}$$

An absorption-with-reaction coefficient, ϕ, can be defined as the ratio of the absorption rate in the presence of chemical reaction to that which would occur by physical absorption only under the same driving force. That is,

$$\phi_{fast} \equiv R_{Vk}^r / R_{Vk} = K_L^r / k_L = (D_{Lk} k_2 B_B)^{1/2} / k_L \tag{2.104}$$

for the case of pseudo-first order reaction in the fast-reaction regime.

d) Previous Methods of Measuring the Specific Interfacial Area (a)

i) Optical Light Scattering

When gas bubbles are dispersed in a transparent liquid, and a parallel beam of light is shone through the dispersion, the light is scattered by the bubbles. The amount of light scattering, as charac-

terized by the ratio of the incident light intensity to the time-averaged transmitted light intensity, varies exponentially with the specific interfacial area, a (10, 65).

However, when a beam of light is passed through a portion of the gas - liquid dispersion onto a receiving photocell, the specific area so determined is a "point" area, that is, it represents the value of a in only that one relatively small section of the total dispersion volume. Since, in general, the value of a varies spatially throughout the agitated tank owing to the variation of turbulent shear forces (being greatest at the impeller zone and least at the baffled walls), the overall average area must be obtained by traversing the tank axially and radially with the light beam-detector apparatus. Space limitations in small tanks generally preclude conducting such a traverse.

ii) Absorption with Chemical Reaction: General Considerations

When the process of gas absorption is accompanied by a fast, pseudo-first order homogeneous reaction with a non-volatile component of the liquid phase, a may be determined directly from Eq. (2.101) in its rearranged form. Further, if the dispersed gas phase is well mixed, and if the absorbing component follows Henry's law, then Eq. (2.101) can be written in the form

$$a = R^{r}_{Vk} / (P_T y_2 / H)(D_{Lk} k_2 B_B)^{1/2} \quad . \qquad (2.105)$$

Equation (2.105) is rigorously valid only for those systems in which reaction occurs in the fast regime, as defined by the criterion of Eq. (2.95), and also in which the pseudo-first order kinetics criterion

of Eq. (2.97) is met. Since both D_{Lk} and B_B usually have limited ranges of values, the major parameter affecting both the foregoing criteria is the second-order reaction velocity constant, k_2, which at the temperature of interest must be of sufficient magnitude to satisfy the fast-reaction criterion without at the same time being too large and thereby invalidating the pseudo-first order reaction criterion.

Two absorption-with-reaction systems which have suitable values of k_2 in the temperature range of 15 to 40°C encountered in most microbiological processes are: for oxygen transfer studies, the cobalt-catalysed oxidation of sodium sulphite under slightly alkaline pH conditions, and for carbon dioxide absorption, the reaction between dissolved carbon dioxide and hydroxyl ion in solutions of strong alkalies. It is possible for both of these reaction systems to proceed in the transitional region between the fast and the instantaneous reaction regimes; experimental conditions must be carefully selected in order to avoid this occurrence.

iii) Carbon Dioxide Absorption with Reaction in Hydroxide Solutions

The kinetics of the reaction of carbon dioxide in aqueous alkaline solutions has been studied by a number of workers (66, 67, 68, 69, 70, 71, 111). The temperature dependency (activation energy) of the reaction velocity constant for the reaction between dissolved carbon dioxide and hydroxyl ion has been well established (111), but its dependency upon the total ionic strength of the aqueous phase and upon the nature of any non-reacting ionic species present has been studied in only a limited number of systems (69, 70, 111).

In carbonate-bicarbonate buffer, the reaction occurs in a stepwise manner, and may be considered to consist of four individual reactions (63, 64)

$$CO_2 + H_2O \underset{}{\overset{k_1}{\rightleftharpoons}} HCO_3^- + H^+ , \qquad (2.106)$$

$$CO_2 + OH^- \underset{}{\overset{k_2}{\rightleftharpoons}} HCO_3^- , \qquad (2.107)$$

$$CO_3^= + H^+ \rightleftharpoons HCO_3^- , \qquad (2.108)$$

$$CO_3^= + H_2O \underset{}{\overset{K_4}{\rightleftharpoons}} HCO_3^- + OH^- . \qquad (2.109)$$

Reactions (2.108) and (2.109) may be considered to occur instantaneously as they involve only proton exchange. In weakly-alkaline solutions, carbon dioxide enters into two reactions directly, namely reactions (2.106) and (2.107).

The overall reaction is given by the summation of the individual steps

$$CO_2 + CO_3^= + H_2O \longrightarrow 2HCO_3^- , \qquad (2.110)$$

and the overall volumetric reaction rate can then be expressed as

$$\bar{R}_V = (k_1 + k_2[OH^-])[CO_2] . \qquad (2.111)$$

At 20°C and infinite dilution, for sodium alkalies $k_1 = 0.016$ sec^{-1} (111), $k_2 = 5.9(10^6)$ cm^3/gmol-sec (111), and K_4, which is also affected by ionic strength and the type of other species present, has a value of about $1.7(10^{-7})$ gmol/cm^3. In carbonate-bicarbonate buffer systems,

the free hydroxyl ion concentration is governed by the equilibrium of reaction (2.109), such that

$$[OH^-] = K_4[CO_3^=]/[HCO_3^-] . \qquad (2.112)$$

Therefore, whenever $[CO_3^=]/[HCO_3^-] > 1$, then $k_2[OH^-] > k_1$, and Eq. (2.111) can be simplified to

$$\bar{R}_V = k_2[OH^-][CO_2] . \qquad (2.113)$$

In aqueous solutions of sodium or potassium hydroxide, whenever $[OH^-] > 0.01M$ the equilibrium of reaction (2.109) may be considered to be completely displaced to the left. Under this condition, the overall reaction may then be considered as being

$$CO_2 + 2OH^- \longrightarrow CO_3^= + H_2O . \qquad (2.114)$$

Reaction (2.114) is essentially irreversible, and has a rate of reaction in accordance with Eq. (2.113).

In carbonate-bicarbonate buffer solutions, $B_B \equiv [OH^-]$ is relatively low as a result of the small value of the equilibrium constant K_4 of the hydroxyl-ion producing reaction (2.109). Therefore, the fast-reaction criterion, Eq. (2.95), cannot be met in practice, and in this system direct evaluation of the specific interfacial area is not possible in the absence of catalysis. On the other hand, both the fast- and pseudo-first order reaction criteria can be concurrently satisfied in aqueous solutions of strong electrolyte alkalies, permitting direct experimental measurement of a .

Westerterp et al. (12) studied the absorption-with-reaction of pure carbon dioxide in sodium hydroxide solution of unspecified concentration in a stirred tank. At equi-impeller rotational speeds they obtained the same value of the specific area a in both the carbon dioxide-hydroxide and the oxygen-sodium sulphite (catalysed by cupric ion) systems. This equivalence of area appears to be fortuitous since, in general, different absorption rates would be expected due to the different gas solubilities and reaction velocity constants, and since the cupric-catalysed sulphite oxidation does not generally occur in the fast-reaction regime wherein a can be evaluated directly (43, 63). Differences in absorption rate would, in turn, be expected to lead to different degrees of bubble shrinkage during their residence time in the dispersion. Bubble shrinkage in the case of pure gases can be appreciable, thereby greatly reducing the specific interfacial area, as has been demonstrated by Linek and Mayrhoferová (45). Westerterp et al. (12) developed an empirical correlation, based largely on their sulphite oxidation work, in which the specific area, a , was directly prportional to the impeller rotational speed, impeller diameter, and to the square-root of the tank diameter.

Yoshida and Miura (72) studied the stirred-tank absorption-with-reaction of dilute carbon dioxide - air mixtures (0.001 to 0.014 mole fraction carbon dioxide in the inlet gas) in aqueous sodium hydroxide solutions (0.005 to 1.0M) at 20°C. They investigated the performance of both 16-vaned disc and 12-blade turbine impellers, each of 0.40 D_I/D_I ratio. Compared to our work, their maximum agitation rate was much lower (400 rpm). They considered that the absorption was proceeding

in the fast-reaction regime in order to calculate the specific area from an equation analogous to Eq. (2.105). However, at the lower half of their rpm range, the specific area was found to be independent of alkali concentration varying from 0.1 to 0.8M; this is precisely the range of solute ionic strength over which the interfacial area exhibited by dispersed gas bubbles in this study was found to be strongly dependent on ionic strength.

iv) Cobalt-Catalysed Sulphite Oxidation

The first-order kinetic constant for this system can attain values on the order of 10^4 sec^{-1} (12, 43). Hence, this system operates in the fast-reaction regime and can be used to directly evaluate a .

Linek and Mayrhoferová (45) investigated the cobalt-catalysed absorption-with-reaction by using pure oxygen. The use of pure oxygen resulted in a greater mass transfer rate than that achieved with air, and hence appreciable bubble shrinkage and concomitant reduction in specific interfacial area was observed. The rate of absorption was varied by varying the concentration of the cobalt catalyst. At their maximum absorption rate, the specific interfacial area was only 38 percent of that found in uncatalysed solution.

e) Determination of the Liquid-Phase Coefficient (k_L) by Classical Methods

To study the behaviour of the liquid-phase mass transfer coefficient, k_L , the traditional experimental approach has been to separately evaluate $K_L a$ and a by conducting two separate absorptions-with reaction: one in the diffusional regime to measure $K_L a$ (alternatively, a purely physical absorption without reaction can be used);

the other, in the fast-reaction regime to measure a. The results have then been combined to evaluate k_L.

For a sparingly-soluble gas, one can write, using Eq. (2.9),

$$k_L \approx K_L = K_L a/a , \qquad (2.115)$$

but the numerical value of K_L obtained therefrom is only meaningful if $K_L a$ and a were both measured under identical conditions of aeration, agitation, and fluid phase physicochemical properties.

Classical absorption-with-reaction experimental techniques for the separate measurement of $K_L a$ and a do not invariably lead to meaningful results from the application of Eq. (2.115). As previously discussed, the separate determination of $K_L a$ and a by these methods requires different liquid-phase conditions, i.e., different composition and/or solute concentrations (ionic strength), which may result in a different gas bubble size distribution even at equivalent agitation and aeration rates. For example, one could measure $K_L a$ for carbon dioxide absorption-with-reaction in the diffusional regime using hydroxide ion of low concentration, and by significantly increasing the hydroxide ion concentration in a separate experiment measure a in the fast-reaction regime. However, by so changing the ionic strength between "duplicate" experiments it is possible for the average bubble size and the fractional gas holdup to change, thereby altering the specific interfacial area as shown by Eq. (3.16). Bubble size change with changing ionic strength is most pronounced at the relatively low total electro-

lyte concentrations used in these reaction regimes if non-buffered systems are being used.

Alternately, one could measure $K_L a$ for the physical absorption of a non-reacting gas, say oxygen, in a hydroxide solution of concentration compatible with the carbon dioxide-hydroxide fast-reaction regime criterion. Then, holding the impeller rotation speed and the gas sparging rate constant, the inlet gas could be switched to one containing carbon dioxide, thereby sequentially measuring a . However, in this case there is the possibility of again having a different bubble size distribution between the first stage of the sequence and the second as during the latter an appreciably greater amount of the gas phase may be absorbed due to the rate enhancement caused by the chemical reaction.

Yoshida and Miura combined their carbon dioxide - hydroxide solution results for interfacial area (72) with values of $K_L a$ measured by Yoshida et al. (14) in an air - water physical absorption system to calculate the behaviour of k_L without reaction. However, even at identical agitation and gas sparging rates, the dispersed bubbles in the two distinct cases may have been subject to significantly different hydrodynamic regimes since the average bubble size in pure water is larger than in electrolyte solutions.

If an absorption-with-reaction is conducted in a regime intermediate to the diffusion and fast-reaction regimes, as shown by Danckwerts, Kennedy, and Roberts (73), a plot of Eq. (2.100) in the form of $(R_{Vk}^r)^2$ versus $k_2 B_B$ yields a straight line of slope $(aC_k^*)^2 D_{Lk}$ and intercept $(aC_k^*)^2 k_L^2$, from which the value of k_L can be obtained. If $k_2 B_B$

can be varied independently of the concentration of the liquid-phase reactant, B_B, for example, by varying the concentration of a catalyst present in trace amount, the determination of k_L can be made in a consistent physicochemical environment. However, the implementation of the method requires several measurements of the overall absorption rate at each agitation - gas flow rate combination and is, therefore, time consuming.

De Waal and Okeson (43) applied the preceding graphical method to evaluate the rate of surface renewal [related to k_L by Eq. (2.91)] in a cobalt-catalysed sulphite oxidation reaction with pure oxygen. They obtained the anticipated straight-line plot, which implies that their bubble size in each separate experiment was in the same size range such that the value of k_L was independent of average bubble diameter. This is a somewhat fortuitous result using a pure gas, since there is no a priori reason to believe that the gas bubble diameters would remain in the same size range since the degree of bubble shrinkage during the gas residence time would be expected to change with increasing reaction rate (45).

Calderbank (9, 10) and Calderbank and Moo-Young (16) measured the specific interfacial area of gases dispersed in liquids by optical means, and combined the results with $K_L a$ values determined in the same systems by unsteady-state or steady-state physical absorption without reaction (9, 16). Calderbank's smaller tank (5 litre working volume) corresponded in geometric ratios to the one used in this study. Interfacial areas measured in the 5-litre tank were "point" values,

whereas the $K_L a$'s were integral volume averages, possibly leading to some inconsistency in the calculated k_L for this size tank.

6. Concurrent Measurement of $K_{L4}a$ and a and Evaluation of k_{L4}

a) Method and Advantages

The previously-discussed inherent or induced differences between the different systems required to separately evaluate $K_L a$ and a can be eliminated by determining these parameters concurrently such that they are both measured under identical conditions of bubble size, ionic strength, phases densities, viscosities, and interfacial tension. One method of accomplishing this is to desorb transiently a non-reactive gas, e.g., oxygen, from a batch aqueous hydroxide solution into an oxygen-free, carbon-dioxide-bearing dispersed gas. The oxygen desorption is essentially complete within a relatively short period of from one to two minutes, and $K_{L4}a$ for the physical mass transfer of oxygen can be computed from the transient response of an oxygen probe, i.e., through the computer evaluation of β in Eq. (2.83). The specific interfacial area may be computed from the appropriate reaction regime model for the absorption-with-reaction of carbon dioxide which occurs over a longer time interval in a pseudo-steady state manner. The carbon dioxide absorption process is described by either Eq. (2.100) or Eq. (2.101).

At high agitation rates in a stirred-tank absorber-reactor, the specific interfacial area may be one order of magnitude greater than that obtained in a stirred tank at low agitation rates or in a packed-tower absorber. Therefore, the absorption-with-reaction rate can be

increased by an order of magnitude, and the initial hydroxide ion concentration in a semi-batch system can be completely depleted in such a short time that accurate absorption rate data cannot be obtained. In order to eliminate this difficulty, a small feed stream of concentrated hydroxide is continuously added under pH control, and effluent withdrawn at the same rate such that the liquid-phase is at steady-state with respect to the hydroxide ion concentration. The small dilution rate is, in general, not sufficient to keep the concentration of the carbonate ion reaction product at a steady-state value; therefore, the reaction velocity constant, k_2, and the Henry's law coefficient for carbon dioxide, H_3, which are dependent upon the total ionic strength of the absorbing solution, change slowly with time and corrected values must be used in each point calculation of the rate.

The use of the oxygen probe transient desorption response model, Eq. (2.83), is predicated on the assumption that the amount of gas absorbed is small compared to the total gas input rate. This assumption would be invalidated if pure carbon dioxide were to be used in the near-fast reaction regime since both C_3^* and a (at high agitation rate) would be relatively large in Eq. (2.101). The degree of bubble shrinkage can be minimized by using a dilute carbon dioxide sparge gas, but the degree of carbon dioxide absorption must still be restricted in order that the exit gas contain an experimentally-measurable concentration of carbon dioxide. Therefore, the use of this concurrent method requires that the absorption-with-reaction proceed at a rate somewhat less than that which would occur in the fast-reaction regime with a sparge gas of

appreciable carbon dioxide concentration. Experimentally, the sparge gas used was 0.10 mole fraction carbon dioxide in nitrogen, and the bulk solution hydroxide ion concentration was less than 0.1M.

b) Absorption-with-Reaction Model

The applicable absorption model is that for pseudo-first order reaction--criterion of Eq. (2.97)--in an absorption-with-reaction regime intermediate between the diffusional and fast-reaction regimes, namely Eq. (2.100), which for carbon dioxide can be written as

$$R_{V3}^{r} = a_3 C_3^{*} (k_{L3}^2 + D_{L3} k_2 B_B)^{1/2} , \qquad (2.116)$$

where a_3 is the specific interfacial area effective for the transfer of carbon dioxide which is denoted by subscript 3.

The use of Eq. (2.116) to determine a_3 requires separate knowledge of the value of k_{L3}. From the concurrent desorption of oxygen, denoted by subscript 4, a value of $K_{L4}a_4$ is obtained. Assuming that the penetration or the random surface renewal models describe the process of desorption or absorption over the entire range of bubble sizes, for identical interfacial hydrodynamic conditions, i.e., identical rates of surface renewal for both the desoprtion and the absorption-with-reaction processes, it follows from Eq. (2.91) that

$$k_{L3} = k_{L4} (D_{L3}/D_{L4})^{1/2} . \qquad (2.117)$$

If we further assume that the effective interfacial area for physical mass transfer of oxygen is the same as that for the absorption-with-reaction of carbon dioxide, then

$$a_3 = a_4 = a \,. \qquad (2.118)$$

In the case of mass transfer with chemical reaction, the effective specific interfacial area, a_3, depends not only upon the average bubble size and the liquid-phase hydrodynamics, but also upon the reaction time, that is the time required for the reaction to proceed to a considerable extent (74). In the fast-reaction regime, the volumetric absorption rate per unit surface area can be independent of the rate of surface renewal or the age of the surface element; absorption into the surface element will continue until all the liquid-phase reactive component has been completely consumed and the liquid surface element reaches a state of physical equilibrium (saturation) with the gaseous component. Therefore, an as-yet-unrenewed surface element can be effective for mass transfer for a considerably longer period than it would be if there were no reaction within it.

In the case of physical absorption without reaction, unrenewed surface elements of large age contribute little to the overall mass transfer rate, and the effective interfacial area may be much less than the total area existent. Such indeed can be the case in packed-tower absorbers where stagnant liquid zones can exist at the ends of packing elements, but in the case of highly-agitated stirred tanks, where the average bubble diameter is much greater than the scale of the small turbulent-liquid eddies, stagnant liquid surface elements are very much less likely, and the assumption of Eq. (2.118) appears to be reasonable.

Substituting Eqs. (2.117) and (2.118) into Eq. (2.116), rearranging, and solving for the specific interfacial area, and using the sparingly-soluble gas approximation that $k_{L4} \approx K_{L4}$, we obtain

$$a = \left\{\left[\left(R^r_{V3}/C^*_3\right)^2 - \left(K_{L4}a\right)^2\left(D_{L3}/D_{L4}\right)\right]/D_{L3}k_2B_B\right\}^{1/2} . \quad (2.119)$$

The liquid volumetric rate of carbon dioxide absorption-with-reaction, R^r_{V3}, is obtained from gas-phase analyses. The exit gas rate, Q_2, can be related to the inlet rate, Q_1, by a nitrogen material balance, which leads to

$$Q_2 = Q_1(1 - y_1)/(1 - y_2) , \quad (2.120)$$

where y_1 and y_2 are the mole fractions of carbon dioxide in the inlet and outlet gas streams, respectively.

Writing a molar material balance for steady-state carbon dioxide absorption-with-reaction, and substituting Eq. (2.120) therein, the result is

$$R^r_{V3} = 1.69(10^{-8})Q_1\left\{y_1 - y_2[(1-y_1)/(1-y_2)]\right\} , \quad (2.121)$$

where the numerical constant $1.69(10^{-8})$ incorporates the conversion factor $23.7\ (10^3)$ cm^3 of gas at 60°F, 1 atm/gmole gas, and the liquid volume of 2500 cm^3. In Eq. (2.121), the y's denote mole fractions of carbon dioxide.

Equation (2.119) is applicable to the case of a well-mixed dispersed gas phase; that is, we have assumed that the interfacial concentration of dissolved carbon dioxide is in physical equilibrium

with the outlet gas stream carbon dioxide partial pressure, the equilibrium following Henry's law, Eq. (2.45).

From the concurrent but separate evaluation of $K_{L4}a$ and a, the liquid-phase mass transfer coefficient for oxygen is calculated following Eq. (2.115), namely

$$k_{L4} \approx K_{L4} = K_{L4}a/a \ . \qquad (2.122)$$

III. EXPERIMENTAL

1. Apparatus

A schematic flow diagram of the entire system is given on Fig. (3.1).

a) Stirred-Tank Absorber-Reactor

The stirred-tank absorber-reactor used in this study consisted of a 1-ft length of 6-in. i.d. "Pyrex" pipe, to which were attached by flanges top and bottom stainless steel cover plates, as shown on Fig. (3.2). Feed and effluent gas and liquid streams were admitted to or withdrawn from the tank through fittings in the head plates, which also held the impeller shaft bearing housing and the ancillary measuring devices such as the oxygen probe, pH electrodes, and thermowells. The internals of the tank were constructed to correspond to the recommended "standard" dimension ratios (75). Four equally-spaced vertical baffles one-tenth of the tank i.d. in width constructed from 11-gauge 316-stainless plate were joined at their tops (above the liquid level) by means of a rigid supporting ring; the bottoms, which were not interconnected, rested on the bottom head plate. Rotation of the baffle assembly was prevented by small retaining pins attached to the bottom head plate on botn sides of two of the baffle strips. The single impeller was a stainless steel, 6-blade, turbine type 2 inches in diameter, thereby having an impeller-to-tank diameter ratio of one-third. The impeller was mounted on a 1/2-in. diameter stainless steel shaft such that the impeller radial centre line was one impeller diameter above the tank bottom.

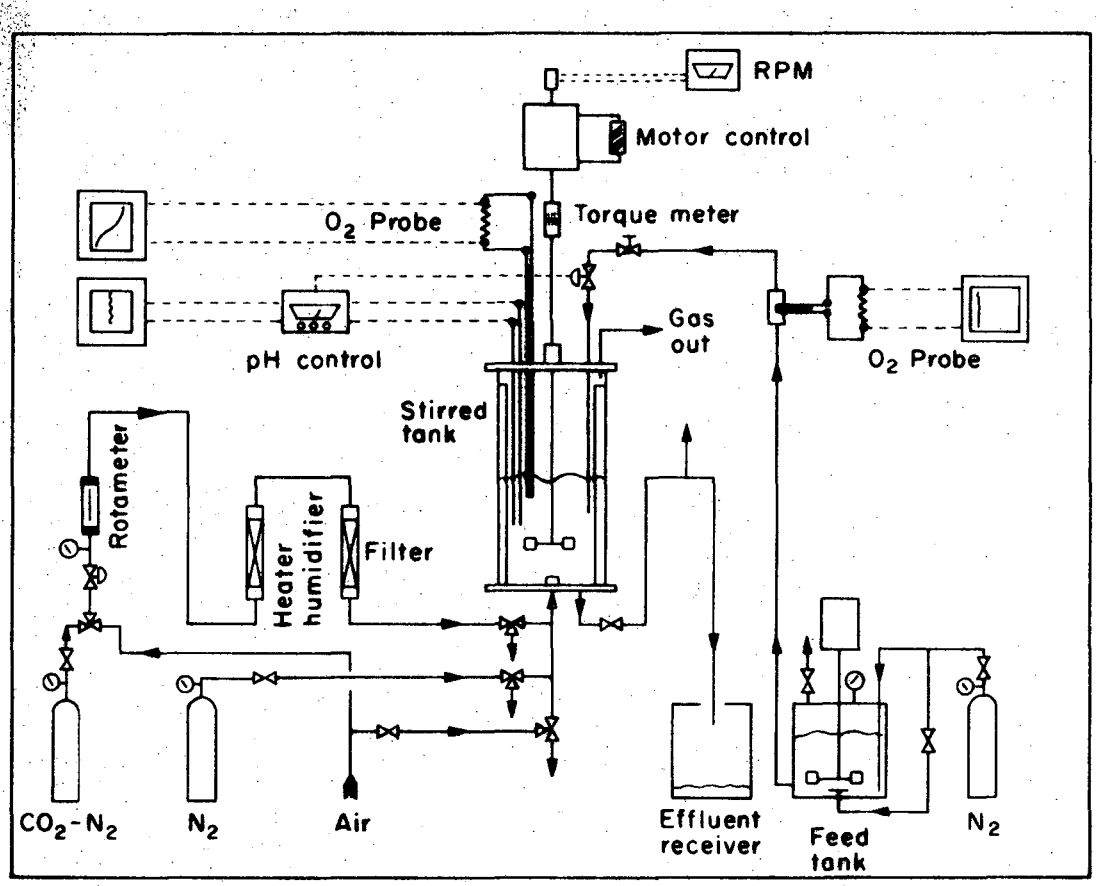

XBL6912-6368

Fig. 3.1. Schematic Flow Diagram of Apparatus.

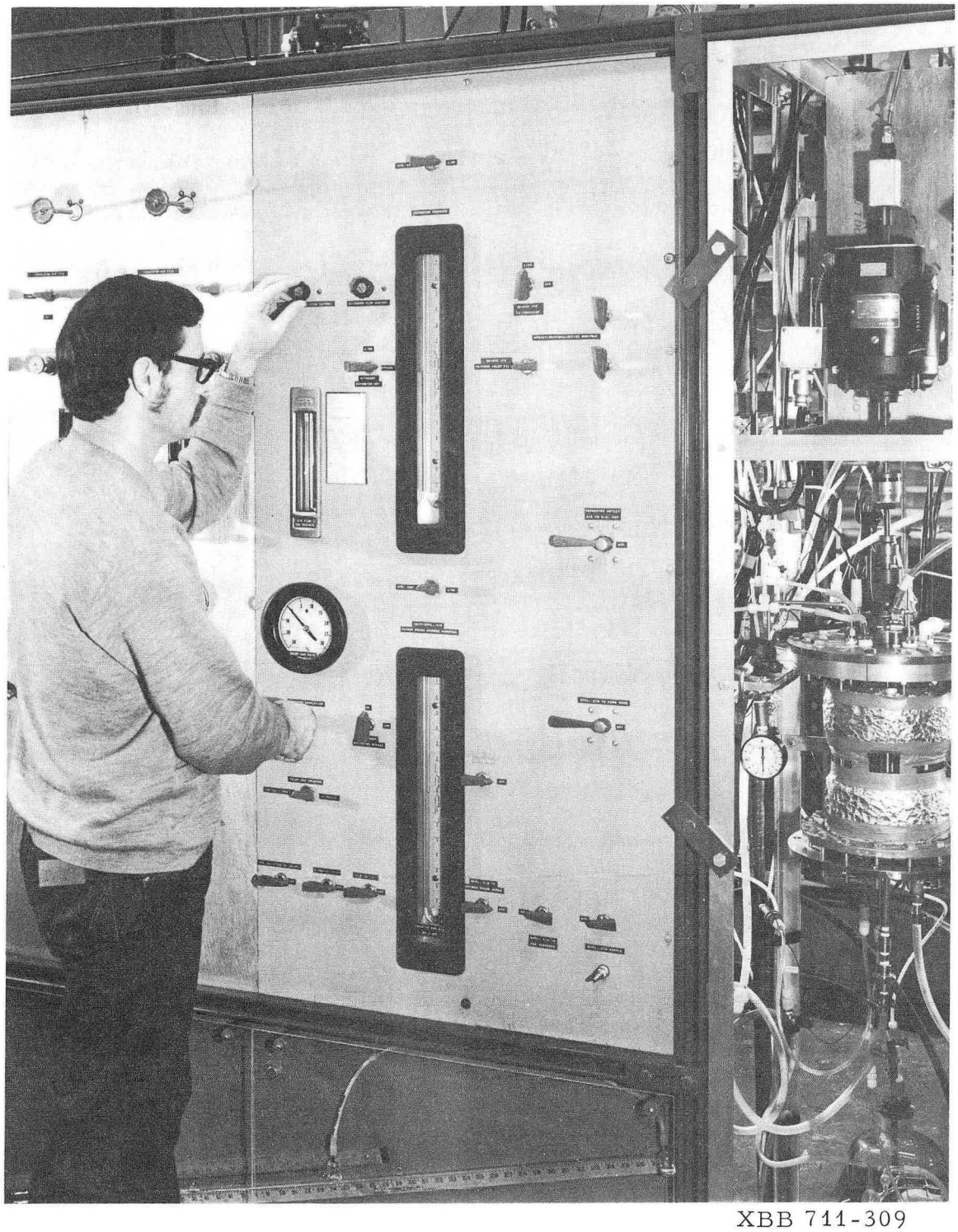

XBB 711-309

Fig. 32. Photograph of Experimental Apparatus.

flow through an electric heating tape wound around the outside of the lower half of the vessel. The entire exterior of the tank, excepting a 1-in. wide observation strip at the midsection, was insulated. The tank contained a cooling coil constructed of 1/4-in. o.d. stainless tubing would in a spiral coil and mounted flat on the bottom head plate. Water entered and left the coil through fittings in the bottom plate; flow regulation was done manually.

b) Ancillary Equipment

The gas supply to the tank was metered through a rotameter, which was calibrated against a wet-test meter. Gas was heated to 30°C and at the same time humidified by passing it through a 2-in. i.d. × 2-ft long "Pyrex" pipe column packed with stainless steel wool and half filled with water. Temperature control of the heat-humidifier was only manual, being effected by regulating the electric current through a heating tape, but was quite invariant even when the system was disturbed by changes in the ambient temperature or gas flow rate due to the fact that the stainless wool packing, in addition to its gas-dispersion function, acted as a heat sink. The gas was then passed through a glass wool filter, flowed to the inlet gas piping manifold, and was admitted to the tank through a 1/8-in. diameter bevelled orifice fitting located in the bottom head plate directly under the impeller axial centre line. The effluent gas left the tank through an open port in the top head; therefore, reactor head space pressure was local atmospheric in all runs.

In the CFST absorption experiments, the liquid feed stream was supplied from a 35-litre, stainless steel tank which was pressurized

to a constant pressure. The tank was equipped with an impeller agitator, internal perforated pipe gas sparger, and heating coil. The contents of the tank were held at 30°C by a second proportional temperature controller acting on an immersion heater. Liquid flow rate was regulated manually by means of a needle valve. The liquid feed flowed through a chamber containing an oxygen probe before entering the stirred tank from the top through a 1/2-in. diameter downpipe which terminated 2 in. below the liquid level near the wall adjacent to one of the baffles. The liquid effluent left the tank from the bottom by gravity flow through a non-syphoning loop (thereby holding the liquid volume in the tank constant) and was directed to a collection vessel.

In the carbon dioxide absorption-with-reaction experiments, the hydroxide ion concentration of the liquid phase was kept at the initial concentration ± 0.02 pH units by the addition of small amounts of concentrated potassium hydroxide solution supplied from a pressurized tank (same tank as described previously). The addition of hydroxide was regulated by a pH controller. Steam-sterilizable pH glass and reference electrodes in stainless steel immersion holders were mounted in the tank through the top head plate. The electrodes were connected to a pH indicator-controller meter with an expanded recorder output scale. The pH was recorded on a 0 to 10 mV recorder with zero point set at pH 12.0, and full-scale corresponding to pH 14.0. Control mode was on-off, acting on a solenoid valve mounted in the concentrated potassium hydroxide solution feed line. The liquid effluent was handled in the same manner as in the aforementioned CFST experiments.

2. Absorber-Reactor Operating Characteristics

a) Power Number (N_P)

Rushton, Costich, and Everett (76) described the unaerated mixing power characteristics of various types of impellers in baffled tanks according to the variation of a dimensionless group denoted the Power number. The Power number is the ratio of the external to the internal forces acting upon the liquid:

$$N_P \equiv P_0 g_c / N^3 D_I^5 \rho_L \quad . \tag{3.1}$$

The Power number is usually correlated with the modified Reynolds number for the particular impeller, defined as

$$N_{Re} \equiv N D_I^2 \rho_L / \mu \quad . \tag{3.2}$$

As shown in Fig. (3.3), the apparatus behaved in accordance with Eq. (3.1) in that the impeller rotational speed was found to be proportional to the cube root of the mixing power.

Over the range of agitation rates in the turbulent region ($N_{Re} > 10^4$) where gas bubble inclusion due to backmixing from the vapour space did not occur, the experimentally-determined Power number was nearly constant, as shown in Table (3.1). The average value of N_P was 3.2, which is on the lower side of the range of values previously reported for turbine-type impellers. Rushton et al. (76) found $N_P = 6.0$, while Bates, Fondy, and Corpstein (77) reported values of N_P ranging from 3 to 5.

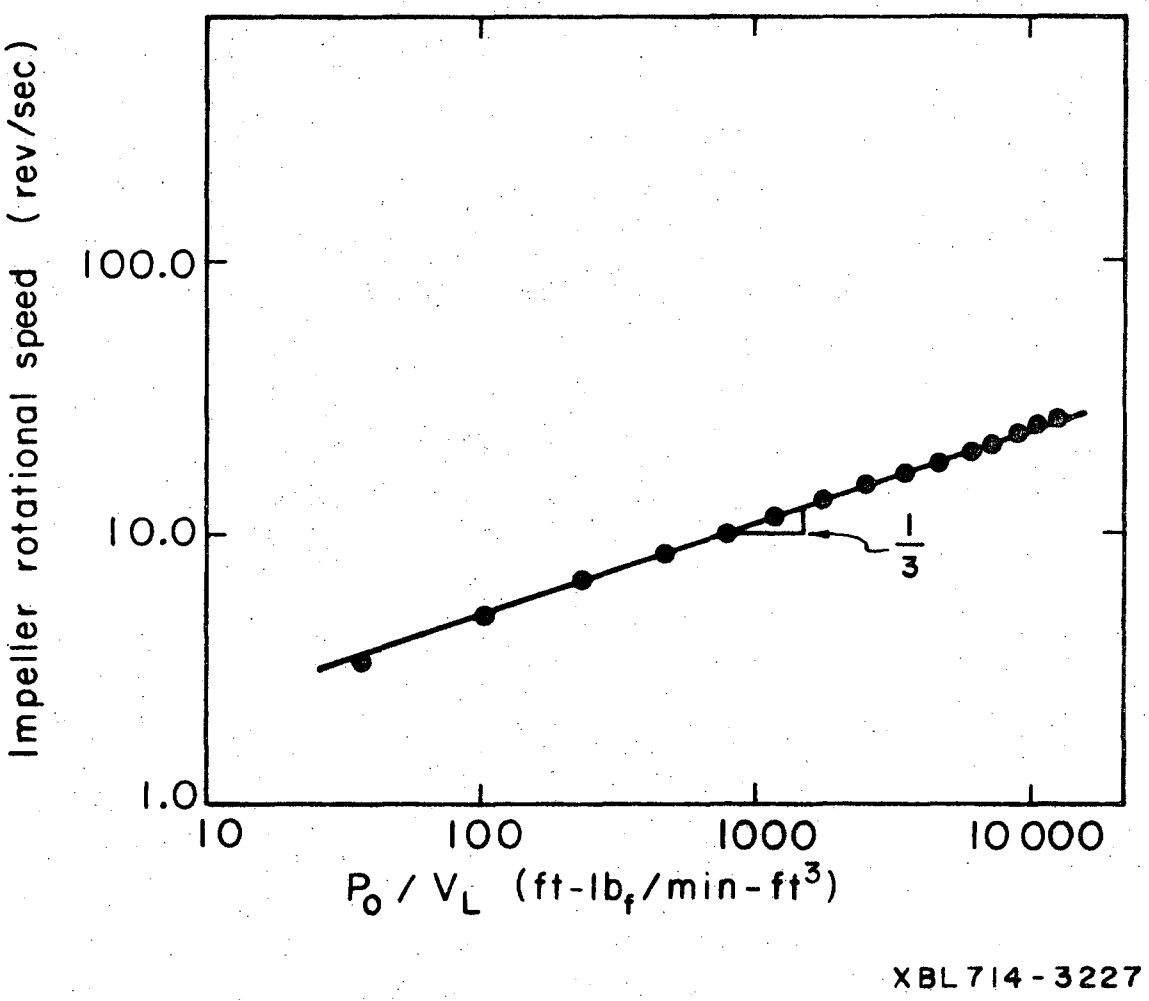

Fig. 3.3. Effect of Impeller Rotational Spped on Unaerated Mixing Power per Unit Volume in Water.

Table 3.1. Mixing power characteristics of fermentation apparatus measured in water.

Impeller rotational speed (N) rpm	N_{Re} $\frac{ND_I^2\rho_L}{\mu}$ $\times 10^{-4}$	No-load[a] torque oz.-in.	Unaerated torque oz.-in.	Unaerated[b] power/unit vol. ft-lb$_f$/min-ft^3	Power number $\frac{Pg_c}{\rho_L N^3 D_I^5}$
200	1.07	0.4	0.9	37	4.16
300	1.60	0.5	1.4	100	5.53
400	2.14	0.65	2.2	230	3.22
500	2.67	0.75	3.2	454	3.26
600	3.21	0.80	4.3	778	3.23
700	3.74	0.9	5.5	1190	3.11
800	4.28	1.0	7.0	1780	3.12
900[c]	4.81	1.0	8.7	2570	3.16
1000	5.35	1.1	10.7	3540	3.17
1100	5.88	1.2	12.7	4680	3.15
1200[d]	6.41	1.2	14.7	6010	3.12
1300	6.95	1.3	16.6	7370	3.01
1400	7.48	1.35	18.6	8950	2.93
1500	8.02	1.4	20.9	10830	2.88
1600[e]	8.55	1.45	22.5	12490	2.73

(a) Measured in air.
(b) Liquid volume 2.5 litres.
(c) Incipient bubble inclusion (drawn in from vapor space).
(d) Start of uniform bubble holdup in liquid.
(e) Limit of torque meter range.

b) Aeration Number (N_A)

When an agitated liquid is subjected to aeration from sparged gas bubbles, the power drawn by the motor at constant rpm decreases. The decrease in power is not due merely to the resultant decrease in the overall fluid density caused by bubble dispersion in the liquid, being greater than the decrease predicted from density considerations only from Eq. (3.1) substituting ρ_D for ρ_L. In practice, the ratio of aerated to unaerated power, P_G/P_0, ranges from 0.3 to 1.0, depending upon the relative agitation and aeration rates.

Empirically, Ohyama and Endoh (15) found that the power ratio could be correlated with a dimensionless group denoted the Aeration number, N_A, which is proportional to the ratio of the superficial gas velocity with respect to the impeller cross-sectional area to the tip velocity of the impeller,

$$N_A \equiv Q_1/ND_I^3 \quad . \tag{3.3}$$

The functional dependency of P_G/P_0 on N_A depends upon the type of impeller. The specific dependency for the impeller used in this work is shown on Fig. (3.4) for water, the experimental data being given in Appendix III. 1.

c) Backmixing from the Vapour Space

Backmixing is defined here as the phenomenon of bubble inclusion into the agitated liquid from the absorber vapour space, resulting from the wave-like motion and localized small-scale vortexing of the free liquid surface. Such backmixing can conceivably increase the gas

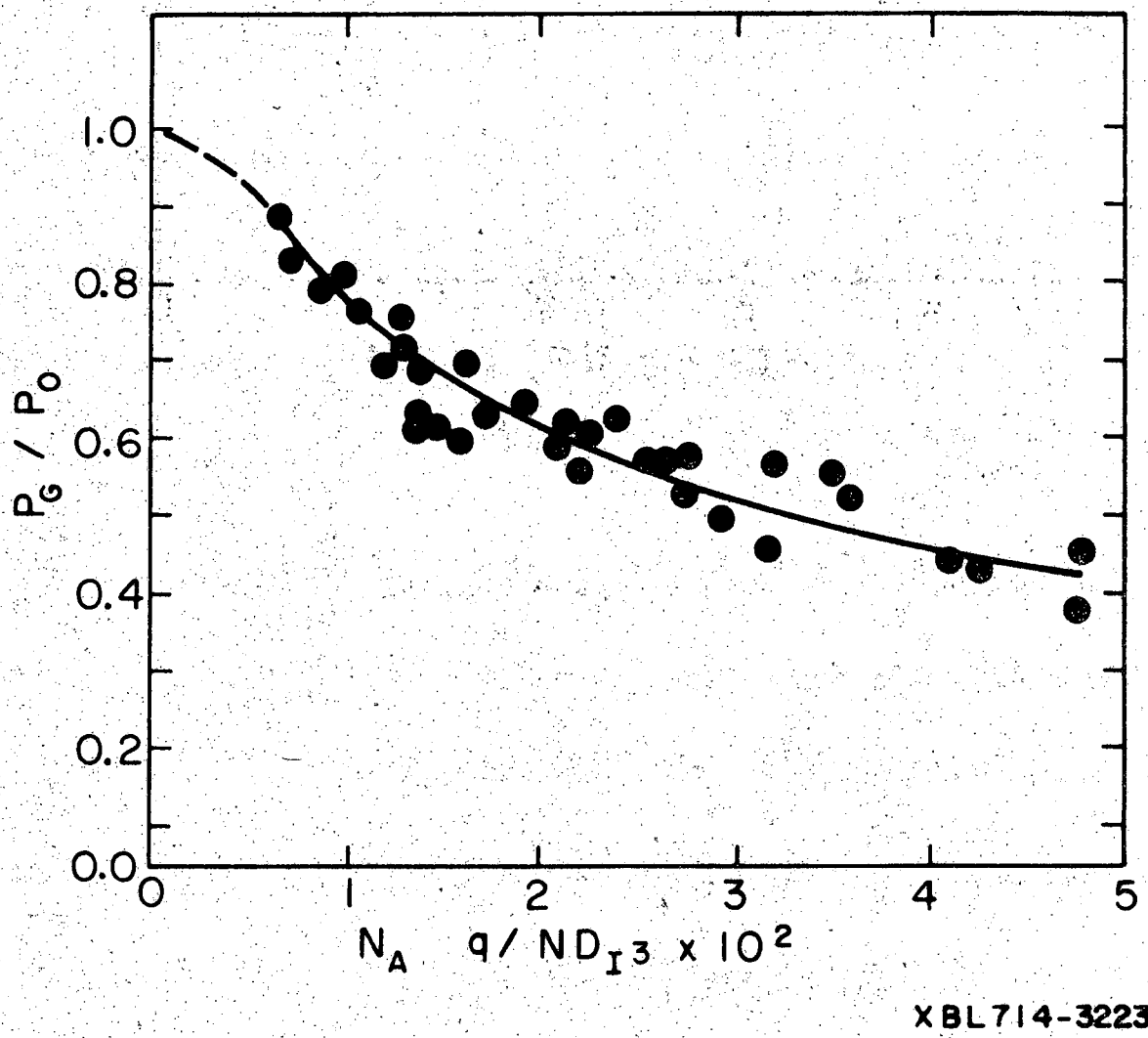

Fig. 3.4. Effect of Aeration on Agitation Power per Unit Volume in Water.

fractional hold-up (especially at low sparging rates where the maximum possible rpm-dependent distribution of dispersed bubbles has not been reached) and/or reduce the mass transfer rate by the recirculation of gas which may already be in physical equilibrium with the liquid.

One should, however, distinguish between two limiting cases of backmixing, namely:

i) backmixing in the absence of concurrent gas sparging into the liquid (which has been the type most commonly investigated)

ii) backmixing with concurrent gas sparging.

Whenever the distribution of dispersed, sparged gas is uniform over the entire absorber cross section, the effective degree of backmixing should be reduced over that experienced in the non-sparged case. As far as the mass transfer capability is concerned, sparged bubbles arriving at the free liquid surface prior to break-up serve as a stripping agent for material returned to the liquid phase by the process of backmixing.

Backmixing characteristics were investigated with concurrent gas sparging in this work. Nitrogen was sparged into the tank at a volumetric rate Q_N. A 4-in. diameter turbine-type impeller was installed in the gaseous head space about 2 in. above the maximum free liquid surface level expected. Air, at a rate Q_A, was admitted to the head space just below the additional impeller. Assuming perfect mixing in the head space between the dispersed gas leaving the free liquid surface and the added air stream, when the liquid and the dispersed nitrogen are in equilibrium, and when $Q_A = Q_N$, then the mole fraction

of oxygen in the head space gas is one-half its value in air, i.e., 0.105 mole fraction. This mole fraction will produce an oxygen probe external voltage E_{max}, which can be measured by sparging both the nitrogen and the air streams together.

The volumetric rate of backmixing is denoted Q_V. When only nitrogen is sparged with air admitted only to the head space, any reading on the oxygen probe voltage recorder must then be due solely to the oxygen content of Q_V being transferred into the liquid by backmixing.

Assuming that the total dispersed gas hold-up consists of sparged gas and backmixed gas in direct proportion to their volumetric rates Q_N and Q_V, the fractional hold-up due to backmixing, f_{BM}, can be defined as

$$f_{BM} \equiv Q_V/(Q_V + Q_N) . \tag{3.4}$$

The mole fraction of oxygen in the dispersed gas of assumed composition distribution then simply becomes

$$y_{4D} = 0.105\, Q_V/(Q_V + Q_N) = 0.105\, f_{BM} . \tag{3.5}$$

An oxygen probe external voltage, E_L, is produced in direct proportion to y_{4D} when steady-state is attained. The oxygen partial pressure corresponding to E_L for a probe with a linear partial pressure - voltage characteristic is then

$$p_{4d} = (E_L/E_{max})(0.105) = P_T y_{4D} . \tag{3.6}$$

Combining Eqs. (3.5) and (3.6) at one atmosphere total pressure, f_{BM} is given by

$$f_{BM} = E_L/E_{max} . \qquad (3.7)$$

Experimental results for the backmixing effect on mass transfer of oxygen in water and 0.125M sodium sulphate solution are shown on Figs. (3.5) and (3.6), respectively. In both cases, f_{BM} is relatively high at low rpm, decreases to a minimum, and then increases again at agitation rates greater than about 1600 rpm. Fractional backmixing with gas sparging decreases as the sparging rate increases at constant rpm.

At low rpm (less than 400 to 500 rpm), the sparged gas is not uniformly distributed, rising in large bubbles in a small zone immediately adjacent to the impeller shaft. A large area of the relatively-quiescent free surface is not contacted by this stripping gas, permitting a relatively high mass transfer rate of oxygen from the head space gas mixture into the liquid. At high rpm (greater than 1500 to 1700 rpm), the free liquid surface is very turbulent with localized surface vortexing readily visible, affording a mechanism for increased backmixing.

Over the range of agitation rates used in this work (700 to 2200 rpm), backmixing into the sparged liquid appears to be negligibly small at the three higher sparging rates, i.e., f_{BM} is less than 2 percent.

Using air to strip sulphur dioxide from aqueous solutions, Calderbank (9), over a range of tank sizes, found that backmixing under some conditions retarded the desorption process. He gives an empirical

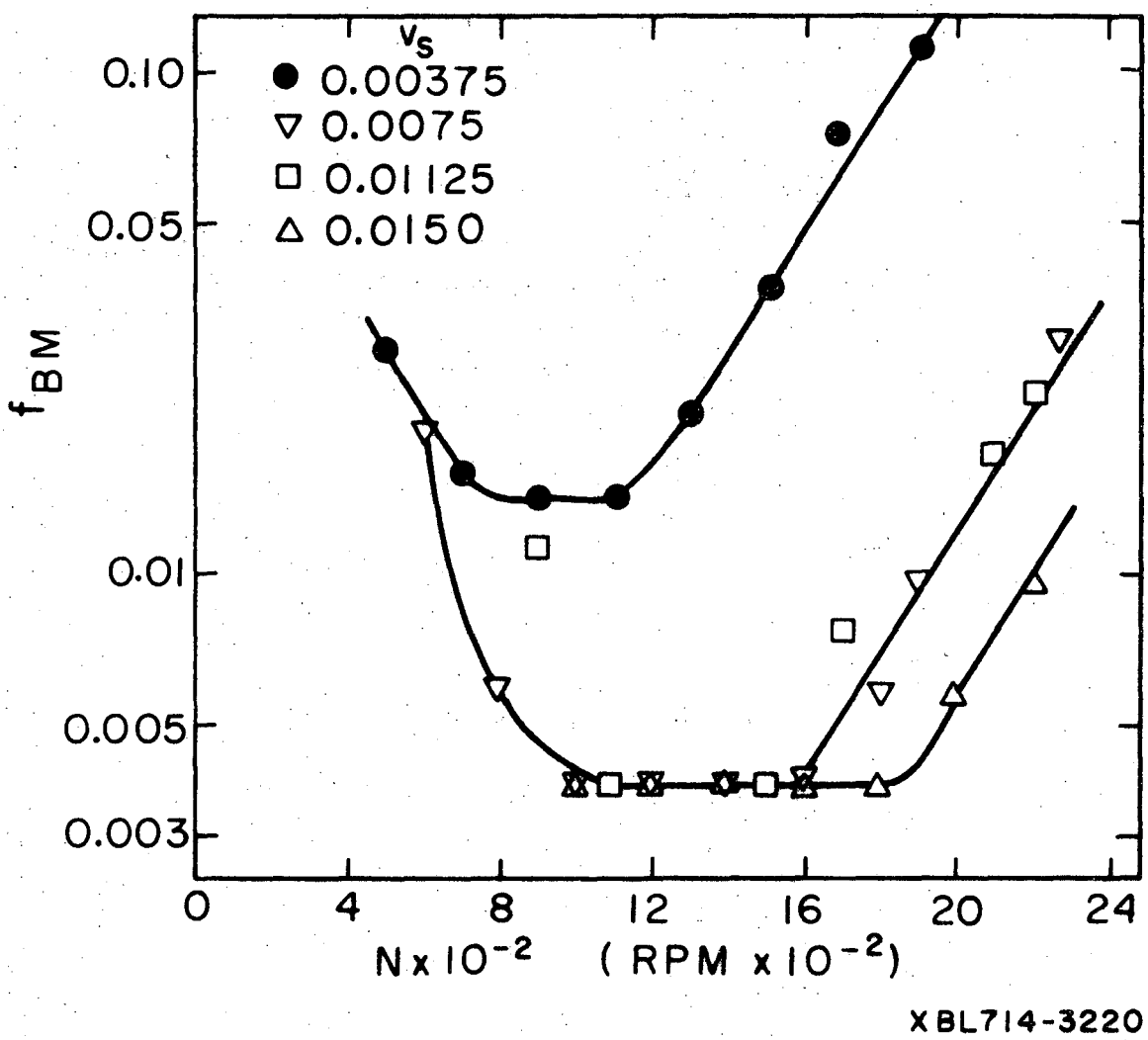

Fig. 3.5. Gas Phase Backmixing Fraction in Water.

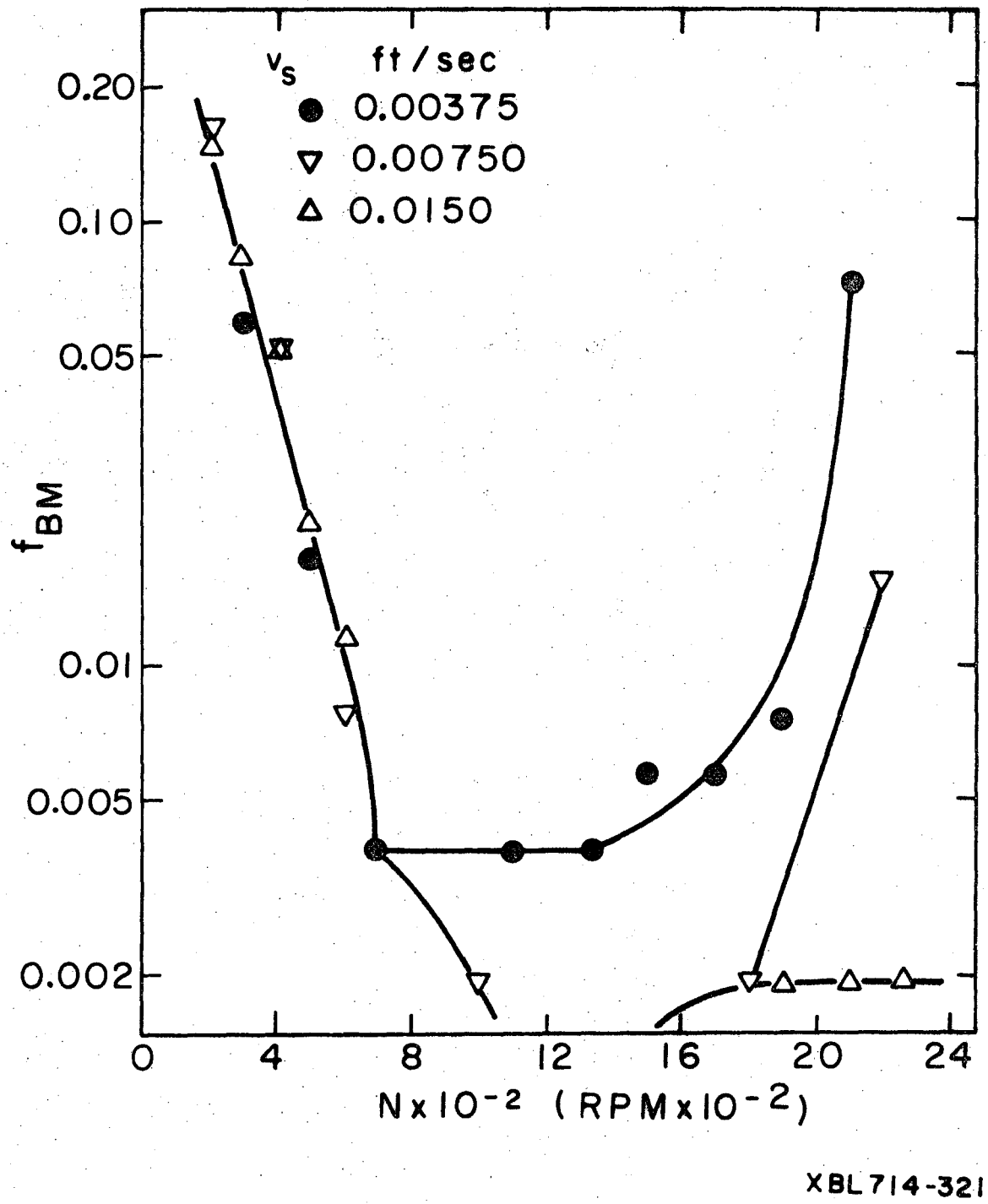

Fig. 3.6. Gas Phase Backmixing Fraction in 0.125M Na_2SO_4 + 0.004M $CuSO_4$.

criterion involving impeller rotational speed, impeller diameter, and gas superficial velocity by which the onset of significant backmixing can be predicted. For the stirred tank used in this work, the criterion predicts negligible backmixing below 1800 rpm, with which the experimental results are in general agreement.

3. Operating Methods

a) Steady-State or Pseudo-Steady State Absorption

i) CFST Absorption Without Reaction

The stirred-tank absorber was filled with 2.5 litres of the test solution, the desired impeller rpm established, and sparging with nitrogen begun at a rate equal to that of the air rate to be eventually used. Air was metered, heated and humidified, and filtered in the manner previously described and then initially vented to the atmosphere at the gas inlet manifold through a three-way valve.

The pressurized liquid feed tank contained deoxygenated test solution (achieved by stripping with sparged nitrogen). Liquid feed to the absorber was begun at a constant flow rate; the feed was passed through an oxygen probe chamber located upstream of the absorber in which the oxygen tension of the feed was measured by oxygen probe calibrated against the probe mounted in the absorber. The oxygen tension in the liquid feed was usually zero, or an extremely low value, depending upon the time period of nitrogen stripping in the feed tank. The effluent liquid from the absorber was collected and, at the conclusion of the run, the total weight collected was determined. Knowing the density of the test solution, the volume of feed supplied over the

known time interval, and hence the dilution rate was calculated. The effluent from each run was returned to the feed tank, where it was reheated and deoxygenated for reuse.

Immediately after the start of the liquid feed, air was switched into and nitrogen switched out of the inlet gas manifold. After a short transient period, the oxygen tension in the absorber liquid, and hence the absorber probe reading reached their steady-state values, which, of course, were less than the saturation value possible with respect to air, the magnitude of the difference being a function of both $K_{L4}{}^{a}$ and the dilution rate, $\bar{D}$, as shown by Eq. (2.35) or Eq. (2.36). Several runs were made holding the impeller rotational speed and the gas sparging rate constant, but varying the dilution rate; the results showed that the dilution rate per se had no effect upon the experimentally-determined value of $K_{L4}{}^{a}$.

The steady-state bulk solution oxygen tension was recorded continuously on a 15 in./hr chart speed recorder. After at least a 5-minute steady-state period, the liquid feed was stopped while agitation and aeration of the then batch liquid volume was continued in order to determine the probe reading at the final equilibrium dissolved oxygen tension with respect to the inlet air.

ii) Absorption of Oxygen with Chemical Reaction: Sulphite Oxidation in SBST

In all runs, reagent grade sodium sulphite was used at an initial concentration of 0.5M (1.0N with respect to the reaction stoichiometry). The reaction was catalysed with cupric ion, $4(10^{-3})$M, obtained from

reagent grade cupric sulphate. This is the same system as used by Cooper, Fernstrom, and Miller (11).

The experiments were terminated before the concentration of sulphite ion reached 0.1N; at sulphite concentration above about 0.02N, the reaction rate is independent of sulphite ion concentration (78).

At suitable time intervals, liquid samples were taken for sulphite ion concentration analysis, and vapour space samples taken for oxygen content determination. $K^r_{L4}a$ was determined by the procedure discussed in Section III. 4(b).

b) Unsteady-State Oxygen Transfer Without Chemical Reaction

The test solution of 2.5 litres volume was stirred at the desired rpm; nitrogen (oxygen absorption) or air (oxygen desorption) was initially sparged at the desired gas volumetric flow rate. Air (absorption) or nitrogen (desorption) was directed through the metering-heating-humidifying-filtering circuit, and was then vented to atmosphere at the inlet gas manifold.

When the oxygen probe readings indicated that the solution had reached its equilibrium deoxygenated state for the case of absorption, or oxygen saturated with respect to air for the case of desorption, the probe output was switched to the high-speed chart recorder (30 in./min chart speed, 0.25 sec full-scale response time). Then, the step change in sparge gas type was made at the inlet manifold. The transient increase or decrease in the probe external millivoltage was recorded continuously until about 90 percent of the total change had occurred. The chart drive was then stopped to conserve paper, but the measuring function of the

instrument was kept operative in order to note the final probe reading when the solution reached its oxygen saturated state for the case of absorption or the fully-deoxygenated state for the case of desorption.

The three-way valves at the inlet gas manifold were then switched to their original positions, the rpm changed to another value, and the procedure repeated.

c) Concurrent Oxygen Desorption and Carbon Dioxide Absorption-with-Reaction

Initially, the test solution containing 0.01 to 0.10M potassium hydroxide was at a fully-oxygenated state, achieved by sparging caustic-scrubbed air (to remove atmospheric carbon dioxide). The dilute carbon dioxide - nitrogen mixture (0.10 mole fraction CO_2) was metered, heated, humidified, filtered, and then vented to atmosphere at the inlet gas manifold.

In the runs made by using 0.11M Na_2SO_4 + KOH - K_2CO_3 or 0.135M KCl + KOH - K_2CO_3, it was essential that the initial total ionic Γ_T, be as uniform as possible. Since the reaction product, K_2CO_3, contributes appreciably to Γ_T, and since it is produced at an unpredictable rate (a priori), it was necessary to adjust its initial concentration before beginning the run. This was done by intermittently switching the CO_2-bearing gas into the absorber-reactor for brief periods until liquid-phase analysis for hydroxyl and carbonate ion concentrations gave the desired Γ_T to within 10 percent.

To start the run, the gas streams were switched at the inlet manifold; the transient response of the oxygen probe was recorded as

previously described. Samples of the reactor liquid and vapour-space gas (the latter from 1 in. above the surface of the dispersion) were taken a suitable intervals for analysis; at least three sets of such samples were taken per run.

The pH controller admitted deoxygenated concentrated KOH (about 1M) at a rate of about 15 to 20 ml/min. The resulting small flow of liquid effluent was withdrawn through the non-syphoning loop, maintaining a constant volume within the tank.

Although the recorded pH was constant to within ± 0.02 pH units, liquid analysis showed that in all runs the concentration of hydroxide ion decreased slowly with time. The insensitivity of the pH electrodes was presumably due to the inherent difficulty in accurately measuring pH's greater than 11 with general-purpose glass electrodes, and to the fact that the response of the glass electrode is influenced by large concentrations of other ions in solutions of high alkalinity (79).

In the experimental system used here, the concentration of carbonate ion produced by the reaction increased with time as the dilution rate was too small to achieve carbonate ion steady-state. The increase in carbonate ion concentration, however, did not significantly affect Γ_T during the transient oxygen desorption period, as this comprised only the first 10 to 20 percent of the total run time. The continuous decrease in hydroxide ion concentration, however, did result in a slight increase in the sampled gas carbon dioxide content, amounting to about a 10 percent increase. As neither the gaseous or the liquid phase concentration were truely invariant, the mode of operation is denoted as pseudo-steady state.

d) Measurement of Dispersed Gas Fractional Holdup

The volume fraction of gas in the dispersion, H_G, was determined manometrically from the decrease in differential hydrostatic pressure between two pressure tap points resulting from the gassing of the clear liquid. The pressure differential was measured by a manometer inclined 15° from the horizontal, using hexadecane (S.G.=0.775) as the manometer fluid.

The two pressure taps were part of a probe which was mounted vertically in the vessel through the top head. The two taps were constructed from sections of 1/4-in. o.d. stainless tubing mounted immediately adjacent to one another. The open ends of the taps were 4-5/8 in. apart, the lower tap end being positioned 1 in. above tank bottom. The vertical axis of the probe was located 4-1/2 in. from the tank centre line. A small bleed stream of nitrogen was passed through each manometer leg (about 10 bubbles/min discharge).

The hydrostatic pressure difference in lb_f/ft^2 between two taps L' feet apart in the gas-free liquid is

$$\Delta\bar{P}_L = L'\rho_L g/g_c \tag{3.8}$$

and in the gas - liquid dispersion is given by

$$\Delta\bar{P}_D = L'\rho_D g/g_c \,. \tag{3.9}$$

Writing a mass balance over the dispersion volume V_D results in

$$\rho_D = \rho_G(V_G/V_D) + \rho_L(V_L/V_D)$$

$$= \rho_G H_G + \rho_L(1 - H_G)$$

$$= \rho_L - (\rho_L - \rho_G) H_G \quad . \tag{3.10}$$

But, since $\rho_L >> \rho_G$, Eq. (3.10) can be simplified to

$$\rho_D = \rho_L(1 - H_G) \quad . \tag{3.11}$$

The difference in manometer reading between the gas-free liquid case and the gas - liquid dispersion, $\Delta\bar{P}_F$, is given by

$$\Delta\bar{P}_F \equiv \Delta\bar{P}_L - \Delta\bar{P}_D \quad . \tag{3.12}$$

The linear differential displacement in inches of the manometer fluid for a manometer inclined η degrees to the horizontal is

$$\Delta\mathcal{H}_F = 12 g_c \Delta\bar{P}_F \sin \eta/\rho_F g \quad . \tag{3.13}$$

Combining Eqs. (3.8), (3.9), (3.11), (3.12), and (3.13) and solving for the dispersed gas volume fraction, we obtain

$$H_G = (12\rho_F \sin \eta/L'\rho_L)\Delta\mathcal{H}_F \quad . \tag{3.14}$$

Although Eq. (3.14) is written to incorporate only the hydrostatic pressure effect, in practice the manometer also detects a time-averaged dynamic pressure difference proportional to $\Delta(u_L^2/g_c)$ resulting from differences in the fluctuating turbulent fluid velocities at the manometer probe openings, one of which is closer to the impeller

than the other. Tests on the apparatus showed that in a non-gassed liquid, the manometer $\Delta\mathcal{H}_F$ increased with increasing rpm just as it would with increasing rpm in a gas-liquid dispersion wherein the gas holdup increases. Therefore, the $\Delta\mathcal{H}_F$ data must be adjusted for the effect of dynamic pressure differences before H_G can be determined from Eq. (3.14). For a turbulent fluid in a stirred-tank absorber, no theoretical means of determining this correction factor is, as yet, known. Empirically, the dynamic $\Delta\mathcal{H}_F$ in gas-free liquid was measured and correlated with the square of the impeller rotational speed. Aiba (80) has shown that the fluid tangential velocity at any point in a stirred tank is proportional to the impeller tip speed, ND_I. The correction was found to be linear in N^2 from 500 to 1600 rpm; values of the dynamic $\Delta\mathcal{H}_F$ are given in Appendix III.2.

All fraction gas holdup values reported were calculated according to

$$H_G = (12\rho_F \sin\eta/L'\rho_L)\left[(\Delta\mathcal{H}_F)_{total} - (\Delta\mathcal{H}_F)_{dyn.}\right], \qquad (3.15)$$

where $(\Delta\mathcal{H}_F)_{total}$ is the linear displacement of the manometer fluid in the agitated gas-liquid dispersion (includes the effects of both gas holdup and fluid dynamic pressure), and $(\Delta\mathcal{H}_F)_{dyn.}$ is the linear displacement of the manometer fluid due to only the dynamic pressure effect in the unsparged liquid at the same rpm.

Equation (3.15) assumes that the dynamic pressure difference at any rpm between the manometer taps is the same in the gas - liquid

dispersion as in the gas-free liquid. This assumption introduces an element of uncertainty into the results of the measurements.

Some previous investigators also measured gas holdup by manometric techniques, for example Calderbank (10) and Yoshida and Miura (72). No mention of the dynamic pressure contribution to $\Delta\mathcal{H}_F$ was made in these works, but it is difficult to see how their manometers were free from this source of interference.

e) Gas Bubble Average Diameter (d_b)

For the relatively small bubbles produced by the fluid shearing forces in the agitated electrolyte solutions, the bubble shape was assumed to be spherical. For such bubbles it can be shown that (10)

$$d_b = 6H_G/a(1 - H_G) . \qquad (3.16)$$

Since the average diameter of the bubbles is calculated from measured values of the fractional gas holdup, H_G , it is subject to the same degree of uncertainty discussed in the preceding section.

4. Analytical Measurements

a) Oxygen Tension

The oxygen tension of the liquid solutions was measured by steam-sterilizable dissolved oxygen probes of the galvanometric type discussed by Johnson, Borkowski, and Engblom (50), which were obtained from J. Borkowski. These probes use a lead anode, a silver cathode, and have an acetate buffer electrolyte; the membrane material is Teflon, 0.002 in. thick (before attaching to the probe). As described by Johnson et al. (50), the probes were found to have a very low residual

current (the current which flows in the absence of oxygen) of about 0.1 percent of the current generated in atmospheric air.

During operation, the electrodes were interconnected externally through a known resistance; resistance values of 500, 1000, 1100, and 1500 ohms could be selected by a rotary switch. The probe current through the resistor gave rise to a potential drop in the external circuit which was measured on either one of two 0 to 10 mV recorders.

The probe tip was located in the stirred tank 2 in. above the impeller radial centre line and 4-1/2 in. from the tank centre line.

As recommended by the supplier, the probes were autoclaved (121°C, 1 hr) while short-circuited as a conditioning step before use. They were calibrated in pure water saturated at 30°C and 1.0 atmosphere total pressure with various oxygen-nitrogen mixtures of known composition. The external potential drop across the resistor(s) was found to be linearly proportional to the solution oxygen tension over the range zero to 0.21 atm.

i) Membrane Oxygen Permeability (K_M)

The membrane's permeability to oxygen, defined by Eq. (2.51), was measured in steady-state by the application of Eq. (2.52), using air-saturated distilled water at 30°C.

For a measured membrane area of 0.203 cm^2 normal to the direction of oxygen flux, and using the nominal thickness of 0.00508 cm, the permeability was found to be $2.17(10^{-12})$ gmole O_2/cm-sec-atm. For similar material at the same temperature, Aiba et al. (57) obtained a K_M of $1.80(10^{-12})$ gmole O_2/cm-sec-atm.

The permeability of the membrane decreases as the probe ages. A decline of about 5 percent was observed over one 6-month period.

ii) Membrane Effective Diffusivity (D_M)

The effective oxygen diffusivity was measured shortly after first commissioning the probe by using the step change in oxygen tension procedure given by Aiba et al. (57). In this procedure, an arithmetic plot of E_t versus t is made. For the case of a step change from a deoxygenated to a completely oxygenated (with respect to air) aqueous phase, the area under the curve is defined as

$$q_t \equiv \int_0^{t_\infty} E_t dt ,$$

where t_∞ is the time following the step change at which E_t reaches its final value of E_∞. q_t is obtained by graphical integration, and the effective diffusivity can then be calculated from

$$D_M = L^2 E_\infty / \left[6(E_\infty t_\infty - q_t) \right] .$$

Step changes in both directions were made in duplicate, the change in probe external millivoltage being measured on the high-speed chart recorder. An example of one set of data is given in Appendix III. 4. The results of all four determinations agreed to within 10 percent, giving an average value of the effective diffusivity of $1.68(10^{-7})$ cm^2/sec, in general agreement with previously reported values (57).

The particular probe tested had a first time constant (1/e) of 9.70 sec, with a 90 percent response time of 48 sec.

b) Sulphite Oxidation

i) Exit Gas Concentration

As the reactor was vented to the atmosphere through open ports in the top head plate, a flow of exit gas confined in a pipe and having sufficient linear velocity to ensure that transport through an oxygen probe membrane was the controlling resistance was not available. A velocity criterion has been given by Aiba and Huang (81). Therefore, the oxygen partial pressure of the gas leaving the dispersion, $p_{4,2}$, was determined by Orsat analysis. The partial pressure so determined was in excellent agreement with the value calculated from a gas phase material balance, using the experimentally-determined absorption rate (see Appendix IV.12).

ii) Sulphite Ion Concentration

The sulphite ion concentration was determined by standard iodometric techniques (82). 2-ml samples of the aqueous phase were taken from the dispersion with a hypodermic syringe and transferred to a sealed serum bottle containing an excess (40 ml) of 0.100N iodine reagent under a nitrogen atmosphere wherein part of the iodine was reduced according to the reaction

$$SO_3^{=} + I_2 + H_2O \longrightarrow SO_4^{=} + 2H^{+} + 2I^{-} .$$

The unreacted iodine was back-titrated with 0.100N sodium thiosulphate, using a starch indicator:

$$I_2 + 2S_2O_3^{=} \longrightarrow 2I^- + S_4O_6^{=} .$$

Finally, the sulphite ion concentration was calculated as

$$\text{gmole } SO_3^{=}/\text{litre} = 1.0 - 0.025(\text{ml } 0.100\text{N Thio. added}).$$

Sulphite concentrations were plotted versus time, giving a straight line as long as the concentration of sulphite was greater than 0.05M. The value of $\Delta[SO_3^{=}]/\Delta t$ was determined from the slope.

The stoichiometry of the reaction of sulphite with oxygen, Eq. (2.37), leads to

$$R^r_{V4} = K^r_{L4}a(C^*_4 - C_{4B}) = -1/2(\Delta[SO_3^{=}]/\Delta t). \qquad (3.17)$$

We assume that the unmeasurable Henry's law coefficient for oxygen in the reactive sodium sulphite solution is the same as in non-reactive sodium sulphate of identical concentration. It is commonly assumed that the reaction proceeds with sufficient velocity such that $C_{4B} = 0$. Using the well-mixed dispersed-gas assumption in addition to the foregoing, Eq. (3.17) may be solved for $K^r_{L4}a$. Incorporating the numerical value of $H_{SO_4^{=}}$, the result is

$$K^r_{L4}a = -(0.184/p_{4,2})(\Delta[SO_3^{=}]/\Delta t. \qquad (3.18)$$

wherein $[SO_3^{=}]$ is expressed as molarity, the other symbols having the normal units used throughout this work.

c) Carbon Dioxide Absorption-with-Reaction

i) Gas Phase Analysis

The carbon dioxide content of the gaseous streams was determined chromatographically, using thermal conductivity detection.

The column used was 80/100 mesh Poropak Q in a 1/8-in. o.d. × 6-ft long stainless steel tube. The carrier gas was helium (Grade A).

The chromatograph operating conditions were: column temperature, 35°C; detector temperature, 42°C; carrier gas flow rate, 30 ml/min. Component elution order was air/nitrogen, carbon dioxide, and, finally, water vapour.

The chromatograph was equipped with a disc integrator. Carbon dioxide - nitrogen mixtures of known composition were used as calibration standards. The peak area - concentration relationship was linear over the range of interest (0.0001 to 0.10 mole fraction carbon dioxide)

ii) Liquid Phase Analaysis

Approximately 12 ml of sample was taken with a hypodermic syringe and transferred to a sealed serum bottle. 5 ml were later pipetted from the bottle into a beaker containing carbon-dioxide-free distilled water. The resulting solution was then titrated with standard HCl using a pH meter to endpoints of 8.30 and 3.70 pH, the former corresponding to neutralization of all the hydroxide plus one-half the carbonate, and the latter corresponding to complete neutralization of both species. The titrations were done in duplicate, the average result being used in the subsequent calculations.

The sodium sulphate and potassium chloride contents of the 0.11M Na_2SO_4 + KOH-K_2CO_3 and the 0.135M KCl + KOH-K_2CO_3 solutions studied consumed 0.18 and 0.10 ml of 0.1183N HCl, respectively, in the pH range 3.7 to 8.3 . These blanks were subtracted from the gross volume of acid titre in this range. The gross volume varied from about 3 ml to 7 ml over the runs.

Denoting T_1 as the volume of 0.1183N HCl titrated to pH 8.3, and T_2 as the net total volume of acid titrated to pH 3.7, the species molarities are calculated according to

$$\text{Molarity KOH} = 0.02366(2T_1 - T_2), \qquad (3.19)$$

$$\text{Molarity } K_2CO_3 = 0.02366(T_2 - T_1). \qquad (3.20)$$

Equations (3.19) and (3.20) are simply derived from the stoichiometry of the two-step neutralization.

5. Evaluation of Physical and Chemical Constants

a) Henry's Law Coefficient (H)

Oxygen and carbon dioxide solubilities at the gas-liquid interface for the electrolyte solutions were calculated from their solubilities in pure water at 30°C (83), using the method of van Krevelen and Hoftijzer (84), by which the solubility of gases in a solution of a single electrolyte can be predicted to within 10 percent. For the mixed electrolyte solutions, the method was modified incorporating the mixing rule suggested by Danckwerts and Sharma (64), the accuracy of which has not been experimentally evaluated. For absorption with reaction in the

fast or near-fast reaction regime, Eq. (2.101) shows that a 10 percent error on H_{kj} results in the same error in the calculated value of a .

b) Molecular Diffusivities (D_{Lk})

The aqueous phase dissolved gas diffusivities were estimated from the data of Ratcliff and Holdcroft for carbon dioxide (85), and the Wilke-Chang correlation (86). For oxygen, the reference diffusivity was taken as $2.41(10^{-5})$ cm^2/sec at 25°C (87).

c) CO_2 - OH^- Reaction Velocity Constant (k_2)

The second-order reaction velocity constant for the reaction described by Eq. (2.107) is dependent upon the species of hydroxyl base, the species of non-reactive electrolyte(s) present, and upon the solution ionic strength, Γ_T . The interaction of these parameters and its effect upon the magnitude of k_2 has not been fully evaluated to date, but a reasonable estimate of the value of k_2 can be obtained by interpolation of the data of Pinsent et al. (111) and Nijsing et al. (70).

For the reaction of CO_2 with potassium hydroxide in the test solutions, the value of k_2 was calculated from

$$k_2 = 12.4(10^6) \exp (0.392\,\Gamma_T) , \qquad (3.21)$$

where Γ_T is the total ionic strength defined as

$$\Gamma_T \equiv 1/2 \sum_j z_j^2 C_j , \qquad (3.22)$$

where z_j is the charge on the ionic species, and C_j is the concentration expressed as g-ion/litre.

For the highest ionic strength solution examined, namely 0.11M Na_2SO_4 + KOH - K_2CO_3 having an average Γ_T of 0.418 g-ion/litre, Eq. (3.21) shows that k_2 has a value 17.8 percent greater than at infinite dilution. For the calculation of a from Eq. (2.119), a 20 percent error in the estimated value of k_2 would result in a 10 percent error in a .

6. Range of Parameters Investigated

a) Solution Types and Ionic Strengths

For oxygen transfer from air, the physical absorption characteristics of the following aqueous solutions were studied: (1) 0.125, 0.250, 0.375, and 0.500M sodium sulphate with $4(10^{-3})$M cupric sulphate; (ii) an electrolyte solution used by Champagant (3) as a source of basal mineral salts in the production of biomass from hydrocarbon substrate, designated here as Medium A-1 and consisting of 1.6 g K_2HPO_4, 0.48 g $MgSO_4 \cdot 7H_2O$, 4.6 g NH_4Cl, 0.02 g NaCl (and 0.03 g HgI_2 -- a biocide to prevent microbial growth in the solution) per litre of distilled water; (iii) 0.11 and 0.22M KCl, and (iv) distilled water. Pertinent physicochemical properties of these solutions are given in Appendix III.3. Ionic strengths ranged from zero to 1.516 g-ion/litre.

The mass transfer of oxygen from air with chemical reaction was studied with the sulphite oxidation system used by Cooper, Fernstrom, and Miller (11). Initial sulphite ion concentration was 0.50M, and the reaction was catalysed by cupric ion, $4(10^{-3})$M.

The behaviour of $K_{L4}a$, k_{L4} , and a evaluated by the concurrent oxygen desorption, carbon dioxide absorption-with-reaction technique were studied in (i) KOH + K_2CO_3 , average Γ_T = 0.0965; (ii) 0.135M KCl + KOH-K_2CO_3, average Γ_T = 0.221, and (iii) 0.11M Na_2SO_4 + KOH-K_2CO_3, average Γ_T = 0.418. The latter two solutions have approximately the same ionic strengths as their counterparts studied solely for oxygen transfer from air, namely 0.22M KCl and 0.125M Na_2SO_4 + $4(10^{-3})$M $CuSO_4$.

b) Agitation - Aeration Parameters

The operating parameters were varied over the following ranges: impeller rotational speed, 400 to 2200 rpm; power input to the dispersion per unit volume of clear liquid, 40 to 22,400 ft-lb_f/min-ft^3, 0.0012 to 0.68 hp/ft^3 or 0.16 to 90.8 hp/1000 gal.; inlet gas rate 0.5 to 2.0 VVM or superficial gas velocity 0.00375 to 0.0150 ft/sec.

IV. RESULTS OF EXPERIMENTS

1. Overall Volumetric Mass Transfer Coefficient for Oxygen Without Chemical Reaction ($K_{L4}a$)

a) Distilled Water (Γ_T = 0.00 g-ion/litre)

Once-distilled water was obtained from the in-house distribution system. The interfacial tension with respect to air was measured by the DuNoüy ring tensiometer method and was found to have a value of 71.9 dynes/cm at 25°C, in close agreement with the reported value of 71.97 dynes/cm (83).

The value of $K_{L4}a$ at a given agitation - aeration rate was determined solely by the SBST, unsteady-state procedure. For the most part, oxygen from air was transiently absorbed; some desorption runs were made and the results of these agreed well with absorption measurements at the same agitation-aeration condition. It was not possible to use the CFST, steady-state method of evaluating $K_{L4}a$ in distilled water since the aqueous feed stream picked up sufficient surface-active trace contaminants from the feed tank and/or tubing such that reproducible results could not be obtained.

$K_{L4}a$ results for distilled water are correlated with agitation power input per unit liquid volume of the dispersion (P_G/V_L) on Fig. (4.1), the value of $K_{L4}a$ being computed from the LSQVMT computer fitting programme. The data are tabulated in Appendix IV.1. P_G/V_L has been expressed in units of ft-lb_f/min-ft^3 on all graphical correlations to facilitate comparison with previous work, e.g. (11).

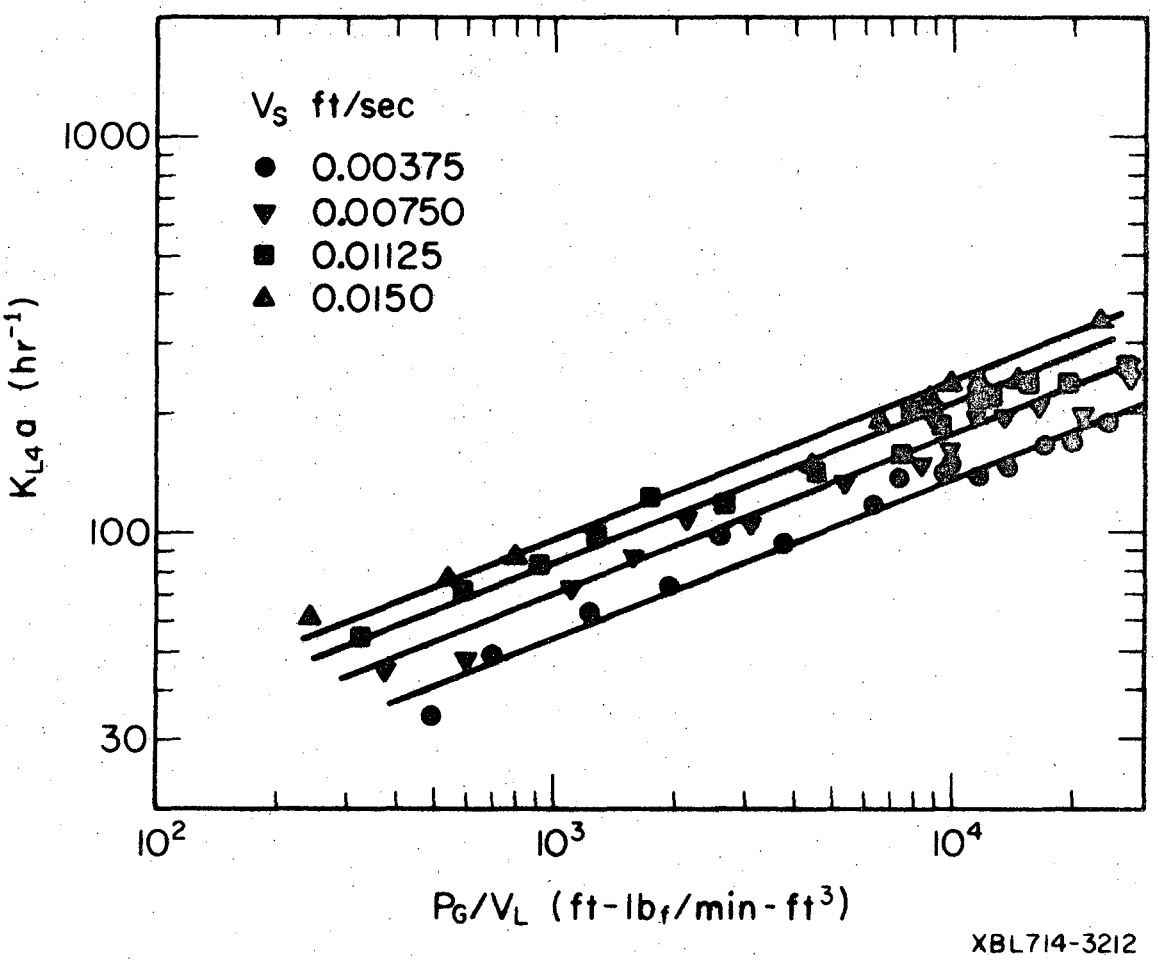

Fig. 4.1. Overall Volumetric Mass Transfer Coefficient for Oxygen in Water.

Figure (4.1) shows that the $K_{L4}a$ - $(P_G/V_L)^n$ relationship is linear over the power input range studied. From cross plots of the data obtained at different aeration rates, $K_{L4}a$ was found to correlate linearly with superficial gas velocity expressed as $(v_S)^m$. Further, there appears to be no effect of v_S on the value of n.

$K_{L4}a$ is plotted against the impeller rotational speed, N, on Fig (4.2). Unlike the correlation with P_G/V_L, the $K_{L4}a$ versus N behaviour is not constant over the entire range of agitation rate, and, when correlated in this manner, v_S has a pronounced effect on the slope of the lines at values of N greater than 1200.

By linear least-squares fitting of the data, for distilled water $K_{L4}a$ varies according to

$$(K_{L4}a)_{H_2O} = 6.62(10^{-3})(P_G/V_L)^{0.4}(v_S)^{0.35} + (1.59)(10^{-3}). \qquad (4.1)$$

The fractional gas holdup at a superficial gas velocity of 0.0150 ft/sec was measured manometrically and calculated from Eq. (3.15). As a check on the manometric method (which incorporates a correction factor for dynamic pressure effects), the initially ungassed tank was completely filled with water (initial volume 5180 cm^3); upon sparging the tank, the gas holdup displaced an equivalent amount of water through an opening in the top head plate, the displaced water being collected in a graduated cylinder. The results of the manometric and displacement measurements are compared in Appendix IV.2. The holdup values computed from the liquid displacements are generally less than the values calculated from the manometric measurements. Visually, it was noted that the holdup was not uniformly distributed over the height

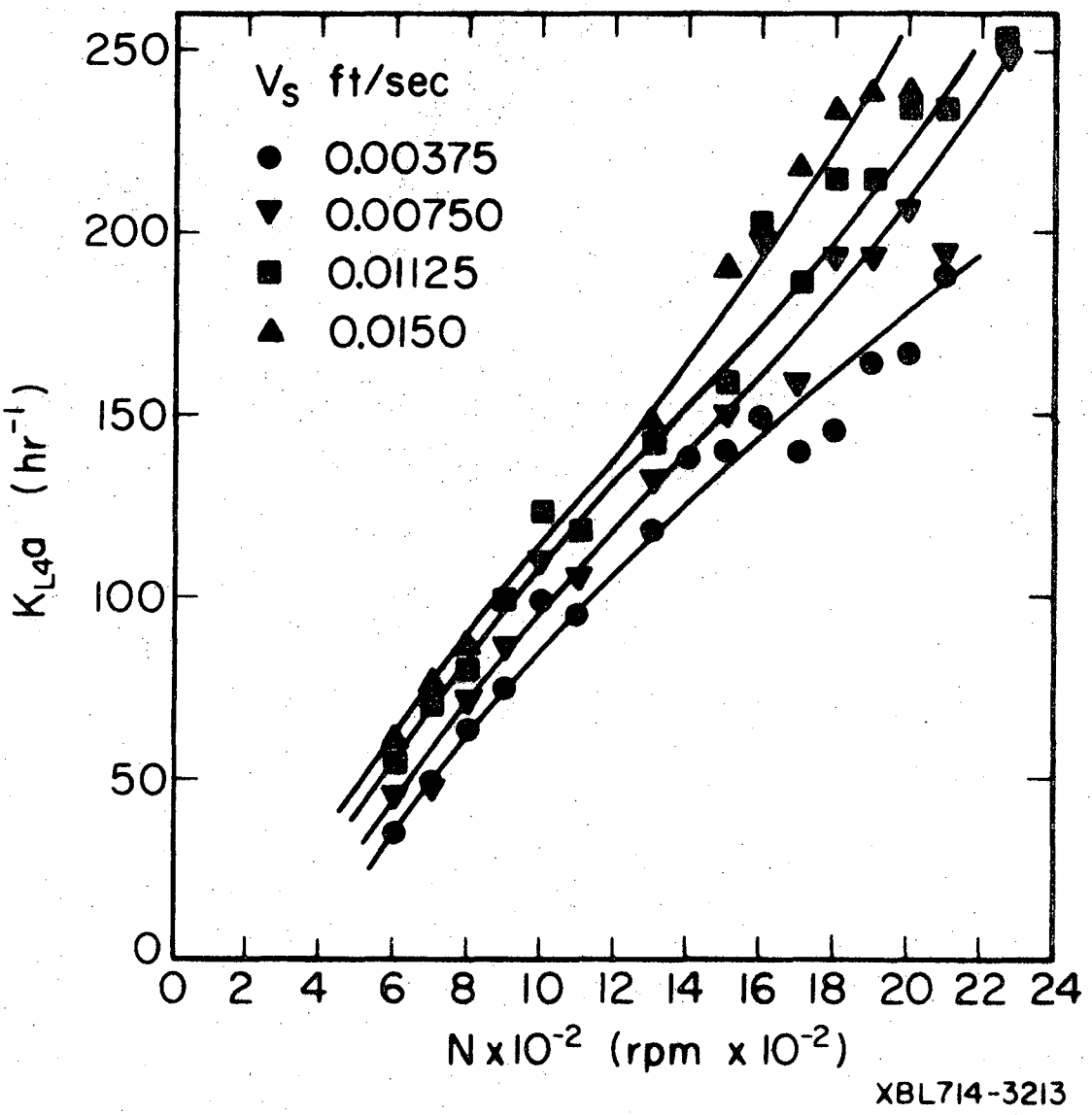

Fig. 4.2. Overall Volumetric Mass Transfer Coefficient for Oxygen in Water.

of the tank, being greater in the bottom half (impeller region) where the manometer probe was located than in the top half; thus, it is reasonable to expect that the displacement method which measures an average holdup in the total tank contents will result in lower holdup values than the manometer method which, in this case, reflected the greater holdup in the bottom region of the tank.

The values of H_G determined from the manometer readings correlate well with $(P_G/V_L)^{0.4}$, in agreement with the results of Calderbank (10) in tanks of identical geometric ratios.

b) 0.10M KCl (Γ_T = 0.10 g-ion/litre)

$K_{L4}a$ behaviour in 0.10M reagent-grade KCl in distilled water was determined at two aeration rates by using the CFST, steady-state method whereby $K_{L4}a$ is calculated from Eq. (2.35) in conjunction with Eq. (2.56). The experimental parameters are tabulated in Appendix IV.3; $K_{L4}a$ correlated well with P_G/V_L, as shown on Fig. (4.3).

In this solution, the $K_{L4}a$ - $(P_G/V_L)^n$ dependency is also linear over the range of power input investigated, n in this case having a value of 0.63. Having investigated the effect of aeration rate at only two different rates, it is tentatively concluded that m is 0.62 in this system, such that overal the $K_{L4}a$ behaviour may be described by

$$(K_{L4}a)_{0.10M\ KCl} \propto (P_G/V_L)^{0.63}(v_S)^{0.62}. \qquad (4.2)$$

Plots of $K_{L4}a$ versus N for this system are non-linear. The value of $K_{L4}a$ when correlated with N depends upon v_S, but, in

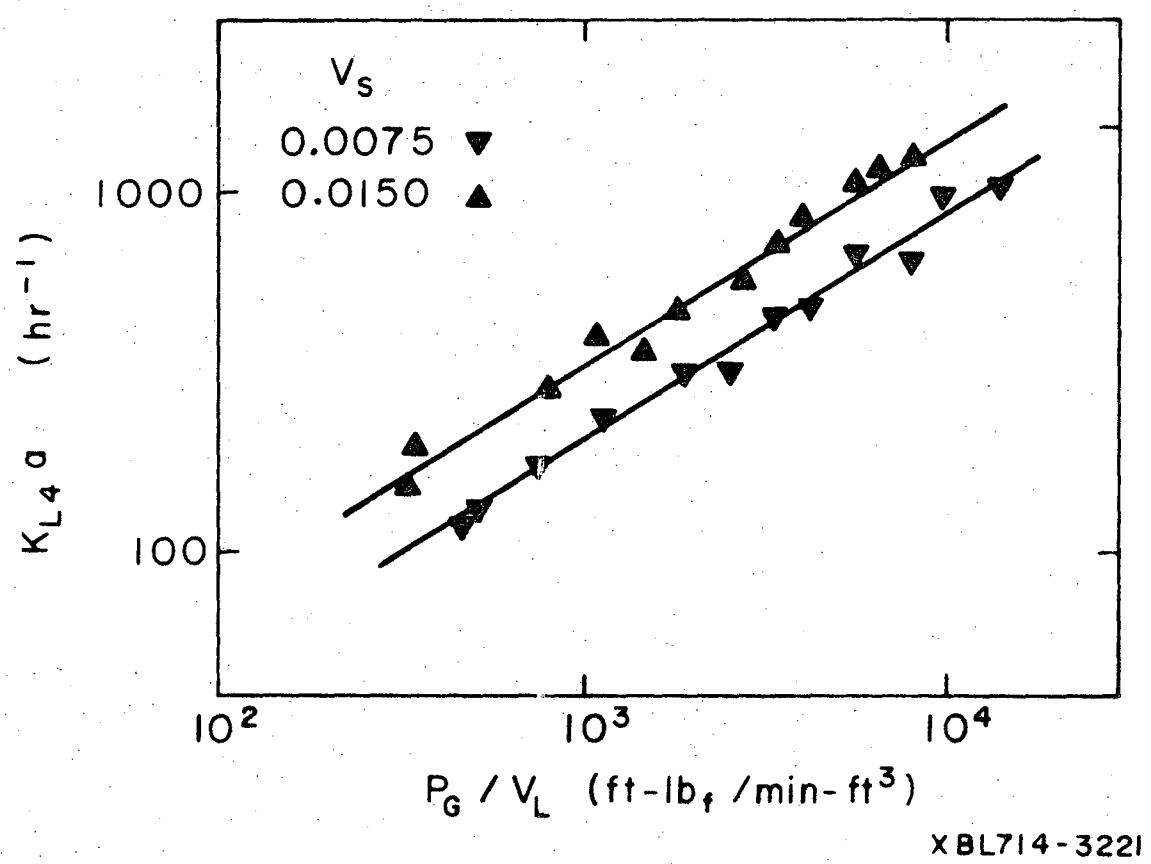

Fig. 4.3. Overall Volumetric Mass Transfer Coefficient for Oxygen in 0.10M KCl.

addition, the value of v_S affects the shape of the $K_{L4}a$ - N relationship at values of N greater than 1200 rpm.

The aeration rate has a greater effect upon $K_{L4}a$ in this solution than in any of the others which were tested in this study; the value of the v_S exponent m being 0.62 in some 50 percent greater than its value in other solutions or in water. The reason for this anomaly is not known.

c) Medium A-1 (Γ_T = 0.136 g-ion/litre)

i) CFST, Steady-State Measurement

The $K_{L4}a$ a behaviour of this basal mineral salt medium was determined over the entire range of aeration rates used in this study.

The experimental data are tabulated in Appendix IV. 4, while the correlation with P_G/V_L is shown on Fig. (4.4). Except at the extreme upper end of the power input range, the correlation is linear in $(P_G/V_L)^n$; $K_{L4}a$ is dependent upon $(v_S)^m$ throughout, such that

$$(K_{L4}a)_{Med.A-1} = 3.29(10^{-3})(P_G/V_L)^{0.71}(v_S)^{0.43} \qquad (4.3)$$

for values of $(P_G/V_L)^{0.71}(v_S)^{0.43}$ less than 60.3.

$K_{L4}a$ for this mixed electrolyte solution did not correlate well with impeller rotational speed, as shown on Fig. (4.5). The behaviour at each aeration rate exhibits a greater degree of non-linearity as compared to the P_G/V_L correlation. Again, the exact nature of the dependency of $K_{L4}a$ upon N is, in turn, dependent upon the particular value of v_S , whereas when correlated with P_G/V_L , the value of the agitation exponent n is independent of the value of v_S .

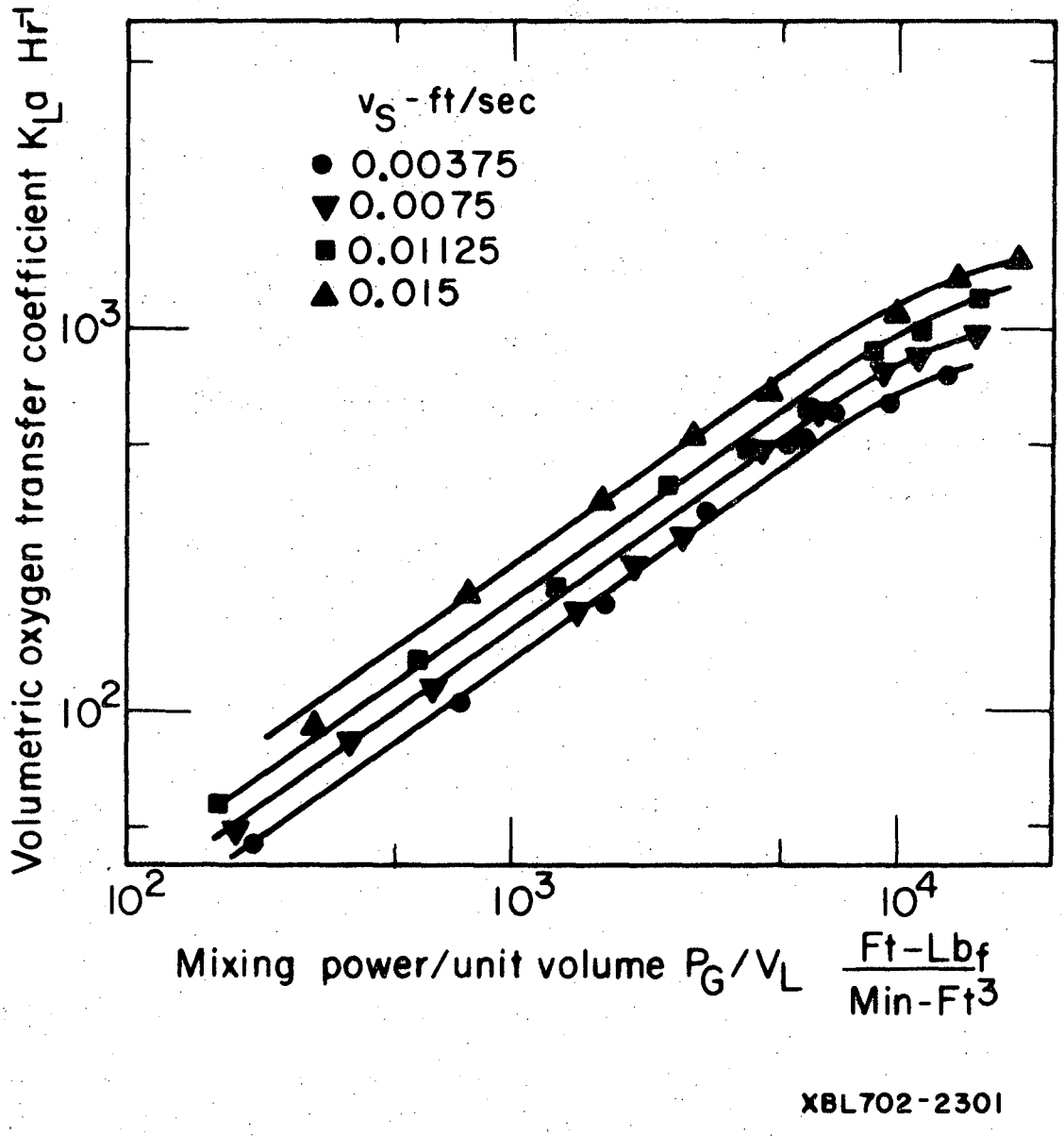

Fig. 4.4. Overall Volumetric Mass Transfer Coefficient for Oxygen in Medium A-1: Steady-State Measurements.

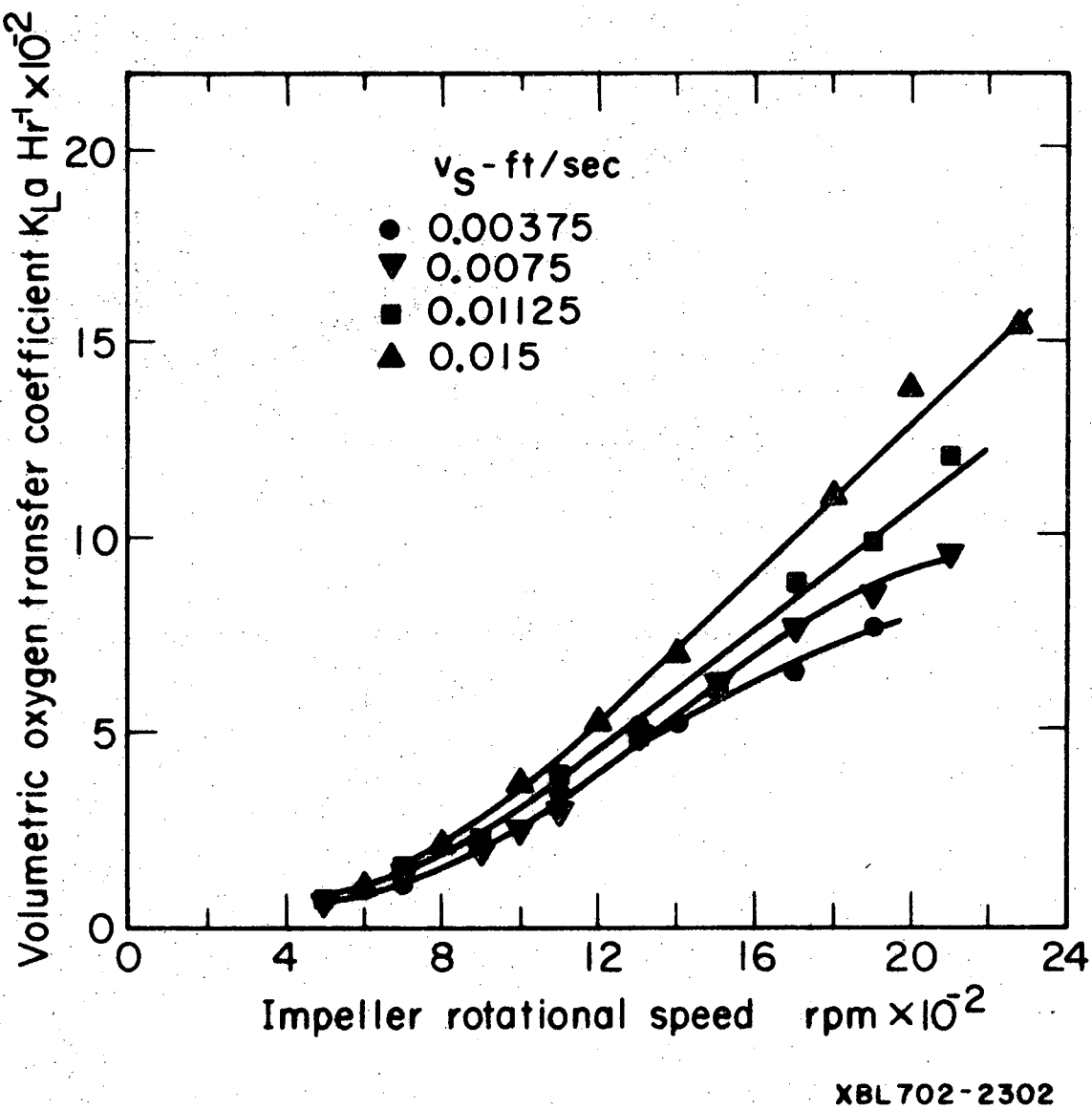

Fig. 4.5. Overall Volumetric Mass Transfer Coefficient for Oxygen in Medium A-1: Steady-State Measurements.

ii) SBST, Unsteady-State Measurement

The validity of the transient absorption model, Eq. (2.75), was tested at each of the four aeration rates over the entire agitation power range. $K_{L4}a$ values computed from the LSQVMT computer programme best-fit value of β are tabulated in Appendix IV.5. The transiently-determined $K_{L4}a$'s are compared to the steady-state results on Fig. (4.6).

On Fig. (4.6), the lines represent the $K_{L4}a$ dependencies upon P_G/V_L as determined by the CFST, steady-state method (Fig. 4.4), while the points are the $K_{L4}a$ values determined from the unsteady-state procedure. The agreement is quite good, regardless of the simplifying assumptions applied in the development of the transient model, except at the lower end of the power range where the impeller rotational speed is less than 1000 rpm. At these low rpm's, it is likely that the dispersed gas phase is not well-mixed, particularly in electrolyte solutions where the bubble coalescence required for gas mixing is hindered (see further discussion in Section V.). As expected, the deviation between the steady-state and the unsteady-state results is greater the smaller the aeration rate where the transient model assumptions regarding the gas-phase behaviour are less valid.

d) 0.22M KCl (Γ_T = 0.22 g-ion/litre)

In this system, $K_{L4}a$ was determined by the CFST, steady-state method at two values of the aeration rate. The data are tabulated in Appendix IV.6, and the $K_{L4}a$ correlation with P_G/V_L is shown on Fig. (4.7). Here again the general linearity of $K_{L4}a$ with $(P_G/V_L)^n$

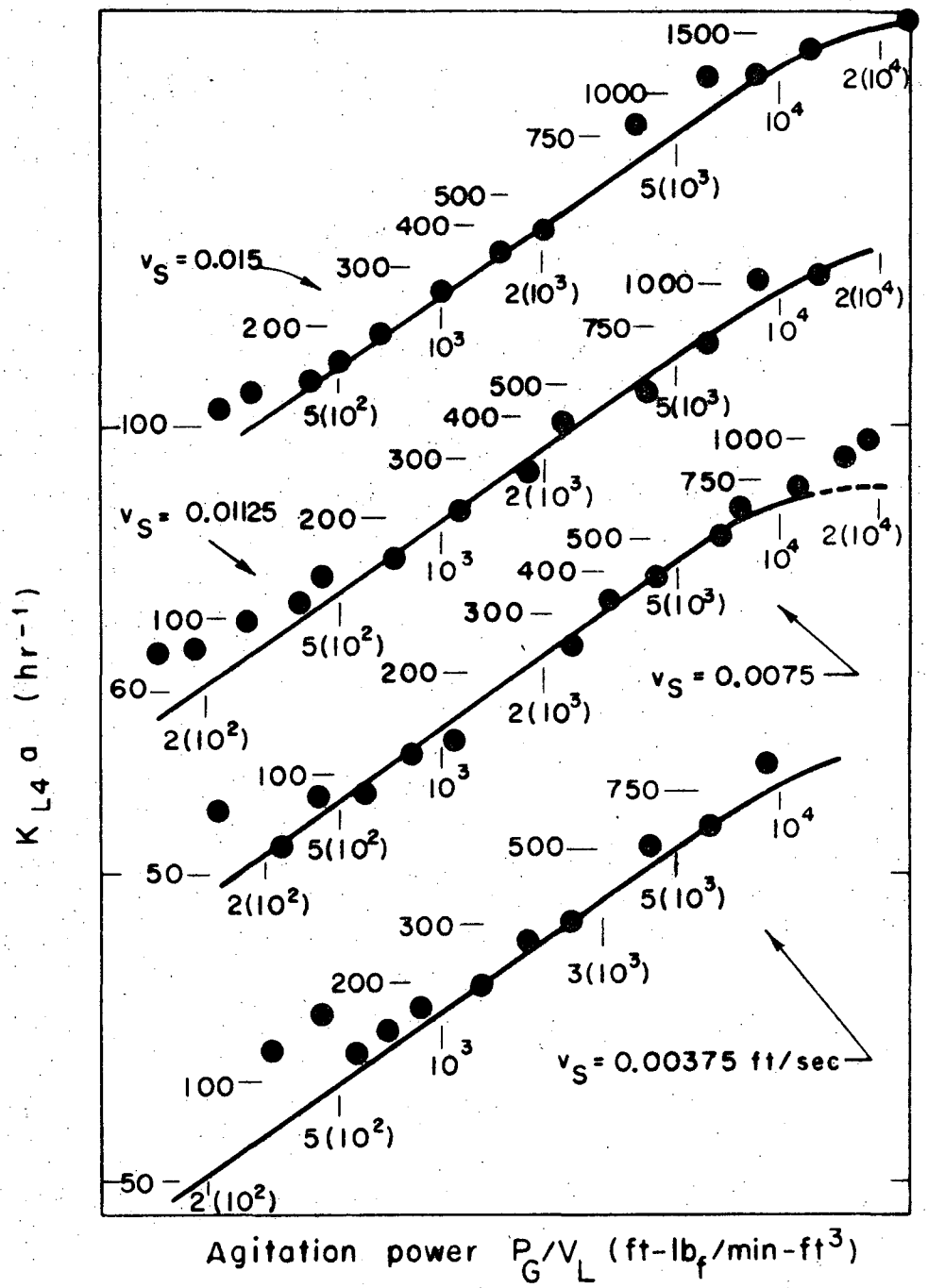

XBL711-2660

Fig. 4.6. Comparison of $K_{L4}a$ Values in Medium A-1 Determined by Unsteady-State Probe Response (Data Points) and Steady-State Measurements (Lines).

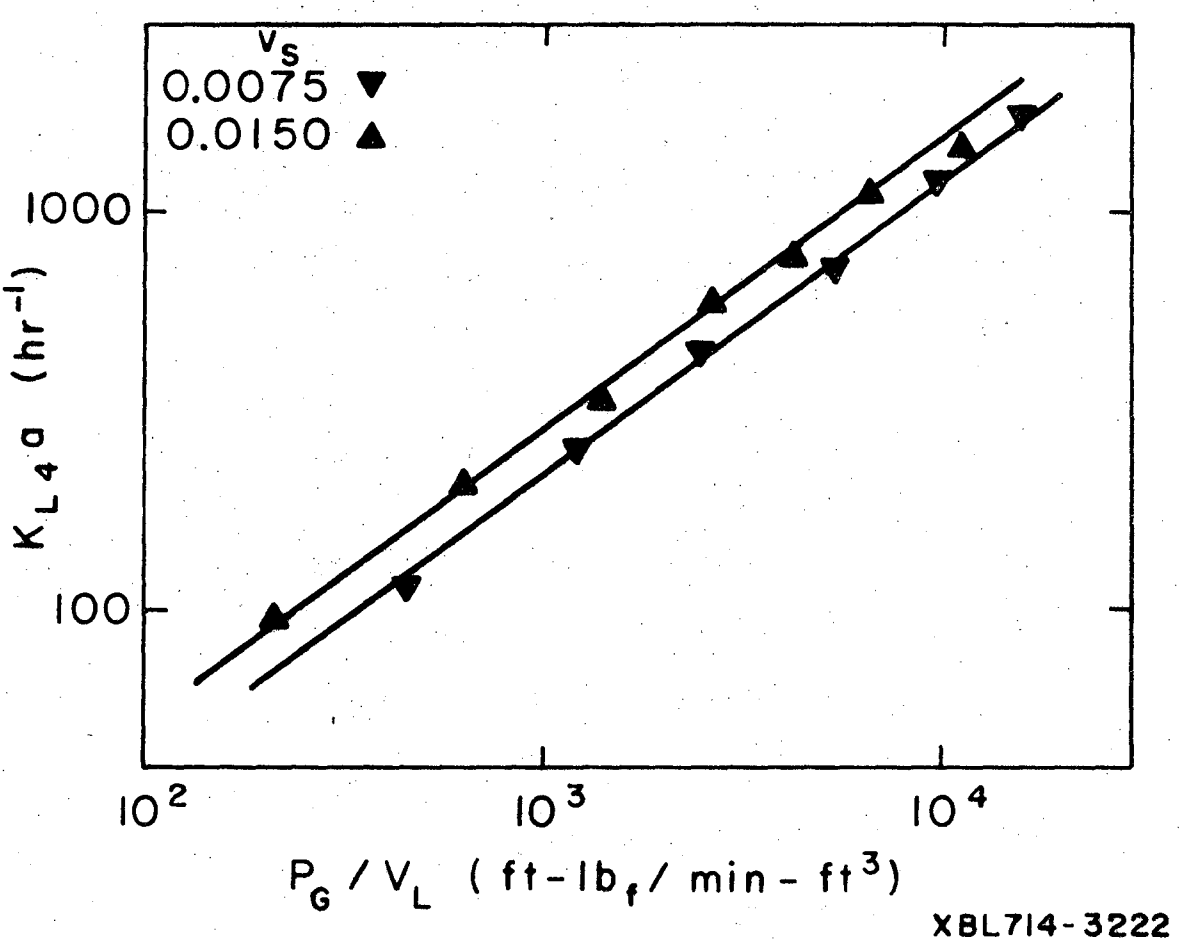

Fig. 4.7. Overall Volumetric Mass Transfer Coefficient for Oxygen in 0.22M KCl.

is clearly evident, as is the dependency of $K_{L4}a$ upon v_S. The value of the aeration exponent m is not precisely defined since only two aeration rates were investigated. However, for the range of parameters investigated with this solution,

$$(K_{L4}a)_{0.22MKCl} = 2.17(10^{-3})\,(P_G/V_L)^{0.74}(v_S)^{0.36} \quad . \qquad (4.4)$$

As in the previous systems, the $K_{L4}a$ correlation with N is non-linear over the entire range of impeller rotational speed. In the region $600 \leq N \leq 1400$, $K_{L4}a$ is directly proportional to N. However, at higher agitation rates, $K_{L4}a$ increases non-linearly with increasing N, the slope of the curve becoming increasingly positive.

e) Sodium Sulphate - 0.004M Cupric Sulphate Solutions

The $K_{L4}a$ behaviour of sodium sulphate solutions was investigated since they are a physical absorption without chemical reaction analog of the sulphite oxidation system. A range of sulphate concentrations was tested, namely: 0.125, 0.250, 0.375, and 0.500M sodium sulphate, each of which contained 0.004M cupric sulphate (the sulphite oxidation catalyst). The total ionic strength of the solutions ranged from 0.391 to 1.516 g-ion/litre.

In a separate series of screening experiments, it was determined that the value of $K_{L4}a$ at a fixed agitation-aeration rate condition was dependent upon the concentration of electrolyte in the solution when the sodium sulphate concentration was less than about 0.1M. The results of one such investigation are shown on Fig. (4.8). It was concluded that the value of $K_{L4}a$ reached an upper limit which was independent of the

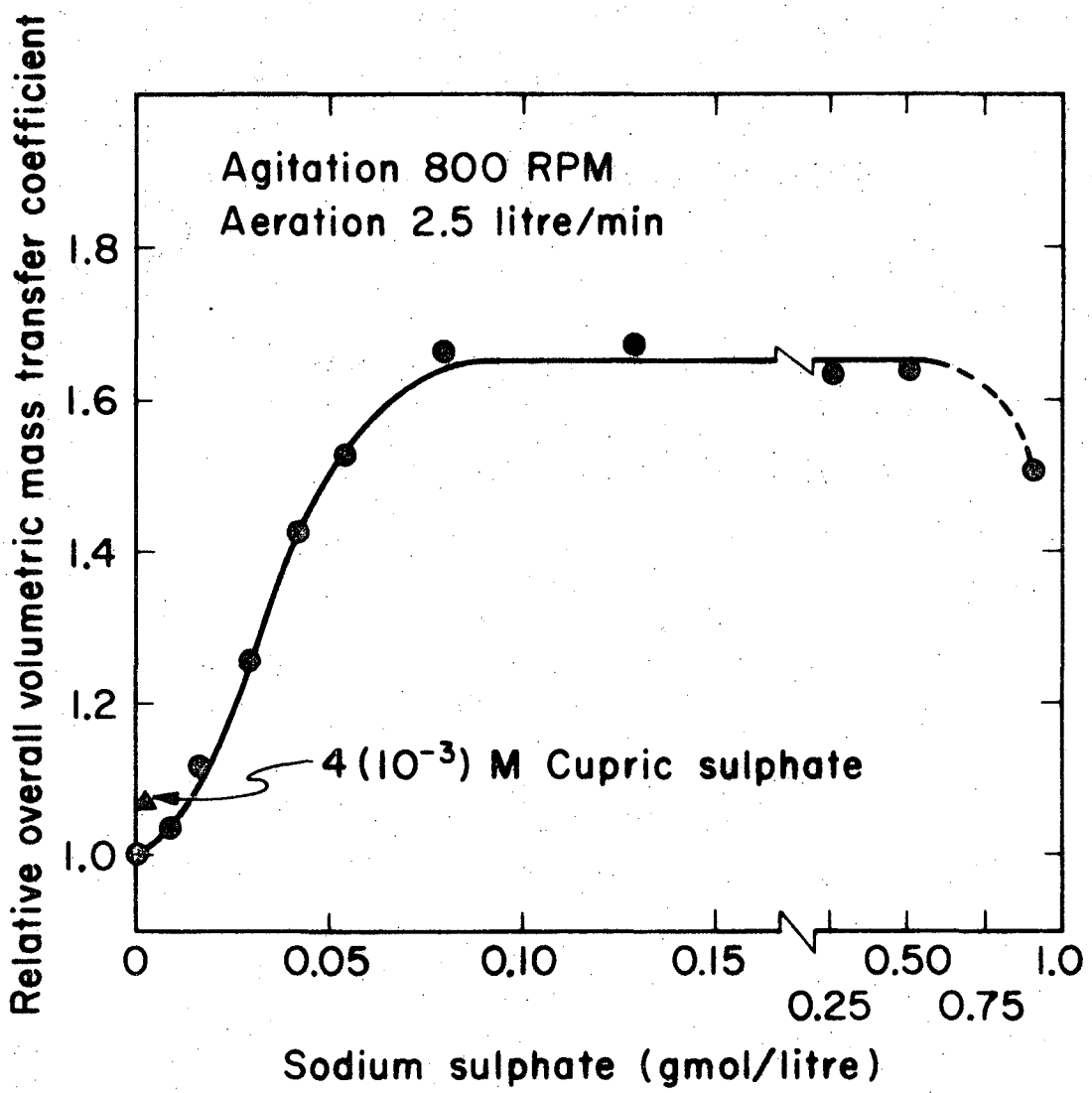

Fig. 4.8. Effect of Sodium Sulphate Concentration on $K_{L4}a$.

electrolyte concentration when the latter exceeded 0.1M. Therefore, the majority of the experimental determination of $K_{L4}a$ were made in 0.125M Na_2SO_4 - 0.004M $CuSO_4$ solution, with the behaviour of the three other sulphate concentrationsolutions being studied less intensively.

i) CFST, Steady-State Measurements with 0.125M Na_2SO_4 - 0.004M $CuSO_4$

Experimental results for this system are tabulated in Appendix IV.7.

The correlation of $K_{L4}a$ with P_G/V_L is given on Fig. (4.9). The correlation is linear with respect to $(P_G/V_L)^n$ in the mid-power range, and exhibits non-linearities at both the low and high ends of the power range.

At agitation power inputs greater than 7000 ft-lb_f/min-ft^3, the behaviour exhibited on Fig. (4.9) indicates that there is little or no effect of v_S upon $K_{L4}a$ if v_S is greater than or equal to 0.0075 ft/sec.

For power inputs in the range of linear $K_{L4}a$ versus $(P_G/V_L)^n$ behaviour

$$(K_{L4}a)_{0.125M\ SO_4^=} = 0.725(10^{-3})(P_G/V_L)^{0.90}(v_S)^{0.39} \qquad (4.5)$$

for values of $(P_G/V_L)^{0.90}(v_S)^{0.39}$ less than 238.

Unlike the other solutions tested (excepting 0.22M KCl), when $K_{L4}a$ for 0.125M sulphate is correlated with impeller rotational speed, the correlation does not appear to be affected by the aeration rate, as shown on Fig. (4.10). The correlation of Fig. (4.10) is linear over a large part of the agitation rate range (a larger part of the range

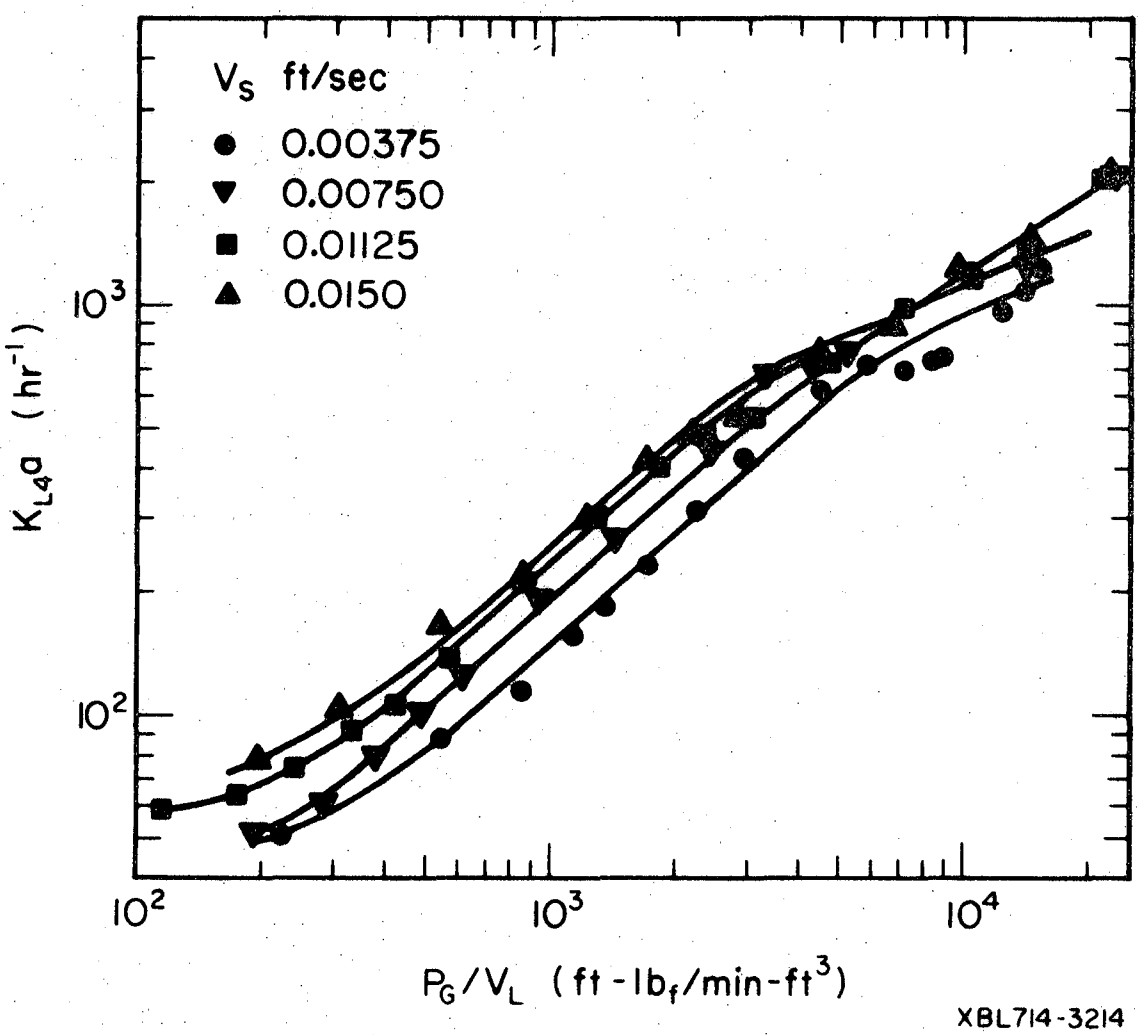

Fig. 4.9. Overall Volumetric Mass Transfer Coefficient for Oxygen in 0.125M Na_2SO_4 + 0.004M $CuSO_4$.

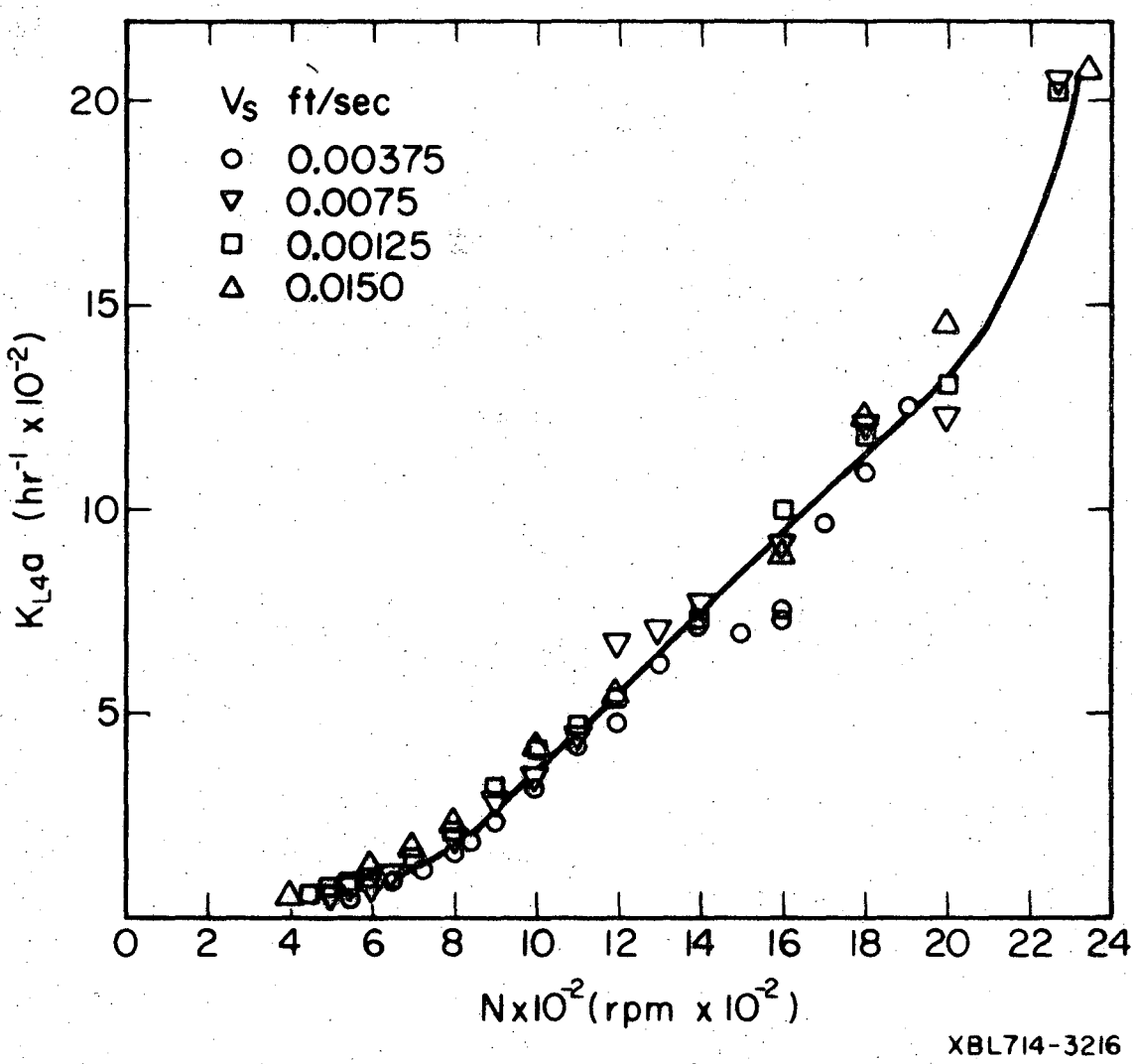

Fig. 4.10. Overall Volumetric Mass Transfer Coefficient for Oxygen in 0.125M Na_2SO_4+ 0.004M $CuSO_4$.

than in the case of 0.22 M KCl).

ii) SBST, Unsteady-State Measurement

All four concentrations of sulphate solution--0.125M, 0.250M, 0.375M, 0.500M, each with 0.004M cupric sulphate--were studied by using the transient absorption technique. The computer-calculated results for the four solutions are tabulated in Appendices IV.8, IV.9, IV.10, and IV.11.

The transiently-determined values of $K_{L4}a$ are compared to the steady-state correlations on Figs. (4.11), (4.12), (4.13), and (4.14). As found for Medium A-1 (Fig. 4.6), the agreement at each value of the aeration rate appears to be reasonably good, except at the low end of the power input range where perfect gas mixing in the dispersion is not assured. From Figs. (4.11) to (4.14), inclusively, it is evident that the value of $K_{L4}a$ at a given agitation - aeration rate is independent of the sulphate concentration over the range 0.125 to 0.500M, in agreement with the results of the preliminary screening tests (Fig. 4.8).

2. Overall Volumetric Mass Transfer Coefficient for Oxygen with Chemical Reaction ($K^r_{L4}a$)

$K^r_{L4}a$ results for the absorption with chemical reaction of oxygen from air in the 0.50M sulphite oxidation system are tabulated in Appendix IV.12.

The correlation of $K^r_{L4}a$ with P_G/V_L is shown on Fig. (4.15). The behaviour of $K^r_{L4}a$ is analogous to that of $K_{L4}a$ in sodium sulphate (Fig. 4.9) in that the slopes of the lines in the linear regions are identical ($n = 0.90$ in both cases), the aeration rate dependency is almost identical ($m = 0.38$ for sulphite, 0.39 for sulphate), and there is a similar deviation

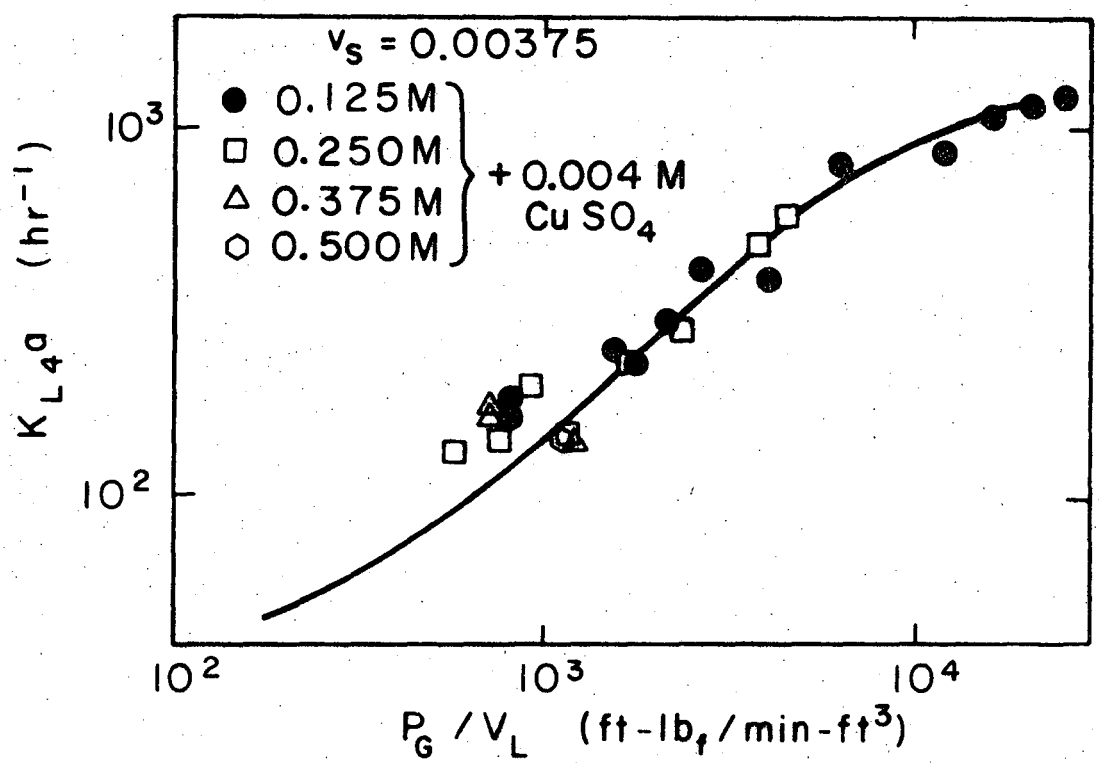

XBL 714-3229

Fig. 4.11. Comparison of $K_{L4}a$ Values in 0.125M Na_2SO_4 + 0.004M $CuSO_4$ Determined by Unsteady-State Probe Response (Data Points) and Steady-State Measurement (Line).

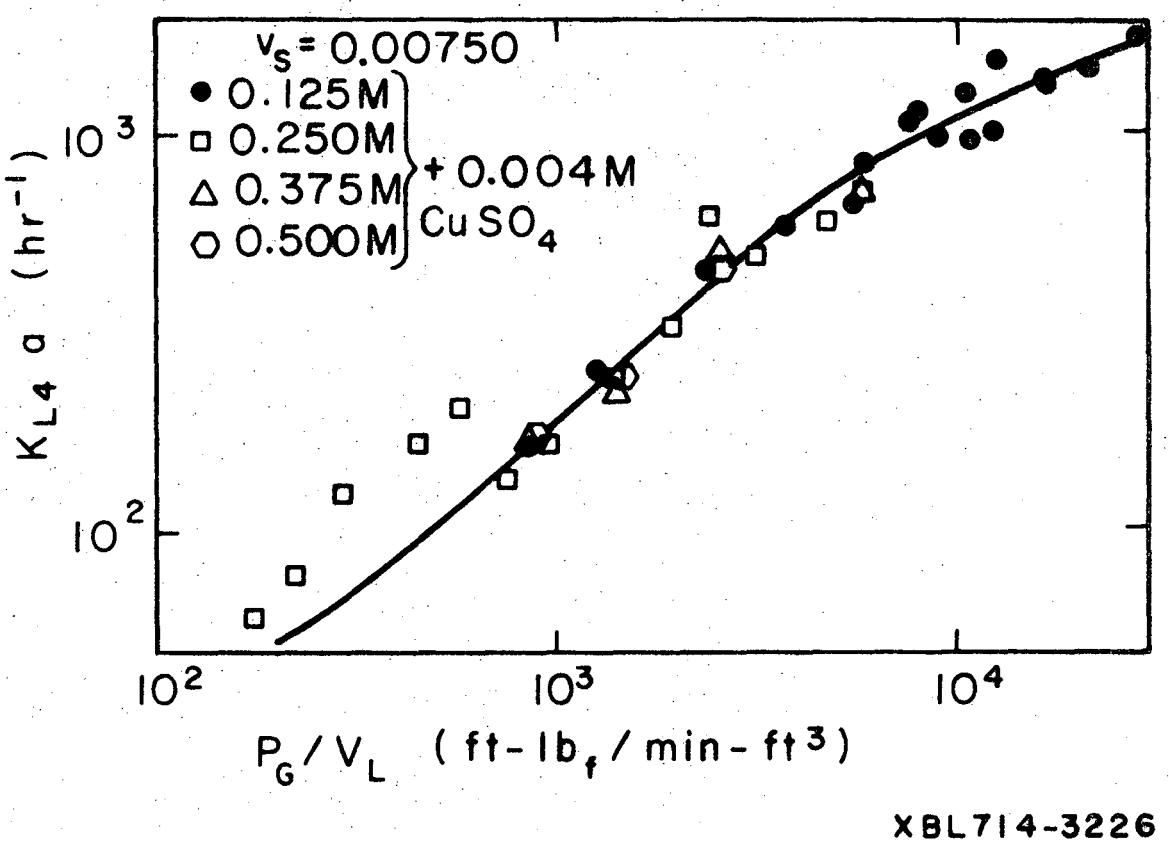

Fig. 4.12. Comparison of $K_{L4}a$ Values in Na_2SO_4 + 0.004M $CuSO_4$ Determined by Unsteady-State Probe Response (Data Points) and Steady-State Measurement (Line).

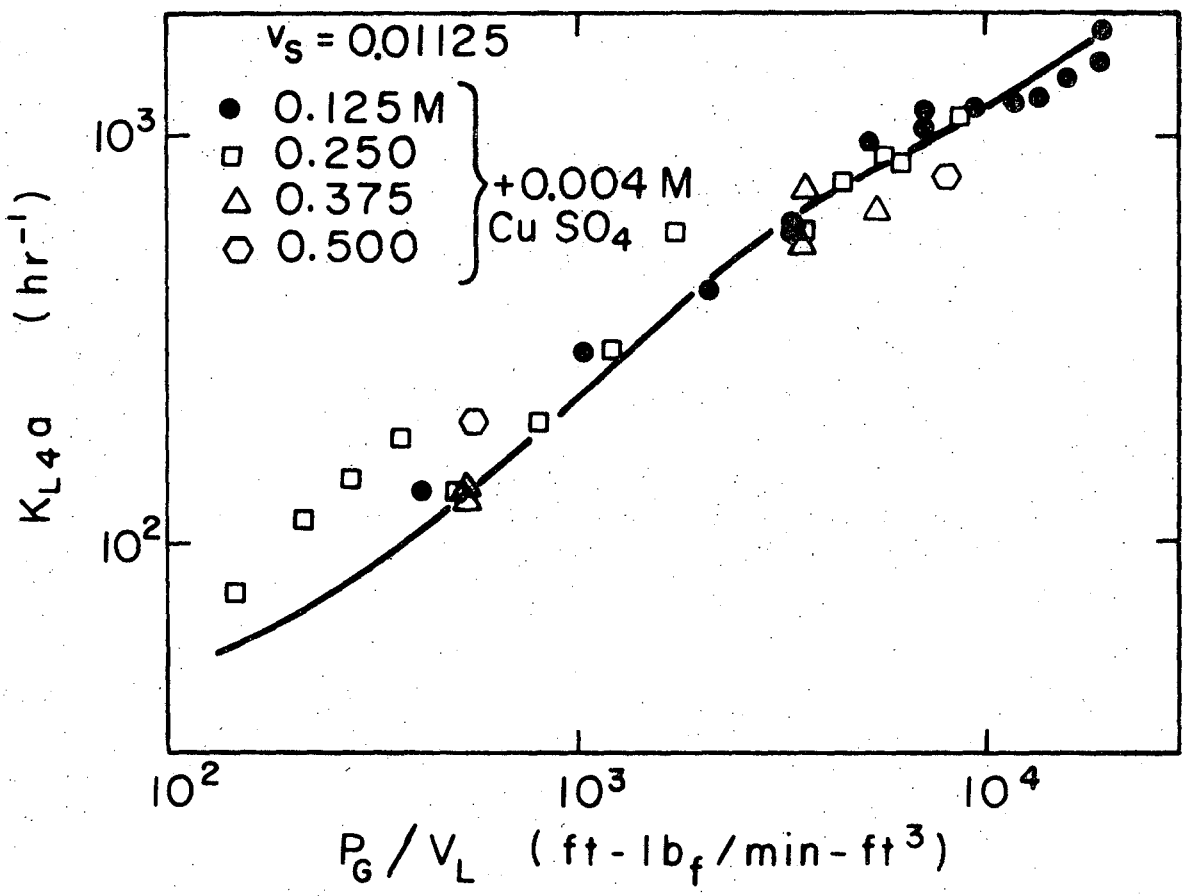

XBL 714-3219

Fig. 4.13. Comparison of $K_{L4}a$ Values in Na_2SO_4 + 0.004M $CuSO_4$ Determined by Unsteady-State Probe Response (Data Points) and Steady-State Measurement (Line).

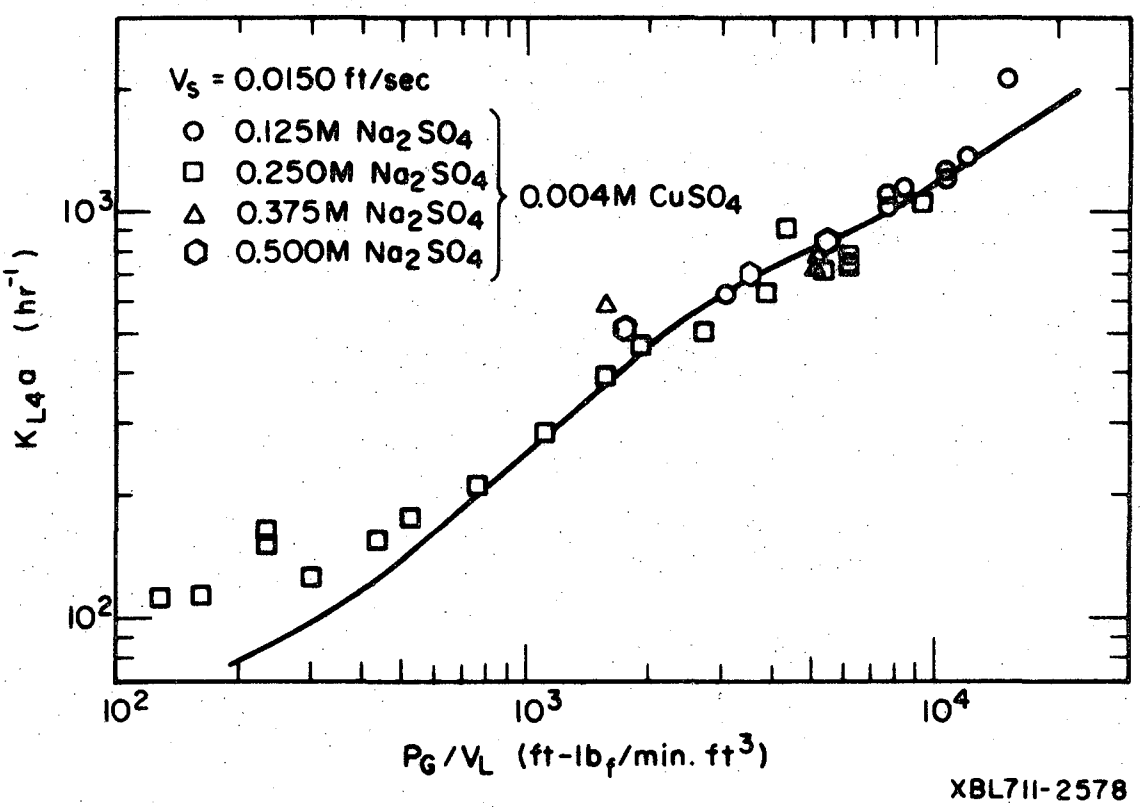

Fig. 4.14. Comparison of $K_{L4}a$ Values in Na_2SO_4 + 0.004M $CuSO_4$ Determined by Unsteady-State Probe Response (Data Points) and Steady-State Measurement (Line).

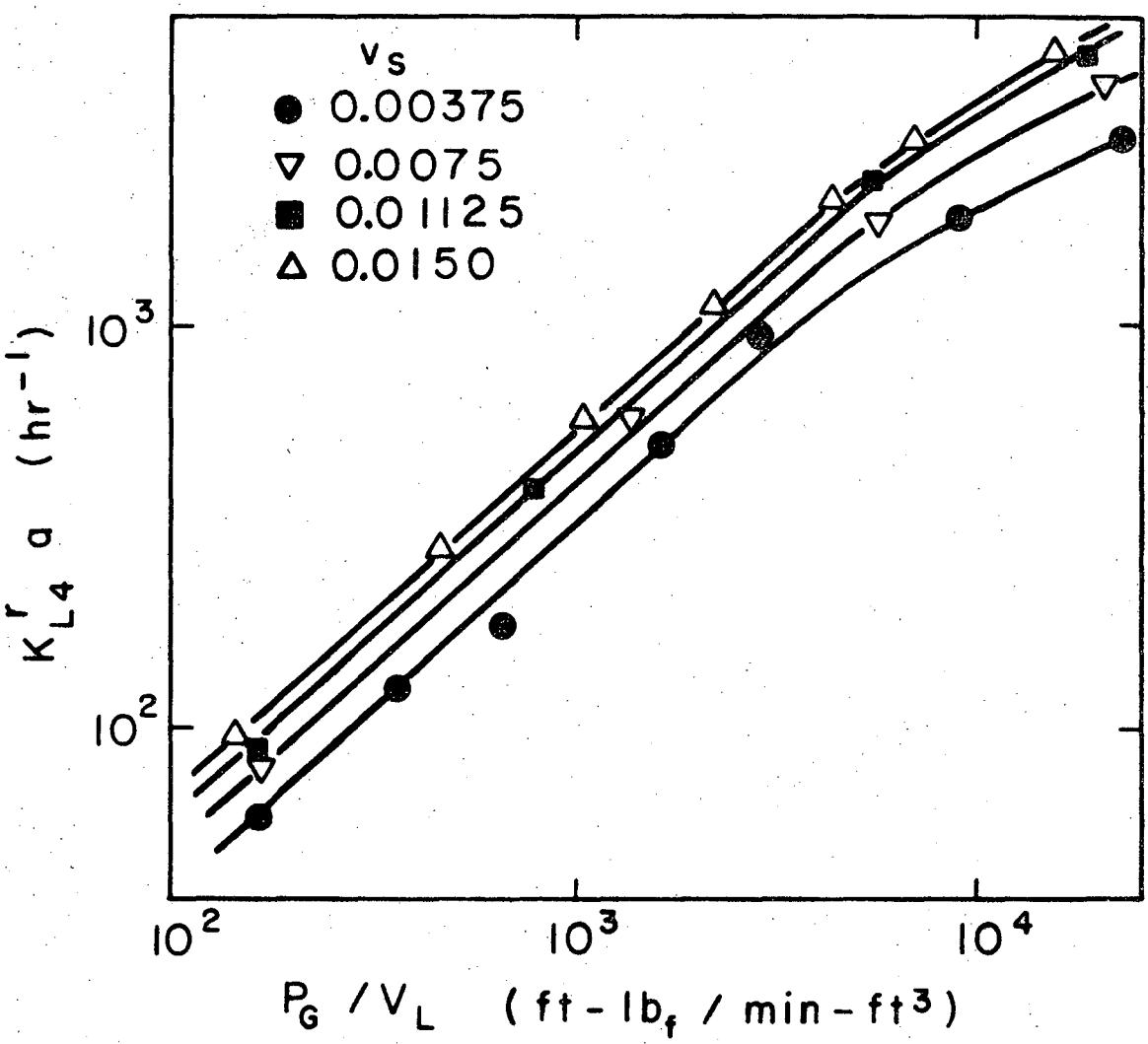

Fig. 4.15. Overall Volumetric Mass Transfer Coefficient for Oxygen with Chemical Reaction in 0.50M Na_2SO_3 + 0.004M $CuSO_4$.

from linearity at the high end of the agitation power range. However, at the same agitation power and rate of aeration, $K^r_{L4}a$ in the sulphite solution is greater than $K_{L4}a$ in sulphate solution by a factor of 2.1.

In the sulphite oxidation system, for the stirred tank used in this study, the $K^r_{L4}a$ dependency upon the agitation and aeration parameters is given by

$$K^r_{L4}a = 1.52(10^{-3})(P_G/V_L)^{0.90}(v_S)^{0.38} \qquad (4.6)$$

for values of $(P_G/V_L)^{0.90}(v_S)^{0.38}$ less than 412.

Correlation of $K^r_{L4}a$ with impeller rotational speed resulted in linear relationships for values of N greater than 1000 rpm, as shown on Fig. (4.16). However, the $K^r_{L4}a$ - N relationship is not independent of the aeration rate at low values of v_S, but appears to become independent of v_S when the superficial velocity reaches 0.01125 ft/sec or greater.

3. Comparison of Oxygen Overall Volumetric Mass Transfer Coefficients

A comparison of the $K_{L4}a$ and $K^r_{L4}a$ dependencies upon P_G/V_L for some of the solutions tested at superficial gas velocities of 0.00375 and 0.0150 ft/sec is given on Figs. (4.17) and (4.18), respectively.

At all aeration rates the $K_{L4}a$ values for purely physical absorption of oxygen in the non-reactive electrolyte solutions examined are appreciably greater than $K_{L4}a$ values in distilled water and are less than $K^r_{L4}a$ values obtained by the sulphite oxidation method. The differences are most pronounced at values of P_G/V_L greater than 5000 ft-lb_f/min-ft^3.

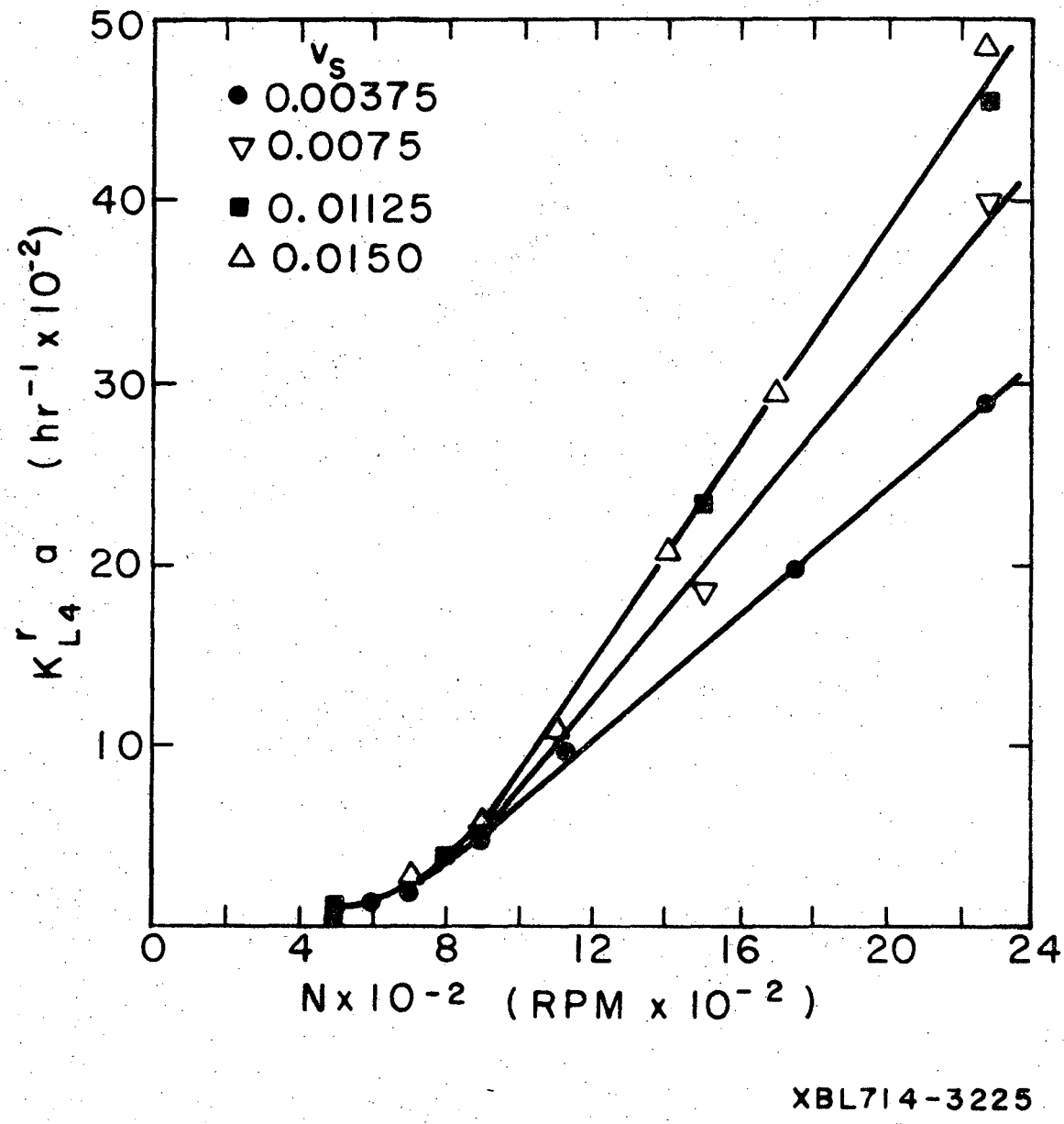

Fig. 4.16. Overall Volumetric Mass Transfer Coefficient for Oxygen with Chemical Reaction in 0.50M Na_2SO_3 + 0.004M $CuSO_4$.

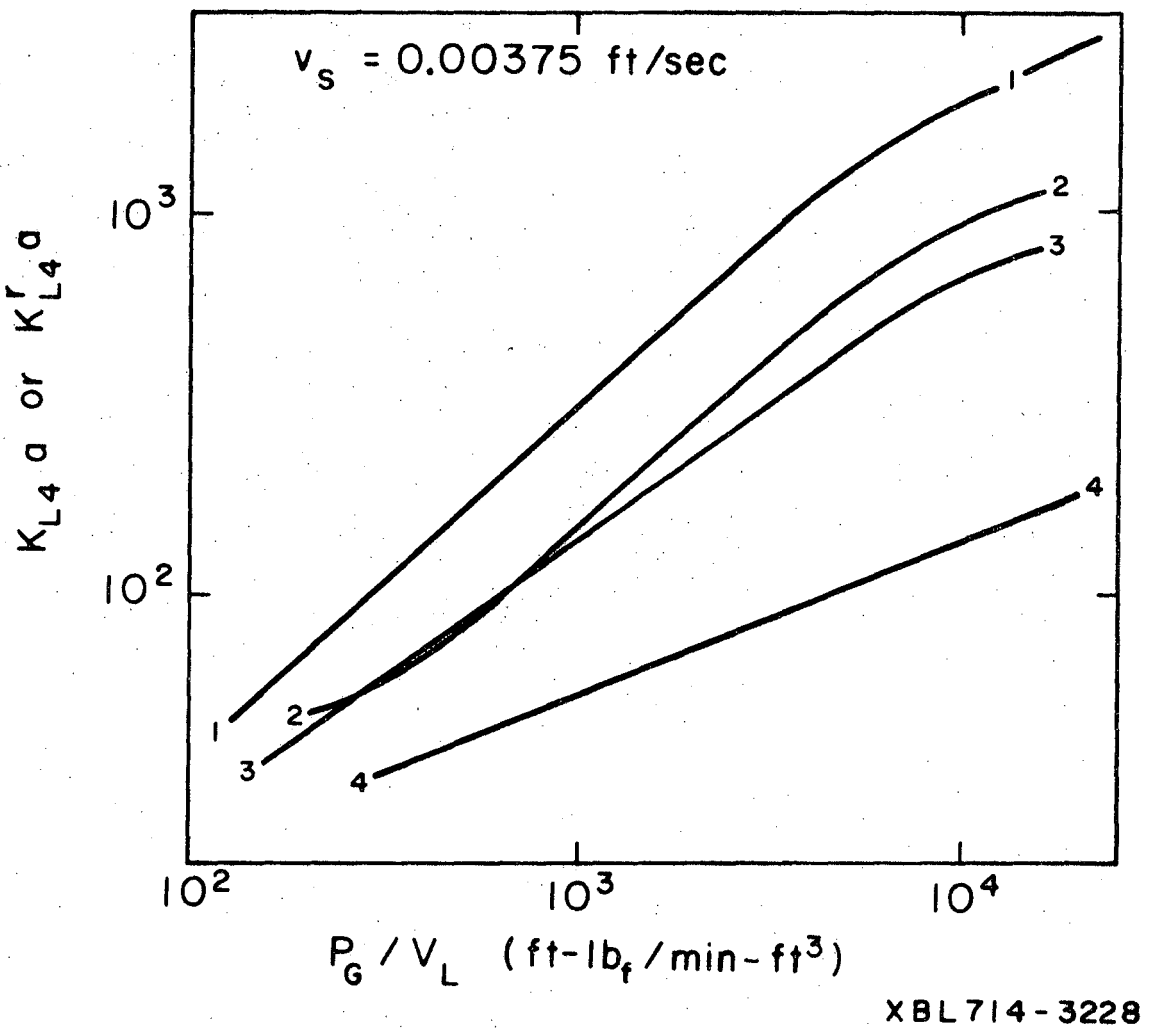

Fig. 4.17. Comparison of Overall Voulmetric Mass Transfer Coefficients for Oxygen. 1 = Sulphite Oxidation, 2 = 0.125M Na_2SO_4 + 0.004M $CuSO_4$, 3 = Medium A-1, 4 = Distilled Water.

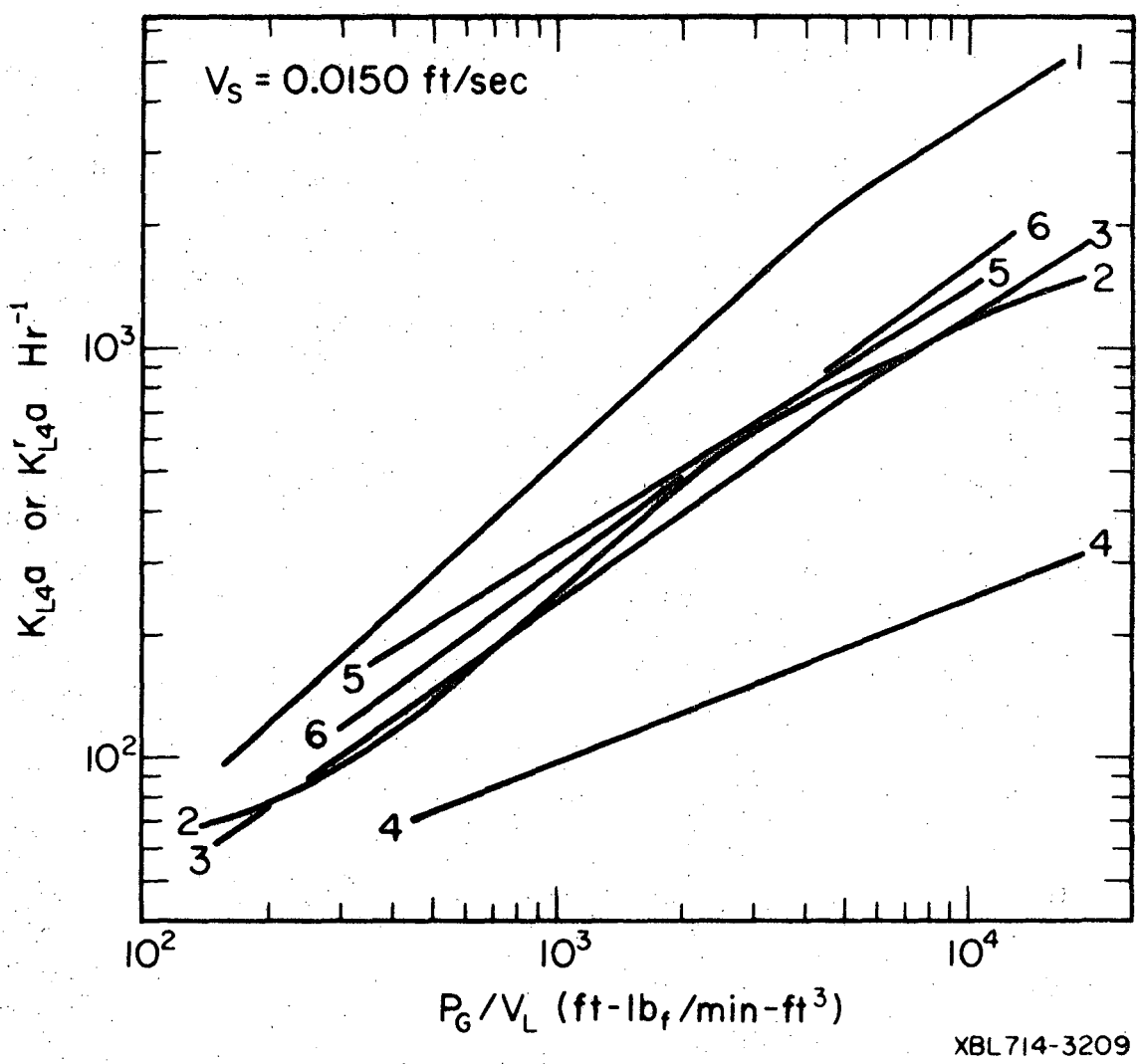

Fig. 4.18. Comparison of Overall Volumetric Mass Transfer Coefficients for Oxygen. 1 = Sulphite Oxidation, 2 = 0.125M Na_2SO_4 + 0.004M $CuSO_4$, 3 = Medium A-1, 4 = Distilled Water, 5 = 0.10M KCl, 6 = 0.22M KCl.

At low aeration rates, but at relatively high power input, as shown on Fig. (4.17), $K_{L4}a$ values in electrolyte solutions appear to be somewhat greater, the greater the concentration of the electrolyte. Little, or no dependency upon the electrolyte concentration is evident at power inputs less than 1000 ft-lb_f/min-ft^3.

At higher aeration rates, as shown on Fig. (4.18), the difference between the $K_{L4}a$'s of the different concentration electrolyte solutions is much reduced. $K_{L4}a$ values in 0.1M Medium A-1 and 0.129M sodium sulphate - cupric sulphate are almost identical to within experimental error at a power input greater than 10,000 ft-lb_f/min-ft^3, whereas at the lower aeration rate of Fig. (4.17), the difference is about three times the maximum estimated experimental error for the CFST, steady-state method.

The effect of solution composition and ionic strength upon the agitation exponent n and the aeration exponent m is summarized on Table 4.1. The aeration exponent m, in general, varies only slightly with solution composition and ionic strength; except for 0.10M KCl, $0.35 \leq m \leq 0.43$. In 0.10M KCl, m was found to have a significantly anomalous value of 0.62. However, the data suggest that there is a general trend of increasing m with increasing ionic strength in the range $0 \leq \Gamma_T \leq 0.40$, as shown on Fig. (4.19).

On the other hand, Table 4.1 shows that there is a consistent trend of increasing value of the agitation exponent n with increasing solution ionic strength regardless of its chemical composition. As shown on Fig. (4.19), n correlates with total ionic strength, increasing uniformly

Table 4.1. Variation of Agitation and Aeration Exponents with Solution Composition.

Solution	Total electrolyte concentration (gmole/ litre)	Γ_T (g-ion/ litre)	n	m
Na_2SO_3 + $CuSO_4$ [a]	0.504	1.516	0.90	0.38
Na_2SO_4 + $CuSO_4$ [a]	0.504	1.516	0.90	0.39
	0.379	1.141	0.90	0.39
	0.254	0.766	0.90	0.39
0.11M Na_2SO_4 + KOH-K_2CO_3		0.418 [b]	(d)	(c)
Na_2SO_4 + $CuSO_4$ [a]	0.129	0.391	0.90	0.39
0.135M KCl + KOH-K_2CO_3		0.221 [b]	0.70	(c)
KCl	0.220	0.220	0.71	0.36
Medium A-1	0.100	0.136	0.71	0.43
KCl	0.100	0.100	0.63	0.62
KOH-K_2CO_3		0.0965 [b]	0.55	(c)
Distilled Water	0.000	0.000	0.40	0.35

[a] $4(10^{-3})$ M $CuSO_4$.
[b] Average of all runs.
[c] Not determined.
[d] 0.90 at P_G/V_L < 2000; 0.60 at P_G/V_L > 3000.

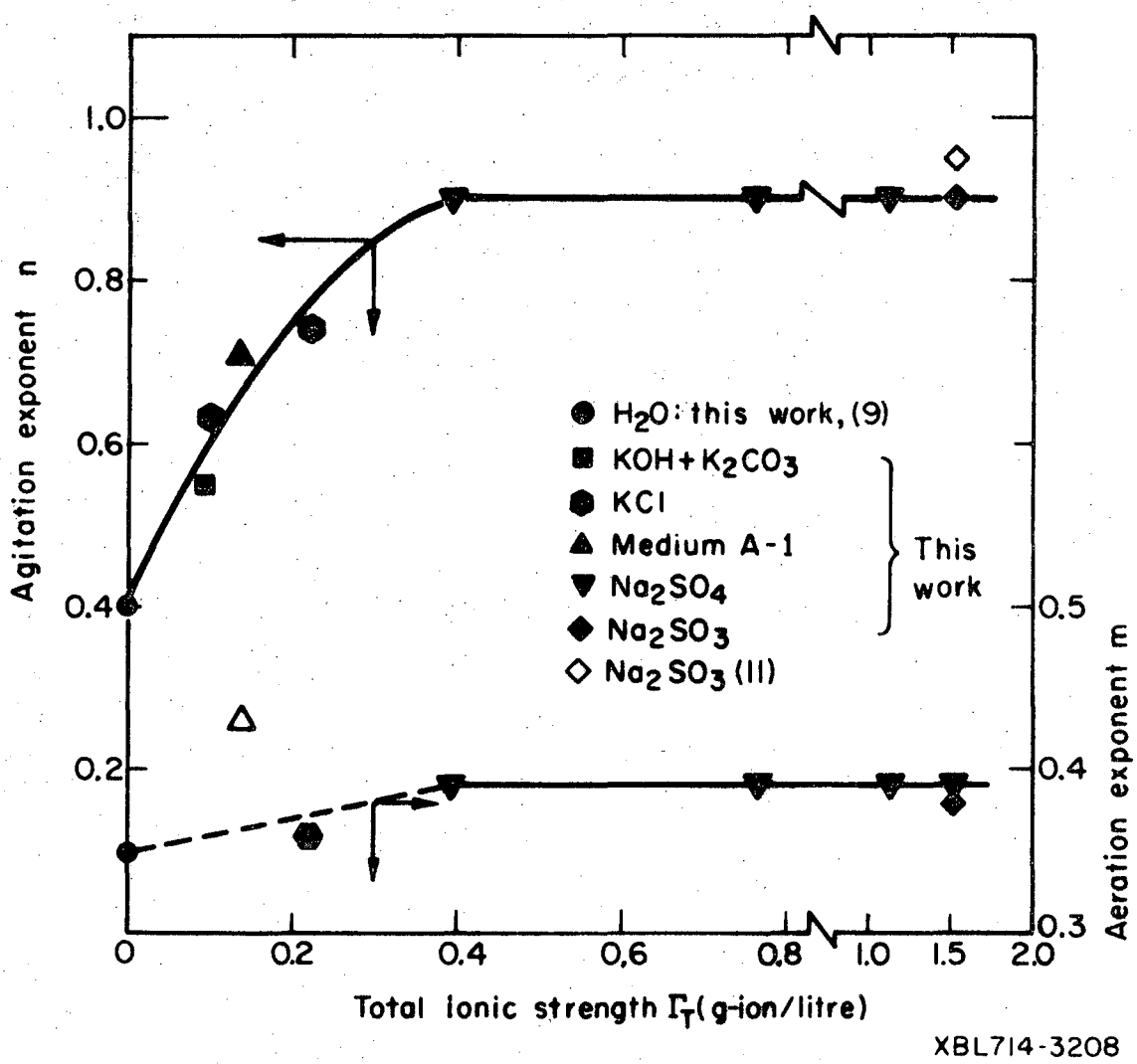

Fig. 4.19. Effect of Ionic Strength on Agitation Power per Unit Volume and Superficial Gas Velocity Exponents.

in the range $0 \leq \Gamma_T \leq 0.4$, and reaches a limiting value of 0.90 for all $\Gamma_T > 0.4$.

The relationship between n and Γ_T is analagous to the type of surface adsorption behaviour described by a Langmuir adsorption isotherm (88). The variation of n with ionic strength, as illustrated on Fig. (4.19), is given by

$$n = 0.40 + 0.862\ \Gamma_T/(0.274 + \Gamma_T)\ . \qquad (4.7)$$

4. Concurrent Oxygen Desorption, Carbon Dioxide Absorption-with-Reaction

Experimental tests of this concurrent absorption - desorption technique could only be made at the highest gas sparging rate possible to measure on the rotameter, i.e., at a superficial gas velocity of 0.0150 ft/sec. At the three lower sparging rates used before in the $K_{L4}a$ or $K^r_{L4}a$ determinations, the degree of carbon dioxide absorption from the dilute inlet gas was too great, particularly at high agitation rates, resulting in the exit gas carbon dioxide mole fraction becoming too small for accurate chromatographic analysis. Therefore, values of the "aeration" exponent m were not determined for the solutions investigated.

a) KOH - K_2CO_3 Solution (Average $\Gamma_T = 0.0965$ g-ion/litre)

The method was first tested experimentally in dilute solutions of potassium hydroxide and potassium carbonate, the latter being produced by the reaction with carbon dioxide. The transiently-determined values of $K_{L4}a$ are tabulated in Appendix IV.13(A), while concurrently-measures values of a , H_G , and the calculated values of k_{L4} , and d_b are tabulated in Appendix IV.13(B).

Figure (4.20), shows data points and correlating lines for $K_{L4}a$, a , and k_{L4} as functions of P_G/V_L . Individual k_{L4} points were calculated from the corresponding paired values of $K_{L4}a$ and a , by Eq. (2.122). The line representing the overall average behaviour of k_{L4} was computed from the least-squares fitted lines for $K_{L4}a$ and a . The result clearly show that for mass transfer of oxygen without reaction the individual parameters k_{L4} and a have distinctly different dependencies upon the agitation power per unit volume. There is a definite trend of decreasing k_{L4} with increasing P_G/V_L in the electrolyte solution, such that over most of the power range

$$k_{L4} \propto (P_G/V_L)^{-0.34} . \qquad (4.8)$$

The decrease in k_{L4} with increasing P_G/V_L accompanies a decrease in average bubble diameter from 0.23 to 0.034 cm, as shown on Fig. (4.21). The correlating line for d_b was calculated from the lines for a and H_G , while the individual d_b data points are calculated from paired values of a and H_G , using Eq. (3.16).

b) 0.135M KCl + KOH - K_2CO_3 (Average Γ_T = 0.221 g-ion/litre)

In order to determine the k_{L4} behaviour in non-reactive 0.22M KCl solution, a reactive (with respect to carbon dioxide) analog solution was prepared by reducing the concentration of KCl to 0.135M and adjusting the initial KOH and K_2CO_3 concentrations such that, on the average, the initial ionic strength of the reactive solution was 0.221 g-ion/litre as compared to 0.22 g-ion/litre for unreactive 0.22M KCl. This consistency of ionic strength ensured that $K_{L4}a$ differences

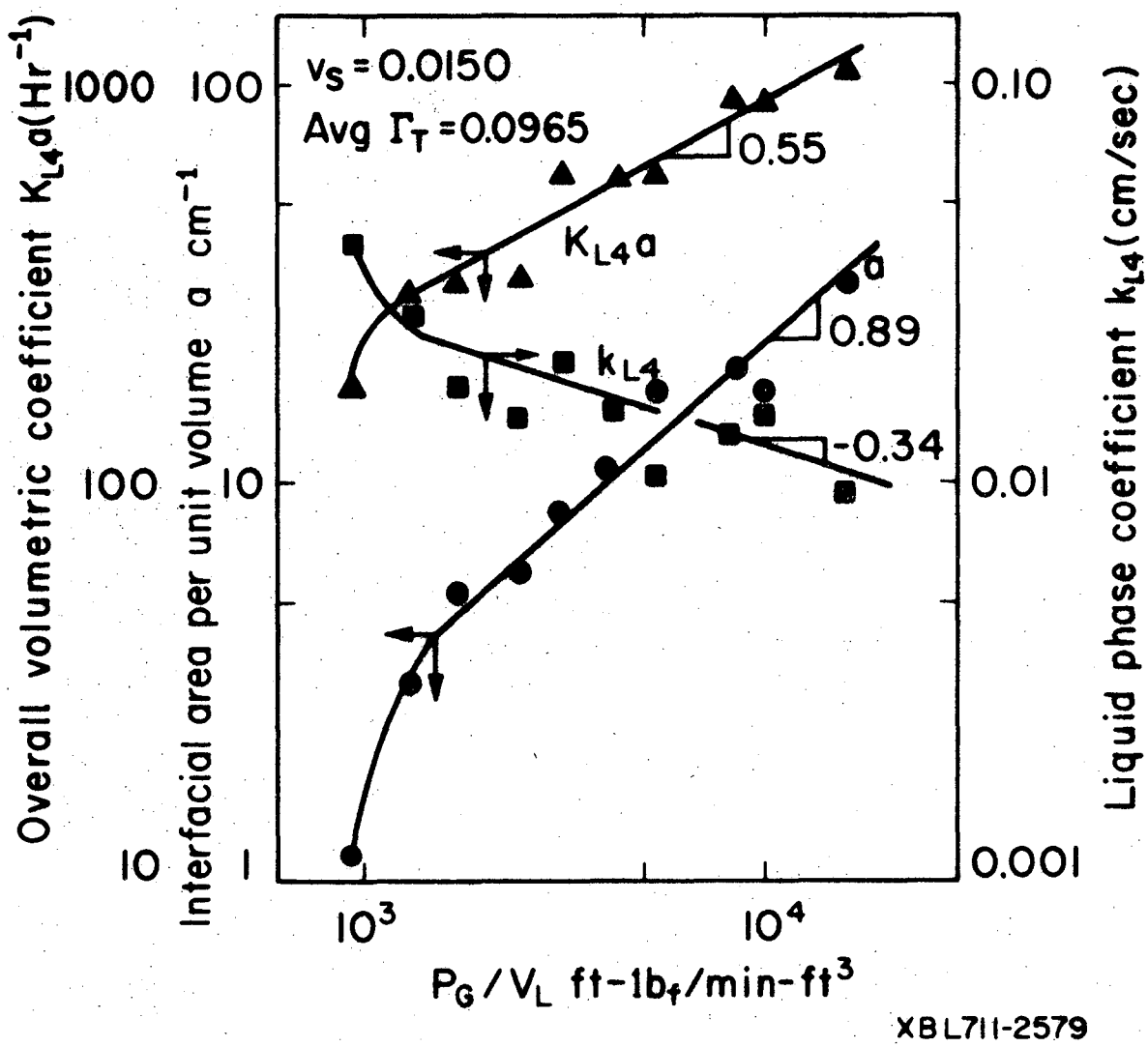

Fig. 4.20. Oxygen Mass Transfer Coefficients and Specific Interfacial Area in KOH - K_2CO_3 Solution.

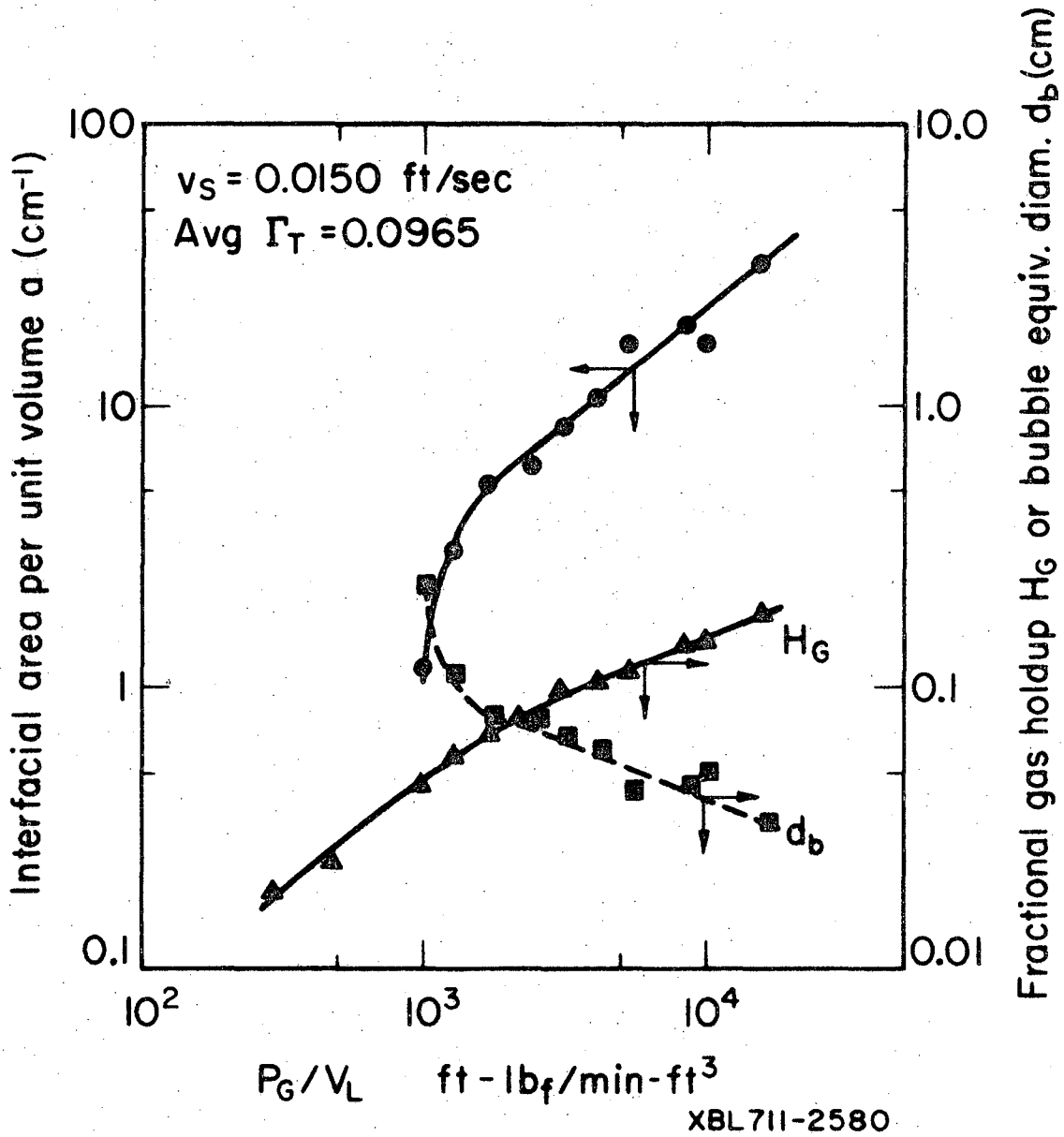

Fig. 4.21. Specific Interfacial Area, Gas Fractional Holdup, and Average Bubble Diameter in KOH - K_2CO_3 Solution.

between the non-reactive and the reactive (with carbon dioxide) KCl solutions would be slight; significantly different $K_{L4}a$ dependencies upon P_G/V_L can result from small changes in the ionic strength in the vicinity of 0.22 g-ion/litre, as illustrated on Fig. (4.19).

$K_{L4}a$ values determined from the transient desoprtion model, Eq. (2.83), are tabulated in Appendix IV.14(A). Concurrently measured values of a and H_G and calculated values of k_{L4} and d_b are listed in Appendix IV.14(B).

The $K_{L4}a$ correlation with P_G/V_L shown on Fig. (4.22) for this reactive solution is in close agreement with the $K_{L4}a$ correlation for 0.22M KCl determined from steady-state experiments and given previously on Fig. (4.7). The transiently-determined values are somewhat greater at the low end of the power range--the same phenomenon as noted before on Fig. (4.6) and Figs. (4.11) to (4.14), inclusive--and slightly lower at the high end.

The k_{L4} data points and correlating line on Fig. (4.22) were determined in the same manner as for Fig. (4.20) discussed previously. Here, too, it is evident that the liquid phase coefficient for oxygen mass transfer without reaction decreases in value with increasing P_G/V_L. The rate of decrease in k_{L4} does not appear to be uniform over the entire power range investigated; the k_{L4} data points on Fig. (4.22) suggest that there may be a plateau-like region in the range $2500 \leq P_G/V_L \leq 8000$ over which k_{L4} is independent of P_G/V_L.

The average bubble diameter decreases concurrently with k_{L4} as shown on Fig. (4.23), going from 0.142 to 0.023 cm. Individual data

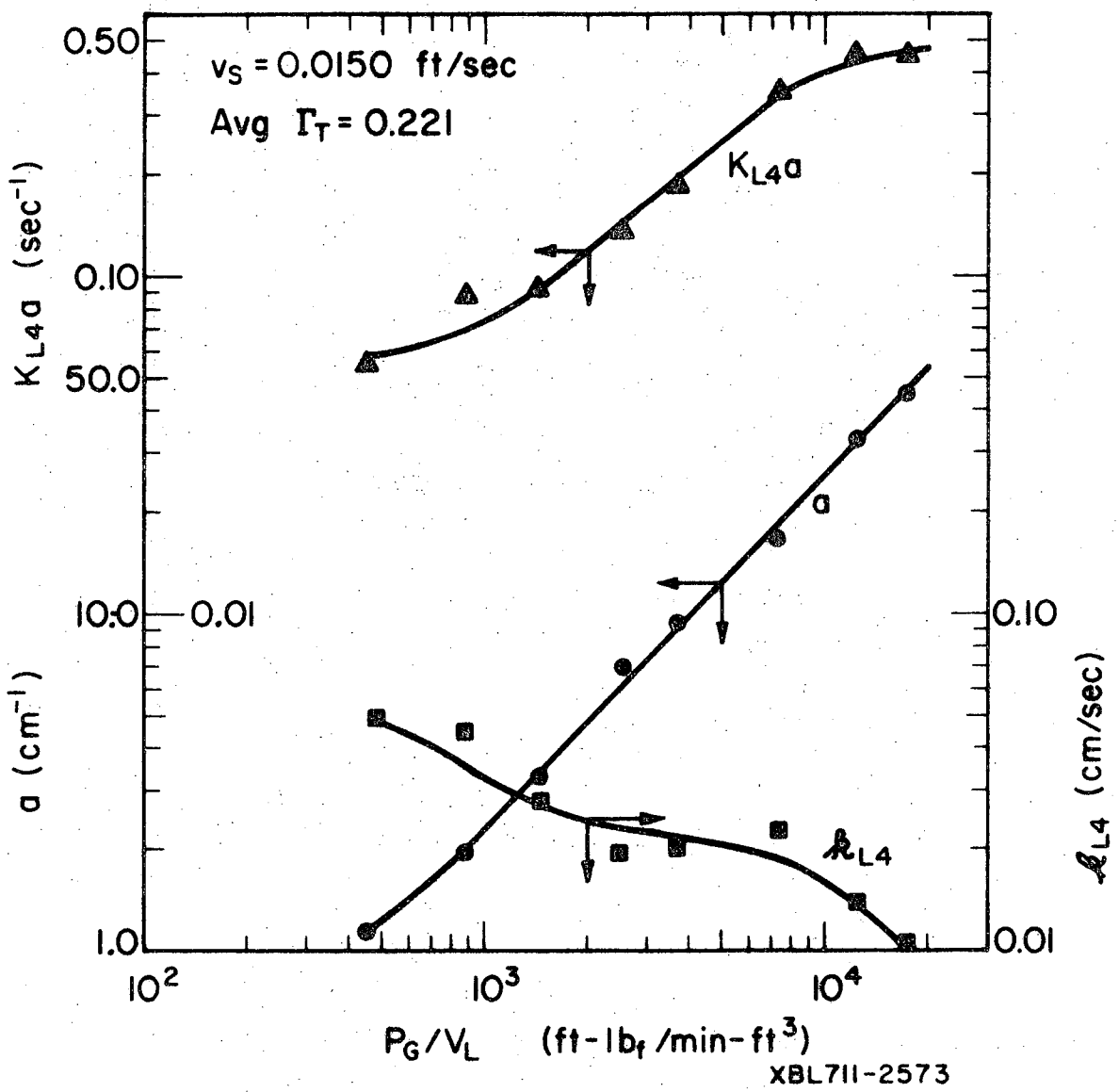

Fig. 4.22. Oxygen Mass Transfer Coefficients and Specific Interfacial Area in 0.135M KCl + KOH - K_2CO_3 Solution.

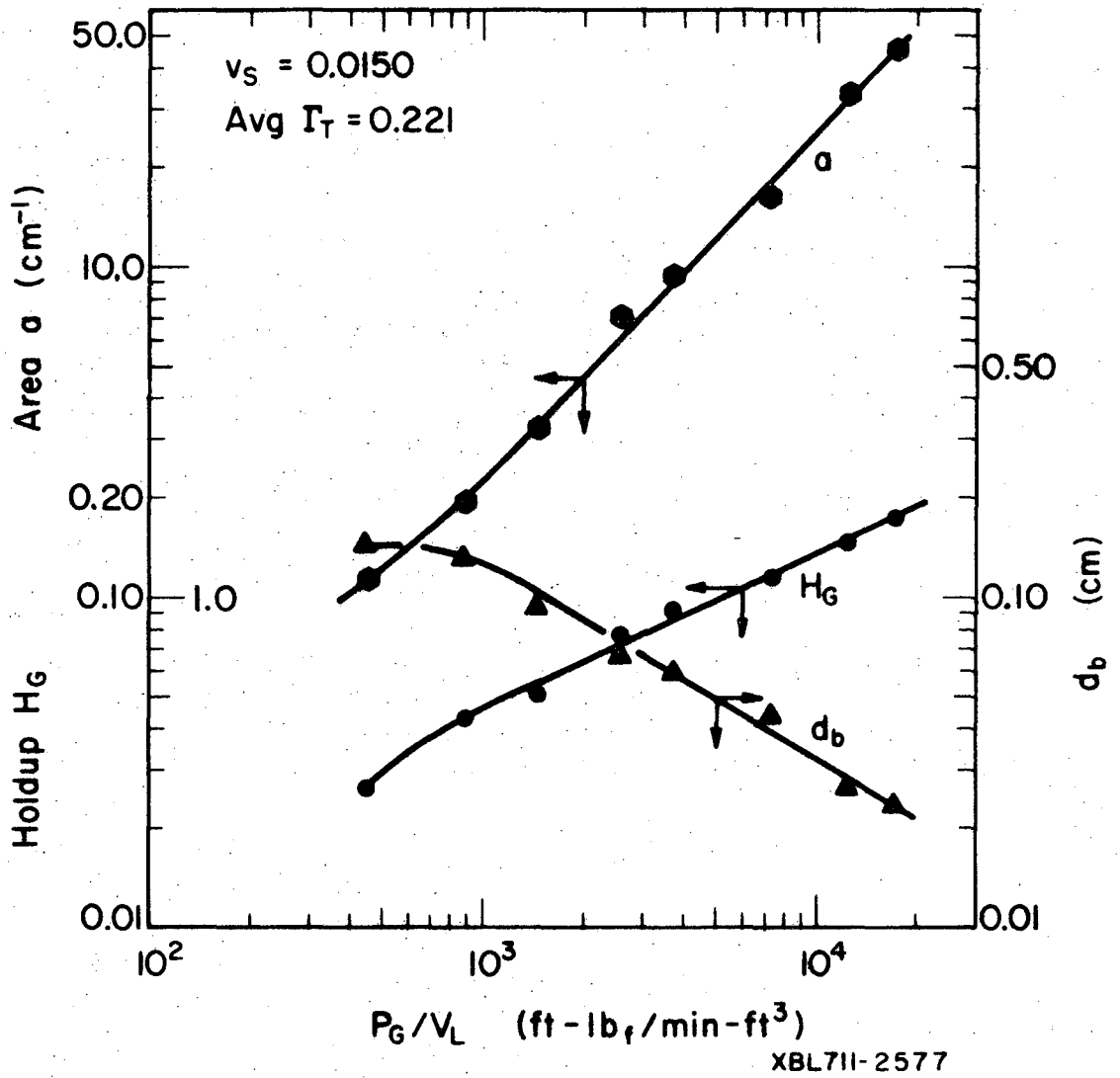

Fig. 4. 23. Specific Interfacial Area, Gas Fractional Holdup, and Average Bubble Diameter in 0.135M KCl + KOH - K_2CO_3 Solution.

points and the correlating line representing the overall behaviour of d_b were located by the procedure discussed in reference to Fig. (4.21).

At the minimum bubble diameter of 0.023 cm, the corresponding k_{L4} is 0.0103 cm/sec. This value of k_{L4} is about seven times greater than that for a stagnant sphere of the same diameter surrounded by an infinite fluid (Sherwood number of 2.0).

c) 0.11M Na_2SO + KOH - K_2CO_3 (Average Γ_T = 0.418 g-ion/litre)

This solution is a carbon dioxide reactive analog of 0.125M Na_2SO_4 - 0.004M $CuSO_4$ (Γ_T = 0.391). The transiently-determined $K_{L4}a$ values are listed in Appendix IV.15(A), with corresponding values of k_{L4}, a, H_G, and d_b given in Appendix IV.15(B).

The $K_{L4}a$ results are shown on Fig. (4.24) and are in general agreement with the behaviour of 0.129M Na_2SO_4 - $CuSO_4$ solution at this superficial gas velocity of 0.0150 ft/sec, as shown on Fig. (4.9). Both correlations have a straight-line portion of slope 0.90 in the region $600 \leq P_G/V_L \leq 2500$, with decreasing slope as the agitation power is increased above this level; for the reactive (with carbon dioxide) sulphate solution, n has a value of 0.60 for $P_G/V_L > 3000$ ft-lb_f/min-ft^3. The individual $K_{L4}a$ data points for the reactive 0.11M Na_2SO_4 + KOH - K_2CO_3 solution agree well with the $K_{L4}a$ correlation for the non-reactive 0.129M Na_2SO_4 - $CuSO_4$ solution, suggesting that the addition of a relatively small concentration of KOH and K_2CO_3 to achieve carbon dioxide reaction in an otherwise non-reactive solution has an insignificant effect on the oxygen mass transfer capability, as long as the total ionic strength is unchanged.

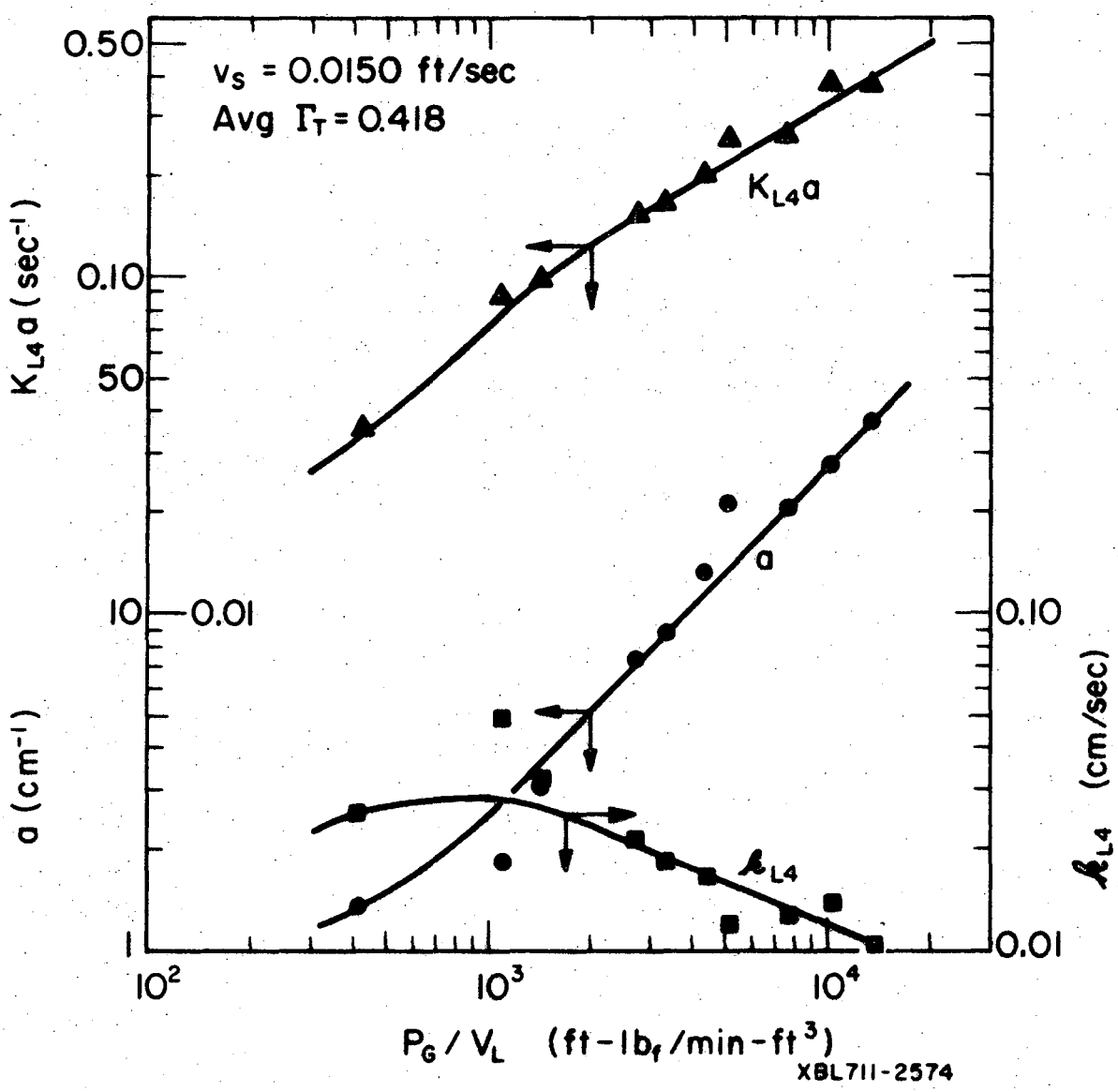

Fig. 4.24. Oxygen Mass Transfer Coefficients and Specific Interfacial Area in 0.11M Na_2SO_4 + KOH - K_2CO_3 Solution.

The individual k_{L4} data points and the average behaviour correlating line on Fig. (4.24) were located in the same manner as for Fig. (4.20). In this solution, k_{L4} remains nearly constant as P_G/V_L increases from 400 to 1000 ft-lb_f/min-ft^3, and then markedly decreases with increasing P_G/V_L in an apparently uniform manner. For $P_G/V_L > 1500$, k_{L4} varies as

$$k_{L4} \propto (P_G/V_L)^{-0.425} . \qquad (4.9)$$

The average bubble diameter behaviour parallels that of k_{L4}, as shown on Fig. (4.25). The specific interfacial area in the 0.11 M Na_2SO_4 + KOH - K_2CO_3 (average $\Gamma_T = 0.418$), is only about 10 percent greater than that in 0.135 MKCl + KOH - K_2CO_3 (average $\Gamma_T = 0.221$), reflecting the fact that there is little difference in the absolute values of K_{L4} at this highest gas sparging rate as shown on Fig. (4.18).

d) Effect of Varying Ionic Strength on Results

As previously discussed, the concurrent oxygen desorption, carbon dioxide chemical absorption technique as applied here results in a pseudo-steady state process wherein the carbonate ion concentration and, hence, the ionic strength increases with time. The percentage increase in Γ_T during a particular run depends upon the rate of carbon dioxide absorption-with-reaction, the rate of addition of concentrated KOH for pH control (which depends on the molarity of this feed stream), and upon the ionic strength contribution of any non-reactive salts present.

The increase in Γ_T is greatest in the KOH - K_2CO_3 solution as these two components are the only electrolytes present which contribute ionic strength. Each mole of carbonate produced from the

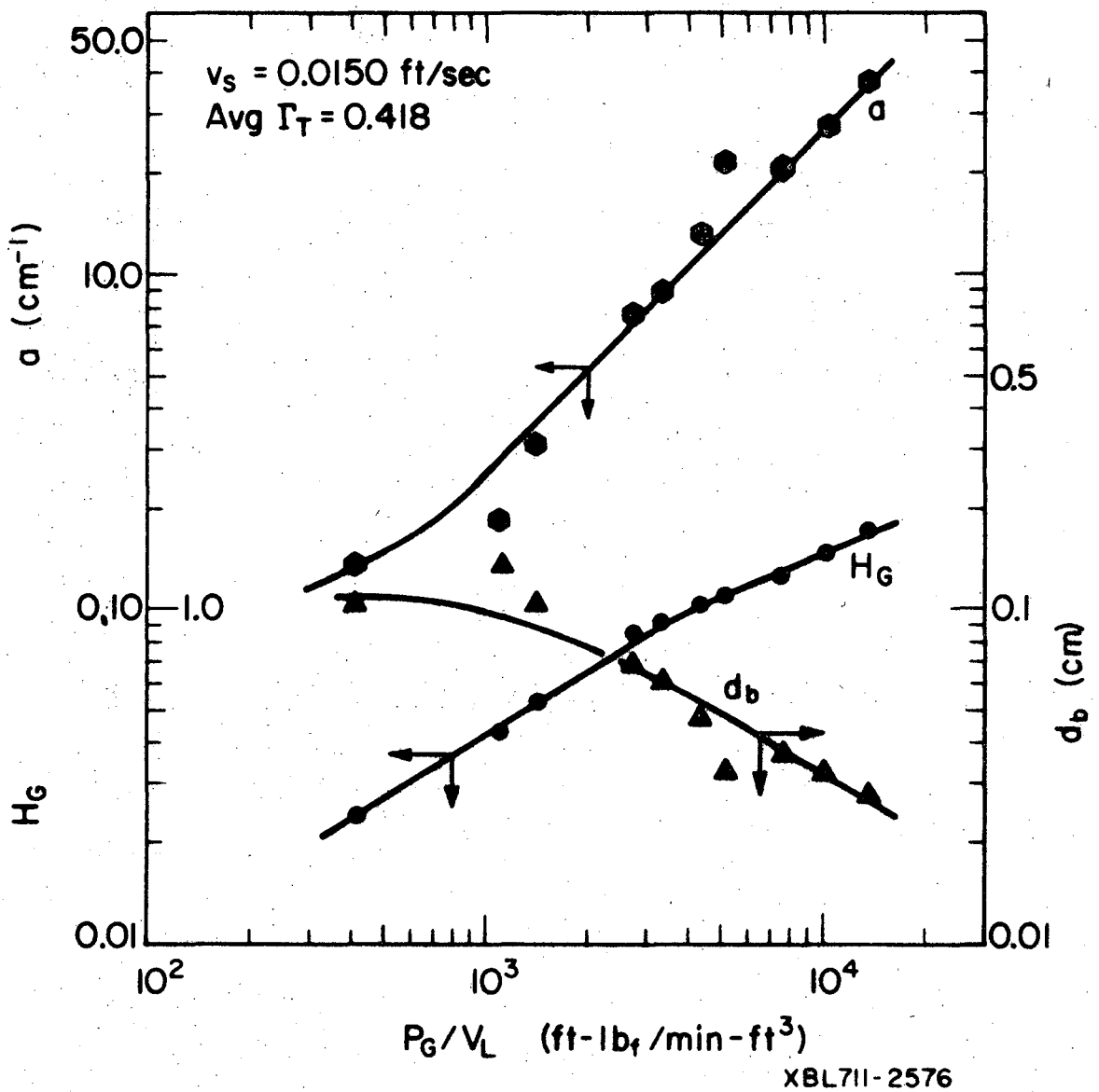

Fig. 4.25. Specific Interfacial Area, Fractional Gas Holdup, and Average Bubble Diameter in 0.11M Na_2SO_4 + KOH - K_2CO_3 Solution.

stoichiometric amount of hydroxide increases the ionic strength contribution of that amount of solute by 50 percent, considering Eq. (3.22) in conjunction with Eq. (2.114). On the other hand, in 0.11M Na_2SO_4 + KOH - K_2CO_3 for example, the greatest contribution to Γ_T comes from the sodium sulphate, and the conversion of hydroxide to carbonate has much less effect on the time variance in ionic strength.

The increase in carbonate ion concentration during a run can be calculated from a material balance differential equation, which upon integration results in

$$[CO_3^{=}]_t = [CO_3^{=}]_0 + 10^3(R^r_{V3}/\bar{D})[1 - \exp(-\bar{D}t)] , \qquad (4.10)$$

where $\bar{D}$ in this case is the dilution rate with respect to the feed of concentrated KOH added on pH control, R^r_{V3} is the volumetric rate of chemical absorption of carbon dioxide, and the concentrations are expressed as gmole/litre.

Equation (4.10) shows that the rate of increase in Γ_T is most pronounced in the initial time portion of a run. Decreasing the concentration of KOH in the pH-control feed stream would result in a decrease in $\bar{D}$ at a given R^r_{V3}, thereby reducing the rate of increase in Γ_T. However, if $\bar{D}$ becomes a significant quantity, the oxygen desorption process can then no longer be considered to be a semi-batch one, and Eq. (2.83) would not be applicable, a more-complicated model being required to describe the process.

In practice, oxygen desorption data for the evaluation of $K_{L4}a$ where taken over a 50 to 90 second time period following the step change

in inlet gas composition, the actual time interval depending upon the rate of oxygen desorption. Carbon dioxide absorption-with-reaction instantaneous point data for the evaluation of a were taken after an elapsed run time of 3 to 6 minutes, the actual sampling time interval varying with the rate of carbon dioxide chemical absorption, smaller time intervals being used at the higher agitation rates.

Because of the transient increase in ionic strength, the physicochemical properties of the aqueous phase at the time of $K_{L4}a$ measurement and at the time of measuring a were not strictly identical. As a , in general, increases with increasing ionic strength, the values of k_{L4} computed from Eq. (2.122) which assumes constancy of a , are, therefore, possibly somewhat low. In the case of the KOH - K_2CO_3 solution, at high agitation rates (high carbon dioxide absorption-with-reaction rates) the ionic strength typically increased about 30 percent over a 3 to 4 minute time interval (e.g., increasing from an initial value of, say, 0.08 to a final value of 0.105 g-ion/litre); at low agitation rates, the increase in Γ_T over the same time period amounted to less than 10 percent. For the 0.11M Na_2SO_4 + KOH - K_2CO_3 solution, the increase in Γ_T at high agitation rates was only about 12 to 15 percent in 3 to 4 minutes, and at the lower end of the agitation rate range was on the order of 3 to 5 percent. A definitive investigation of the effect of ionic strength on a was not done as part of this investigation. However, comparison of the area data on Figs. (4.20), (4.22), and (4.24) indicates that a increases about 20 to 30 percent with an increase in Γ_T from 0.09 to 0.40 g-ion/litre. Therefore, it is considered that the difference

between the value of a during the initial time period pertinent to oxygen desorption and the later-time measured a , and hence the error from this source in the calculated value of k_{L4} for 0.135M KCl + KOH - K_2CO_3 and 0.11M Na_2SO_4 + KOH - K_2CO_3 solutions, amounts to less than 5 percent over the entire agitation range.

A few CFSTR runs were made with KOH - K_2CO_3 solutions of average Γ_T equal to 0.0886 in order to evaluate $K_{L4}a$, a , and k_{L4} in steady-state. The results are compared to those obtained from transient oxygen desorption with pseudo-steady state carbon dioxide absorption-with reaction runs in 0.0965 Γ_T (average) KOH - K_2CO_3 at the same agitation rates in Table 4.2.

5. Generalized Correlation for K_La

Knowledge of the variation of the agitation power exponent (n) with solution ionic strength as given by Eq. (4.7) and illustrated on Fig. (4.19) does not, by itself, enable $K_{L4}a$ to be predicted a priori for a particular electrolyte solution which is agitated and aerated at prescribed rates. To predict the oxygen mass transfer capabilities under these circumstances, it is desirable to have a generalized empirical correlation relating K_La to the agitation and sparging rates, as well as to the pertinent physicochemical properties of the solution, namely, ionic strength, interfacial tension, viscosity, diffusion coefficient, and density.

The aqueous-phase viscosity, density, and diffusivity and the interfacial tension of the various solutions investigated in this study for the most part did not differ from the corresponding values in water by more

Table 4.2. Concurrent Oxygen Desorption, Carbon Dioxide Absorption-With-Reaction: Comparison of Steady-State and Unsteady-State/Pseudo-Steady State Methods

Agitation rate N	$K_{L4}a$ (sec^{-1}) (a)	(b)	a (cm^{-1}) (a)	(b)	k_{L4}(cm/sec) (a)	(b)
900	0.0717	0.0820	3.14	3.10	0.0228	0.0271
1000	0.0907	0.0944	4.75	5.23	0.0191	0.0180
1300	0.167	0.164	11.6	10.5	0.0144	0.0156
1600	0.248	0.253	18.1	19.0	0.0137	0.0133

(a) CFST, steady-state method.

(b) Unsteady-state O_2 desorption, pseudo-steady state CO_2 absorption-with-reaction.

than 15 percent. Therefore, any effects upon $K_{L4}a$ or $K^r_{L4}a$ behaviour due to these physicochemical parameters cannot be meaningfully determined from the experimental results. The effect of these particular parameters upon $K_{L4}a$ must, therefore, be obtained from the results of others in systems wherein these properties were varied over a significantly wide range of values.

For non-electrolyte solutions or for pure liquids, combining the results of Calderbank for a (10) with his results for k_L (9) or with the k_L correlation of Calderbank and Moo-Young (16) obtained in stirred tanks having geometric ratios identical to those for the tank used in our work shows for "small" bubbles ($d_b < 0.2$ cm) that

$$k_L a \propto (\rho_L)^{0.2}(\Delta\rho)^{1/3}(D_L)^{2/3}/(\sigma)^{0.60}(\mu_L)^{1/3}, \qquad (4.11)$$

where $\Delta\rho$ is the density difference between the liquid and dispersed gas phases.

Using the close approximation that $\Delta\rho \approx \rho_L$, Eq. (4.11) may be written as

$$k_L a \propto (\rho_L)^{0.533}(D_L)^{2/3}/\sigma^{0.6}(\mu_L)^{1/3} \equiv \xi , \qquad (4.12)$$

whereby the physical property factor ξ is defined.

Westerterp et al. (12) introduced physical property factors into their correlation for $K^r_{L4}a$ in sodium sulphite. Experimentally, for pure carbon dioxide absorption-with-reaction in viscous sodium hydroxide solutions containing varying amounts of glycerol such that μ_L was varied by one order of magnitude, they found that what they considered to be a (see discussion in Section V. 4) varied directly with viscosity. Using, in addition, the empirical result of Vermeulen et al. (101) which predicts that a varies inversely with σ for gas dispersions in non-electrolytic liquids, and the theoretical considerations of Hinze (112) concerning the effects of σ and ρ_L upon a , Westerterp et al. correlated sulphite oxidation data obtained in various size tanks on the basis of

$$K^r_{L4}a \propto \mu_L(\rho_L D_T/\sigma)^{0.50} D_I(N - N_0) , \qquad (4.13)$$

in which K^r_{L4} is unaffected by viscosity, density, and interfacial tension. However, as their sulphite soluitons were all of one fixed concentration, μ_L , ρ_L , and σ were not, in fact, variables, and variation in the values of the data points reflected only variations in tank diameter (D_T), impeller diameter (D_I), and N .

Equation (4.13) is in general agreement with Eq. (4.12) as far as the effects of density and interfacial tension are concerned. However, the two equations are in disagreement with respect to the effect of viscosity, Eq. (4.12) predicting that $K_L a$ decreases with increasing μ while Eq. (4.13) predicts the opposite behaviour.

The dependency of $k_L a$ upon μ, ρ, D_L, and σ determined from the works of Calderbank (10) and Calderbank and Moo-Young (16), namely Eq. (4.12), was adopted for use in the development of the generalized correlation. Equation (4.12) has been experimentally tested over a wider range of values of these variables than has Eq. (4.13) based on the work of Westerterp et al. It is thereby assumed that the empirical or semi-empirical values of the exponents in Eq. (4.12), which were obtained by varying the physical properties of non-electrolyte solutions, are directly applicable to solutions of electrolytes.

To develope a generalized correlation in a form useful for predicting $K_L a$ or $K_L^r a$ values for other sparingly-soluble gases in addition to oxygen, it was assumed that, in general,

$$\epsilon = \lambda(P_G/V_L)^n (v_S)^m \xi , \qquad (4.14)$$

where ϵ denotes either $K_L a$ or $K_L^r a/\phi$, and the proportionality constant λ is assumed to be a function of ionic strength.

Ratcliff and Holdcroft (85) studied the effect of viscosity upon diffusivity, specifically in electrolyte solutions of the same general solute concentration range used here. Using carbon dioxide as the diffusing solute at 25°C, the results of their study showed that

$$D_L = D_W (\mu_W/\mu_L)^{0.637}, \qquad (4.15)$$

where subscript W denotes the value in water. Diffusivities predicted from Eq. (4.15) agreed with their experimental measurements to within 4 percent. Assuming that Eq. (4.15) also describes the variation of oxygen diffusivity with electrolyte solution viscosity, values of D_{L4} for the solutions tested in our work were calculated by using the reference D_{W4} and experimentally-determined μ_W/μ_L data of Appendix III.3. Electrolyte solution viscosities relative to that of water at 30°C were measured by using an Ostwald capillary viscometer.

Values of ξ for the systems which were studied the most intensively are shown on Table 4.3. The pertinent physical property data for these solutions are given in Appendix III.3.

The original correlating equations for these systems--Eqs. (4.1), (4.3), (4.4), (4.5), and (4.6)--did not include the physical property factor ξ as incorporated in the generalized correlation given by Eq. (4.14). The values of λ given in Table 4.3 were therefore calculated by dividing the proportionality constants of Eqs. (4.1) and (4.3) to (4.6), inclusive, by the corresponding values of ξ.

As shown on Fig. (4.26), λ decreases uniformly with increasing Γ_T until a lower limiting value of 2.10 is reached at an ionic strength of 0.40 g-ion/litre (the same value of Γ_T at which n reaches an upper limiting value as shown on Fig. 4.19). In the region $0 \leqslant \Gamma_T \leqslant 0.40$, the correlating line of Fig. (4.26) follows a Langmuir adsorption type of behavior. The overall behavior of λ with respect to Γ_T is well described by

Table 4.3. Values of ξ and λ (Eq. 4.14) for experimental Solutions.

Aqueous phase	$\xi \times 10^4$	λ
Water	3.51	18.9
Medium A-1	3.49	9.41
0.22M KCl	3.49	6.21
0.125M Na_2SO_4 + 0.004M $CuSO_4$	3.46	2.09
0.250M Na_2SO_4 + 0.004M $CuSO_4$	3.45	2.16
0.500M Na_2SO_4 + 0.004M $CuSO_4$	3.08	2.35
0.500M Na_2SO_3 + 0.004M $CuSO_4$	2.96	2.45

$$\lambda = 18.9 - 28.7\,\Gamma'/(0.276 + \Gamma') , \qquad (4.16)$$

where

$$\Gamma' = \Gamma_T , \quad 0 \leq \Gamma_T \leq 0.40 ,$$
$$\Gamma' = 0.40 , \quad \Gamma_T > 0.40 . \qquad (4.17)$$

The generalized correlation in the form of Eq. (4.14) is shown on Fig. (4.27) for seven of the systems investigated. For sulphite oxidation, the value of ϕ_4 defined as the ratio of $K_{L4}^r a$ in the sulphite solution to $K_{L4}a$ in 0.125 to 0.500M Na_2SO_4 + 0.004M $CuSO_4$ solutions is 2.1, as obtained by dividing Eq. (4.6) by Eq. (4.5), neglecting the minor difference between the two aeration exponents. For the solutions used in conjunction with the concurrent measurement technique for separately evaluating k_{L4} and a, the value of the aeration exponent was not determined experimentally. For inclusion in the generalized correlation, the carbon-dioxide reactive solutions were assumed to have the same value of m as their corresponding non-reactive analogs.

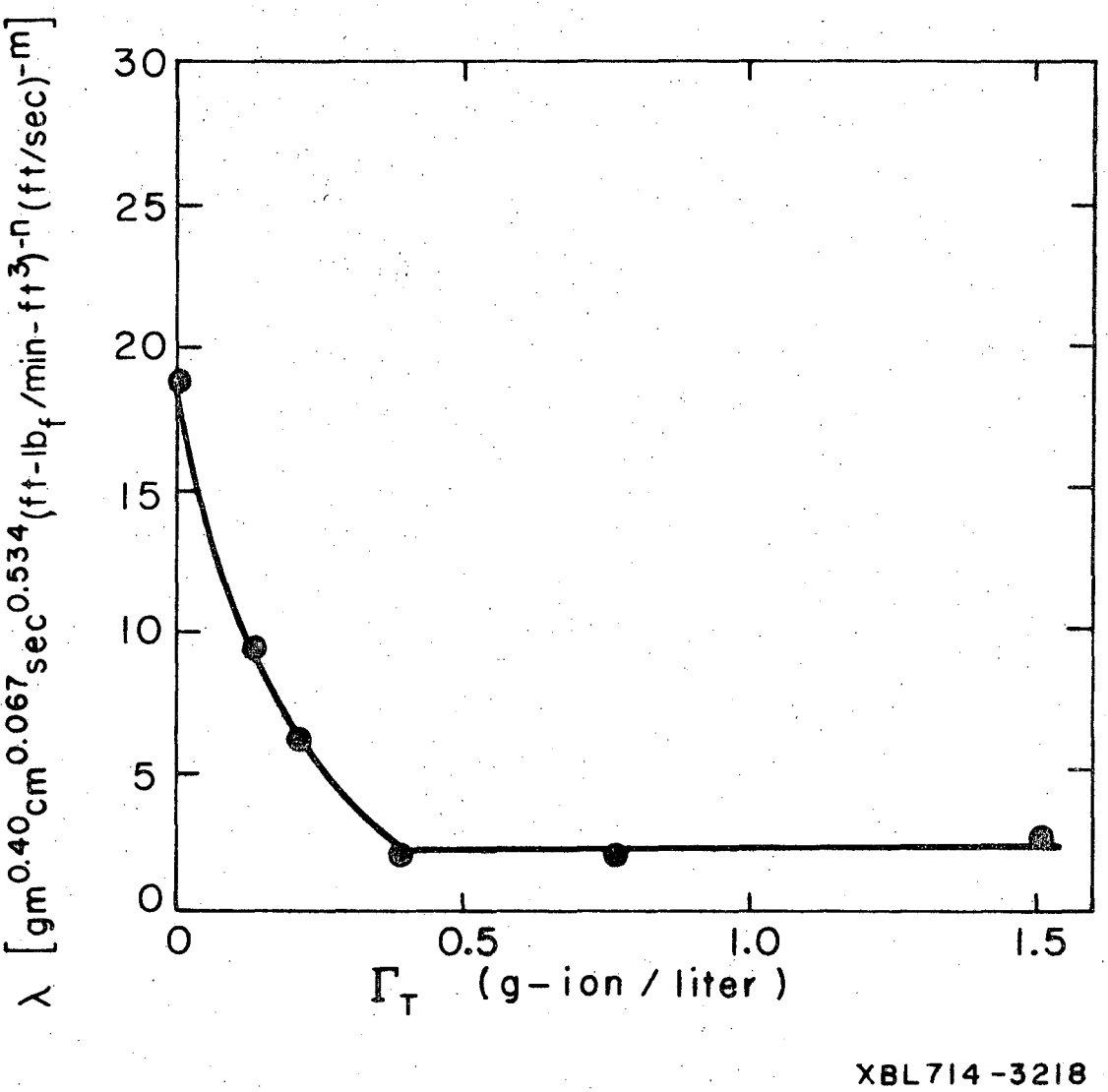

Fig. 4.26. Variation of λ with Ionic Strength.

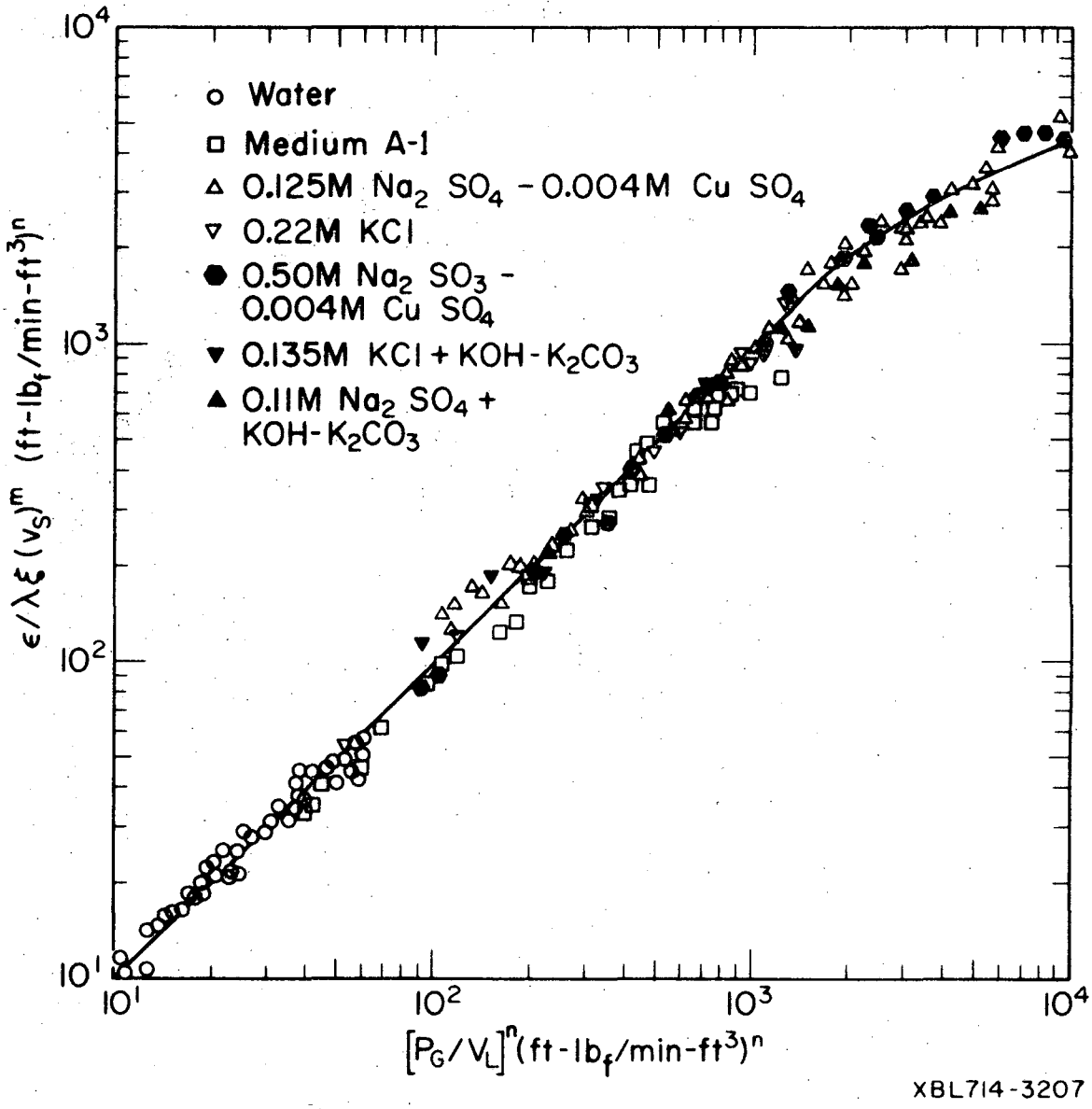

Fig. 4.27. Generalized Correlation for Oxygen Mass Transfer Overall Volumetric Coefficients in Aerated and Agitated Aqueous Phases.

That is, the values of m in 0.135M KCl + KOH - K_2CO_3 and 0.11M Na_2SO_4 + KOH - K_2CO_3 were taken as being 0.36 and 0.39, respectively.

The linear portion of the correlating line of Fig. (4.27) has a slope of unity in accordance with the prediction of Eq. (4.14). For values of the two correlating parameters varying by nearly three orders of magnitude, the vast majority of the data points agree with the correlating line to within 15 percent. The correlating line deviates from linearity at abcissa values greater than 2000. This deviation reflects the declining rate of increase in $K_{L4}a$ and $K^r_{L4}a$ with increasing P_G/V_L which was observed with both the 0.125M Na_2SO_4 + 0.004M $CuSO_4$ and sulphite oxidation solutions at values of P_G/V_L greater than 6000 ft-lb_f/min-ft^3, as shown on Figs. (4.9) and (4.15).

Data points for KOH - K_2CO_3 and 0.10M KCl solutions are not shown on Fig. (4.27) as they do not fit the correlation within 40 percent. The difficulty in minimizing the ionic strength increase in the KOH - K_2CO_3 solution over a run may have resulted in the data points for this system not following the generalized correlation. 0.10M KCl solution exhibited an anomalous value of m as previously discussed, and in addition the values of $K_{L4}a$ at given values of P_G/V_L and v_S are greater than would be anticipated with respect to the other solutions tested, assuming $K_{L4}a$ increases uniformly with increasing ionic strength at ionic strengths less than 0.40.

V. DISCUSSION OF RESULTS

1. Oxygen Probe Transient Response Models and Computer Evaluation $K_{L4}a$

The LSQVMT computer programme for the evaluation of β which best fit the experimental data to the theoretical transient response behaviour of the dissolved oxygen probe--Eq. (2.75) for absorption and Eq. (2.83) for desorption--resulted in values of $K_{L4}a$ which agreed well with the steady-state experimental values of $K_{L4}a$ computed from Eq. (2.35), at the same agitation and aeration rates. The close agreement, except at values of P_G/V_L less than about 1000 ft-lb_f/min-ft^3, is illustrated on Fig. (4.6) and Figs. (4.11) to (4.14), inclusive.

However, referring to Fig. (4.9) for 0.125M Na_2SO_4 - 0.004M $CuSO_4$, it may be noted that there is not a great deal of difference between the values of $K_{L4}a$ obtained at a given agitation power input but with varying aeration rate. Even at power inputs greater than 1000 ft-lb_f/min-ft^3, it is evident from Figs. (4.11) to (4.14), inclusive, that the degree of scatter of the transiently-determined $K_{L4}a$ points about the steady-state correlation lines is of the same magnitude as the spread in $K_{L4}a$ values at different aeration rates found on Fig. (4.9). At the relatively-high values of $K_{L4}a$ exhibited by the sulphate solutions wherein $\Gamma_T \geq 0.40$ g-ion/litre, the oxygen probe transient response becomes less sensitive to differences in the aeration rate. Therefore, in solutions of high $K_{L4}a$ potential, it appears that the oxygen probe unsteady-state response method is inadequate for the precise determination of the effect of v_S upon $K_{L4}a$, i.e., it is not sufficiently sensitive to the effect of v_S such that the aeration exponent m may be

accurately evaluated. However, as the effect of v_S upon $K_{L4}a$, although being measurable in steady-state, is small, the oxygen probe transient response technique of $K_{L4}a$ measurement results in reasonably accurate values of $K_{L4}a$ as long as the well-mixed disperse gas assumption is met in practice. The lower limit of applicability of the models appears to occur at a value of P_G/V_L in the vicinity of 1000 ft-lb_f/min-ft^3 for electrolyte solutions and less than 300 ft-lb_f/min-ft^3 for distilled water.

2. Overall Volumetric Mass Transfer Coefficient for Oxygen ($K_{L4}a$)

a) Water

Calderbank (9), for air dispersions in pure liquids including water, measured K_La at 15°C in stirred tanks having geometric ratios identical to the one used here; the power range investigated in his work was $330 \leq P_G/V_L \leq 3300$. In a previous work, Calderbank (10) measured a by optical light scattering and found that a varied as $(P_G/V_L)^{0.4}(v_S)^{0.5}$; combining the results for K_La and a, k_L was found to be independent of the agitation power input for both "large" (> 0.25 cm. diameter) and "small" (< 0.25 cm. diameter) bubble size ranges, being dependent only on the component's liquid phase diffusivity. Hence, K_La also varied as $(P_G/V_L)^{0.4}(v_S)^{0.5}$. The results of the present study at 30°C over a wider range of agitation power are in agreement with Calderbank's power exponent, but the aeration exponent was found to have a smaller value (m = 0.35) as shown by Eq. (4.1).

Calderbank and Moo-Young (16) developed generalized correlations for the agitation-rate independent behaviour of k_L in dispersions,

the "large" and "small" bubble size ranges having different dependencies on the Schmidt and Raleigh numbers. Small bubble k_L was found to be less than large bubble k_L, as shown by Eqs. (5.5) and (5.6) in Section V.7. Combining "large" bubble k_{L4} results (16) with the correlation for specific interfacial area (10) permits the numerical evaluation of $K_{L4}a$ in air-water dispersions at 30°C. Using a diffusivity of $2.74(10^{-5})$ cm^2/sec for oxygen in water at 30°C, the generalized correlation of Calderbank and Moo-Young (16) predicts the value of k_{L4} to be 0.0489 cm/sec for "large" bubbles. The specific area correlation of Calderbank (10) predicts values of a ranging from 0.329 to 0.82 cm^{-1} over the range $300 \leq P_G/V_L \leq 3000$. The Calderbank:Calderbank-Moo-Young combination of correlations results in

$$(k_{L4}a)_{H_2O} = 13.7(10^{-3})(P_G/V_L)^{0.40}(v_S)^{0.50}. \qquad (5.0)$$

The proportionality constant in Eq. (5.0) is slightly more than double that of Eq. (4.1) which correlates the water $K_{L4}a$ results of this present study. However, over the range $0.00375 \leq v_S \leq 0.0150$, values of $(v_S)^{0.50}$ in Eq. (5.0) are about one-half the values of $(v_S)^{0.35}$ in Eq. (4.1), the net effect being that values of $K_{L4}a$ computed from Eqs. (4.1) and (5.0) generally agree to within 10 percent at the same agitation and aeration rates.

Using 12-blade turbine impellers of D_I/D_T ratio of 0.40 in tanks of various diameters, Yoshida et al. (14) measured $K_{L4}a$ in water at 20°C by using only the simplified "gassing-in" model of Eq. (2.16) to describe the overall transient phase behaviour. They found

that $K_{L4}a$ varied as $(N^3D_T^2)^{0.67}(v_S)^{0.67}$ for values of $N^3D_T^2$ greater than about $3(10^6)$ ft^2/min^3. They further found that the effect of temperature on $K_{L4}a$ in water to be negligible; values of $K_{L4}a$ determined at 20 and 40°C were reported to coincide over the entire range of agitation rates.

b) Electrolyte Solutions

Values of $K_{L4}a$ for the various electrolyte solutions were appreciably greater than $K_{L4}a$ values obtained in distilled water, the magnitude of the difference increasing with increasing P_G/V_L. As shown by Fig. (4.17) and Fig. (4.18), at 10,000 ft-lb_f/min-ft^3, $K_{L4}a$ in non-reactive electrolyte solutions has a value on the order of 1200 hr^{-1} (0.3 sec^{-1}), while in pure water $K_{L4}a$ is only about 200 hr^{-1} (0.0556 sec^{-1}), differing by a factor of about 6. In many cases the extent of microbial growth in mineral salts media utilizing dispersed n-alkane as the carbon and energy source substrate is limited by the oxygen supply capability of the stirred tank. Cell productivity estimates based on a $K_{L4}a$ correlation for pure water would, therefore, be erroneously low by a wide margin.

The higher value of $K_{L4}a$ in electrolyte solutions results in large values of the agitation power exponent n as the ionic strength of the solution increases to an upper limiting value, as shown on Fig. (4.19). Although the density, viscosity, and interfacial surface tension of electrolyte solutions vary with both the nature and concentration of the solute, the values of these three physicochemical parameters differ

from those of water by less than 15 percent for the solutions tested (Appendix III.3).

The separate effects of variations in viscosity, density, and interfacial tension obtained from direct experimentation with electrolyte solutions have not been well defined in the literature. However, for pure liquids or non-electrolyte solutions, the works of Calderbank (9,10) and Calderbank and Moo-Young (16) indicate that $K_L a$ for dispersed bubbles of average diameter less than 0.2 cm varies as $(\rho_L)^{0.533}(D_L)^{2/3}/\sigma^{0.6}(\mu_L)^{1/3}$, as given by Eqs. (5.10) and (5.11). It is not certain that the dependency of $K_{L4}a$ upon these parameters is the same in electrolyte solutions, but as a first approximation it appears that the increase in n shown on Fig. (4.19) cannot be attributed to these factors to any significant degree. It is known that the addition of small quantities of solutes to water may appreciably decrease the bubble size, even though other physicochemical properties remain essentially constant (14,89). In the case of electrolyte solutions, this phenomenon has been attributed to electrical effects at the gas-liquid interface as discussed in Section V.4; repulsive forces generated by the surface potentials hinder bubble coalescence, and the average equilibrium bubble size is therefore smaller. Visual observation indicated that upon addition of increasing amounts of ionic solute, the average bubble diameter decreased and the dispersed gas fractional holdup increased. These observations are in qualitative agreement with the work of Calderbank (10), who measured the average bubble diameter of air dispersions in solutions of sodium chloride, sodium sulphate, and sodium phosphate. He found that when

the ionic strength exceeded 0.5 for sodium chloride, 0.75 for sodium sulphate, and 0.6 g-ion/litre for sodium phosphate, the average bubble diameter reached a minimum limiting size which was about one-half the bubble diameter in pure water at the same agitation power input.

Marrucci and Nicodemo (89) studied the effect of electrolyte concentration on nitrogen bubble diameters in a bubble column. They found that d_b decreased with increasing electrolyte concentration until a minimum value was reached at which point d_b was unaffected by further increases in electrolyte concentration; the minimum bubble diameter was 0.041 cm, regardless of the nature of the electrolyte. The electrolyte concentration at which this lower d_b limit was reached depended upon the chemical nature of the electrolyte used, ranging from 0.05M for $AlCl_3$(Γ = 0.3), 0.28M for KCl (Γ = 0.28), to 0.71M for KI (Γ = 0.71).

In this present study, the agitation exponent n reaches an upper limiting value of 0.90 at an ionic strength of 0.40 g-ion/litre, as shown on Fig. (4.19) or by Eq. (4.7). Hence, the behaviour of n with Γ_T for bubble swarms in stirred tanks is in general agreement with the values of Γ_T at which the dispersed bubbles of Marrucci and Nicodemo reached a lower limiting value of d_b (corresponding to an upper limiting value of a for any H_G). It appears, therefore, that the variation in n with varying ionic strength primarily reflects variation in a, there perhaps being a secondary effect due to variation in k_{L4}.

Microbial processes for the production of single-cell protein from hydrocarbon substrates are generally conducted in a basal mineral salts aqueous solution of ionic strength less than those which are commonly used in soluble substrate (e.g., glucose) media. These processes, and other fermentations utilizing a medium of initial ionic strength less than 0.4 g-ion/litre, if conducted in a batch manner may experience an appreciable depletion of ionic strength due to microbial uptake of essential inorganic nutrients (phosphate, sulphate, nitrogen), which, in turn, could lead to significantly lower values of $K_{L4}a$ as the growth process proceeds.

3. Sulphite Oxidation ($K^r_{L4}a$)

In this work, $K_{L4}a$ for oxygen absorption in sodium sulphate and $K^r_{L4}a$ for absorption with reaction in sodium sulphite solutions of identical ionic strengths exhibit the same dependency upon power input in the range $300 \leq P_G/V_L \leq 4000$, and Table 4.1 shows that the dependency upon aeration rate is nearly the same in both cases. $K^r_{L4}a/K_{L4}a$, however, is greater than 1.0, as predicted by the theory of mass transfer in the diffusional-to-fast intermediate reaction regime, Eq. (2.116), assuming that the value of a is the same in both solutions. Comparing Figs. (4.9) and (4.15), the decline in $K_{L4}a$ in sulphate at high power levels may be due to a decrease in K_{L4} as a minimum bubble diameter is approached; K^r_{L4}, of course, depends as well on the kinetics of the reaction and is less dependent on the hydrodynamics.

Defining an absorption coefficient for oxygen, ϕ_4, in the diffusional-to-fast reaction regime as

$$\phi_4 \equiv k^r_{L4}/k_{L4} = [(k_{L4})^2 + D_{L4}k_{SO_3^=}]^{1/2}/k_{L4}\,, \qquad (5.1)$$

then, for $0.01 \leq k_{L4} \leq 0.03$, comparison of the sulphate and sulphite overall volumetric coefficient results, assuming the specific areas are identical in both solutions, leads to the conclusion that the first-order reaction velocity constant for sulphite oxidation has a possible range of values given by

$$18 \leq k_{SO_3^=} \leq 160 \text{ sec}^{-1} \qquad (5.2)$$

The values given by Eq. (5.2) satisfy the pseudo-first order reaction criterion of Eq. (2.97), but fail to satisfy the fast-reaction criterion of Eq. (2.95). Equation (5.2) is in general agreement with the work of de Waal and Okeson (43), who obtained a value of 56 sec^{-1} at 30°C for cupric ion catalysed sulphite oxidation .

Mass transfer coefficients obtained by the sulphite oxdiation method are normally measured at ionic strengths greater than 1.5 g-ion/litre, and in addition are greater than $K_{L4}a$ values for purely physical absorption under otherwise identical conditions. Therefore, application of sulphite oxidation results to microbial processes conducted in media of lower ionic strength and in which the absorption is not accompanied by a homogeneous reaction in the liquid phase may not be valid.

In the only other work in which comparison of sulphate and cupric ion catalysed sulphite oxygen mass transfer behaviour was made in the same tank, Yoshida et al. (14) found the value of $K^r_{L4}a$ in 0.125M

sulphite absorption-with-reaction to be the same as $K_{L4}a$ for absorption only in sulphate solution of the same concentration at the same agitation rate. They concluded that the sulphite oxidation system is rate controlled by the rate of physical absorption of oxygen. However, these results are not in agreement with the theory of mass transfer with chemical reaction, suggesting that perhaps their sulphite solution was, in fact, less reactive towards oxygen than is normally the case.

Cooper, Fernstrom, and Miller (11) measured, in effect, $K^r_{G4}a$ at 20°C by means of sulphite oxidation, using vaned disc impellers of D_I/D_T ratio 0.40 to 0.41 to disperse the gas at $P_G/V_L < 3600$ in a series of tanks ranging in capacity from 0.104 ft^3 to 2.33 ft^3.

For comparison with our results, it is necessary to convert $K^r_{G4}a$ values at 20°C to the corresponding $K^r_{L4}a$ at 30°C. Sulphite oxidations are usually represented by the diffusional-to-fast reaction regime model of Eq. (2.100), but the temperature dependency of the absorption rate given by this model can only be evaluated if values of both k_L and $k_1 = k_2 B_B$ are separately known. Since such is not the case for the work of Cooper et al., a simplifying assumption was introduced, namely that the diffusional regime model of Eq. (2.92) could be used to evaluate the temperature change effect; thus, we considered that $K^r_{L4} \approx k_{L4} \approx K_{L4}$. The temperature variation of k_{L4} for small, rigid, spherical gas bubbles was then obtained by combining the fact that k_{L4} varies as $(D_{L4})^{2/3}$ (16) and that D_{L4}, in turn, varies as $(\mu_L)^{-0.637}$ (85). $K^r_{L4}a$ values at 20°C were obtained from the corresponding $K^r_{G4}a$ values using the approximate relationship

$$K^r_{L4}a \approx (K^r_{G4}a)H \ ,$$

where the Henry's law coefficient H was assumed to have the same value as in sodium sulphate solution of the same ionic strength.

The temperature-corrected absorption rate coefficient data of Cooper et al. were then further corrected for the effect of oxygen partial pressure driving force. Cooper et al. based their calculations on the logarithmic mean gas mole fraction rather than on the exit gas mole fraction of oxygen which subsequently has been shown to be the correct driving force when the dispersed gas phase is well mixed (29).

The sulphite oxidation $K^r_{L4}a$ values of this present study agree remarkably well with the corrected results of Cooper et al. up to the same power level (regardless of the fact that the impeller types and geometric ratios are quite dissimilar), as may be seen by comparing $K^r_{L4}a$ values obtained from Fig. (.1) and Fig. (4.15). However, the results of our work do not agree with Cooper et al.'s conclusion that $K^r_{L4}a$ varies as $(P_G/V_L)^{0.95}(v_S)^{0.67}$, the main difference being in the aeration exponent.

Cooper et al. found that $K^r_{G4}a$ was independent of the tank size over the range of tank diameters investigated (6 to 17.3 in.).

Augenstein and Wang (110) conducted cupric ion catalysed sulphite oxidations (0.5M sulphite, 0.001M cupric ion) at 30°C in a 3-litre tank equipped with a turbine-type impeller of D_I/D_T ratio of 0.51. The power input was measured by a D.C. wattmeter, and ranged from 2 to 150 hp/1000 U.S. gallons (494 to 37,000 ft-lb_f/min-ft^3). The aeration rate was varied from 0.33 to 4.0 VVM. $K^r_{L4}a$ values ranging

from 230 to 6500 hr^{-1} were obtained; these values agree well with those found in this work, which ranged from 60 to 4900 hr^{-1} over a smaller range of power. At power inputs less than 10,000 $ft\text{-}lb_f/min\text{-}ft^3$, Augenstein and Wang found that $K^r_{L4}a$ varied as $(P_G/V_L)^{0.85}$; above this level of agitation power, they found that $K^r_{L4}a$ dependency upon P_G/V_L was reduced, $K^r_{L4}a$ varying as $(P_G/V_L)^{0.57}$. A similar decrease in the rate of increase of $K^r_{L4}a$ with increasing P_G/V_L was noted in our work once P_G/V_L exceeded about 6000 $ft\text{-}lb_f/min\text{-}ft^3$. Augenstein and Wang's results showed that $K^r_{L4}a$ varied as $(v_S)^{0.2}$ at gas flow rates up to 0.011 ft/sec; at higher superficial gas velocities, $K^r_{L4}a$ was independent of v_S.

Westerterp, van Dierendonck, and de Kraa (12) investigated the behaviour of copper-catalysed sulphite oxidation (0.79M) at 30°C, using superficial air velocities at least double the maximum used in this work. Defining N_0 as a critical (minimum) agitation rate, $K^r_{L4}a$ in their system varied as $(N - N_0)D_I$, being completely independent of the aeration rate when $N>N_0$, an observation unique to their work and that of Friedman and Lightfoot (90). Westerterp et al. conclude that $K^r_{L4}a$ or a in stirred tanks depends on aeration rate only if the experiments are done at very low rpm ($N<N_0$) where agitation rate has no effect, or if the log mean partial pressure driving force is used instead of the exit gas partial pressure. However, Westerterp's criterion indicates that N_0 = 950 rpm for the stirred tank used in this work, and a measurable dependency of $K_{L4}a$ or $K^r_{L4}a$ upon v_S at $N>N_0$ was found for all solutions tested, except 0.125M sodium sulphate and 0.22M potassium chloride which, coincidentally, were the only ones that had characteristics

that could be well correlated with N as well as P_G/V_L. It appears, then, that mass transfer rate may be generally independent of gas sparging rate only at relatively high superficial gas velocities, greater than those normally used in submerged fermentation processes, for example.

Robinson (91) in discussing the implications of the results of Westerterp et al. (12) consideres that at impeller rotational speeds less than N_0 the gas rate affects K_La due to an increase in a and an increase in interphase turbulence with increasing v_S. At impeller speeds greater than N_0, the specific area is postulated to be independent of the gas sparging rate because the dispersed gas circulation rates are much greater than the gas supply rate. Therefore, bubbles will remain in contact with the liquid for long periods before escaping the circulation pattern and rising to the surface. The chance of bubble escape becomes independent of its age, and for a significant fraction of the bubbles the actual contact time is much greater than the mean residence time computed from the gas holdup and the sparging rate.

4. Specific Interfacial Area (a)

Values of a measured in this work by dilute carbon dioxide absorption with reaction in electrolyte solutions containing hydroxyl ion are greater than the values obtained by other workers at lower agitation rates, in non-electrolyte solutions, or with pure reactive gases. With pure gases, of course, the degree of absorption is much greater, resulting in appreciable bubble shrinkage during the gas-liquid contact time and subsequent reduction in a. In non-electrolyte solutions, as will be discussed in detail later, the rate of gas bubble coalescence is greater,

resulting in large values of d_b, and hence smaller values of a at constant H_G.

In this work, at constant P_G/V_L, a appears to increase fractionally with increasing ionic strength in the range of $0.09 \leq \Gamma_T \leq 0.40$. Generally, a varied from about 1.0 to 45 cm^{-1} over the agitation power range investigated. The dependency of a upon P_G/V_L increased somewhat with increasing ionic strength of the liquid solution. For KOH - K_2CO_3 solution, a varied as $(P_G/V_L)^{0.89}$; in 0.135M KCl + KOH - K_2CO_3, a was proportional to $(P_G/V_L)^{1.06}$, and for 0.11M Na_2SO_4 + KOH - K_2CO_3, a was dependent upon $(P_G/V_L)^{1.01}$.

In contrast to the results of this investigation in electrolytic solutions, Calderbank (10) reported an optically-measured maximum integral a of about 1.1 cm^{-1} for air dispersions in pure-non-electrolytic liquids at 15°C; in these non-electrolytes, a varied as $(P_G/V_L)^{0.40}$ and was dependent upon the interfacial tension, varying as $(1/\sigma)^{0.6}$. Yoshida and Muira (72) at $60 \leq N \leq 400$ measured a by dilute carbon dioxide absorption and reaction in sodium hydroxide solutions at 20°C and reported a maximum a of 0.8 cm^{-1}. In their work, a varied as $N^{1.1}$, or approximately as $(P_G/V_L)^{0.33}$ for the turbine impeller used.

Westerterp et al. (12) investigated both the cupric ion and the cobaltous ion catalysed sulphite oxidation absorption with reaction, using air, in several stirred tanks of different size and with turbine impellers of varying D_I/D_T ratios. They compared the absorption rate dependency upon N in a cobalt-catalysed sulphite oxidation with the dependency exhibited in the cupric-catalysed systems, the latter comprising the bulk

of their work. They then deduced that the first-order reaction rate constant for the cupric-catalysed oxidation was 9,800 sec^{-1}, based on a rate constant of 37,000 sec^{-1} for the cobaltous system which was measured in a separate laminar liquid jet experiment. If, in fact, the cupric-catalysed kinetic constant were 9,800 sec^{-1}, the absorption with reaction would have proceeded in the fast-reaction regime where the mass transfer rate is independent of k_{L4}, and Westerterp et al.'s conclusion that the absorption rate dependency upon N reflected only the variation in a with N would be valid. However, as discussed by Linek and Myerhoferova (45), in calculating the value of the kinetic constant for the cupric-catalysed oxidation reaction, Westerterp et al. compared the cobaltous and cupric-catalysed absorption rate results using an expression analogous to Eq. (2.101), that is, they assumed a priori that the cupric-catalysed reaction proceeded in the fast-reaction regime. Linek and Myerhoferova (45) also point out that some recent studies (92, 93) have found that the cobaltous-catalysed reaction is second order in oxygen. Therefore, a comparison of cobalt and copper-catalysed absorption rates on the basis of a first-order kinetic model being applicable to both types of solutions could result in an erroneous evaluation of the kinetic constant for the cupric-catalysed reaction. Westerterp et al.'s value of the first-order kinetic constant for the cupric-catalysed reaction is two orders of magnitude greater than the value deduced in this work, Eq. (5.2), and the value obtained by deWaal and Okeson (43). The latter two values do not meet the fast-reaction regime criterion.

Westerterp et al. (12) report specific areas ranging up to 5cm^{-1} in cupric-catalysed 0.793M sulphite at an impeller rotational speed of 1300 rpm; this is about 50 to 60 percent of the values of a determined in 0.11M Na_2SO_4 + KOH - K_2CO_3 (Γ_T = 0.418) at the same N. In addition, Westerterp et al. reported that specific interfacial areas in a pure carbon dioxide - concentrated sodium hydroxide system were identical to those in the cupric ion catalysed sulphite oxidation system using air. As previously discussed in Section II. 5(d)(ii), such agreement would not generally be anticipated. In this present study, pure carbon dioxide was sparged into 0.5M sodium hydroxide at 1000 rpm; the absorption-with-reaction rate was so great, that few, if any, bubbles were observed to leave the dispersion at the free liquid surface. The interfacial area under these conditions was only about one-twentieth the value obtained with 10 percent carbon dioxide absorption with reaction in 0.06M potassium hydroxide at the same agitation rate.

Using sodium hydroxide solutions with added glycerine having viscosities up to ten times that of pure water, Westerterp et al. (12) obtained values of a up to 23 cm^{-1} in stirred-tank dispersions. The effect of the added glycerine on the kinetics of the carbon dioxide - hydroxide reaction, if any, was not considered. The increase in a was apparently due solely to the effect of viscosity.

Based on the questionable premise that the cupric ion catalysed sulphite oxidation system studied by Westerterp et al. (12) was operating in the fast-reaction regime, the results of the study were used by Westerterp to develope a generalized correlation for predicting a in

stirred-tank gas absorbers in terms of the liquid volume fraction, liquid depth, liquid density, the interfacial tension, the tank diameter, and the impeller rotational speed (94). According to Westerterp, a is directly proportional to N for $N > N_0$. In constrast to the results of Westerterp, for the three solutions studied in this work, the interfacial area determined from the rate of absorption-with-reaction of dilute carbon dioxide are not found to be directly proportional to N over most of the agitation rate range investigated. Only one solution, the KOH - K_2CO_3 (average $\Gamma_T = 0.0965$), exhibited a linear dependency of a upon N, and then only over a limited range of N, i.e., $800 \leq N \leq 1300$.

Linek and Myerhoferova (45) studied the absorption with reaction of pure oxygen in cobaltous-catalysed sodium sulphite solution using a stirred tank with a 6-blade turbine impeller having a D_I/D_T ratio of 0.345. Over a range of impeller rotational speeds $250 \leq N \leq 550$, they obtained values of a ranging from 0.24 to 2.24 cm^{-1}. The interfacial areas are less than those that would be obtained using air due to the greater degree of bubble shrinkage with pure oxygen.

In pure liquids having interfacial surface tensions less than that of water, or in viscous aqueous solutions (e.g., glycerol-water mixtures) values of a are significantly greater than the specific area obtained in pure water under otherwise identical conditions. In these cases, the increase in a could be correlated directly with the differences in interfacial tension and/or density and viscosity (10, 12). In relatively dilute aqueous solutions of electrolytes such as those used in this work, the interfacial tensions, and solution viscosities and densities do not, in

general, vary appreciably from their values in pure water, and the large increase in specific interfacial area cannot, therefore, be attributed to these factors to any significant degree.

As far as the effect of interfacial tension is concerned, theory and experimental work indicate that, in general, the addition of an electrolyte to water, at concentrations greater than a certain minimum, increases the surface tension of the solution over that of the pure solvent. For example, the work of Jones and Ray (95) shows that at low concentrations of inorganic solute surface tension first decreases slightly with increasing solute concentration, reaches a minimum at a solute concentration of about 0.01M, and then increases with further increases in solute concentration. Such ions are, therefore, said to be surface inactive.

Drost-Hansen has recently reviewed the state of knowledge about ionic effects at phase interfaces (96). In most aqueous solutions, an electric potential exists at the interface due to either the water dipole orientation alone or, in addition, to the preferential adsorption of ions. Ion hydration may affect the surface structure of water, some ions are structure breakers, while others serve to promote water structure. How, and under what conditions these effects are operative is not clearly understood at present, and no general theory exists whereby the effect of ionic solutes on interfacial stability in dispersions can be quantitatively predicted.

As previously mention in Section V.2(b), Marrucci and Nicodemo (89) found that gas bubble diameters decreased with increasing concentration of inorganic electrolyte until a minimum diameter was reached

at which point the diameter was unaffected by further increases in solute concentration in the bubble column aqueous phase. They attributed the decrease in gas bubble diameter to a decrease in the bubble coalescence rate which, in turn, was due to an increase in repulsive electrical effects at the gas-liquid interface as electrolyte concentration increased. Marrucci and Nicodemo postulate that when two or more kinds of ions are present in solution, they will have different interface-to-bulk solution concentration differences, resulting in the generation of a surface potential difference. This postulation follows from a thermodynamic relationship of Gibbs, namely

$$\zeta = -(\bar{a}/RT)(d\sigma/d\bar{a}) , \qquad (5.3)$$

where ζ is the surface excess concentration.

Equation (5.3) shows that for electrolyte solutions above a minimum concentration, the surface excess molar concentration of an ionic species is negative, since $d\sigma/d\bar{a}$ is positive; that is, ions are generally less concentrated at the interface than in the bulk solution. For bi-ionic electrolytes wherein the ion species have common valence, Marrucci and Nicodemo assumed that a surface potential, Λ, would be generated in proportion to ζ such that

$$\Lambda \propto 0.5\ zC(d\sigma/dC)/[1/(1+d\ln\gamma/d\ln C] . \qquad (5.4)$$

Equation (5.4) predicts that polyvalent electrolytes ($z>1$) are more effective than univalent electrolytes in hindering bubble coalescence. The results of Marrucci and Nicodemo (89) for electrolytes having

common ion valencies showed that the average bubble diameter decreased with increasing Λ, reaching the asymptotic minimum diameter at values of the right-hand side of Eq. (5.4) in excess of about 0.3 dynes/cm. However, Eq. (5.4) alone did not account for the observed behaviour as there was a residual dependency upon the nature of the electrolyte, resulting in deviations of up to 50 percent from the average-behaviour curve.

Reith and Beek recently compared dispersed gas bubble coalescence rates in water and 0.793M sodium sulphite in a stirred-tank gas absorber (97). The coalescence frequency in the sulphite solution was on the order of 10 times smaller that that in water, particularly at impeller speeds below 900 rpm. Bubble segregation in the electrolyte solution was significant (i.e., less than 10 coalescences per bubble during its mean residence time) until the impeller rotational speed exceeded 1000 rpm. The higher coalescence rates in water lead to the conclusion that the gas dispersion was perfectly mixed if $N \geq 480$ for water, but that perfect gas mixing was not obtained in sulphite until $N \geq 800$ rpm.

Howarth studied liquid droplet coalescence rates in a stirred tank using benzene-carbon tetrachloride dispersed in water or in dilute aqueous electrolyte solutions (98). The coalescence rates were determing by using a light transmission method to follow the change in mean drop diameter when the impeller rotational speed was changed from one value to another. In water, for $110 \leq N \leq 360$, the coalescence frequency at a dispersed phase volume fraction of 0.10 ranged from about 0.0018 to 0.0078 sec^{-1}. Coalescence frequency increased by about a factor of four

when the dispersed phase volume fraction was increased to 0.25. The addition of a small amount of electrolytic solute, 0.05M sodium chloride, was found to reduce the coalescence rates by a factor of about 5; the use of sodium sulphate in place of sodium chloride at the same concentration further reduced the coalescence frequency some 45 percent. The mechanism by which the electrolytes hindered drop coalescence was not clear.

5. Dispersed Gas Fractional Holdup (H_G)

The dispersed gas holdup was measured in water and in the three KOH-containing electrolyte solutions at a gas superficial velocity of 0.0150 ft/sec. In water, the dispersed gas was air; in the electrolyte solutions, the dispersed gas was 10 percent carbon dioxide in nitrogen.

For water, H_G varied from 0.0160 to 0.0853 over an agitation power range of $74 \leq P_G/V_L \leq 17{,}700$. He was found that H_G varied as $(P_G/V_L)^{0.40}$, in agreement with the results of Calderbank for pure, non-electrolytic liquids (10). Rushton and Bimbinet studied the effect of tank diameter, D_I/D_T ratio, superficial gas velocity, and total power input (agitation plus aeration) upon air holdup in water (99). The holdup was found to vary as $\left[(P_G)_{Tot.}/V_L\right]^n (v_S)^{0.60}$, where the value of n depended upon the tank diameter and the D_I/D_T ratio. For a 9-in. diameter tank having a D_I/D_T ratio of 0.335, n was 0.28; in a 12-in. diameter tank at a superficial gas velocity of 0.020 ft/sec over a power range of 1.2 to 11 hp/1000 gal, H_G for air varied from 0.022 to 0.045, with which the results of this present investigation are in general agreement.

In the KOH - K_2CO_3 solution (average $\Gamma_T = 0.0965$), H_G varied from 0.0453 to 0.181 with P_G/V_L increasing from 980 to 15,850 ft-lb_f/min-ft^3; H_G varied as $(P_G/V_L)^{0.60}$ for $1000 \leq P_G/V_L \leq 3000$, and as $(P_G/V_L)^{0.38}$ for $3000 \leq P_G/V_L \leq 16{,}000$. Yoshida and Muira (72), who studied the absorption with reaction of dilute carbon dioxide in sodium hydroxide solutions, measured H_G manometrically and found that H_G varied as $N^{0.8}$ for $60 \leq N \leq 180$ at all gas sparging rates; at $N > 180$, the impeller rotational speed exponent became greater than 1.0, the value depending upon the gas sparging rate. At 400 rpm in a 25-cm diameter tank with a D_I/D_T ratio of 0.4, H_G in their work was 0.25, a value about double the H_G at equivalent power input determined in the tank used in this study when the manometer reading is corrected for dynamic pressure effects. Assuming the usual proportionality between N and the power input as given by the Power number, N_P, Yoshida and Muira's results suggest that H_G is proportional to $(P_0/V_L)^{0.26}$, the value of the exponent being considerably less than the value 0.60 found in this present work at the low end of the power range.

In the 0.135M KCl + KOH - K_2CO_3 solution (average $\Gamma_T = 0.221$), H_G varied from 0.0267 to 0.171. The values of H_G were greater than those in water, particularly at high levels of power input, but were about 10 to 15 percent less than those in the KOH - K_2CO_3 solution of lower ionic strength at equal power inputs. For the 0.135M KCl + KOH - K_2CO_3 solution, H_G was found to vary as $(P_G/V_L)^{0.48}$ for $1000 \leq P_G/V_L \leq 18{,}000$.

For 0.11M Na_2SO_4 + KOH - K_2CO_3 (average Γ_T = 0.418), H_G varied as $(P_G/V_L)^{0.63}$ for $400 \leq P_G/V_L \leq 3000$, and as $(P_G/V_L)^{0.53}$ for $3000 \leq P_G/V_L \leq 14{,}000$. Values of H_G ranged from 0.024 to 0.171 over the range of power input investigated at the superficial gas velocity of 0.0150 ft/sec; these values of H_G, at $P_G/V_L > 3000$, are some 10 to 15 percent greater than corresponding holdups in 0.135M KCl + KOH - K_2CO_3, are about the same as corresponding H_G values in the KOH - K_2CO_3 solution.

Holdup was not measured in the sulphite oxidation experiments. However, the $K_{L4}a$ values in the 0.11M Na_2SO_4 + KOH - K_2CO_3 carbon dioxide-reactive analog of the 0.125M Na_2SO_4 + 0.004M $CuSO_4$ solution were in close agreement, and $K_{L4}a$ values in the latter had the same dependency upon P_G/V_L as did the $K^r_{L4}a$ values determined from sulphite oxidation, differing only in magnitude due to the effect of the chemical reaction. Therefore, as a first approximation, one may consider the 0.11M Na_2SO_4 + KOH - K_2CO_3 results to be indicative of the behaviour in sulphite solution. Over an agitation rate range of $0 \leq N \leq 1800$, at a superficial gas velocity of 0.0384 ft/sec, Westerterp in 0.793M sulphite found that H_G varied from 0.01 to 0.27(94), being proportional to $N^{1.0}$ for $250 \leq N \leq 1800$. Westerterp's values of H_G in a 19-cm diameter tank having a D_I/D_T ratio of 0.40 are greater than those determined in this work from corrected manometer readings, and his dependency upon agitation rate is less than that indicated in this investigation.

In the sulphite oxidation system studied by Augenstein and Wang (110), in a 14.7-cm diameter tank using a turbine impeller with a D_I/D_T ratio of 0.51, gas holdup varied from 0.05 to 0.25 at a superficial gas velocity of 0.00834 ft/sec over an agitation power input range of 700 to 37,000 ft-lb_f/min-ft^3. For $P_G/V_L < 9{,}800$, H_G varied as $(P_G/V_L)^{0.40}$ at the highest superficial gas velocity (0.0415 ft/sec) to $(P_G/V_L)^{0.53}$ at v_S equal to 0.00834 ft/sec. At P_G/V_L values greater than 9,800, H_G asymptotically approached an apparent upper limit of 0.25 at all superficial gas velocities greater than 0.00834 ft/sec. At a power input equal to the maximum used with 0.11M Na_2SO_4 + KOH - K_2CO_3, and at a superficial gas velocity of 0.00834 ft/sec, Augenstein and Wang obtained H_G equal to 0.19, in close agreement with the value of 0.171 found in this investigation.

6. Average Gas Bubble Diameter (d_b)

The average gas bubble diameters in the three electrolyte solutions studied range from 0.231 to 0.024 cm as the power input was increased from 900 to 16,000 ft-lb_f/min-ft^3. Bubble diameter appears to decrease significantly with increasing ionic strength at constant P_G/V_L, particularly at relatively low values of P_G/V_L. For example, at 980 ft-lb_f/min-ft^3, the average bubble diameters in KOH - K_2CO_3 (average $\Gamma_T = 0.0965$), 0.135M KCl + KOH - K_2CO_3 (average $\Gamma_T = 0.221$), and 0.11M Na_2SO_4 + KOH - K_2CO_3 (average $\Gamma_T = 0.418$) were 0.231, 0.128, and 0.100 cm; when the power input has reached 15, 900 ft-lb_f/min-ft^3, average bubble diameters in the three aforementioned solutions were 0.034, 0.025, and 0.0245 cm, respectively.

From gas holdup and interfacial area measurements in cupric-catalysed 0.793M sodium sulphite solution (areas being evaluated on the questionable conclusion that the absorption with reaction was in the fast-reaction regime), Westerterp reports much greater values of the average bubble diameter, even at appreciably greater agitation rates than the maximum used in this study (94). In Westerterp's work, the average bubble diameter decreased rapidly from 0.8 cm at 900 rpm to an agitation-rate independent value of 0.47 cm over the range $1500 \leq N \leq 2500$, then decreased slowly to 0.35 cm at 3600 rpm; measurements were reported for a 19-cm diameter tank with a turbine impeller of D_I/D_T ratio 0.40.

Yoshida and Muira (72) for dilute carbon dioxide absorption with reaction in sodium hydroxide solutions found that d_b ranged from 0.45 to 0.15 cm for $60 \leq N \leq 330$ rpm, d_b varying as $N^{-0.3}$.

For pure, non-electrolytic liquids, Calderbank (10) found that d_b varied as $(P_G/V_L)^{-0.40} (H_G)^{0.50} \sigma^{0.60}$. The average bubble diameter in both 5- and 100-litre tanks ranged from 0.2 to 0.5 cm for dispersed air in the range $3300 \geq P_G/V_L \geq 330$.

7. Liquid-Phase Mass Transfer Coefficient (k_{L4})

As shown on Figs. (4.20), (4.22), and (4.24), in the aqueous electrolyte solutions of $0.0965 \leq \Gamma_T \leq 0.418$ over the agitation power range $1000 \leq P_G/V_L \leq 17{,}200$, the liquid-phase mass transfer coefficient for oxygen, k_{L4}, decreases with increasing P_G/V_L. Values of k_{L4} ranged from 0.0484 down to 0.0098 cm/sec, concomitantly with a decrease in average gas bubble diameter from 0.231 to 0.0231 cm. This decrease in k_{L4} with decreasing d_b in this bubble diameter range has not previously been reported for bubble dispersions

in electrolyte solutions, but is consistent with prior results for bubbles of the same general size range for dispersions and for single bubbles in viscous, Newtonian, non-electrolytic aqueous solutions.

Calderbank investigated k_L behaviour in pure liquids and in aqueous solutions of glycol and glycerol at 20°C for sparingly-soluble gas dispersions using both pulsed sieve plates and stirred tanks (9). He investigated two bubble size regimes: "large" bubbles, defined as having an average diameter greater than 0.25 cm, and "small" bubbles, defined as having an average diameter less than 0.25 cm; in practice, the small bubbles were apparently generally less than 0.1 cm in diameter (16). For both of these bubble size ranges, he found that the value of k_L was independent of the bubble size, and hence independent of the agitation power on which the bubble size was dependent (9). For "small" bubbles, k_L ranged from 0.003 to 0.05 cm/sec, and was proportional to $(D_{Lk})^{2/3}$, in agreement with the results for mass transfer from solid particles dispersed in liquid phases, leading to the conclusion that "small" bubbles behave as rigid spheres (9). The "large" bubbles' k_L values ranged from 0.05 to 0.11 cm/sec. For the same dispersed gas - liquid phase combination, "large" bubble k_L was about an order of magnitude greater than the corresponding value for "small" bubbles. "Large" bubble k_L was also independent of P_G/V_L, varying only as $(D_{Lk})^{0.86}$. Calderbank's work indicated that the value of D_{Lk} was the major factor affecting the value k_L for a given size range of bubbles; however, the effect of liquid-phase viscosity upon k_L was not separable from its effect on D_{Lk}.

Calderbank and Moo-Young (16) presented generalized correlations for the k_L behaviour of bubble swarms in both sieve-plate columns and stirred tanks. For both "large" and "small" bubbles, the mass transfer coefficient was independent of the agitation power input in stirred tanks or the fluid flow rates in bubble columns, being merely dependent upon the physical properties of the phase according to

"Small" bubbles: $$N_{Sh} = 2.0 + 0.31\left[d^3 \Delta\rho g/\mu_L D_{Lk}\right]^{1/3}, \qquad (5.5)$$

"Large" bubbles: $$N_{Sh} = 0.42(N_{Sc})^{1/2}(N_{Gr})^{1/3}. \qquad (5.6)$$

Equation (5.5) is consistent with Frossling's equation for solid spheres (19), leading to the conclusion that "small" bubbles behave as rigid particles with their motion relative to the liquid phase being retarded (16); k_L is proportional to $(D_{Lk})^{2/3}$ in this case. Equation (5.6) predicts that k_L for "large" bubbles varies as $(D_{Lk})^{1/2}$, in agreement with Higbie's penetration theory (17), Eq. (2.87), and Danckwert's random surface renewal model (18), Eq. (2.91).

For carbon dioxide absorption in viscous aqueous solutions of glycerol, Calderbank and Moo-Young (16) demonstrated the existence of a transitional bubble regime intermediate between those of "small" and "large" bubbles. In this transitional regime, characterized by $0.05 \leq d_b \leq 0.25$ cm, k_L decreased with decreasing d_b. Hence, in general, as P_G/V_L is increased, thereby decreasing d_b, k_L remains constant until d_b decreases to a value of about 0.25 cm, decreases more-or-less in direct proportion to d_b until d_b reaches

about 0.05 cm, and then assumes a smaller, constant value as d_b is further decreased with increasing P_G/V_L. The results of the present study of k_{L4} behaviour in non-viscous aqueous solutions of electrolytes are in general agreement with the work of Calderbank and Moo-Young in the same average bubble size range characteristic of the transitional regime. It appears, then, that the decrease in k_{L4} over the range $0.25 \geq d_b \geq 0.02$ cm is due solely to the change in bubble-liquid interfacial motion characteristics; the interfacial relative motion and the subsequent mass transfer behaviour is dependent on the bubble size for the most part, there being, perhaps, only a relatively minor effect due to the nature of the solution (e.g., viscosity) in which the bubble is produced.

Kintner has reviewed the hydrodynamic characteristics of dispersed liquid droplets (or gas bubbles) (100). Small bubbles have relatively low values of bubble Reynolds number; the inertial forces are negligible, and the bubbles maintain a rigid, spherical shape, the bubble surface area (at low mass transfer rates) and shape thereby being constant during the entire lifetime of the bubble (the time interval between successive coalescences and break-up). Small bubbles are surrounded by a liquid laminar sub-layer and a very thick laminar transition boundary layer, resulting in relatively low values of k_L. On the other hand, large bubbles behave as fluid bodies, having internal circulation and mobile interfaces. The large bubbles have higher values of bubble Reynolds number; consequently, inertial forces predominate, and the surface shape is continually distorted as the bubble moves relative to the liquid

from near-spherical, to oblate ellipsoid to prolate, with oscillation between the two latter shapes occurring in large drops or bubbles. The deformation of the large bubble surface enhances the rate of formation of fresh mass transfer surface, thereby resulting in large bubbles having greater values of k_L than smaller bubbles. Intermediate behaviour results in the transition regime between small and large bubbles.

Equivalent behaviour has been found for single bubbles in a bubble column. Garner and Hammerton (62) studied the mass transfer behaviour of single bubbles of oxygen or ethylene in aqueous glycerol solutions at 17°C. For $d_b > 0.3$ cm, they found that k_L behaviour followed the prediction of the penetration theory (17), while for $d_b < 0.10$ cm, k_L approached smaller values in accordance with Frössling's equation for solid spheres (19). For intermediate size bubbles, $0.15 \leq d_b \leq 0.30$, k_L values were some 20 percent less than those predicted from the penetration theory, but were some 300 to 400 percent greater than predictions based on the Frössling equation; k_L decreased with decreasing bubble diameter in this intermediate size range. Garner and Hammerton concluded that the Higbie penetration theory ($k_L \propto D_{Lk}^{1/2}$). is valid for oscillating and deforming single bubbles of $0.3 \leq d_b \leq 0.8$, while single bubbles of $d_b < 0.1$ behave as rigid spheres ($k_L \propto D_{Lk}^{2/3}$).

Sieminski and Raymond (102) studied single-bubble behaviour using the system carbon dioxide - distilled water at 25°C. Bubble size was regulated by the rate of injection of a volume of gas contained in a glass capillary inside the bottom of the bubble column. Large bubbles of size range $0.30 \leq d_b \leq 0.38$ rose through the liquid with a helical motion with consequent surface shape deformation; for these

bubbles, k_L increased with decreasing bubble diameter in agreement with the Higbie model for circulating bubbles (17), ranging in value from 0.04 to 0.06 cm/sec. The value of k_L reached a maximum at a bubble diameter of about 0.30 cm, and then decreased as the bubble diameter was further reduced to 0.27 cm. For these smaller sized bubbles, the helical motion was much less pronounced, the bubbles tending to rise vertically through the aqueous phase. Zieminski and Raymond considered a bubble diameter of 0.30 cm to be the point at which the transition from circulating bubbles to rigid spheres began.

Yoshida and Muira combined their carbon dioxide - hydroxide solution results for the specific interfacial area (72) with values of $K_{L4}a$ measured in an air-water system by Yoshida et al. (14) to calculate the variation of k_L without reaction. For $d_b > 0.15$ cm, they found that the Sherwood number could be correlated with the impeller Reynolds number and the Schmidt number such that k_L increased with increasing agitation rate, varying as $(ND_I)^{0.6}/d_b^{0.4}$, in the range $60 \leq N \leq 400$. However, this method does not ensure (i) that the specific interfacial area in the physical absorption runs in water is the same as the a in the chemical reaction runs since a varies with ionic strength, and (ii) that the average d_b is the same in both types of liquids since d_b decreases with increasing electrolyte concentration. Therefore, the dispersed bubbles may have been subjected to significantly different hydrodynamic regimes.

In applying our new concurrent oxygen desorption, carbon dioxide absorption-with-reaction technique for the simultaneous evaluation of

k_{L4} and a , it is implicitly assumed that the gas-phase mass transfer resistance is negligible, and further that the temperature rise at the interface (resulting from the heats of absorption and reaction of carbon dioxide) is insignificant such that interfacial physical properties may be evaluated at the bulk solution temperature.

The temperature rise at the interface, ΔT_i , was predicted by the method of Danckwerts based on the random surface renewal model of interfacial hydrodynamics (103). For a carbon dioxide heat of solution of -4.755 kcal/gmole (83), and heat of reaction of -21.2 kcal/gmole (111), the maximum temperature rise at the interface corresponding to a minimum rate of surface renewal (k_L = 0.01) is predicted to be

$$(\Delta T_i)_{MAX} = 1.21 y_{3,2} \quad (°C) \qquad (5.7)$$

such that at the maximum experimental exit gas mole fraction of carbon dioxide of 0.0319, $(\Delta T_i)_{MAX}$ was only 0.0385°C.

Based on the Chilton-Colburn analogy between heat and mass transfer (104), the actual temperature rise at the interface can be predicted from

$$\Delta T_i = R^r_{V3}(\Delta H_{rx} + \Delta H_{soln})/19.5\, K_{L3}\, a. \qquad (5.8)$$

In the KOH - K_2CO_3 solution, ΔT_i's calculated from Eq. (5.8) were less than 0.004°C.

Gas-phase mass transfer resistance can, of course, be made identically zero by using pure carbon dioxide. However, the large degree

of bubble shrinkage which would be experienced would result in the bubble sizes and interfacial areas being appreciably different with carbon dioxide sparge gas than with air, making the results of the study with respect to a, d_b, and k_L, inapplicable to air-sparged fermentation systems. For this reason, dilute carbon dioxide was used as the sparge gas; with 0.10 mole fraction carbon dioxide in the inlet gas, the maximum degree of absorption is limited to the maximum experienced in the sulphite oxidation system using air.

The gas-phase fractional mass transfer resistance was calculated in accordance with the theoretical model of Kronig and Brink for liquid droplet internal mass transfer (105). As discussed by Westerterp et al. (12), for gas bubbles the internal Sherwood number, $k_G H\, d_b/D_{Gk}$, varies between 10 for small, rigid bubbles and 25 for large bubbles with completely developed internal circulation. Defining the fractional gas-phase mass transfer resistance, f_3^*, for carbon dioxide in an absorption-with-reaction system operating in the fast-reaction regime (wherein the effect of gas-phase resistance is even more pronounced than in the diffusional-to-fast reaction regime used in this work) as

$$f_3^* \equiv (1/Hk_G)/\left[(1/Hk_G) + (k_2 D_{L3}\,[OH^-])^{1/2}\right] , \qquad (5.9)$$

the maximum value of f_3^* for small, rigid bubbles corresponding to a maximum average bubble diameter of 0.23 cm is only 0.013, being, therefore, negligible as expected for a sparingly-solute gas.

8. Generalized Correlation for $K_L a$ or $K_L^r a/\phi$

The generalized correlation of Fig. (4.27) appears to represent well the majority of the experimental data for oxygen mass transfer in the 2.5 litre working volume tank used in this study. It is not known if this same correlation can be applied directly to scale-up, that is, if the correlation will remain valid for larger sized tanks having the same pertinent geometric ratios. Calderbank's correlation for a (10) was independent of tank size over a twenty-fold volume variation; Cooper et al.'s sulphite oxidation correlation (11) was valid for varying tank liquid volume by a factor of 22. However, Westerterp et al. (12), varying tank liquid volumes by factors ranging from about 1.2 to 40, found that $K_{L4}^r a$ was proportional to the square root of the tank diameter.

The generalized correlation in its present form likely is restricted for use with only those types of solutions or fermentation media which exhibit Newtonian viscosity behaviour, and in which the viscosity is of the same order of magnitude as that in water. In the microbial processing industries, such solutions are represented by media in which the growing microorganisms are unicellular, utilizing either a soluble or insoluble carbon source, and into which the microorganisms do not excrete significant amounts of polymeric materials. Without further experimental verification, the correlation should be used only for systems operating within the normal biological temperature range of 20 to 40°C.

Like all other previous correlations for the prediction of $K_L a$, the generalized correlation of Fig. (4.27) does not account for the effects

of foaming which occurs in, or for the effects of anti-foam agents which are added to many microbial processing systems. However, the generalized correlation of Fig. (4.27) is considered preferable to correlations based solely on pure water (as obtained from the results of 9, 10, 16) because of the significant ionic strength effect, and preferable to correlations based on sulphite oxidation (11, 12) because of the chemical kinetics effect in the latter system.

The generalized correlation was developed specifically for the case of mass transfer from "small" bubbles ($d_b < 0.10$ cm). However, by applying an appropriate correction factor, it may be used for estimating the value of $K_L a$ for the mass transfer of sparingly-soluble gases in aqueous solutions in which the average bubble diameter may be classified as "large" ($d_b > 0.20$ cm). As shown on Figs. (4.23) and (4.25), the average bubble diameters in highly-agitated electrolyte solutions are intermediate to the "small" and "large" size limits. For "small" bubbles, k_L varies as $(D_L)^{2/3}$, as used in Eq. (4.12), while for "large" bubbles, k_L varies as $(D_L)^{1/2}$ (16). In addition, "large" bubble k_L is greater in magnitude than "small" bubble k_L all other physical property factors being constant.

Combing Eq. (5.5) for "small" bubbles with Eq. (5.6) for "large" bubbles, it follows that

$$(k_L)_{large} = 1.36(N_{Sc})^{0.167}(k_L)_{small} \quad (5.10)$$

The work of Calderbank (10) showed that the interfacial area dependency upon physicochemical factors was independent of bubble size. Therefore, for evaluating $K_L a$ in "large" bubble systems such

as might be produced in near-zero ionic strength solutions at low agitation rates, the ordinate value of Fig. (4.27) must be multiplied by the factor $1.36(N_{Sc})^{0.167}$.

As shown in Table 4.1, experimental values of the aeration exponent m did not vary in a mathematically-describable manner with ionic strength. However, as shown on Fig. (4.19), it appears that there is a trend of increasing m with increasing Γ_T. In the development of the generalized correlation, actual experimental values of m were used. For Medium A-1, the experimental value of m was 0.43; the trend correlation of Fig. (4.19) would result in a value of 0.36 for m in a solution of this ionic strength. If the value 0.36 were to have been used in the correlation of Fig. (4.27), the data points for Medium A-1 would have decreased some 30 to 35 percent in ordinate value.

To use the generalized correlation for predictive purposes, one must first know, or be able to estimate, the physicochemical properties Γ_T, σ, μ_L, D_L, and ρ_L. The physical property factor ξ is then calculated from Eq. (4.12). Values of n are obtained from Fig. (4.19) or from Eq. (4.7), while λ is obtained from either Fig. (4.26) or Eqs. (4.16) and (4.17). The diffusivity of the absorbing gaseous species in an electrolyte solution at 20 to 40°C may be estimated from Eq. (4.15). The required diffusivity in water, D_W, may be estimated from tabulations (33) or correlations (86) in the literature. Alternatively, the diffusivity may be measured experimentally, using one of several methods that have been applied previously (e.g., 85, 86); diffusivity measurement methods are reviewed by Reid and Sherwood (33).

For an aqeuous electrolyte solution of (a priori) unknown value of the superficial gas velocity exponent, m , it is suggested that m be chosen from the trend correlation given on Fig. (4.19) as a first approximation. However, until such time as the effect of ionic strength upon m is better defined, it must be recognized that the resultant value of $K_L a$ obtained from Fig. (4.27) may be subject to an error or some 30 to 40 percent in the range $0.00375 \leq v_S \leq 0.0150$ ft/sec (the computed $K_L a$ perhaps being low for solutions of ionic strength in the range $0 \leq \Gamma_T \leq 0.20$).

VI. CONCLUSIONS

A membrane-covered dissolved oxygen probe is an ideal tool for the experimental measurement of the oxygen overall volumetric mass transfer coefficient applicable to any solution of desired composition contained in a stirred tank gas absorber of given design. $K_{L4}a$ can be measured by using either CFST, steady-state or SBST, unsteady-state procedures. The latter procedure requires a minimum of experimental complexity, but its use is contingent upon having an applicable mathematical model of the time response characteristics of the stirred tank - oxygen probe system. The probe membrane should be sufficiently rugged in construction to ensure a reasonably long service life, but at the same time the membrane thickness must be limited in order to have adequate time response characteristics, particularly if $K_{L4}a$ is to be measured at high agitation rates.

For unsteady-state work, the diffusional time lag in the probe membrane must be taken into account if significant errors in $K_{L4}a$ measurement are to be avoided. Using the well-stirred dispersed gas phase mass transfer model of Hanhart et al. (29), mathematical models of the probe transient response were derived for both absorption and desorption, Eqs. (2.75) and (2.83), respectively. The results of this study showed that at agitation power inputs per unit liquid volume (P_G/V_L) greater than about 1000 ft-lb_f/min-ft^3 (which, apparently, is the limit below which the well-stirred gas phase assumption is not valid) $K_{L4}a$ values obtained by the unsteady-state methods are consistent with steady-state results; for example, see Fig. (4.6) and Figs. (4.11) to

(4.14), inclusive. It is concluded, therefore, that the probe transient response models, Eqs. (2.75) and (2.83), adequately characterize the overall unsteady-state behaviour of a stirred tank - oxygen probe system in which both the gas and liquid phases may be considered to be well mixed, and in which $K_{L4}a$ values up to the order of 2000 hr^{-1} can be produced. However, the sensivity of a particular probe used was not sufficiently adequate to determine accurately the effect of the superficial gas velocity (v_S) upon $K_{L4}a$ (which effect is relatively small with respect to the effect of agitation power), particularly at values of $K_{L4}a$ in excess of 200 to 300 hr^{-1}. To evaluate the effect of v_S under these circumstances, recourse must be made to the CFST, steady-state model described by Eq. (2.35) or Eq. (2.36) in which probe external voltage readings are substituted for the corresponding oxygen concentrations.

Where computer facilities are available, $K_{L4}a$ values obtained by either the transient absorption or desorption techniques utilizing a dissolved oxygen probe are as readily obtainable as $K^r_{L4}a$ values from cupric ion catalysed sulphite oxidation tests. In addition, the $K_{L4}a$ results are directly applicable to the aqueous phase in which they were obtained. Appropriately correcting the mass transfer models for microbial respiration, the aqueous phase may be the actual growth medium containing suspended cells and, possibly, excreted metabolic products. On the other hand, $K^r_{L4}a$ results are subject to a possibly uncertain interpretation as far as their direct application to microbial growth media or other gas absorption systems is concerned.

For the particular tank of 2.5 litres working liquid volume used in this study, $K_{L4}a$ generally correlated better with P_G/V_L than with impeller rotational speed (N); for example, compare Figs. (4.4) and (4.5). However, the effect, if any, of tank size was not investigated, and hence the results merely suggest rather than establish the use of P_G/V_L rather than N in scale-up calculations.

The superficial gas velocity range investigated, $0.00375 \leq v_S \leq 0.0150$ ft/sec, corresponded to an air supply rate of $0.5 \leq VVM \leq 2.0$, a range commonly used in the submerged cultivation of aerobic micro-organisms. In this range, $K_{L4}a$ was found to have a relatively small but nonetheless experimentally-detectible (in steady-state) dependency upon v_S. Contrary to the work of Westerterp et al. (12), it is therefore concluded that v_S is a design parameter to be included in most microbial cultivation processes.

The variation in $K_{L4}a$ with P_G/V_L (and to some extent with v_S) was found to be significantly dependent upon the ionic strength of the aqueous phase, a fact not heretofore deduced in other studies. The value of the agitation power exponent (n) is particularly sensitive to ionic strength in the range $0 \leq \Gamma_T \leq 0.40$, as shown on Fig. (4.19). For the most part, n is independent of P_G/V_L. However, for solutions of low ionic strength ($\Gamma_T < 0.20$), excluding water, n appears to become dependent upon P_G/V_L for $P_G/V_L > 10^4$ ft-lb$_f$/min-ft^3 as shown, for example, on Fig. (4.4). For solutions of higher ionic strength ($\Gamma_T \geq 0.40$), the dependency of n upon P_G/V_L becomes evident at about 6000 ft-lb$_f$/min-ft^3, as shown on Figs. (4.9) and (4.15).

It appears that the presence of ionic solutes, even in low concentration, greatly reduces the rate of gas bubble coalescence, thereby resulting in a smaller average bubble diameter which, in conjunction with an increase in dispersed gas holdup with ionic strength, in turn results in a significant increase in the specific interfacial area for mass transfer (a). As ionic strength increases, the smaller bubbles have inherently lower values of K_{L4} in accordance with both theory (17, 18, 19) and experiment (e.g., Figs. 4.24 and 4.25), but this decrease is more than compensated for by an increase in a , such that the combined coefficient $K_{L4}a$ increases with increasing Γ_T at constant P_G/V_L and v_S in the aforementioned range of Γ_T.

The mechanism by which ionic strength influences the equilibrium bubble size is not known, although it has been suggested by a number of workers that the effect arises from a differential concentration of ionic species between the bulk solution and the gas-liquid interface regions and the resultant effect on water dipole orientation (89, 96, 98). Whatever the specific mechanism may be at the molecular level, its gross manifestation in the overall system appears to be described by the same type of model which characterizes molecular adsorption of the Langmuir type. As shown by Fig. (4.19), as far as the value of n is concerned the ionic strength phenomenon reaches a saturation point such that n becomes independent of Γ_T when $\Gamma_T \geq 0.40$ g-ion/litre.

The variation of n with Γ_T undoubtedly accounts for part of the differences in $K_{L4}a$ values predicted from previous correlations, such as shown on Fig. (1.1), particularly when comparing the results in

electrolyte solutions to those in water. However, these previous correlations were obtained, for the most part, in stirred tanks of different geometry and the effect of ionic strength differences cannot be separated readily from the effects of geometry differences.

In microbial growth systems using dispersed liquid hydrocarbons as the carbon source, the rate of supply of this insoluble substrate is generally growth-rate limiting when the aeration rate is adequate, more so than in the case of conventional soluble-substrate processes utilizing dissolved carbohydrates. Hence, in hydrocarbon substrate systems, the concentrations of essential inorganic nutrients can be lower than in soluble-substrate systems without one of the inorganic species itself becoming the growth rate limiting factor. Media recipes suggested for hydrocarbon systems specify a lower total concentration of inorganic salts than is generally the case for carbohydrate substrate systems. Consequently, media of initially low ionic strength, for example Medium A-1 at an initial value of 0.136 g-ion/litre, could lose a significant amount of oxygen mass transfer capacity in batch growth situations due to the decrease in $K_{L4}a$ with decreasing Γ_T as the inorganic nutrient concentration decreases with time.

A generalized correlation, Fig. (4.27), has been developed for predicting $K_L a$ for the mass transfer of sparingly-soluble gases in stirred tanks or for predicting $K_L^r a/\phi$ in stirred tank absorber-reactors having the same impeller type and geometric ratios as the tank used in this study. The correlation incorporates the significant effect of ionic strength found in this present work, and the effects of the other pertinent

physicochemical parameters previously determined by Calderbank (9) and Calderbank and Moo-Young (16). The generalized correlation was developed specifically for use with bubble dispersions having the average bubble diameters typically found in agitated electrolyte solutions and described as being "small" bubbles, that is, having bubble diameters less than 0.10 to 0.15 cm. A means of adjusting the correlation so that it may be used for predicting the mass transfer behaviour of "large" bubble systems ($d_b > 0.20$ cm) is suggested.

A new experimental technique utilizing concurrent oxygen desorption and carbon dioxide absorption-with-reaction was developed to separately evaluate a and the liquid-phase oxygen mass transfer coefficient (k_{L4}) under reasonably consistent hydrodynamic conditions. The technique was tested experimentally in three different systems, two of which were carbon dioxide-reactive analogs of solutions previously studied with respect to $K_{L4}a$ behaviour only. The experimental results, Figs. (4.20) to (4.25), inclusive, lead to the conclusion that k_L and a have diametrically opposite dependencies upon P_G/V_L ; k_L decreases with increasing P_G/V_L (concomitantly with decreasing average bubble diameter), while a increases with increasing P_G/V_L . The decrease in k_L with decreasing d_b may be attributed to change in bubble hydrodynamic regimes from the deformable, circulating bubbles of large diameter to the rigid, spherical bubbles of small diameter.

Sideman, Hortacsu, and Fulton (113), based on works such as those of Calderbank (9), Calderbank and Moo-Young (16), and Hyman (114) which indicate that k_L is independent of P_G/V_L or nearly so, suggested that

for all practical purposes $K_L a$ depends only on the variation of a with agitation rate and superficial gas velocity. It is concluded from the results of this present study that such is not the case of electrolyte solutions of $0.10 \leq \Gamma_T \leq 0.40$ agitated over the power range $10^3 \leq P_G/V_L \leq 2(10)^4$.

A definitive study of the effect of ionic strength upon H_G, d_b, and k_L was not part of this present work. However, the results of the three systems examined suggest that it would be profitable to fully define the ionic strength effect on these three parameters (and upon a), applying the concurrent measurement technique to solutions of ionic strength range $0.05 \leq \Gamma_T \leq 1.0$. The results of such a separate study could lead to even better predictions for $K_L a$ in electrolyte solutions based on the separate behaviour of k_L and a than that presently available from Fig. (4.27).

NOMENCLATURE

a	gas-liquid interfacial area per unit liquid volume, cm^{-1}
$\bar{a}$	activity of component in the liquid phase
A	surface area of oxygen probe membrane, cm^2
B	concentration of non-volatile liquid-phase reactant, $gmole/cm^3$
C	concentration, $gmole/cm^3$
$\overline{C}$	LaPlace-transformed concentration of oxygen in probe membrane, $gmole/cm^3$
d_b	gas bubble average diameter $(\sum_i n_i d_i^3 / \sum_i n_i d_i^2)$, cm
$\bar{D}$	dilution rate in CFST, defined by Eq. (2.35), sec^{-1}
D_I	impeller diameter, cm
D_{Lk}	diffusivity of species k in liquid phase, cm^2/sec
D_M	effective diffusivity of oxygen in probe membrane, cm^2/sec
D_T	tank internal diameter, cm
E	potential difference across external resistor in oxygen probe circuit, volt
f	fugacity, atm
f^0	standard state fugacity, atm

f_{BM} backmixing fraction, defined by Eq. (3.4), dimensionless

f^* fractional gas-phase mass transfer resistance defined by Eq. (5.9), dimensionless

F liquid flow rate, cm^3/sec

$\overline{F}$ Faraday constant, amp-sec/equiv

G gas flow rate, gmole/sec

g gravitational acceleration, ft/sec^2

g_c conversion factor, 32.2 $ft\text{-}lb_m/lb_f\text{-}sec^2$

h molar gas holdup in the liquid phase, gmole gas/cm^3 gas-free liquid

H Henry's law coefficient, $atm\text{-}cm^3/gmole$

H_L fractional liquid holdup, volume of gas-free liquid per volume of gas-liquid dispersion, dimensionless

H_G fractional gas holdup, volume of dispersed gas per volume of gas - liquid dispersion, dimensionless

$\mathcal{H}_F$ linear displacement of manometer fluid, inches

i the fundamental imaginary number, $(-1)^{1/2}$

I current generated by oxygen probe, ampere

k_1 first-order reaction velocity constant, sec^{-1}

k_2 second-order reaction velocity constant, $cm^3/gmole\text{-}sec$

k_L liquid-phase mass transfer coefficient in non-reactive system, cm/sec

k_L^r effective liquid-phase mass transfer coefficient for absorption with chemical reaction, cm/sec

K_L overall mass transfer coefficient based on liquid-phase concentration difference driving force for absorption without reaction, cm/sec

K_L^r effective overall mass transfer coefficient based on liquid-phase concentration difference driving force for absorption with chemical reaction, cm/sec

K_M permeability of probe membrance to oxygen defined by Eq. (2.51), gmole/cm-sec-atm

$K_G a$ overall volumetric mass transfer coefficient based on partial pressure difference driving force for absorption without reaction, gmole/cm^3-sec-atm

$K_L a$ overall volumetric mass transfer coefficient based on liquid-phase concentration difference driving force for absorption without reaction, sec^{-1}

$K_L^r a$ effective overall volumetric mass transfer coefficient based on liquid-phase concentration difference driving force for absorption with chemical reaction, sec^{-1}

K_4 equilibrium constant for hydrolysis of carbonate ion defined by Eq. (2.109), gmole/cm^3

L	thickness of oxygen probe membrane, cm
L'	distance between manometer taps, ft
m	exponent of v_S, dimensionless
n	exponent of P_G/V_L, or an integer in a mathematical series, dimensionless
n_I	number of electrons transferred in the oxygen probe electrochemical reaction
N	impeller rotational speed, rev/min
$\underline{N}$	diffusive molar flux relative to fixed coordinates, gmole/cm^2-sec
N_A	Aeration number, defined by Eq. (3.3), dimensionless
N_{Gr}	Grashof number $d^3 \rho_L \Delta\rho\, g/\mu_L^2$
N_P	Power number, defined by Eq. (3.1), dimensionless
N_{Re}	impeller Reynolds number defined by Eq. (3.2), dimensionless
N_{Sc}	Schmidt number $\mu_L/\rho_L D_{Lk}$, dimensionless
N_{Sh}	Sherwood number $k_L d_b/D_{Lk}$, dimensionless
p	partial pressure, atm
$\bar{P}$	hydrostatic pressure, lb_f/ft^2
P_G	agitation power input to gassed liquid, ft-lb_f/min
P_0	agitation power input to ungassed liquid, ft-lb_f/min

P_T	total pressure in absorber-reactor vapour space, atm
q	LaPlace transformation parameter, defined by Eq. (2), Appendix II. 1
Q	volumetric gas flow rate at 60°F, 1 atm, cm^3/sec
R	resistance of resistor in oxygen probe external circuit, Ohm
$\bar{R}$	universal gas constant, cal/gmole-°K
R_V	liquid-phase absorption rate of gaseous component, $gmole/cm^3$-sec
$\bar{R}_V$	liquid-phase reaction rate of dissolved gaseous component, $gmole/cm^3$-sec
s	LaPlace transform parameter
$\bar{s}$	fractional rate of renewal of surface liquid elements, sec^{-1}
S	solubility of oxygen in oxygen probe membrane, defined by Eq. (2.50), $gmole/cm^3$-atm
t	time, sec
T	absolute temperature, °K
$\underline{u}$	local mass average fluid velocity (vector), cm/sec
v_S	superficial gas velocity based on empty tank cross-sectional area, ft/sec
V_L	volume of gas-free liquid, cm^3 (ft^3 with P_G/V_L)

x	distance measured in x-coordinate direction, cm
x'	liquid-phase mole fraction, dimensionless
y	mole fraction of component in gas phase, dimensionless
z	electric charge carried by ionic species
Z	reaction stoichiometric coefficient defined by Eq. (2.96), dimensionless

GREEK LETTERS

α	aeration-agitation parameter defined by Eq. (2.26), $gmole/cm^3\text{-}sec$
β	aeration-agitation parameter defined by Eq. (2.25), sec^{-1}
γ	liquid-phase activity coefficient, dimensionless
Γ	ionic strength, defined by Eq. (3.22), g-ion/litre
δ	thickness of stagnant liquid film, cm
∇	Nabla operator, cm^{-1}
∇^2	LaPlacian operator, cm^{-2}
ϵ	denotes $K_L a$ or $K_L^r a/\phi$
ζ	surface excess concentration defined by Eq. (5.3), $gmole/cm^2$

λ proportionality constant defined by Eq. (4.14), $gm^{0.40}\,cm^{0.067}\,sec^{0.534}(ft\text{-}lb_f/min\text{-}ft^3)^{-n}(ft/sec)^{-m}$

Λ interfacial surface potential defined by Eq. (5.4), volt

μ viscosity, gm/cm-sec (poise)

ξ physical property factor defined by Eq. (4.12), $gm^{-0.40}\,sec^{-0.067}\,sec^{-1.534}$

ϕ' gas-phase fugacity coefficient, dimensionless

ϕ absorption factor for mass transfer with chemical reaction defined by Eq. (2.104), dimensionless

ρ density, g/cm^3

η angle of inclination of manometer to the horizontal, degree

θ^* average lifetime of surface liquid elements, sec

θ time for which liquid surface element has been exposed; "age" of surface, sec

σ interfacial surface tension, dyne/cm

τ rate ratio parameter defined by Eq. (2.76), dimensionless

ψ age distribution function defined by Eq. (2.89)

SUBSCRIPTS

0 initial condition

1 inlet stream

2	exit stream
3	carbon dioxide species
4	oxygen species
5	hydroxyl ion
6	carbonate ion
∞	final equilibrium condition (after infinite time)
B	bulk phase; cup-mixed property
D	dispersed phase
E	value at chemical equilibrium
F	manometer fluid property
G	gas phase
i	value at gas-liquid interface; ionic species
j	solvent (pure or multicomponent fluid) for solute k
k	absorbing solute in a liquid phase
L	property of gas-free liquid
M	value in oxygen probe polymeric membrane
n	ionic species
t	unsteady-state condition
T	property of total phase or system
V	per unit volume of gas-free liquid

SUPERSCRIPTS

r	property determined in and affected by a chemically-reacting system
*	hypothetical gas-phase property in physical equlibrium with bulk liquid-phase property, or vice-versa

ABBREVIATIONS

CFST	continuous flow stirred-tank absorber
CFSTR	continuous flow stirred-tank absorber-reactor
SBST	semi-batch stirred-tank absorber (batch liquid)
SBSTR	semi-batch stirred-tank absorber-reactor (batch liquid)
VVM	volume of inlet gas per unit volume of liquid per minute

APPENDIX II.1

Derivation of Oxygen Probe Transient Response to Continuous Concentration Change in Bulk Solution (Absorption)

Applying the initial condition, Eq. (2.72) to the partial differential Eq. (2.71), the Laplace transformed diffusion equation becomes

$$\frac{d^2\bar{C}}{dx^2} - q^2\bar{C} = 0 \qquad (1)$$

where

$$q^2 = s/D_M \qquad (2)$$

Using the shifting theorem, boundary condition Eq. (2.73) becomes

$$x = 0, \quad \bar{C} = SHC_\infty \left[\frac{\beta}{s(s+\beta)}\right] \qquad (3)$$

while the second boundary condition, Eq. (2.74), transform to

$$x = L, \quad \bar{C} = 0 \qquad (4)$$

Substituting the assumed solution, $C = A_n \exp(nx)$, in Eq. (1) we find that $n = \pm q$, and it therefore follows that

$$\bar{C} = A_1 \exp(qx) + A_2 \exp(-qx) \qquad (5)$$

Applying the boundary conditions Eq. (3) and Eq. (4) sequentially to Eq. (5), collecting exponential terms and re-arranging, the transformed solution is found to be

$$\overline{C} = \frac{SHC_\infty}{s}\left[\frac{\exp[q(L-x)] - \exp[-q(L-x)]}{\exp[qL] - \exp[-qL]}\right] - \frac{SHC_\infty}{s+\beta}\left[\frac{\exp[q(L-x)] - \exp[-q(L-x)]}{\exp[qL] - \exp[-qL]}\right] \quad (6)$$

Inversion will be done by contour integration (method of residues).

Inversion of the first term of Eq. (6)

The first term contains a singularity (the denominator becomes zero) when either $s = 0$, or $q_n L = in\pi$, i.e.

$$s_n = n^2\pi^2 D_M/L^2 \quad (7)$$

The residue of the function at the pole $s = 0$ is given by (108)

$$(r)_{s=0} = \left[(s-0)\frac{SHC_\infty}{s}\frac{\exp[q(L-x)] - \exp[-q(L-x)]}{\exp[qL] - \exp[-qL]}\exp(st)\right]_{s=q=0} \quad (8)$$

Since Eq. (8) is indeterminant, it is evaluated by means of L'Hôpital's rule, and the residue is thereby found to be

$$(r)_{s=0} = SHC_\infty(1 - x/L) \quad (9)$$

which is, of course, the final steady-state concentration profile in the membrane.

Writing the first term of Eq. (6) in the equivalent hyperbolic form, functions f(s) and g(s) are defined according to

$$\frac{SHC_\infty (s_n^{-1}) \sinh[(s_n/D_M)^{1/2}(L-x)]}{\sinh[(s_n/D_M)^{1/2}L]} = \frac{f(s_n)}{g(s_n)} \qquad (10)$$

The residue of the function at the pole s_n is given by

$$(r)_{s=s_n} = \frac{f(s_n)\exp(s_n t)}{\left.\frac{dg(s_n)}{ds}\right|_{s=s_n}} \qquad (11)$$

Applying Eq. (11) to Eq. (10), and substituting in the result Eq. (7) and the following identity,

$$\left(\frac{s_n}{D_M}\right)^{1/2} = in\pi/L$$

we obtain

$$(r)_{s=s_n} = \frac{2SHC_\infty}{in\pi} \cdot \frac{\sinh[in\pi(1 - x/L)]}{\cosh[in\pi]} \exp\left(-\frac{n^2\pi^2 D_M t}{L^2}\right) \qquad (12)$$

Eq. (12) may be further simplified by using the identities

$$\sinh[in\pi(1 - x/L)] = i\sin[n\pi(1 - x/L)]$$

$$\cosh[in\pi] = \cos[n\pi] = (-1)^n = 1/(-1)^n$$

from which it follows that

$$(r)_{s=s_n} = SHC_\infty \sum_{n=0}^{\infty} \frac{2}{n\pi} \sin[n\pi(1 - x/L](-1)^n \exp\left(-\frac{n^2\pi^2 D_M t}{L^2}\right) \qquad (13)$$

Inversion of the second term of Eq. (6)

The second term has singularities at either $s = -\beta$, or $s_n = -n^2\pi^2 D_M/L^2$.

The residue at the pole $s = -\beta$ is found by the same procedure used to evaluate the residue at $s = 0$ for the first term of Eq. (6). The result is

$$(r)_{s=-\beta} = -SHC_\infty \exp(-\beta t) \frac{\sin[(\beta/D_M)^{1/2}(L-x)]}{\sin[(\beta/D_M)^{1/2}L]}$$

wherein we have applied the identity

$$\exp(iy) - \exp(-iy) = 2i \sin(y)$$

where y represents either $(\beta/D_M)^{1/2}L$ or $(\beta/D_M)^{1/2}(L-x)$.

The residue at s_n is found by writing the second term of Eq. (6) in the equivalent hyperbolic form and proceeding analogously to the evaluation of this residue in the first term of Eq. (6). The result is

$$(r)_{s=s_n} = \sum_{n=0}^{\infty} \frac{2SHC_\infty}{(\beta L^2/D_M) - n^2\pi^2} \cdot (-1)^n (n\pi) \sin[n\pi(1-x/L)] \times \exp\left(-\frac{n^2\pi^2 D_M t}{L^2}\right) \quad (15)$$

C_M is found by summing all the residues, Eqs. (9), (13), (14), and (15). Applying the identity

$$\sin(a - b) = (\sin a)(\cos b) - (\cos a)(\sin b)$$

Therefore,

$$\sin[n\pi(1 - x/L)] = -\cos(n\pi)\sin(n\pi x/L) = -(-1)^n \sin(n\pi x/L)$$

the sum of the residues is

$$C_M = SHC_\infty \left\{ (1 - x/L) - 2/\pi \sum_{n=0}^{\infty} \frac{1}{n} \frac{\sin(n\pi x/L)}{1 - \frac{n^2\pi^2}{\tau}} \exp\left(- \frac{n^2\pi^2 D_M t}{L^2} \right) \right.$$
$$\left. - \frac{\sin[(\tau)^{1/2}(1-x/L)]}{\sin(\tau)^{1/2}} \exp(-\beta t) \right\} \qquad (16)$$

where $\tau = \beta L^2/D_M$

The concentration gradient $(\partial C_M/\partial x)_{x=L}$ is found from Eq. (16) and substituted into Eq. (2.52), along with Eqs. (2.50) and (2.51) to give the final result

$$E_t = E_\infty \left\{ 1 + 2 \sum_{n=0}^{\infty} \frac{(-1)^n}{1 - \frac{n^2\pi^2}{\tau}} \exp\left(- \frac{n^2\pi^2 D_M t}{L^2} \right) - \frac{\tau^{0.5}}{\sin\tau^{0.5}} \exp(-\beta t) \right\} \qquad (2.75)$$

NOMENCLATURE FOR APPENDICES II.2 AND II.2

F denotes the fitting function

X(1) denotes β

X(2) denotes D_M/L^2

G(1) denotes the partial derivative of F with respect to X(1)

G(2) denotes the partial derivative of F with respect to X(2)

M1 a programme-incorporated control parameter which permits additional calculations on the first and/or last entry into TABLE, e.g., calculation of $K_{L4}a$ from the best-fit value of β.

APPENDIX II.2

Subroutine Table: Two-Parameter Fitting - Absorption

```
      SUBROUTINE TABLE (F,G,X,T,M1)
C VOL MASS TRANS COEFF KLA IN WATER
C TWO PARAMETER FITTING - X(1)=BETA,1/SEC AND X(2)=D*L**2 ,1/SEC
C DETERMINED BY TRANSIENT RESPONSE OF OXYGEN PROBE DURING GASSING IN
C OXYGEN ABSORPTION      STEP CHANGE FROM NITROGEN TO AIR
C AERATION RATE Q=LITRE/MIN, HENRY COEFF H=ATM*CC/GM-MOLE
C PROBE VOLTAGES F(TRANSIENT), ESTART(INITIAL), AND FINFIN IN MILLIVOLTS
C TIME IN SECONDS, L=CM, V=CU.CM., P=ATM, X(1)=BETA/60., 1/SEC
C MEMBRANE DIFFUSIVITY   D=SQ.CM./SEC      X(2)=D/L**2  ,1/SEC
C BETA=1/MIN, KLAHR=1/HR, KLAMIN=1/MIN
C  DATA CONTROL PARAMETERS  K=2, ISTEP=0, IWRITE=0, ICON=1
C CONVERGENCE CRITERION  ICONVRG=0
      DIMENSION X(2),G(2),T(1),THETA(1)
      REAL L,LAMBDA,KLAHR,KLAMIN
      DATA L,V,P,Q,H/5.08E-3,2500.,1.0,2.50,8.345E5/
      IF(M1.EQ.1) GO TO 8
      READ 9,ESTART,FINFIN
    9 FORMAT(2F5.2)
      RETURN
    8 CONTINUE
      TAU1=(X(1)/X(2))**2
      TAU=SQRT(TAU1)
      CHI1=(1./(X(1)*X(2)))**2
      CHI=SQRT(CHI1)
C TAU1,CHI1 AVOID INDETERMINANT SQRTS IF X VALUES NEG ON RANDOM STEPS
      THETA(1)=T(1) +10.
C T(1)=0 AT THE INSTANT OF THE INITIAL INCREASE IN PROBE VOLTAGE
C THETA=0 AT THE INSTANT OF THE STEP CHANGE IN INLET GAS COMPOSITION
      ZETA=SIN(SQRT(TAU))*SIN(SQRT(TAU))
      GAMMA=THETA(1)*SQRT(TAU)*SIN(SQRT(TAU))
      DELTA=0.5*SQRT(CHI)*(SIN(SQRT(TAU))-SQRT(TAU)*COS(SQRT(TAU)))
      LAMBDA=X(1)*DELTA*SQRT(TAU)*EXP(-X(1)*THETA(1))/ZETA
      Y=0.
      DER1Y=0.
      DER2Y=0.
      DO 10 K=1,8
      M=K
      ALPHA=(K**2)*9.8696*THETA(1)*X(2)
      EPSILON=(1.0-9.8696*M**2/TAU)*(1.0-9.8696*M**2/TAU)
      RHO=(1./X(1))-(THETA(1)*SQRT(EPSILON))
      Y=Y+((-1)**K)*EXP(-ALPHA)/(1.-((K**2)*9.8696/TAU))
      DER1Y=DER1Y+((-1)**M)*(M**2)*9.8696*EXP(-ALPHA)/(X(1)*TAU*EPSILON)
      DER2Y=DER2Y+((-1)**M)*(M**2)*9.8696*RHO*EXP(-ALPHA)/EPSILON
   10 CONTINUE
      F=ESTART+FINFIN*(1.-SQRT(TAU)*EXP(-X(1)*THETA(1))/SIN(SQRT(TAU))+2
     1.*Y)
      G(1)=FINFIN*(EXP(-X(1)*THETA(1)))*(GAMMA-DELTA)/ZETA-2.*DER1Y)
      G(2)=FINFIN*(LAMBDA+2.*DER2Y)
      IF(M1.NE.4) RETURN
      BETA=60.*X(1)
      KLAHR=60.*BETA*C*H/(Q*H-23.7*V*P*BETA)
      KLAMIN=KLAHR/60.
      D=X(2)*L**2
      PRINT 20
   20 FORMAT(1HO,9X,4HBETA,5X,5HKLAHR,4X,6HKLAMIN,3X,6HESTART,3X,6HFINFI
     1N,9X,1HD)

      WRITE(3,30) BETA,KLAHR,KLAMIN,ESTART,FINFIN,D
   30 FORMAT(1HO,5X,F10.4,2X,F7.1,3X,F6.2,3X,F6.2,3X,F6.2,4X,F11.10)
      PRINT 40
   40 FORMAT(1HO,7X,4HX(2))
      WRITE(3,50) X(2)
   50 FORMAT(1HO,4X,F9.7)
      RETURN
      END
```

APPENDIX II.3

Subroutine Table: Two-Parameter Fitting - Desorption

```
      SUBROUTINE TABLE (F,G,X,T,M1)
C VOL MASS TRANSFER COEFF KLA IN 0.135M KCL-KOH-K2CO3 SOLUTION
C TWO PARAMETER FITTING - X(1)=BETA,1/SEC AND X(2)=D*L**2 ,1/SEC
C DETERMINED BY TRANSIENT RESPONSE OF OXYGEN PROBE DURING GASSING OUT
C OXYGEN DESORPTION    STEP CHANGE FROM AIR TO 0.1CO2/0.9N2
C AERATION RATE Q=LITRE/MIN, HENRY COEFF H=ATM*CC/GM-MOLE
C TRANSIENT PROBE VOLTAGE F,FINAL VOLTAGE EFINAL, AND INITIAL SATURATION
C VOLTAGE EINFIN IN MILLIVOLTS
C T(1)=0 WHEN THE PROBE VOLTAGE FIRST BEGINS TO DECREASE FROM EINFIN
C THETA(1)=   AT THE INSTANT OF THE STEP CHANGE IN INLET GAS COMPOSITION
C TIME T(1) IN SECONDS, L=CM, V=CU.CM., P=ATM, X(1)=BETA/60., 1/SEC
C MEMBRANE DIFFUSIVITY D=SQ.CM./SEC              X(2)=D/L**2 , 1/SEC
C BETA=1/MIN              KLAHR=1/HR             KLAMIN=1/MIN
C  DATA CONTROL PARAMETERS  K=2, ISTEP=0, IWRITE=0, ICON=1
C CONVERGENCE CRITERION   ICONVRG=0
      DIMENSION X(2),G(2),T(1),THETA(1)
      REAL L,LAMBDA,KLAHR,KLAMIN
      DATA L,V,P,Q,H/5.08E-3,2500.,1.0,5.00,8.76E5/                    .135MKCL
      IF(M1.GT.1) GO TO 8
      READ 5,EINFIN,EFINAL
    5 FORMAT(2F5.2)
      RETURN
    8 CONTINUE
      TAU1=(X(1)/X(2))**2
      TAU=SQRT(TAU1)
      CHI1=(1./(X(1)*X(2)))**2
      CHI=SQRT(CHI1)
C TAU1,CHI1 AVOID INDETERMINANT SQRTS IF X VALUES NEG ON RANDOM STEPS
      THETA(1)=T(1)+5.
      ZETA=SIN(SQRT(TAU))*SIN(SQRT(TAU))
      GAMMA=THETA(1)*SQRT(TAU)*SIN(SQRT(TAU))
      DELTA=0.5*SQRT(CHI)*(SIN(SQRT(TAU))-SQRT(TAU)*COS(SQRT(TAU)))
      LAMBDA=-X(1)*DELTA*SQRT(TAU)*EXP(-X(1)*THETA(1))/ZETA
      Y=0.
      DER1Y=0.
      DER2Y=0.
      DO 10 K=1,8
      M=K
      ALPHA=(K**2)*9.8696*X(2)*THETA(1)
      EPSILON=(1.-M**2*9.8696/TAU)*(1.-M**2*9.8696/TAU)
      RHO=(1./X(1))-(THETA(1)*SQRT(EPSILON))
      Y=Y+(-1)**K*EXP(-ALPHA)/(1.-K**2*9.8696/TAU)
      DER1Y=DER1Y+((-1)**M)*(M**2)*9.8696*EXP(-ALPHA)/(X(1)*TAU*EPSILON)
      DER2Y=DER2Y+((-1)**M)*(M**2)*9.8696*RHO*EXP(-ALPHA)/EPSILON
   10 CONTINUE
      F=EFINAL+EINFIN*(SQRT(TAU)*EXP(-X(1)*THETA(1))/SIN(SQRT(TAU))-2.*Y
     1)
      G(1)=EINFIN*(2.*DER1Y-(EXP(-X(1)*THETA(1)))*(GAMMA-DELTA)/ZETA))
      G(2)=EINFIN*(LAMBDA-2.*DER2Y)
      IF(M1.NE.4) RETURN
      BETA=60.*X(1)
      KLAHR=60.*BETA*Q*H/(Q*H+23.7*V*P*BETA)
      KLAMIN=KLAHR/60.
      D=X(2)*L**2
      PRINT 20
   20 FORMAT(1HO,9X,4HBETA,5X,5HKLAHR,4X,6HKLAMIN,3X,6HEINFIN,3X,6HEFINA
     1L,9X,1HD)
      WRITE(3,30) BETA,KLAHR,KLAMIN,EINFIN,EFINAL,D
   30 FORMAT(1HO,5X,F10.4,2X,F7.1,3X,F6.2,3X,F6.2,3X,F6.2,4X,F11.10)
      PRINT 40
   40 FORMAT(1HO,7X,4HX(2))
      WRITE(3,50) X(2)
   50 FORMAT(1HO,4X,F9.7)
      RETURN
      END
```

APPENDIX III.1

Effect of Aeration on Mixing Power Unit Volume for Water at 30°C

Impeller rotational speed (N) rpm	Aeration rate (q) scc/min	Aeration number (N_A) $\frac{q}{ND_I^3}$	Aerated/unaerated power ratio $\frac{P_G}{P_0}$
600	1250	0.0158	0.595
	2500	0.0316	0.459
	3750	0.0474	0.378
700	1250	0.0136	0.628
			0.617
	2500	0.0272	0.535
	3750	0.0408	0.447
	5000	0.0544	0.488
800	1250	0.0119	0.695
	2500	0.0238	0.627
	3750	0.0357	0.525
	5000	0.0476	0.458
900	1250	0.0106	0.763
	2500	0.0212	0.618
	3750	0.0318	0.566
	5000	0.0424	0.432
1000	1250	0.0127	0.753
	2500	0.0145	0.613
	3750	0.0218	0.559
	5000	0.0291	0.495
1100	1250	0.0087	0.793
	2500	0.0174	0.638
	3750	0.0261	0.574
	5000	0.0348	0.552
1300	1250	0.00691	0.830
	2500	0.0138	0.692
	3750	0.0207	0.597
	5000	0.0276	0.572
1500	1250	0.00638	0.885
	1875	0.00957	0.811
	2500	0.0128	0.713
	3125	0.0160	0.697
	3750	0.0191	0.646
	4375	0.0223	0.607
	5000	0.0255	0.565

APPENDIX III.2

Dynamic Pressure Corrections to Manometric Gas Holdup Measurements

Impeller Rotational Speed

N	$N^2 \times 10^{-4}$	$(\Delta\mathcal{H}_F)_{dyn}$ inches
500	25	0.125
600	36	0.125
700	49	0.225
800	64	0.275
900	81	0.350
1000	100	0.450
1100	121	0.525
1200	144	0.625
1300	169	0.750
1400	196	0.850
1500	225	0.975
1600	256	1.10
1700	289	1.18
1800	324	1.25
1900	361	1.30
2000	400	1.32
2100	441	1.32

Manometer $\rho_F = 0.775$; $\eta = 15°$

Appendix III.3

Physicochemical Properties of Experimental Solutions

	Ionic strength Γ_T g-ion/litre	Density $\rho(30°C)$ g/cm^3	Viscosity $\mu_{°C}$ cp	Interfacial tension $\sigma_{°C}$ Expt'l	Interfacial tension dynes/cm Literature (Ref.)	pH	H_4 (atm-cm^3/gmole) $\times 10^{-5}$
Distilled Water	0.00	0.9957	0.8949_{25}(106)	71.9_{25}	71.97_{25}(83)	6.45	8.345 (Ref. 83)
			0.801_{30}(106)		71.18_{30}(107)		
KOH - K_2CO_3	0.0965[a]						8.530
0.1M KCl	0.100	1.003				7.35	8.547
0.22M KCl	0.220	1.012	0.801_{30}	72.7_{30}		7.93	8.796
0.135M KCl + KOH - K_2CO_3	0.221[a]						8.760
Medium A-1[b]	0.136	1.003	0.8012_{30}	72.4_{30}		5.45	8.570
0.125M Na_2SO_4 - 0.004M $CuSO_4$	0.391	1.014	0.841_{30}	71.7_{30}			9.300
0.250M Na_2SO_4 - 0.004M $CuSO_4$	0.766	1.032	0.9942_{25}(106)	72.2_{30}		5.50	10.38
0.375M Na_2SO_4 -0.004M $CuSO_4$	1.141	1.045		72.9_{30}			11.68
0.500M Na_2SO_4 - 0.004M $CuSO_4$	1.516	1.067	1.098_{25}(106)		72.58_{30}(83)		12.88
0.500M Na_2SO_3 - 0.004M $CuSO_4$	1.516	1.059	1.031_{30}	72.6_{30}		8.94	12.88[c]
0.11M Na_2SO_4 + KOH - K_2CO_3	0.418[a]						9.646

(a) Average of all runs.

(b) Composition: 1.6g K_2HPO_4, 0.48g $MgSO_4 \cdot 7H_2O$, 4.6g NH_4Cl, 0.02g NaCl, 0.03g HgI_2 per litre distilled water.

(c) Assumed equal to value in 0.500M Na_2SO_4 - 0.004M $CuSO_4$.

APPENDIX III.4

Measurement of Oxygen Probe Membrane Effective Diffusivity by Step Change in Oxygen Tension (30°C)

Time sec	Potential drop across external resistor (1100 ohm) millivolts
0	0.11 (deoxygenated)
1	0.15
2	0.33
3	0.63
4	0.88
5	1.22
6	1.58
7	1.98
8	2.37
9	2.76
10	3.13
11	3.50
12	3.84
14	4.41
16	4.87
18	5.27
20	5.60
22	5.88
24	6.12
26	6.32
28	6.49
30	6.62
40	7.06
60	7.42
80	7.59
100	7.69
∞	8.05

APPENDIX IV.1

Oxygen Volumetric Mass Transfer Coefficient in Distilled Water Computed from Unsteady-State Data

Aeration rate			Agitation P_G/V_L		Calculated D_M	$K_{L4}a$	
Q_1 ℓ/min	v_S ft/sec	N rpm	hp/ft^3	$\frac{\text{ft-lb}_f}{\text{min-ft}^3}$	cm^2/sec $\times 10^7$	hr^{-1}	Best fit CHISQ(X)
1.25	0.00375	600	0.0148	488	1.77	35.1	1.42
		700	0.0212	700	1.53	48.9	0.190
		800	0.0368	1215	1.64	62.2	0.157
		900	0.0588	1940	1.58	74.1	0.201
		1000	0.0785	2590	1.44	98.4	0.727
		1100	0.114	3750	1.34	94.8	2.52
		1300	0.193	6370	1.55	118	0.250
		1400	0.223	7365	1.56	138	0.224
		1500	0.285	9400	1.56	140	0.095
		1600	0.298	9850	1.56	149	0.327
		1700	0.351	11590	1.56	139	1.03
		1800	0.419	13830	1.56	145	0.510
		1900	0.514	16960	1.56	164	0.241
		2000	0.610	20150	1.56	166	0.889
		2100	0.745	24570	1.56	188	0.431
2.50	0.0075	600	0.0114	377	1.69	44.8	0.294
		700	0.0182	599	1.63	46.4	1.31
		800	0.0333	1100	1.54	71.6	0.132
		900	0.0476	1570	1.50	85.6	0.616
		1000	0.0639	2110	1.53	109	0.469
		1100	0.0912	3010	1.55	105	0.765
		1300	0.161	5300	1.56	132	0.122
		1500	0.251	8280	1.56	149	0.087
		1600	0.269	8870	1.56	197	1.33
		1700	0.298	9820	1.56	158	0.139
		1800	0.344	11360	1.56	193	0.148
		1900	0.409	13500	1.56	193	0.854
		2000	0.503	16590	1.56	206	0.077
		2100	0.639	21075	1.56	194	2.36
		2270	0.833	27490	1.56	248	0.298
3.75	0.01125	600	0.00942	311	1.81	54.3	0.686
		700	0.0182	599	1.67	70.2	0.384
		800	0.0279	922	1.64	81.4	0.928
		900	0.0385	1270	1.59	99.0	0.394
		1000	0.0517	1705	1.56	123	0.781
		1100	0.0789	2605	1.49	118	1.23
		1300	0.139	4580	1.56	141	0.718
		1500	0.227	7500	1.56	158	1.01
		1600	0.237	7805	1.56	206	1.89
		1700	0.275	9065	1.56	186	0.240
		1800	0.349	11525	1.46	214	0.097
		1900	0.372	12265	1.56	214	0.263
		2000	0.458	15100	1.56	234	0.089
		2100	0.589	19440	1.56	234	0.279
		2270	0.828	27320	1.56	253	0.794
5.00	0.0150	600	0.00739	244	1.70	60.6	0.468
		700	0.0165	546	1.66	76.9	0.213
		800	0.0242	800	1.59	87.4	0.192
		900	0.0385	1270	1.48	99.3	0.896
		1000	0.0517	1705	1.56	123	1.71
		1100	0.0789	2605	1.65	118	0.669
		1300	0.133	4390	1.56	148	0.073
		1500	0.199	6560	1.58	190	0.182
		1700	0.271	8940	1.56	218	0.171
		1800	0.302	9955	1.56	234	0.265
		1900	0.360	11890	1.56	238	0.041
		2000	0.451	14885	1.56	238	0.305
		2270	0.718	23740	1.56	323	0.264

APPENDIX IV.2

Fractional Gas Holdup in Water (30°C)

Superficial Gas Velocity 0.0150 ft/sec

N rpm	P_G/V_L ft-lb$_f$/min-ft^3	H_G Eq. (3.15)	H_G Liquid displacement
500	74	0.0160	0.0319
700	546	0.0213	0.0319
800	800	0.0245	0.0323
900	1270	0.0320	0.0373
1000	1705	0.0407	0.0419
1100	2605	0.0480	0.0454
1200		0.0480	0.0475
1300	4390	0.0533	0.0498
1400		0.0587	0.0522
1500	6560	0.0587	0.0547
1600		0.0693	0.0562
1700	8950	0.0670	0.0587
1800	9955	0.0747	0.0603
1900	11890	0.0747	0.0622
2000	14890	0.0823	0.0647
2100	17700	0.0853	0.0682

APPENDIX IV.3

Oxygen Overall Volumetric Mass Transfer Coefficient in 0.10M KCl Solution Computed from Steady-State Data (Deoxygenated Feed)

Aeration rate		Agitation rate		Feed rate			Fermentor probe millivolts		
Q_1	v_S	N	P_G/V_L	F_1	V_L	D_L	E_L	E_∞	$K_{L4}{}^a$
ℓ/min	ft/sec	rpm	ft-lb$_f$/min-ft^3	ℓ/min	ℓ	min^{-1}			hr^{-1}
2.50	0.00750	700	475	1.251	2.50	0.500	4.34	5.51	118
			533	1.008	2.55	0.395	5.12	6.10	131
		800	736	1.251	2.57	0.487	8.04	9.50	174
		900	1160	1.251	2.59	0.483	4.94	5.55	238
		1000	1890	1.271	2.60	0.489	8.08	8.95	318
		1100	2540	2.158	2.57	0.840	5.25	6.20	320
		1200	3380	1.271	2.60	0.489	8.34	8.95	451
		1300	4215	2.158	2.57	0.840	5.48	6.20	466
		1400	5700	1.271	2.60	0.489	8.52	8.95	670
		1600	7980	1.281	2.59	0.495	8.62	9.06	674
		1700	9880	2.543	2.58	0.986	5.89	6.40	998
		1900	14050	1.281	2.59	0.495	8.75	9.06	1020
5.00	0.0150	600	322	0.921	2.50	0.368	6.07	6.95	158
		700	344	1.053	2.64	0.399	5.51	6.20	200
		800	816	0.921	2.50	0.368	6.52	7.04	296
		900	1100	1.224	2.49	0.492	6.89	7.44	402
		1000	1490	1.260	2.58	0.488	8.24	9.00	364
		1100	1830	1.456	2.62	0.556	8.90	9.60	470
		1200	2740	1.466	2.48	0.591	9.14	9.78	574
		1300	3470	1.488	2.50	0.579	9.30	9.83	710
		1400	4060	1.453	2.69	0.540	9.33	9.75	863
		1500	5680	1.053	2.64	0.399	6.10	6.27	1070
		1600	6620	1.558	2.51	0.621	9.45	9.83	1180
		1800	9260	1.489	2.67	0.558	9.62	9.96	1212

Appendix IV.4 Oxygen Overall Volumetric Mass Transfer Coefficient in Medium A-1 Computed from Steady-State Data

Aeration rate		Feed Rate			Probe millivolts			Agitation		
					Feed	Reactor				
Q_1	v_S	F_1	V_L	D_L	E_{L1}	E_L	E_∞	N	P_G/V_L	$K_{L4}a$
ℓ/min	ft/sec	ℓ/min	ℓ	min^{-1}				rpm	hp/ft^3	hr^{-1}
1.25	0.00375	1.344	2.50	0.538	0.43	3.35	5.55	500	0.00645	44.6
		1.344	2.50	0.538	0.43	4.27	5.55	700	0.0219	106
		1.357	2.50	0.543	0.58	4.79	5.64	900	0.0530	190
		1.357	2.50	0.543	0.58	5.07	5.64	1100	0.0951	338
		1.356	2.51	0.540	0.35	5.09	5.54	1300	0.155	501
		2.480	2.54	0.976	0.22	5.89	6.84	1400	0.172	519
		2.437	2.42	1.007	0.21	6.01	6.92	1500	0.209	600
		2.471	2.47	1.00	0.25	6.11	6.98	1700	0.286	648
		2.471	2.58	0.958	0.22	6.20	6.97	1900	0.400	765
2.50	0.00750	1.370	2.53	0.542	0.35	3.43	5.55	500	0.00591	48.3
		1.370	2.53	0.542	0.35	4.05	5.55	600	0.0115	83.4
		1.385	2.48	0.558	0.28	4.35	5.60	700	0.0188	115
		1.397	2.50	0.559	0.54	4.85	5.70	900	0.0451	181
		1.397	2.50	0.559	0.54	5.02	5.70	1000	0.0629	242
		1.353	2.56	0.529	0.44	5.08	5.67	1100	0.0839	282
		1.353	2.56	0.529	0.44	5.28	5.67	1300	0.134	482
		2.260	2.62	0.863	0.24	6.97	7.70	1500	0.192	614
		2.299	2.44	0.942	0.12	6.48	7.12	1700	0.274	761
		2.364	2.70	0.876	0.24	6.58	7.13	1900	0.338	845
		2.440	2.71	0.900	0.24	6.58	7.10	2100	0.480	951
3.75	0.01125	1.373	2.60	0.528	0.47	3.65	5.45	500	0.00533	57.0
		1.373	2.60	0.528	0.47	4.48	5.45	700	0.0173	137
		1.376	2.59	0.531	0.62	4.78	5.45	900	0.0389	211
		1.376	2.59	0.531	0.62	5.04	5.45	1100	0.0764	385
		1.369	2.50	0.548	0.31	5.10	5.43	1300	0.121	484
		2.508	2.56	0.980	0.21	6.92	7.68	1500	0.178	618
		2.533	2.64	0.959	0.16	7.10	7.68	1700	0.263	877
		2.528	2.61	0.969	0.16	7.17	7.71	1900	0.347	986
		2.495	2.46	1.014	0.14	7.21	7.71	2100	0.485	1200
5.00	0.0150	1.379	2.52	0.547	0.32	3.99	5.35	600	0.00939	91.1
		1.379	2.52	0.547	0.32	4.61	5.35	800	0.0233	202
		1.386	2.50	0.554	0.40	4.88	5.34	1000	0.0515	360
		1.386	2.50	0.554	0.40	5.00	5.34	1200	0.0891	523
		2.416	2.57	0.940	0.44	4.81	5.24	1400	0.142	698
		2.467	2.44	1.011	0.70	4.75	5.05	1800	0.301	1100
		2.435	2.53	0.962	0.25	9.79	10.36	2000	0.427	1380
		2.471	2.53	0.977	0.21	7.35	7.75	2270	0.621	1540

APPENDIX IV.5

Oxygen Overall Volumetric Mass Transfer Coefficient in Medium A-1 Computed from Unsteady-State Data

Aeration rate			Agitation		Calculated D_M	$K_{L4}a$	
Q_1	v_S		P_G/V_L	$\frac{ft\text{-}lb_f}{min\text{-}ft^3}$	cm^2/sec		Best fit
ℓ/min	ft/sec	rpm	hp/ft^3		$\times 10^7$	hr^{-1}	CHISQ(X)
1.25	0.00375	500	0.01515	212	1.87	77.0	1.03
		600	0.0101	333	1.62	61.5	0.478
		650	0.0131	433	1.38	86.1	1.31
		700	0.0181	596	1.45	88.3	0.755
		750	0.0244	805	1.42	116	1.00
		800	0.0332	1095	1.46	129	0.843
		1000	0.0752	2480	1.46	242	0.338
		1100	0.0962	3180	1.46	339	0.451
		1200	0.131	4315	1.46	392	0.391
		1400	0.206	6800	1.45	512	0.729
		1500	0.231	7610	1.60	625	0.526
		1700	0.353	11650	1.54	728	0.374
		1900	0.473	15600	1.78	862	0.543
		2000	0.563	18600	1.68	947	0.617
		2270	0.894	29500	1.82	1122	0.840
2.50	0.0075	600	0.00942	311	1.55	125	2.52
		650	0.0131	433	1.34	160	2.75
		700	0.0165	544	1.56	123	4.77
		750	0.0210	694	1.56	144	2.42
		800	0.0261	860	1.56	166	1.91
		900	0.0395	1300	1.56	195	2.67
					1.52	194	0.307
		1000	0.0548	1810	1.56	261	3.47
		1100	0.0727	2400	1.56	305	2.99
		1300	0.127	4190	1.57	516	0.482
		1400	0.192	6330	1.45	590	0.433
		1700	0.273	9000	1.48	914	0.927
		2270	0.792	26140	1.58	1308	0.552
3.75	0.01125	500	0.00448	148	1.87	77.0	1.026
		550	0.00554	183	1.72	80.7	0.917
		600	0.00809	267	1.54	99.2	0.915
		650	0.0117	385	1.51	116	1.15
					1.44	111	1.20
		700	0.0134	441	1.38	135	1.21
		800	0.0225	742	1.46	151	1.92
		900	0.0344	1140	1.46	211	0.259
		1000	0.0550	1815	1.46	273	0.188
		1100	0.0703	2320	1.48	385	0.283
		1300	0.124	4090	1.53	481	0.413
		1500	0.183	6055	1.70	670	0.462
		1700	0.265	8750	1.61	1020	0.324
		1900	0.399	13160	1.53	1077	0.491
		2270	0.886	29250	1.58	1496	0.444
5.00	0.0150	600	0.00673	222	1.61	114	0.970
		650	0.00839	277	1.47	128	0.606
		700	0.0126	415	1.56	139	0.788
		750	0.0152	500	1.56	159	0.573
		800	0.0198	653	1.56	190	0.789
		900	0.0303	1000	1.56	258	0.405
		1000	0.0462	1520	1.56	332	0.472
		1100	0.0617	2035	1.54	393	0.161
		1300	0.144	3755	1.41	799	0.235
		1500	0.185	6110	1.47	1129	0.167
		1700	0.265	8750	1.47	1174	0.312
		1900	0.386	12740	1.56	1319	0.320
		2270	0.881	29100	1.54	1647	0.577

APPENDIX IV.6
Oxygen Overall Volumetric Mass Transfer Coefficient in 0.22M KCl Solution Computed from Steady-State Data (Deoxygenated Feed)

Aeration rate		Agitation rate		Feed rate			Fermentor probe millivolts		
Q_1	v_S	N	P_G/V_L	F_1	V_L	D_L	E_L	E_∞	$K_{L4}a$
ℓ/min	ft/sec	rpm	ft-lb$_f$/min-ft^3	ℓ/min	ℓ	min^{-1}			hr^{-1}
2.50	0.0075	700	458	1.899	2.55	0.745	4.34	6.15	113
		900	1245	1.899	2.55	0.745	5.14	6.15	253
		1100	2485	1.782	2.50	0.713	5.35	5.96	451
		1400	5395	1.695	2.50	0.678	5.63	6.05	722
		1700	9730	1.747	2.62	0.667	5.90	6.20	1218
		2000	15900	1.819	2.56	0.711	6.06	6.32	1794
5.00	0.0150	600	211	1.255	2.50	0.502	6.75	8.96	94
		800	638	1.255	2.50	0.502	7.78	8.96	208
		1000	1410	1.283	2.55	0.503	8.28	9.06	342
		1200	2630	1.283	2.55	0.503	8.57	9.06	599
		1400	4240	1.277	2.63	0.486	8.72	9.10	771
		1600	6540	1.277	2.63	0.486	8.82	9.10	1160
		1880	11090	1.273	2.57	0.495	8.88	9.12	1460

Appendix IV.7 Oxygen Overall Volumetric Mass Transfer Coefficient in 0.125M Sodium Sulphate - 0.004M Cupric Sulphate Solution (Computed from Steady-State Data)

Aeration rate		Feed rate			Probe millivolts			Agitation		
					Feed	Reactor				
Q_1	v_S	F_1	V_L	D_L	E_{L1}	E_L	E_∞	N	P_G/V_L	$K_{L4}{}^a$
ℓ/min	ft/sec	ℓ/min	ℓ	min^{-1}				rpm	hp/ft^3	hr^{-1}
1.25	0.00375	1.428	2.50	0.571	Nil	4.95	8.44	550	0.00679	50.7
		1.310	2.52	0.520	Nil	6.14	8.47	650	0.0168	88.4
		1.408	2.50	0.563	0.20	6.88	8.50	800	0.0348	158
		1.346	2.50	0.538	0.13	7.40	8.62	900	0.0527	230
		1.396	2.50	0.558	0.30	6.51	8.50	725	0.0261	115
		1.427	2.54	0.562	0.30	7.65	8.65	1000	0.0685	314
		1.249	2.46	0.508	0.24	7.86	8.61	1100	0.0902	420
		1.244	2.45	0.508	0.31	8.00	8.70	1200	0.117	467
		1.249	2.44	0.512	0.31	8.11	8.70	1300	0.137	620
		1.284	2.49	0.516	0.40	8.16	8.70	1400	0.177	714
		1.280	2.50	0.512	0.31	8.15	8.70	1500	0.219	696
		1.115	2.86	0.390	0.26	8.30	8.72	1600	0.258	726
		2.503	2.50	1.00	0.10	6.20	8.51	850	0.0420	183
		2.774	2.50	1.11	0.09	7.60	8.70	1600	0.264	744
		2.457	2.48	0.991	Nil	7.82	8.70	1700	0.370	960
		2.460	2.55	0.965	Nil	7.90	8.71	1800	0.424	1090
		2.416	2.59	0.933	0.08	7.99	8.72	1900	0.467	1250
2.50	0.00750	1.063	2.46	0.432	Nil	5.50	8.40	500	0.00588	50.2
		1.063	2.46	0.432	Nil	6.26	8.40	600	0.0115	78.6
		1.066	2.50	0.426	0.11	5.92	8.45	550	0.00864	60.0
		1.066	2.50	0.426	0.11	6.70	8.45	650	0.0150	100
		1.260	2.46	0.512	0.07	6.71	8.47	700	0.0188	122
		1.257	2.50	0.503	0.10	7.28	8.52	800	0.0288	189
		1.258	2.50	0.503	0.12	7.62	8.56	900	0.0439	268
		1.476	2.53	0.583	0.14	7.68	8.59	1000	0.0594	329
		1.339	2.56	0.523	0.07	7.91	8.59	1100	0.0748	428
		1.384	2.43	0.570	0.13	8.07	8.59	1200	0.100	672
		1.337	2.43	0.550	Nil	8.16	8.66	1300	0.129	696
		2.445	2.40	1.02	0.43	7.90	8.70	1400	0.158	756
		2.390	2.67	0.895	0.17	8.08	8.73	1600	0.213	906
		2.418	2.49	0.971	0.28	8.17	8.75	1800	0.309	1195
		2.384	2.59	0.920	0.10	8.24	8.80	2000	0.444	1220
		2.419	2.42	1.00	0.14	8.35	8.80	2270	0.709	2050

Appendix IV.7 (Contd.)

Aeration rate		Feed rate			Probe millivolts			Agitation		
					Feed	Reactor				
Q_1	v_S	F_1	V_L	D_L	E_{L1}	E_L	E_∞	N	P_G/V_L	$K_{L4}a$
ℓ/min	ft/sec	ℓ/min	ℓ	min^{-1}				rpm	hp/ft^3	hr^{-1}
3.75	0.01125	0.943	2.50	0.377	Nil	6.01	8.35	450	0.00355	59.0
		0.943	2.50	0.377	Nil	6.15	8.35	500	0.00533	64.2
		0.958	2.47	0.388	0.12	6.42	8.44	550	0.00739	74.4
		0.958	2.47	0.388	0.12	6.70	8.44	600	0.0101	90.6
		0.944	2.50	0.378	0.02	6.96	8.49	650	0.0128	106
		0.944	2.50	0.378	0.02	7.25	8.49	700	0.0173	137
		0.956	2.48	0.385	0.14	7.64	8.52	800	0.0261	208
		0.956	2.48	0.385	0.14	7.88	8.52	900	0.0391	304
		1.160	2.44	0.475	0.14	7.94	8.55	1000	0.0548	406
		2.086	2.50	0.834	0.19	7.65	8.55	1100	0.0727	470
		2.532	2.50	0.941	0.70	7.58	8.52	1100	0.0727	468
		2.359	2.50	0.944	0.34	7.68	8.57	1200	0.0958	538
		2.358	2.53	0.943	0.34	7.89	8.61	1400	0.145	714
		2.378	2.56	0.929	0.43	8.09	8.64	1600	0.217	996
		2.409	2.45	0.983	0.24	8.19	8.72	1800	0.315	1180
		2.387	2.62	0.911	0.08	8.28	8.75	2000	0.426	1310
		2.419	2.47	0.979	0.04	8.39	8.77	2270	0.655	2035
5.00	0.0150	1.409	2.50	0.564	0.10	4.49	8.20	400	0.00122	40.2
		1.432	2.50	0.573	0.12	5.72	8.25	500	0.00591	77.4
		1.429	2.51	0.569	0.12	6.25	8.30	600	0.00939	104
		1.449	2.53	0.573	0.11	6.82	8.25	700	0.0165	167
		1.438	2.59	0.555	0.13	7.20	8.32	800	0.0261	220
		1.420	2.52	0.563	0.08	7.45	8.34	900	0.0379	297
		1.411	2.56	0.551	0.06	7.70	8.37	1000	0.0527	410
		1.877	2.58	0.728	0.06	7.60	8.35	1100	0.0667	484
		2.258	2.55	0.903	0.06	7.51	8.35	1200	0.0864	535
		2.284	2.48	0.921	0.02	7.74	8.40	1400	0.134	750
		2.363	2.52	0.938	0.01	7.85	8.44	1600	0.208	888
		2.457	2.53	0.971	0.06	8.04	8.52	1800	0.297	1220
		2.513	2.50	1.005	0.02	8.11	8.55	2000	0.436	1450
		2.488	2.67	0.932	0.02	8.25	8.57	2340	0.679	2070

APPENDIX IV.8

Oxygen Overall Volumetric Mass Transfer Coefficient in 0.125M Sodium Sulphate - 0.004M Cupric Sulphate Solution (Computed from Unsteady-State Data)

Aeration Rate			Agitation		Calculated		
			P_G/V_L		D_M	$K_{L4}a$	
Q_1	v_S	N		$\frac{ft\text{-}lb_f}{min\text{-}ft^3}$	cm^2/sec		Best fit
ℓ/min	ft/sec	rpm	hp/ft^3		$\times 10^7$	hr^{-1}	CHISQ(X)
1.25	0.00375	750	0.0244	805	1.68	164	0.532
					1.71	185	0.804
		800	0.0288	950	1.39	207	3.84
		900	0.0465	1535	1.56	250	4.64
		1000	0.0652	2150	1.56	300	0.817
		1100	0.0815	2690	1.56	463	1.51
					1.56	461	1.68
		1300	0.124	4090	1.85	383	1.02
		1500	0.192	6335	1.61	813	0.967
		1800	0.373	12300	1.03	895	0.061
		1900	0.495	16320	1.04	1114	0.055
		2000	0.626	20670	1.12	1179	0.317
		2100	0.773	25500	1.09	1254	0.788
2.50	0.00750	800	0.0261	860	1.56	169	10.7
		900	0.0385	1270	1.56	252	16.4
		1100	0.0703	2320	1.69	448	0.880
		1300	0.114	3755	1.68	591	0.975
		1500	0.172	5665	1.73	677	0.922
		1700	0.235	7750	1.66	1064	0.512
			0.273	9000	1.41	961	0.281
			0.242	8000	1.56	1102	0.575
		1800	0.329	10860	1.22	941	0.113
		1900	0.324	10700	1.64	1299	0.479
			0.377	12450	1.41	1577	0.104
			0.377	12450	1.53	1018	0.934
		2000	0.507	16740	1.36	1367	0.080
					1.36	1368	0.079
		2100	0.649	21390	1.33	1475	0.034
		2270	0.867	28600	1.18	1790	0.030
3.75	0.01125	700	0.0126	415	1.55	133	11.8
		900	0.0314	1035	1.56	292	5.67
		1100	0.0629	2075	2.00	362	1.01
		1300	0.102	3370	1.52	594	1.40
					1.76	607	1.21
		1500	0.158	5220	1.57	971	0.640
		1700	0.217	7175	1.58	1160	0.507
					1.61	1028	0.422
		1800	0.283	9355	1.38	1172	0.491
		1900	0.360	11890	1.42	1238	0.283
		2000	0.415	13700	1.32	1289	0.646
		2100	0.482	15900	1.33	1401	0.358
		2270	0.586	19360	1.61	1817	0.595
					1.37	1537	0.236
5.00	0.0150	1300	0.0977	3225	1.80	634	1.01
		1700	0.231	7630	1.46	1047	0.499
					1.61	1111	0.570
		1800	0.257	8490	1.47	1166	0.484
		1900	0.324	10700	1.33	1235	0.530
					1.40	1270	0.523
		2000	0.366	12070	1.41	1392	0.390
		2270	0.456	15045	1.56	2138	0.456
6.75	0.0203	2000	0.310	10200	1.43	1120	1.03

APPENDIX IV.9

Oxygen Overall Volumetric Mass Transfer Coefficient in 0.250M Sodium Sulphate - 0.004M Cupric Sulphate Solution (Computed from Unsteady-State Data)

Aeration rate Q_1' f/min	v_S ft/sec	N rpm	Agitation P_G/V_L hp/ft^3	P_G/V_L ft-lb$_f$/min-ft^3	Calculated D_M cm^2/sec $\times 10^7$	$K_{L4}a$ hr^{-1}	Best fit CHISQ(X)
1.25	0.00375	650	0.0172	566	1.76	133	0.947
		700	0.0228	750	1.72	145	0.324
		750	0.0286	944	1.60	201	1.63
		800	0.0352	1160	1.56	150	0.814
		900	0.0506	1670	1.56	245	1.85
		1000	0.0708	2335	1.56	292	4.80
		1200	0.116	3830	1.54	496	0.628
		1300	0.139	4575	1.42	581	0.947
2.50	0.00750	500	0.00506	167	2.47	60.9	0.319
		550	0.00679	224	2.41	76.5	0.008
		600	0.00876	289	1.68	126	1.96
		650	0.0135	445	1.72	166	1.46
		700	0.0173	570	1.39	201	5.08
		750	0.0227	750	1.54	137	1.45
		800	0.0288	950	1.56	168	1.63
		900	0.0415	1370	1.56	249	5.38
		1000	0.0583	1925	1.56	325	6.63
		1100	0.0755	2490	1.48	610	0.608
		1200	0.0958	3160	1.68	488	0.871
		1400	0.148	4875	1.45	609	0.491
		1500	0.179	5895	1.33	739	0.200
3.75	0.01125	500	0.00452	149	2.01	75.6	1.26
		550	0.00648	214	1.70	116	2.24
		600	0.00842	278	1.67	141	0.932
		650	0.0113	373	1.53	182	1.67
		700	0.0157	518	1.55	133	1.38
					1.55	133	1.69
		800	0.0242	800	1.56	198	0.993
		900	0.0365	1205	1.56	299	0.688
		1000	0.0527	1740	1.58	584	0.738
		1300	0.113	3715	1.67	588	1.01
		1400	0.135	4460	1.46	782	0.508
		1500	0.175	5780	1.41	892	1.18
		1600	0.190	6260	1.38	852	0.409
		1800	0.263	8690	1.33	1129	0.129
5.00	0.0150	500	0.00394	130	1.68	112	1.94
		550	0.00494	163	1.64	115	1.84
		600	0.00706	233	1.56	151	1.38
					1.57	167	1.60
		650	0.00912	300	1.55	128	7.34
		700	0.0134	440	1.56	159	7.63
		750	0.0160	528	1.56	179	1.18
		800	0.0233	770	1.56	210	2.02
		900	0.0344	1135	1.56	284	1.10
		1000	0.0482	1590	1.87	394	1.09
		1100	0.0580	1915	1.69	472	0.873
		1200	0.0823	2715	1.71	503	1.26
		1300	0.118	3900	1.29	627	0.152
		1400	0.132	4360	1.39	901	0.588
		1500	0.162	5340	1.35	718	0.766
		1600	0.183	6025	1.32	788	0.452
					1.41	770	0.444
					1.31	764	0.870
		1800	0.253	9355	1.23	1067	1.04

APPENDIX IV.10

Oxygen Overall Volumetric Mass Transfer Coefficient in 0.375M Sodium Sulphate - 0.004M Cupric Sulphate Solution (Computed from Unsteady-State Data)

Aeration rate			Agitation P_G/V_L		Calculated D_M	$K_{L4}a$	
Q_1 ℓ/min	v_S ft/sec	N rpm	hp/ft^3	$\frac{\text{ft-lb}_f}{\text{min-ft}^3}$	cm^2/sec $\times 10^7$	hr^{-1}	Best fit CHISQ(X)
1.25	0.00375	700	0.0220	725	1.82	172	1.16
					1.85	169	0.512
		800	0.0368	1215	1.56	149	1.89
					1.56	149	1.52
2.50	0.00750	800	0.0261	860	1.56	167	0.992
		900	0.0445	1470	1.56	246	1.32
		1100	0.0770	2565	1.70	517	0.696
		1500	0.1790	5895	1.29	726	0.140
3.75	0.01125	700	0.0165	545	1.56	131	2.71
			0.0157	520	1.52	137	3.64
		1300	0.1090	3610	1.63	556	0.682
		1400	0.1130	3715	1.37	742	0.473
		1500	0.165	5450	1.20	666	1.04
5.00	0.0150	1000	0.0482	1590	1.66	589	0.574
		1500	0.155	5115	1.44	794	0.539
					1.43	724	0.492

APPENDIX IV.11

Oxygen Overal Volumetric Mass Transfer Coefficient in 0.500M Sodium Sulphate - 0.004M Cupric Sulphate Solution (Computed from Unsteady-State Data)

Aeration rate			Agitation P_G/V_L		Calculated D_M	$K_{L4}a$	
Q_1 ℓ/min	v_S ft/sec	N rpm	hp/ft^3	$\frac{\text{ft-lb}_f}{\text{min-ft}^3}$	cm^2/sec $\times 10^7$	hr^{-1}	Best fit CHISQ(X)
1.25	0.00375	800	0.0342	1130	1.56	147	2.80
		900	0.0517	1700	1.56	236	5.15
2.50	0.0075	800	0.0270	890	1.56	166	0.821
		900	0.0445	1470	1.56	245	0.643
		1100	0.0777	2565	1.66	465	0.348
		1500	0.179	5900	1.24	847	0.301
3.75	0.01125	600	0.0165	544	1.91	196	0.991
		1600	0.242	8000	1.27	812	0.164
5.00	0.0150	1000	0.0517	1705	1.56	537	0.785
		1300	0.107	3520	1.32	707	0.332
		1500	0.162	5340	1.34	831	0.109

APPENDIX IV.12

Oxygen Overall Volumetric Mass Transfer Coefficient by Sulphite Oxidation

Q_1		Agitation rate N	P_G/V_L	Partial pressure O_2 in exit gas atm		$K^r_{L4}a$
ℓ/min	ft/sec	rpm	hp/ft^3	Calc.	Measured	hr^{-1}
1.25	0.00375	500	0.00506	0.204		59.4
		600	0.0111	0.199	0.199	123
		700	0.0204	0.194		180
		900	0.0497	0.169		502
		1125	0.0871	0.142		966
		1750	0.278	0.106		1895
		2270	0.688	0.083		2900
2.50	0.00750	500	0.00506	0.207	0.206	79.1
		900	0.0415	0.184	0.182	591
		1500	0.175	0.144	0.139	1840
		2270	0.609	0.103		4000
3.75	0.01125	500	0.0050	0.207	0.206	88.7
		800	0.0242	0.198	0.196	399
		1500	0.167	0.152		2340
		2270	0.548	0.118		4590
5.00	0.0150	500	0.00448	0.208		92.8
		700	0.0142	0.203		279
		900	0.0324	0.197	0.196	581
		1100	0.0697	0.186	0.186	1110
		1400	0.134	0.168	0.160	2070
		1700	0.216	0.155		2945
		2270	0.484	0.130		4900

$K^r_{L4}a$ based on calculated oxygen partial pressure in exit gas.

APPENDIX IV.13(A)

Oxygen Overall Volumetric Mass Transfer Coefficient in KOH - K_2CO_3 (Average Γ_T = 0.0965) Unsteady-State Data; Simultaneous CO_2 Absorption with Chemical Reaction

Aeration rate		Agitation			Calculated		
			P_G/V_L		D_M	$K_{L4}a$	
Q_1	v_S	N		$\frac{\text{ft-lb}_f}{\text{min-ft}^3}$	cm^2/sec		Best fit
ℓ/min	ft/sec	rpm	hp/ft^3		$\times 10^7$	sec^{-1}	CHISQ(X)
5.00	0.0150	800	0.0297	980	1.56	0.0523	0.533
		900	0.0391	1290	1.56	0.0820	3.58
		1000	0.0515	1700	1.56	0.0944	0.386
		1100	0.0730	2410	1.56	0.0892	0.781
		1200	0.0942	3110	1.61	0.166	0.208
		1300	0.124	4090	1.65	0.164	0.765
		1400	0.161	5320	1.62	0.173	1.03
		1600	0.256	8460	1.64	0.253	1.36
		1700	0.302	9950	1.56	0.252	0.798
		2000	0.480	15850	1.58	0.315	0.831

Appendix IV.13(B)

Interfacial Area, Liquid-Phase Oxygen Mass Transfer Coefficient, Gas Holdup, and Average Bubble Diameter in KOH - K_2CO_3: v_S = 0.0150 ft/sec

rpm N	Concentrations OH^- g-ion/ℓ	$CO_3^=$ g-ion/ℓ	Γ_T g-ion/ℓ	CO_2 mole fraction exit gas* $y_{3,2}$	Specific area a cm^{-1}	Reaction factor ϕ_3	k_{L4} cm/sec	Gas holdup H_G	Bubble avg. diameter d_b cm
500								0.0183	
700								0.0240	
800	0.0827	0.0057	0.0998	0.02230	1.18	3.76	0.0443	0.0453	0.231
900	0.0862	0.0063	0.1051	0.00988	3.10	6.14	0.0271	0.0573	0.111
1000	0.0758	0.0071	0.0971	0.00586	5.23	9.47	0.0180	0.0693	0.0796
1100	0.0828	0.0036	0.0936	0.00472	6.07	11.3	0.0148	0.0800	0.0791
1200	0.0798	0.0061	0.0981	0.00399	8.34	8.19	0.0200	0.0990	0.0690
1300	0.0650	0.0091	0.0923	0.00350	10.5	9.35	0.0156	0.107	0.0609
1400	0.0830	0.0042	0.0956	0.00250	16.5	15.4	0.0105	0.116	0.0422
1600	0.0189	0.0241	0.0912	0.00439	19.0	6.39	0.0133	0.140	0.0441
1700	0.0136	0.0267	0.0937	0.00478	16.8	4.38	0.0150	0.144	0.0514
2000	0.0211	0.0257	0.0982	0.00219	32.1	7.64	0.0098	0.181	0.0340
		Avg.	0.0965						

$H_3 = 0.331(10^5)\exp[0.26\,\Gamma_5 + 0.168\,\Gamma_6]$.

*Inlet gas $y_{3,1}$ = 0.10 (0.90 N_2).

APPENDIX IV.14(A)

Oxygen Overall Volumetric Mass Transfer Coefficient in 0.135M KCl + KOH - K_2CO_3 (Average $\Gamma_T = 0.221$). Unsteady-State Data; Simultaneous CO_2 Absorption with Reaction

Aeration rate			Agitation		Calculated	$K_{L4}a$	
			P_G/V_L		D_M		
Q_1	v_S	N		$\frac{\text{ft-lb}_f}{\text{min-ft}^3}$	cm^2/sec		Best fit
ℓ/min	ft/sec	rpm	hp/ft^3		$\times 10^7$	sec^{-1}	CHISQ(X)
5.00	0.0150	700	0.0134	441	1.40	0.0547	0.602
		850	0.0267	880	1.35	0.0894	0.130
		1000	0.0442	1460	1.45	0.0903	0.780
		1150	0.0776	2560	1.51	0.135	0.179
		1300	0.112	3710	1.53	0.186	0.059
		1600	0.223	7360	1.44	0.356	0.046
		1900	0.377	12450	1.60	0.456	1.46
		2100	0.523	17260	1.44	0.457	0.048

APPENDIX IV.14(B)

Interfacial Area, Liquid-Phase Oxygen Mass Transfer Coefficient, Gas Holdup, and Average Bubble Diameter in 0.135M KCl + KOH - K_2CO_3 : v_S = 0.0150 ft/sec

N	Concentrations			CO_2 mole fraction exit gas*	Specific area	Reaction factor	k_{L4}	Gas holdup	Bubble average diameter d_b
	OH^-	$CO_3^=$	Γ_T	$y_{3,2}$	a	ϕ_3		H_G	
rpm	g-ion/ℓ	g-ion/ℓ	g-ion/ℓ		cm^{-1}		cm/sec		cm
700	0.02130	0.01787	0.210	0.0319	1.13	2.19	0.0484	0.0267	0.142
850	0.02106	0.02532	0.232	0.0212	3.86	2.31	0.0451	0.0427	0.130
1000	0.02082	0.02030	0.216	0.01415	3.25	3.70	0.0278	0.0507	0.0936
1150	0.02461	0.02271	0.228	0.00736	7.00	5.11	0.0193	0.0760	0.0651
1300	0.02129	0.01881	0.213	0.00547	9.32	5.92	0.0200	0.0907	0.0584
1600	0.02189	0.02100	0.0219	0.00293	15.9	5.41	0.0224	0.115	0.0434
1900	0.02603	0.02082	0.223	0.00146	33.3	8.06	0.0137	0.145	0.0261
2100	0.02307	0.02189	0.223	0.00116	44.5	10.1	0.0103	0.171	0.0231

$H_3 = 0.331(10^5) \exp [0.26\ \Gamma_5 + 0.168\ \Gamma_6 + 0.0268]$.

*Inlet gas $y_{3,1} = 0.10\ (0.90\ N_2)$.

APPENDIX IV.15(A)

Oxygen Overall Volumetric Mass Transfer Coefficient in 0.11M Na_2SO_4 + KOH - K_2CO_3 (Average Γ_T = 0.418). Unsteady-State Data; Simultaneous CO_2 Absorption with Reaction

Aeration Rate			Agitation P_G/V_L		Calculated D_M	$K_{L4}a$	
Q_1 ℓ/min	v_S ft/sec	N rpm	hp/ft^3	$\frac{\text{ft-lb}_f}{\text{min-ft}^3}$	cm^2/sec $\times 10^7$	sec^{-1}	Best fit CHISQ(X)
5.00	0.0150	700	0.0126	415	1.39	0.0357	0.910
		900	0.0333	1100	1.39	0.0894	0.783
		1000	0.0432	1425	1.39	0.0986	0.542
		1200	0.0823	2715	1.48	0.159	0.057
		1300	0.102	3370	1.52	0.163	0.387
		1400	0.132	4360	1.44	0.215	0.021
		1500	0.157	5170	1.40	0.256	0.476
		1700	0.233	7680	1.42	0.262	0.056
		1900	0.307	10130	1.43	0.378	0.171
		2100	0.412	13600	1.43	0.379	0.106

Appendix IV.15(B)

Interfacial Area, Liquid-Phase Oxygen Mass Transfer Coefficient, Gas Holdup, and Average Bubble Diameter in 0.11M Na_2SO_4 + KOH - K_2CO_3: v_S = 0.0150 ft/sec

rpm N	Concentrations OH^- g-ion/ℓ	$CO_3^=$ g-ion/ℓ	Γ_T g-ion/ℓ	CO_2 mole fraction exit gas* $y_{3,2}$	Specific area a cm^{-1}	Reaction factor ϕ_3	k_{L4} cm/sec	Gas holdup H_G	Bubble avg. diameter d_b cm
700	0.02892	0.01408	0.402	0.0254	1.38	4.77	0.0259	0.0240	0.104
900	0.03691	0.02674	0.447	0.0181	1.85	2.95	0.0483	0.0427	0.138
1000	0.02425	0.02035	0.415	0.0143	3.04	3.58	0.0318	0.0534	0.105
1200	0.02240	0.01916	0.410	0.00664	7.49	5.06	0.0212	0.0853	0.0684
1300	0.02035	0.02650	0.430	0.00588	8.91	5.62	0.0183	0.0906	0.0611
1400	0.02295	0.01514	0.398	0.00387	13.1	6.55	0.0164	0.104	0.0476
1500	0.02106	0.02252	0.419	0.00252	21.5	8.63	0.0119	0.112	0.0313
1700	0.02058	0.02662	0.430	0.00261	20.8	8.13	0.0126	0.128	0.0369
1900	0.01881	0.01964	0.408	0.00209	27.4	8.83	0.0138	0.147	0.0322
2100	0.02023	0.02284	0.419	0.00149	37.5	9.99	0.0101	0.171	0.0274

$H_3 = 0.331(10^5)\exp[0.26\,\Gamma_5 + 0.168\,\Gamma_6 + 0.0719]$.

*Inlet gas $y_{3,1} = 0.10$ (0.90 N_2).

REFERENCES

1. Strohm, J., Dale, H. F., and Peppler, H. J., Appl. Microbiol., 7, 235 (1959).

2. Karow, E. O., Bartholomew, W. H., and Sfat, M. R., J. Agr. Food Chem., 1, 302 (1953).

3. Champagant, A., Gudin, C., and Moutard, A.-M., French Patent 1, 387, 842 (1963).

4. Darlington, W. A., Biotech. Bioeng., 6, 241 (1964).

5. Webb, F. C., Lilly, M. D., and Ertola, R. T., Biotech. Bioeng., 7, 309 (1965).

6. Johnson, M. J., and Miller, T. L., Biotech. Bioeng., 8, 549 (1966).

7. Johnson, M. J., and Miller, T. L., Biotech. Bioeng., 8, 567 (1966).

8. Johnson, M. J., Lie, S., and Miller, T. L., Biotech. Bioeng., 6, 299 (1964).

9. Calderbank, P. H., Trans. Inst. Chem. Engrs. (London), 37, 173 (1959).

10. Calderbank, P. H., Trans. Inst. Chem. Engrs. (London), 36, 443 (1958).

11. Copper, C. M., Fernstrom, G. A., and Miller, S. A., Ind. Eng. Chem., 36, 504 (1944).

12. Westerterp, K. R., van Dierendonck, L. L., and de Kraa, J. A., Chem. Eng. Sci., 18, 157 (1963).

13. Phillips, D. H., and Johnson, M. J., Ind. Eng. Chem., 51(1), 83 (1959).

14. Yoshida, F., Ikeda, A., Imakawa, A., and Miura, Y., Ind. Eng. Chem., 52(5), 435 (1960).

15. Ohyama, Y., and Endoh, K., Chem. Eng. (Japan), 19, 2 (1955), as given in Aiba, S., Humphrey, A. E., and Millis, N., Biochemical Engineering (Academic Press, New York, 1965), p. 142.

16. Calderbank, P. H., and Moo-Young, M. M., Chem. Eng. Sci., 16, 39 (1961).

17. Higbie, R., Trans. Amer. Inst. Chem. Engrs., 31, 365 (1935).

18. Danckwerts, P. V., Ind. Eng. Chem., 43, 1460 (1951).

19. Frössling, N., Gerlands Beitrage Zur Geophysik, 52, 170 (1938).

20. Treybal, R. E., Mass Transfer Operations, 1st. ed. (McGraw-Hill, New York, 1955), p. 85.

21. Ibid, p. 86.

22. Resnick, W., and Gal-Or, B., Adv. in Chem. Eng., 7, 295 (1968), Drew, T. B., ed. (Academic Press, New York).

23. Schaftlein, R W., and Russell, T. W. F., Ind. Eng. Chem., 60(5), 13 (1968).

24. Kolmogoroff, A. N , as given in Levich, V G., Physiochemical Hydrodynamics (Prentice-Hall, Englewood Cliffs, N. J., 1962).

25. Gal-Or, B., and Resnick, W., Chem. Eng. Sci., 13, 653 (1964).

26. Gal-Or, B., and Hoelscher, H. E., A. I. Ch. E. Jr., 12, 499 (1966).

27. Gal-Or, B., and Walatka, V., A. I. Ch. E. Jr., 13, 650 (1967).

28. Gal-Or, B., Hauck, J. P., and Hoelscher, H. E., Int. J. Heat Mass Transfer, 10, 1559 (1967).

29. Hanhart, J., Kramers, H., and Westerterp, K. R., Chem. Eng. Sci., 18, 503 (1963).

30. Richards, J. W., Prog. Ind. Microbiol., 3, 143 (1961).

31. Finn, R. K., in Biological and Biochemical Engineering Science, Blakebrough, N., ed. (Academic Press, New York, 1967), p. 69.

32. Yoshida, F., Yamaguchi, T., and Hattori, K., J. Ferment. Technol., 46, 1019 (1968).

33. Reid, R. C., and Sherwood, T. K., The Properties of Gases and Liquids. Their Estimation and Correlation (McGraw-Hill, New York, 1958).

34. Finn, R. K., Bact. Rev., 18, 254 (1954).

35. Bartholomew, W. H., Karow, E. O., Sfat, M. R., and Wilhelm, R. H., Ind. Eng. Chem., 42, 1810 (1950).

36. Tsao, G. T., and Kempe, L. L., J. Biochem. Microbiol. Tech. Eng., 2, 129 (1960).

37. Humphrey, A. E., and Reilly, P. J., Biotech. Bioeng., 7, 229 (1965).

38. Hsieh, D. P. H., Silver, R. S , and Mateles, R. I., Biotech. Bioeng., 9, 1 (1969).

39. Heineken, F G., On The Use of Fast-Response Dissolved Oxygen Probes for Oxygen Transfer Studies, paper presented at 3rd International Fermentation Symposium, Rutgers, N. J., Sept. 2-6, 1968.

40. Akiba, T., and Fukimbara, T., J. Ferment. Technol., 46, 1013 (1968).

41. Barron, C. H., and O'Hern, H. A., Chem. Eng. Sci., 21, 397 (1966).

42. Srivastava, R. D., McMillan, A. F., and Harris, I. J., Can. Jr. Chem. Eng., 46, 181 (1968).

43. DeWaal, K. J. A., and Okeson, J. C., Chem. Eng. Sci., 21, 559 (1966).

44. Bigelow, S. L., Z. phys. Chem., 26, 493 (1898).

45. Linek, V., and Mayrhoferová, J., Chem. Eng. Sci., 24, 481 (1969).

46. Clark, L. C., Jr., Weld, R. G., and Taylor, Z., J. Appl. Physiol., 6, 189 (1953).

47. Phillips, D. H., and Johnson, M. J., J. Biochem. Microbiol. Technol. Eng., 3, 261 (1961).

48. Carritt, D. E., and Kanwisher, J. W., Anal. Chem., 31, 5 (1959).

49. Mancy, K. H., Okun, D. A., and Reilley, C. N., J. Electroanal. Chem., 4, 65 (1962).

50. Johnson, M. J., Borkowski, J., and Engblom, C., Biotech. Bioeng., 6, 457 (1964).

51. Ričica, J., in Theoretical and Methodological Basis of Continuous Culture of Microorganisms, Málek, I., and Fencl, Z., eds. (Academic Press, New York, 1966), p. 241.

52. Paul, D. R., and DiBenedetto, A. T., J. Polymer Sci., 9(10), Part C, 17 (1965).

53. Whitman, W. G., Chem. Met. Eng., 29, 146 (1923).

54. Crank, J., The Mathematics of Diffusion (The Clarendon Press, Oxford, 1956), p. 5.

55. Daynes, H., Proc. Roy. Soc., 97A, 286 (1920).

56. Barrer, R. M., Diffusion in and Through Solids (Cambridge, 1941), p. 19.

57. Aiba, S., Minoru, O., and Huang, S.-Y., Ind. Eng. Chem. Fundamentals, 7, 497 (1968).

58. Churchill, R. V., Operational Mathematics, 2nd. ed. (McGraw-Hill, New York, 1958), Chap. 6.

59. Beals, E., LRL Computer Centre Programme Description E2BKY LSQVMT (1966).

60. Beals, E., LRL Computer Centre Programme Description E4BKY VARMIT.

61. Davidon, W. C., Variable Metric Minimization, Argonne National Laboratory Report ANL 5990 (Rev. 1959).

62. Garner, F. H., and Hammerton, D., Trans. Inst. Chem. Engrs. (London), 32, S18 (1954).

63. Astarita, G., Mass Transfer With Chemical Reaction (Elsevier Publ. Co., Amsterdam, 1967), Chap. 1.

64. Danckwerts, P. V., and Sharma, M. M., Chem. Eng. (London), 44, 244 (1966).

65. Trice, Jr., V. G., and Rodger, W. A., A. I. Ch. E. Jr., 2, 205 (1956).

66. Faurholt, C., J. Chem. Phys., 21, 400 (1924).

67. Himmelblau, D. M., and Babb, A. L., A. I. Ch. E. Jr., 4, 143 (1958).

68. Sharma, M. M., and Danckwerts, P. V., Trans. Faraday Soc., 59, 386 (1963).

69. Sharma, M. M., and Danckwerts, P. V., Chem. Eng. Sci., 18, 729 (1963).

70. Nijsing, R. A T. O., Hendriksz, R. H., and Kramers, H., Chem. Eng. Sci., 10, 88 (1959).

71. Pearson, L., Pinsent, B. R W., and Roughton, F. J. W., Faraday Soc. Discussions, 17, 141 (1954).

72. Yoshida, F., and Miura, Y., Ind. Eng. Chem. Process Design Develop., 2, 263 (1963).

73. Danckwerts, P. V., Kennedy, A. M., and Roberts, D., Chem. Eng. Sci., 18, 63 (1963).

74. Astarita, G., Mass Transfer With Chemical Reaction (Elsevier Publ. Co., Amsterdam, 1967), p. 90.

75. Aiba, S., Humphrey, A. E., and Millis, N. F., Biochemical Engineering, (Academic Press, New York, 1965), p. 141.

76. Rushton, J. H., Costich, E. W., and Everett, H. J., Chem. Eng. Prog., 46, 467 (1950).

77. Bates, R. L., Fondy, P. L., and Corpstein, R. R., Ind. Eng. Chem. Process Design Develop., 2, 310 (1963).

78. Fuller, E C., and Crist, R. H., J. Amer. Chem. Soc., 63, 1644 (1941).

79. Trujillo, E., Instruction Manual 1381-A (Beckman Instruments, Inc., Fullerton, California 1964), p. 17.

80. Aiba, S., A. I. Ch. E. Jr., 4, 485 (1958).

81. Aiba, S., and Huang, S.-Y., J. Ferment. Technol., 47, 372 (1969).

82. Vogel, A. I., Quantitative Inorganic Analysis, 2nd. ed. (Longmans, Green and Co., London, 1951), p. 328.

83. Handbook of Chemistry and Physics, 44th. ed. (Chemical Rubber Publ. Co., Cleveland, Ohio, 1962).

84. Van Krevelen, D. W., and Hoftijzer, P. J., Chimie et Industrie: Numéro Spéciale du XXIe Congrés International de Chimie Industrielle, Brussels, Sept., 1948, p. 148.

85. Ratcliff, G. A., and Holdcroft, J. G., Trans. Inst. Chem. Engrs. (London), 41, 315 (1963).

86. Wilke, C. R., and Chang, P., A. I. Ch. E. Jr., 1, 264 (1955).

87. Vivian, J. E., and King, C. J., A. I. Ch. E. Jr., 10, 220 (1964).

88. Bond, G. C., Catalysis by Metals (Academic Press, New York, 1962), p. 70.

89. Marrucci, G., and Nicodemo, L., Chem. Eng. Sci., 22, 1257 (1967).

90. Friedman, A. M., and Lightfoot, Jr., E. N., Ind. Eng. Chem., 48(8), 1227 (1957).

91. Robinson, R. G., Ind. Eng. Chem. Process Design Develop., 3, 191 (1964).

92. Reith, T., Dissertation, Technological University of Delft (1968).

93. Astarita, G., Marrucci, G., and Coleti, L., La Chimica e l' Ind., 46, 1021 (1964).

94. Westerterp, K. R., Chem. Eng. Sci., 18, 495 (1963).

95. Jones, G., and Ray, W. A., J. Am. Chem. Soc., 59, 187 (1937).

96. Drost-Hansen, W., in Chemistry and Physics of Interfaces (American Chemical Society Publications, Washington, D. C., 1965), p. 22.

97. Reith, T., and Beek, W. J., Trans. Inst. Chem. Engrs. (London), 48, T63 (1970).

98. Howarth, W. J., A. I. Ch. E. Jr., 13, 1007 (1967).

99. Rushton, J. H., and Bimbinet, J.-J., Can. Jr. Chem. Eng., 46, 16 (1968).

100. Kintner, R. C., Adv. in Chem. Eng., 4, 52 (1963), Drew, T. B., ed. (Academic Press, New York).

101. Vermeulen, T., Williams, G. M., and Langlois, G. E., Chem. Eng. Prog., 51(2), 85F (1955).

102. Zieminski, S. A., and Raymond, D. R., Chem. Eng. Sci., 23, 17 (1968).

103. Danckwerts, P. V., Appl. Sci. Res., A3, 385 (1952).

104. Sherwood, T. K., and Pigford, R. L., Absorption and Extraction, 2nd. ed. (McGraw-Hill, New York, 1952), p. 61.

105. Kronig, R., and Brink, J. C., Appl. Sci. Res., A2, 142 (1950).

106. International Critical Tables, vol. 5 (McGraw-Hill, New York, 1929).

107. International Critical Tables, vol. 4 (McGraw-Hill, New York, 1928).

108. Jenson, V. G., and Jeffreys, G. V., Mathematical Methods in Chemical Engineering (Academic Press, New York, 1963), Chap. 6.

109. Bird, R. B., Stewart, W. E., and Lightfoot, E. N., Transport Phenomena (John Wiley and Sons, New York, 1960), Chap. 18.

110. Augenstein, D. C., and Wang, D. I. C., Mass Transfer in Fermentation Vessels at High Power Input, paper presented at the 17th Canadian Chemical Engineering Conference, Niagara Falls, Ont., October 18, 1967.

111. Pinsent, B. R. W., Pearson, L., and Roughton, F. J. W., Trans. Faraday Soc., 52, 1512 (1956).

112. Hinze, J. O., A. I. Ch. E. Jr., 1, 289 (1955).

113. Sideman, S., Hortacsu, O., and Fulton, J. W., Ind. Eng. Chem., 58(7), 32 (1966).

114. Hyman, D., Adv. in Chem. Eng., 3, 157 (1962), Drew, T. B., ed. (Academic Press, New York).

TECHNICAL INFORMATION DIVISION
LAWRENCE RADIATION LABORATORY
UNIVERSITY OF CALIFORNIA
BERKELEY, CALIFORNIA 94720